Aus dem Biomedizinischen Centrum
der Fakultät der Medizin
Ludwig-Maximilians-Universität München
Lehrstuhl für Molekularbiologie
Vorstand: Prof. Dr. rer. nat. Peter B. Becker

Proteomic analysis of assembled chromatin with SWATH-MS

Dissertation
zum Erwerb des Doktorgrades der Naturwissenschaften
an der Medizinischen Fakultät der
Ludwig-Maximilians-Universität zu München

vorgelegt von
Moritz Carl Völker-Albert

aus
Königstein im Taunus

2017

Mit Genehmigung der Medizinischen Fakultät
der Universität München

Betreuer:	Prof. Dr. Axel Imhof
Zweitgutachter:	PD Dr. Anton Eberharter
Dekan:	Prof. Dr. med. dent. Reinhard Hickel
Tag der mündlichen Prüfung:	20.12.2017

Eidesstattliche Versicherung

Völker-Albert, Moritz Carl

Ich erkläre hiermit an Eides statt,
dass ich die vorliegende Dissertation mit dem Thema

Proteomic analysis of assembled chromatin with SWATH-MS

selbständig verfasst, mich außer der angegebenen keiner weiteren Hilfsmittel bedient und alle Erkenntnisse, die ich aus dem Schrifttum ganz oder annährend übernommen sind, als solche kenntlich gemacht und nach ihrer Herkunft unter Bezeichnung der Fundstelle einzeln nachgewiesen habe.
Ich erkläre des Weiteren, dass die hier vorgelegte Dissertation nicht in gleicher oder in ähnlicher Form bei einer anderen Stelle zur Erlangung eines akademischen Grades eingereicht wurde.

München, den 02.01.2018 _____

Ort, Datum Unterschrift Doktorand

Parts of this thesis have been published in:

Molecular and Cellular Proteomics, 2016 January 25, doi: 10.1074/mcp.M115.053553

A quantitative proteomic analysis of in vitro assembled chromatin.

Völker-Albert, M.C.*, Pusch, M.C.*, Fedisch, A., Schilcher, P., Schmidt, A., Imhof, A.,

*equal contribution

Used excerpts of the publication within this thesis are marked in *italic.*

Teile dieser Arbeit sind veröffentlicht in:

Molecular and Cellular Proteomics, 2016 January 25, doi: 10.1074/mcp.M115.053553

A quantitative proteomic analysis of in vitro assembled chromatin.

Völker-Albert, M.C.*, Pusch, M.C.*, Fedisch, A., Schilcher, P., Schmidt, A., Imhof, A.,

*gleiche Beteiligung

Verwendete Auszüge aus der Publikation in dieser Dissertation sind *kursiv* markiert.

TABLE OF CONTENTS

SUMMARY

In all eukaryotes, the large DNA molecule must be packed into the nucleus of a cell in a very compact manner. The compacted structure consisting of histones, non-histone proteins and nucleic acids is called chromatin. To transcribe, repair or replicate the DNA, chromatin must be regulated in a highly dynamic manner. The regulators are mostly proteins that can remodel and assemble chromatin by altering the accessibility for DNA-templated processes.

Acquired results in this thesis show temporal changes in protein binding using an *in vitro* reconstitution system based on *Drosophila melanogaster* embryos for 15 min, 1 h and 4 hrs of chromatin assembly.
In addition, newly synthesized DNA and its associated proteins were isolated after replication by nascent chromatin capture (NCC) in human cell lines and quantified at various times of chromatin assembly. Results from a comparison of both systems indicate that the principles of chromatin assembly are conserved between *Homo sapiens* and *Drosophila melanogaster*. In addition, results from both approaches show the association of proteasomal proteins with chromatin that are well-known for their function in protein degradation. Proteasome inhibition causes protein aggregates to form during assembly indicating an important role of the proteasome during chromatin assembly.

Both experimental methods rely on the analysis of proteins with mass spectrometry. Comparative experiments using different mass spectrometric techniques show that using a data-independent acquisition method (SWATH-MS) greatly improves the number of identified and quantified proteins in comparison to classical data-dependent techniques, thereby facilitating the downstream statistical analysis.

Data presented here, contribute new insights about the binding kinetics of proteins during chromatin assembly and suggest that the proteasome functions as a quality control during chromatin assembly.

ZUSAMMENFASSUNG

Die DNA aller Lebewesen mit abgegrenztem Zellkern muss stark kompaktiert werden, um in den Zellkern zu passen. Diese Verdichtung der DNA passiert mit Hilfe von Histonen, Nicht-Histon Proteinen und zusätzlichen Nukleinsäuren und wird Chromatin genannt. Damit jedoch die DNA zugänglich bleibt, um transkribiert, repariert oder verdoppelt zu werden, muss das Chromatin dynamisch reguliert werden. Diese Regulierung findet mit einer Vielzahl von Proteinen statt, die das Chromatin öffnen und auch wieder assemblieren können.

Mithilfe eines *in vitro* Rekonstitutionssystems, das auf einem Extrakt von *Drosophila melanogaster* Embryonen basiert, wurden die zeitlichen Veränderungen der Proteinbindungen nach 15 Minuten, 1 Stunde und 4 Stunden Chromatinassemblierung untersucht.

Diese Studien wurden mit Ergebnissen einer Methode untermauert, mit Hilfe der die neu-synthetisierte DNA nach der Replikation isoliert und aufgereinigt werden kann. Die Ergebnisse der sogenannten „Nascent Chromatin Capture“ (NCC) Methode zeigen hohe Übereinstimmungen zum *in vitro* Rekonstitutionsystem in Bezug auf Proteinintensitäten zu unterschiedlichen Zeitpunkten der Chromatinassemblierung. Darüber hinaus zeigt der Vergleich beider Systeme, dass die Prinzipien der Chromatinassemblierung zwischen *Drosophila melanogaster* und *Homo sapiens* deutlich konserviert sind. Außerdem konnte in dieser Arbeit gezeigt werden, dass proteasomale Proteine an das Chromatin binden, die wiederum andere Proteine abbauen. Sobald diese Klasse an Proteinen im *in vitro* Rekonstitutionssystem inhibiert wird, kommt es zu Aggregaten, die darauf schließen lassen, dass das Proteasom eine wichtige Rolle während der Chromatinassemblierung spielt.

Beide Methoden, die zur Untersuchung der Chromatinassemblierung verwendet wurden, basieren auf der Analyse mit massenspektrometrischen Techniken. Dabei zeigte sich, dass weitläufig benutze datenabhängige Messungen zu Schwierigkeiten beim Vergleich biologischer Replikate führten und somit die statistische Auswertung erschwerten. Durch die Anwendung einer datenunabhängigen Methode (SWATH-MS), konnten deutlich mehr Proteine in allen Replikaten und zu allen gemessen Zeitpunkten identifiziert und quantifiziert werden, für eine schlussendlich robuste statistische Analyse.

Diese Arbeit erweitert die Kenntnisse über das Bindungsverhalten von Proteinen während der Chromatinassemblierung und beschreibt zudem die Rolle des Proteasoms als Qualitätssicherung darin. Die Ergebnisse sind Anknüpfungspunkte für zukünftige Experimente in diesem Bereich.

1. INTRODUCTION

1. 1. Chromatin

In eukaryotic cells, the genomic DNA is packaged together with RNA, histone and non-histone proteins in the cell nucleus. The network of nucleic acids and associated proteins is called chromatin and enables the approximately 2 m long DNA molecule to be fitted into the nucleus of a cell with a diameter of ca. 10 µm.

The compact structure of chromatin must however accommodate functionality for all DNA-templated processes. To achieve this, chromatin is regulated on different levels (Figure 1. 1.). The fundamental unit of chromatin is the nucleosome, consisting of 147 bp of DNA wrapped 1.65 times in a left-handed, superhelical turn around an octamer of core histones (Luger K. et al., 1997).

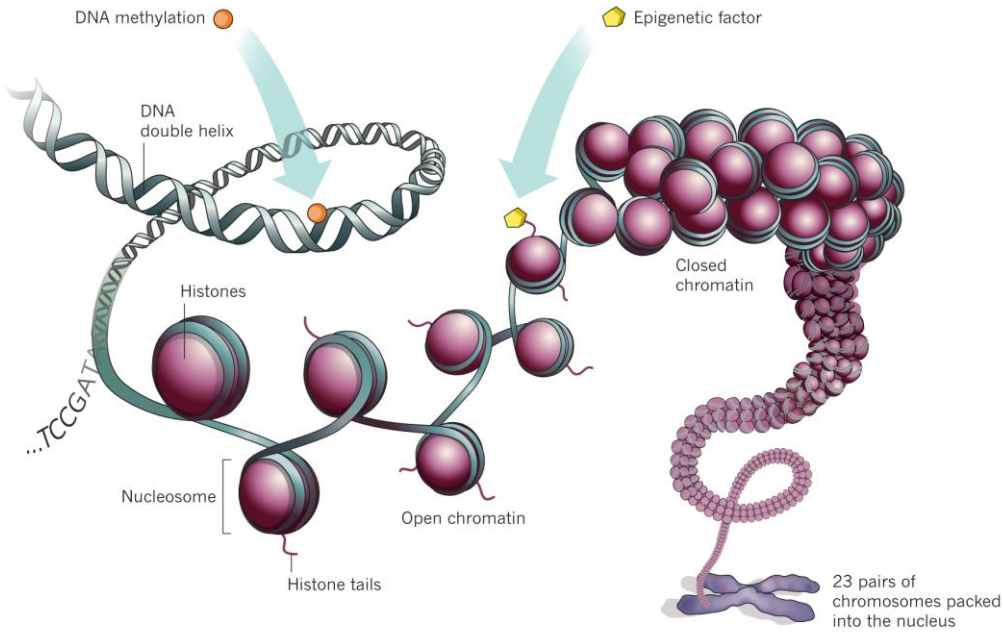

Figure 1. 1.: Packaging of DNA into chromatin.

DNA double helix wraps around nucleosomes composed of histones. DNA and histone tails can be modified to regulate chromatin compaction (Marx, 2012).

Arrays of nucleosomes form distinct fibres of defined size depending on nucleosome-nucleosome interactions or the salt concentration (Hansen, 2002; Maeshima et al., 2016). The status of DNA compaction can dramatically alter the function of the underlying DNA. Densely packed chromatin is referred as heterochromatin whereas more open and accessible chromatin is called euchromatin. Both structures were initially described by Emil Heitz in 1935 who observed morphological differences between different nuclear regions during the cell cycle (Heitz, 1935). The cell cycle of each cell is a continuous succession of stages that lead to cell division and DNA duplication. During each S-phase of the cell cycle, DNA is duplicated and it

was possible to visualise both chromatin states during the cell cycle according to morphological differences of euchromatin and heterochromatin with light microscopy (Elgin, 1996).

After decades of research on both chromatin states, it is known that euchromatin is replicated early during S-phase whereas heterochromatin replicates during middle and late S-phase (Grewal and Elgin, 2002; Grewal and Jia, 2007). Moreover, heterochromatin is characterised by low transcriptional activity and contains only a small number of genetic functions in proportion to its overall length (Lohe et al., 1993).

In addition to their differences in gene activity, both chromatin states have been shown to localize in the nucleus differently. Heterochromatin localizes preferentially at the nuclear periphery, whereas euchromatin is mainly found in the centre of the nucleus resulting in more flexible chromosome territories (Shopland et al., 2006). But also some exceptions to this rule were shown in mouse rod photoreceptor cells and distinct unicellular organisms (Postberg et al., 2005). These studies show that the above canonical pattern is inverted and heterochromatin localizes to the nuclear center whereas euchromatin is mainly found at the nuclear periphery (Solovei et al., 2009).

Very recently, the 3D compaction of DNA in the nucleus has been investigated in a genome-wide scope, confirming that different nuclear compartments can be distinguished within a cell nucleus (Stevens et al., 2017). Whereas compartments of individual topologically-associated domains and loops vary from cell to cell, lamina-associated domains and active enhancers and promoters are organized in a consistent way suggesting that these could drive chromatin folding and genome organisation.

1. 2. Histones

Histone proteins can be classified into canonical histones (H2A, H2B, H3, H4, H1) and non-canonical histones (e.g. H3.3, CenpA, H2A.Z, H3.Y etc.) (Buschbeck and Hake, 2017). Different histone variants are incorporated into nucleosomes under specific circumstances fulfilling specific functions (Van Holde, 1989; Zink and Hake, 2016). The variation of canonical with non-canonical histones enables a dynamic regulation of chromatin. Histone pairs within a nucleosome can be individually exchanged without exchanging an entire nucleosome (Kimura and Cook, 2001; Venkatesh and Workman, 2015).

Canonical histone genes are organized in a gene cluster that is preferentially expressed during early S-phase of the cell cycle to be present during DNA replication. The exception to this rule is H1, which was shown to be transcribed throughout the whole S-phase (Guglielmi et al.,

2013). Non-canonical histones are expressed throughout the cell cycle and function in many replication-independent processes.

The interaction between DNA and histones is mainly mediated by ionic interactions. Histones are small positively charged proteins that interact with the negatively charged phosphate groups of the phosphate-sugar backbone of the DNA leading to a tight binding between histones and DNA.

Each nucleosome consists of an octamer of "core histones": a tetramer of H3-H4 flanked by two dimers of H2A-H2B (Figure 1. 2. a and 1. 2. b). H1 is not part of the nucleosome octamer but is rather located at the top of this structure and keeps the DNA wrapped around the nucleosome in place by binding to the linker DNA between nucleosomes.

All core histones possess a so-called histone fold domain, which consists of three alpha helices linked by two loops (Luger K. et al., 1997). This helical structure leads to the dimer conformation between core histones in a "handshake" configuration (Arents and Moudrianakis, 1995). In contrast to the globular domain, the relatively unstructured N-terminal domain of histones protrudes out of the nucleosome and therefore becomes the target for covalent post-translational modifications (PTMs) by specific enzymes (Figure 1. 2. c), (Alabert et al., 2015; Barth and Imhof, 2010; Fischle et al., 2003).

These epigenetic modifications regulate chromatin via the recruitment of proteins that alter the histone-DNA interaction. For example, histone modifications can recruit remodelling enzymes that utilize the energy from ATP hydrolysis and subsequently change chromatin structure (Becker and Horz, 2002; Clapier et al., 2017; Maier et al., 2008; Mueller-Planitz et al., 2013; Narlikar et al., 2013; Varga-Weisz, 2001). The recruitment of proteins and protein complexes with specific enzymatic activities is now an accepted dogma of how PTMs mediate specific function. The most abundant modifications are methylation, acetylation and phosphorylation. Moreover, ubiquitination and sumoylation as well as crotonylation, succinylation and others have been described as additional PTMs on histone tails (Alabert et al., 2015; Bannister and Kouzarides, 2011; Barth and Imhof, 2010; Fischle et al., 2003; Tan et al., 2011).

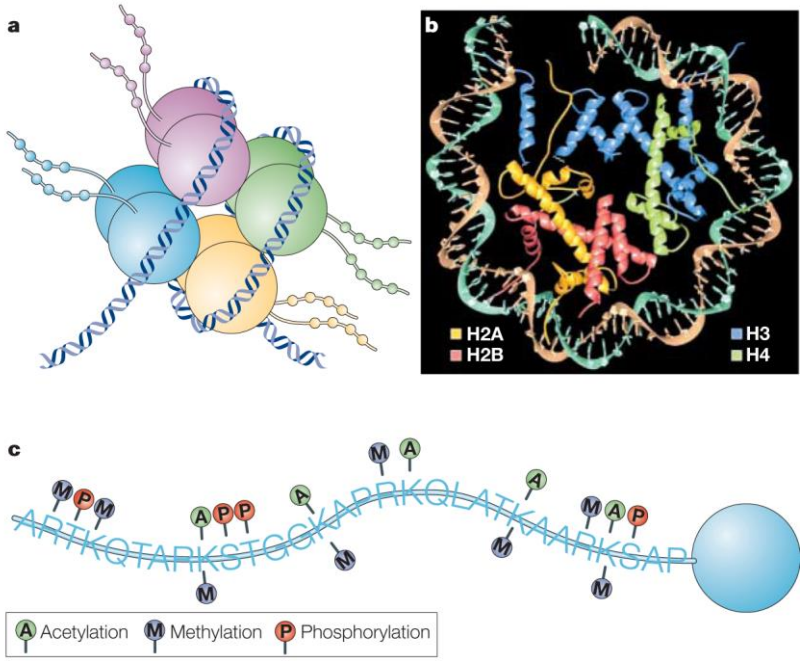

Figure 1. 2.: Nucleosomal composition and histone modifications.

a: Nucleosomes consist of a tetramer of H3-H4 histones together with two dimers of H2A and H2B. Histone tails protrude out the nucleosome.
b: Crystal structure of the nucleosome illustrating the interaction of nucleosome and DNA. (Luger K. et al., 1997).
c: Histone tails can be modified with post-translational modifications. Adapted from (Levenson and Sweatt, 2005).

1. 2. 1. Histone acetylation

Histone acetylation occurs on lysine residues and is facilitated by histone acetyltransferases (HATs). This reaction is reversed by histone deacetylases (HDACs), regulating the steady state of the dynamic histone acetylation modification (Strahl and Allis, 2000).

All HATs catalyse the transfer of an acetyl group from its cofactor acetyl-CoA to the ε-amino group of lysine side chains. Acetylated lysine residues lose their positive charge, which weakens the interaction of DNA and histones (Bannister and Kouzarides, 2011). This reaction has been described in several studies to "open up" the chromatin and to lead to a more accessible DNA structure (Hebbes et al., 1994; Krajewski and Becker, 1998).

Histone acetylation has been found among species predominantly on newly synthesized histone H4 at K5 and K12. This mark is deposited via the histone acetyltransferase HAT1 which interacts with the H3-H4 dimer, CAF and ASF1 before deposition (Loyola et al., 2006; Tagami et al., 2004). But the acetylation of K5 and K12 is not required for any interaction of H4 with ASF1 or CAF arguing for being a transient mark of newly synthesized histones (Ma et al., 1998).

1. 2. 2. Histone methylation

In contrast to acetylation, methylation of lysine and arginine residues on the histone tail does not change the charge of the histone. Lysines can be mono-, di- and tri- methylated and

arginines can be mono-, symmetrically or asymmetrically di-methylated (Bedford and Clarke, 2009; Ng et al., 2008). Methylation is placed by histone methyltransferases (HMT) that catalyse the transfer of a methyl group from S-adenosylmethionine (SAM) to a lysine's ε-amino group or to the ω-guanidino group of an arginine.

For many years, methylation was considered to be a stable mark and demethylases were unknown. However, since 2004, several demethylases have been found (Table 1. 1.). For example, LSD1 in complex with the co-rest repressor complex and JMJD2 were the first demethylases found that can remove methyl groups from H3K4me1/2 or H3K9me3 and H3K36me3 respectively (Shi et al., 2004).

Table 1. 1.: Overview of human demethylase families and proteins with respective substrates.

Adapted from (Pedersen and Helin, 2010). Empty cells illustrate missing data in literature that need to be obtained.

Protein family	Protein name	Substrate
KDM1	KDM1A (LSD1/AOF2/BHC110)	H3K4me1/me2 H3K9me1/me2
	KDM1B (LSD2/AOF1)	H3K4me1/me2
	JMJD7	
	HIF1AN	
	HSPBAP1	
	JMJD5	
	JMJD4	
	JMJD6 (PSR/PTDSR)	H3R2 H4R3
	JMJD8	
KDM2	KDM2A (JHDM1A/FBXL11)	H3K36me1/me2
	KDM2B (JHDM1B/FBXL10)	H3K36me1/me2 H3K4me3
	JHDM1D (KIAA 1718	
	PHF8 (JHDM1F	
	PHF2 (JHDM1E)	
	HR	
KDM3	KDM3A (JHDM2A/JMJD1A/TSGA)	H3K9me1/me2
	KDM3B (JHDM2B/JMJD1B)	
	JMJD1C (JHDM2C/TRIP8)	
KDM4	KDM4A (JMDM3A/JMJD2A)	H3K9me2/me3 H3K36me2/me3 H1K26me1/me3
	KDM4B (JMDM3B/JMJD2B)	
	KDM4C (JMDM3C/JMJD2C)	
	KDM4D (JMDM3D/JMJD2D)	
KDM5	KDM5A (JARID1A/RBP2)	H3K4me2/me3
	KDM5B (JARID1B/PLU1)	
	KDM5C (JARID1C/SMCX)	
	KDM5D (JARID1D/SMCY)	
KDM6	KDM6A (UTX)	H3K27me2/me3
	KDM6B (JMJD3)	
	UTY	
	JARID2	
	MINA	
	NO66	H3K4me2/me3 H3K36me3/me2

1. 2. 3. Histone phosphorylation

Histone phosphorylation takes place at serines, threonines and tyrosines and it is regulated by kinases and phosphatases that add and remove phosphorylation modifications respectively.

Phosphorylation is a highly dynamic modification and has been found to play a role in cell cycle regulation. In particular, the phosphorylation of serine 10 and serine 28 of H3 have been described to regulate mitosis and is deposited by the Aurora B kinase in a genome-wide manner (Goto et al., 2002).

An additional layer of information generated by these modifications is the combination and interaction of specific modifications at the same time. All together these modifications alter the interaction of histones with the DNA to influence gene accessibility and finally regulate gene transcription, chromatin compaction or protein recruitment to the DNA.

This interplay of specific enzymes with various combinations of histone modifications has been termed the "histone code" (Strahl Allis, 2000). To dynamically modify the code, some proteins act as histone code *writers* and *erasers*. Effector proteins contain domains that specifically recognize certain modifications and therefore are able to *read* the histone code and initiate downstream effects (Strahl and Allis, 2000).

1. 3. Histone chaperones

Histone chaperones are a group of proteins that help to regulate nucleosome deposition by binding to the positively charged histones and shielding their charge from the highly negatively charged nucleic acids. In this way, chaperone proteins channel newly synthesized histones from the cytoplasm into the nucleus and control the correct incorporation during chromatin assembly (Laskey et al., 1978).

During nucleosome assembly, parental H3-H4 as well as newly synthesized H3-H4 molecules are incorporated first and then followed by rapid deposition of H2A-H2B dimers (Smith et al., 1984; Worcel et al., 1978). In general, H3-H4 molecules remain stably bound to the DNA, whereas H2A-H2B can be deposited and exchanged more rapidly. Based on this principle, chaperones have preferences either to bind to H3-H4 or to H2A-H2B dimers. Nucleosome incorporation occurs either in the context of DNA replication or during DNA repair or transcription. Therefore, one can distinguish between replication-coupled and replication-independent nucleosome assembly (Figure 1. 3.).

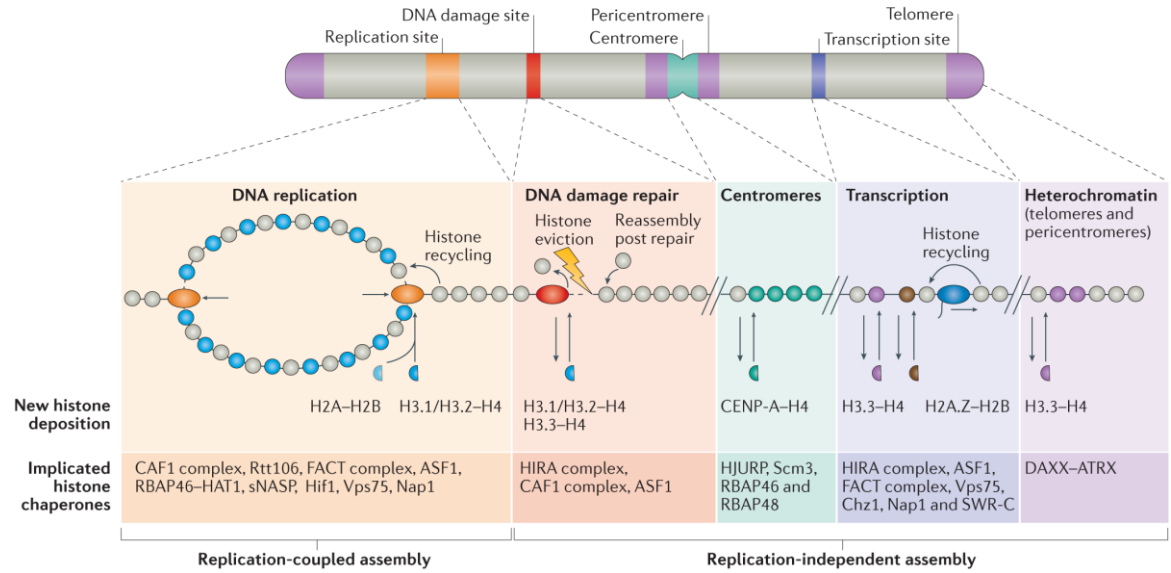

Figure 1. 3.: Histone deposition mechanisms.

Replication-coupled assembly occurs during DNA replication. Specific subset of chaperones is mediating the nucleosome deposition in this context. All other nucleosome deposition mechanisms are classified as replication-independent assembly and can occur in different regions of the genome and with specific histone chaperones. Adapted from (Hammond et al., 2017).

1. 3. 1. Replication-coupled nucleosome assembly

During S-phase of each cell cycle, in which chromatin is disassembled and reassembled, nucleosomes must be evicted from chromatin and newly incorporated after replication. This process is highly regulated and still not fully understood.

The interdependency between DNA replication and nucleosome incorporation has been investigated using the Okazaki fragment length as indicator of chromatin assembly function (Smith and Whitehouse, 2012; Yadav and Whitehouse, 2016). During replication of the lagging strand of DNA, Okazaki fragments are produced and subsequently ligated together. Okazaki fragment ligation occurs at the midpoint of DNA that wraps around a nucleosome, rather than in internucleosomal regions. In addition, alterations in chromatin assembly or lagging-strand polymerization affect Okazaki fragment size, suggesting that the assembly of chromatin is a signal for termination of Okazaki fragment synthesis (Yadav and Whitehouse, 2016).

It could be further shown that nucleosome assembly *in vivo* requires key histone chaperones CAF and Rtt106. CAF is a trimeric complex (Caf-1, Caf-150, Caf-180 in Drosophila) that incorporates H3-H4 into newly synthesized DNA by interacting with PCNA, which helps to recruit it to the replication fork (Moggs et al., 2000; Shibahara and Stillman, 1999; Winkler et al., 2012).

The Caf-150 subunit preferably binds to DNA fragments longer than 40-bp in size. This interaction supports further binding by the other subunits of the CAF chaperone leading to two

CAF-H3-H4 complexes concertedly associating with DNA resulting in the deposition of H3-H4 tetramers (Mattiroli et al., 2017a; Mattiroli et al., 2017b; Sauer et al., 2017).

Rtt106 is a more recently discovered chaperone, first identified in a genetic screen for regulators of Ty1 transposition in budding yeast (Scholes et al., 2001). Rtt106 was shown to interact with PCNA and to incorporate H3-H4 similarly to CAF during replication-coupled nucleosome assembly (Li et al., 2008; Su et al., 2012).

Both chaperones, CAF and Rtt106, rely on the assistance of an additional chaperone ASF1. ASF1 functions in replication-coupled as well as in replication-independent nucleosome assembly. It interacts with cytosolic and nuclear H3-H4 dimers through an H3 interface and transports these complexes to the nucleus. There it forms a complex with the Minichromosomal complex proteins (Mcm) 2-7 to facilitate replication fork progression (Jasencakova et al., 2010). Most importantly, ASF1 is required for acetylation of H3K56 by Rtt109, a mark of newly synthesized histones that has been found to be important for the transfer of H3-H4 from ASF1 to CAF and Rtt106 for assembly of newly synthesized H3-H4 onto replicating DNA (Han et al., 2007).

Another chaperone complex, FACT, has been shown to be involved in nucleosome assembly. The FACT complex interacts with H3-H4 tetramers via its SPT16 subunit. The middle domain of SPT16 (SPT16-M) forms a tandem arrangement of pleckstrin homology domains and can bind to H2A-H2B dimers as well as to H3-H4 tetramers (Tsunaka et al., 2016). Other factors such as Rtt106 and Pob3 also contain pleckstrin homology domains (Rtt106-M and Pob3-M) and it is under current investigation whether these domains bind to H3-H4 in a similar manner than the SPT16-M domain (Liu et al., 2010). Rtt106-M exhibits specificity for H3-H4 by its recognition of H3K56Ac (Li et al., 2008) and together with FACT, it facilitates the incorporation of H3-H4 into chromatin during DNA replication (Tsunaka et al., 2016).

Taken together, many possible pathways have been described that mediate the assembly or disassembly of histones from DNA. This has been confirmed by studies with hemisomes/half-nucleosomes (one copy of H2A/H2B/H3/H4) and hexasomes (two copies of H3/H4 and one copy of H2A/H2B) proposing synergistical pathways for nucleosome assembly (Furuyama et al., 2013; Rhee et al., 2014).

1. 3. 2. Replication-independent chromatin assembly

Other than during S-phase, chromatin is also remodelled after DNA repair and gene transcription using replication-independent pathways. Although no DNA is replicated during these processes, similar chaperones are involved in replication-independent chromatin

assembly. However, some of the identified factors have been described to be only involved in DNA-independent chromatin assembly.

During DNA transcription, histone chaperones remove nucleosomes from occupied DNA sequences in cooperation with histone modifiers and chromatin remodelers (Avvakumov et al., 2011). The chaperones CAF, ASF1, HIRA and NAP1 are involved in nucleosome disassembly during transcription to either disassemble nucleosomes before transcription or reassemble nucleosomes after transcription of RNA polymerase II (RNA pol II) (Ray-Gallet et al., 2011).

NAP1 is a well-known chaperone for H2A-H2B and shows high sequence similarity to other chaperones belonging to the NAP1-like proteins (NAPL) and Vps75 in *yeast* (Selth and Svejstrup, 2007). NAP1 is involved in many processes during nucleosome incorporation. It imports H2A-H2B from cytoplasm into the nucleus via an interaction with importin Kap114 (Mosammaparast et al., 2002). Moreover, it regulates the spacing of nucleosomes through an interaction with the chromatin and remodelling factor ACF in an ATP-dependent manner (Ito et al., 1997).

Additionally, replication-independent pathways have been described in which other chaperones, DAXX and ATRX, control H3.3 deposition at telomeres and regulatory DNA elements showing that multiple chaperones can play roles during transcription (Tagami et al., 2004).

Other chaperones have distinct functions during DNA transcription. For example, the histone chaperone, HIRA, assists in the incorporation of the histone variant H3.3 into DNA. HIRA binds to the DNA directly with the help of the replication protein A (RPA) and is active throughout the entire cell cycle (Zhang et al., 2017). HIRA transfers H3.3 to active genes or promoters, whereas it incorporates canonical histone H3.1 solely during DNA replication.

Replication-independent chromatin assembly is also important during DNA repair. In general, DNA breaks lead to an increased phosphorylation of the H2A variant H2AX (H2Av in Drosophila) at the site of a DNA lesion. Upon modification, DNA repair mechanisms like non-homologous end joining (NHER) or homologous recombination (HR) take place. These processes rely on proteins such as ATM, BRAC1, Rad50 as well as additional repair factors such as the acetyltransferase complex Tip60 in Drosophila. This complex specifically acetylates phosphoH2Av and exchanges it with unmodified H2Av. This unique H2A variant is maintained in the chromatin until repair is completed (Kusch, 2004).

Furthermore, chromatin assembly following DNA repair is dependent on ASF1. Cells depleted of ASF1 and CAF showed upon DNA damage a constant activation of DNA damage

checkpoints although cell cycle progression was not impaired (Kim and Haber, 2009). These results suggest that both chaperones play roles during nucleosome assembly during DNA repair. Indeed, CAF and PCNA are recruited to sites of DNA lesions in an ATP-dependent manner (Moggs et al., 2000), and are responsible for post-repair deposition of new histones. Additionally, CAF is related to monoubiquinitation of H2A histones, although the exact mechanism is still elusive (Polo et al., 2006; Zhu et al., 2009).

1. 4. Kinetics of chromatin assembly

In the beginning of 2017, researchers from the European Molecular Biology Laboratory in Heidelberg and from the Erasmus University Medical Center in Rotterdam published a movie animation illustrating the compaction of DNA in the nucleus (Knoch et al., 2016; Wachsmuth et al., 2016).

Although these studies contribute enormously to our understanding of temporal DNA compaction in the nucleus, the dynamic changes of the DNA-bound proteome during assembly remained largely elusive so far.

Several studies in recent years have shed light into the investigation of the proteomic composition during chromatin assembly (Alabert et al., 2014; Sirbu et al., 2012). However, quality control mechanisms, sequence specificity and inheritance of (epi-) genetic modifications during chromatin assembly are still not fully understood. To address these questions, this thesis is based on two main approaches to shed light on these key cellular processes using: *in vivo* chromatin assembly techniques and *in vitro* assembly systems.

1. 4. 1. *In vitro* chromatin assembly systems

Crude extracts from Drosophila embryos or Xenopus egg extracts have been used to study chromatin assembly *in vitro* (Bulger et al., 1995; Kleinschmidt and Franke, 1982). Both systems are unique to study the mechanisms of cell cycle regulated processes at a biochemical level (Gillespie et al., 2012). This is due to the fact that crude extracts from *Drosophila melanogaster* embryos and *Xenopus laevis* eggs contain sufficient maternal proteins and RNAs to support at least 12 rounds of cell cycle in the absence of transcription (Newport and Kirschner, 1982). Furthermore, these cell-free systems mimic many key aspects of chromatin assembly *in vivo* (Becker and Wu, 1992; Kamakaka et al., 1993; Völker-Albert et al., 2016).

Using *in vitro* assembly systems, it was shown, that H3 and H4 assemble first as tetramer before two dimers of H2A and H2B complete nucleosome formation (Ladoux et al., 2000; Wagner et al., 2005; Worcel et al., 1978). Soluble H4 is stored in a pre-acetylated form (Alvarez et al.,

2011), which gets rapidly deacetylated upon nucleosome assembly (Scharf et al., 2009; Shimamura and Worcel, 1989). This deacetylation step is facilitated by the monomethylation of H4K20 and requires the continuous presence of ATP suggesting that it is coupled to chromatin maturation (Scharf et al., 2009).

Due to the absence of a cell membrane, these *in vitro* assembly systems are also particularly well-suited for the investigation of DNA replication and its associated chromatin assembly mechanisms. First, labelled nucleotides can be added to the extract so that the kinetics of nucleotide incorporation can be observed and monitored (Hashimoto et al., 2011). Secondly, this system can be also used to perform functional studies that elucidate processes of DNA replication as for example the active termination of replication once duplication is complete. In particular, the Mcm7 subunit of the helicase complex during replication gets polyubiquitylated and this subsequently leads to its disassembly at the converging terminating forks because of the action of the p97/Vcp/Cdc48 protein remodeler (Moreno et al., 2014).

Furthermore, the addition of DNA to the extracts with subsequent quantification of DNA-bound proteins enables a detailed investigation of protein binding kinetics. Therefore, *X. laevis* demembranated sperm nuclei recovered from isolated testes were incubated with *X. laevis* egg extract. It was shown that highly condensed chromosomes from sperm nuclei are decondensed and sperm-specific histone variants were exchanged directly with histones from the egg extract establishing newly remodelled chromatin (Gillespie et al., 2012; Hashimoto et al., 2011).

Another approach investigated chromatin interaction dynamics of DNA repair pathways in combination with mass spectrometry. DNA, containing interstrand crosslinks, was incubated with Xenopus egg extracts to measure assembly and disassembly of proteins involved in DNA repair. Among many expected DNA repair factors, it was shown that SLF1 and SLF2 form a complex with Rad18 and recruit the SMC5/6 cohesion complex to DNA lesions (Raschle et al., 2015).

Finally, recently chromatin replication has been reconstituted from highly purified factors. The effects of purified factors on chromatin replication were compared to results from *in vitro* extracts (Kurat et al., 2017). In this work Kurat and colleagues could demonstrate that the progression of the replisome through chromatin requires a complex interplay between FACT, Nhp6, chromatin remodelers (INO80 or Isw1a) and lysine acetyltransferases (Gcn5 and Esa1). In this system, parental nucleosomes are efficiently reassembled in the back of the replisome and positively influence lagging-strand synthesis.

In summary, cell-free assays have been used to describe key aspects of histone deposition, DNA repair and DNA replication. Levels of histone chaperones and chromatin modifiers were

measured and can be easily manipulated within such an assay. Another advantage of *in vitro* systems is the usage of inhibitors, modulators or other reagents to inhibit or change specific functions within the *in vitro* assembly system without risking unspecific side effects that can occur in complex organisms by means of *in vivo* experiments. Nevertheless, the combination of *in vitro* as well as *in vivo* experiments reveals profound insights into biological questions.

1. 4. 2. *In vivo* chromatin assembly techniques

Recent advantages in the field of *in vivo* chromatin assembly systems have been made using a technique that is based on the isolation of nascent chromatin with subsequent mass spectrometric analysis (Alabert et al., 2014). This nascent chromatin capture (NCC) technique relies on the incorporation of biotin-deoxyuridinetriphosphate (dUTP) in newly synthesized DNA during S-phase. The subsequent proteomic analysis captures the first well-established steps in chromatin replication: DNA unwinding (CMG helicase), DNA synthesis (Pol α, β and ε), Okazaki fragment processing (DNA ligase 1, FEN1), nucleosome assembly (CAF), maintenance of DNA methylation (DNMT1-UHRF1) and establishment of sister chromatid cohesion (Esco2). The comprehensive identification of known fork components by NCC describes the isolation of replicated chromatin in combination with quantitative mass spectrometry at two distinct maturation states. Additionally, the analysis is based on a multi-classifier combinatorial proteomics approach that was used to predict functional significance of associated proteins named Index of chromatin probability (ICP) (Kustatscher et al., 2014).
Alternative methods that have also been applied to label and isolate nascent chromatin – albeit with a lower number of identified proteins – are called the iPOND technique and Dm-ChP. Both techniques are based on the use of ethynyl deoxyuridine (EdU) as a thymidine analogue, which can be modified with biotin using copper based “click-chemistry” (Dungrawala et al., 2015; Kliszak et al., 2011; Sirbu et al., 2012; Sirbu et al., 2013). As EdU is cell permeable, it can be used to label newly replicating chromatin in living cells and does not require prior cell permeabilization.
Above described *in vitro* as well as *in vivo* chromatin assembly techniques revealed the presence of proteasomal proteins. In addition, the combination of mass spectrometry with chromatin assembly techniques could show, that all subunits of the proteasome were identified during chromatin assembly and replication consistently between different techniques and among several biological replicates (Alabert et al., 2014; Moreno et al., 2014; Sirbu et al., 2013).

1. 5. Proteasome

1. 5. 1. The proteasome as a protein regulator

The 26S proteasome is a key player in eukaryotic protein quality control and in the regulation of numerous cellular processes in the cytoplasm as well as in the nucleus (Brooks et al., 2000; Peters et al., 1994). It is part of the ubiquitin proteasome system (UPS) and catalyses the processive degradation of proteins marked for destruction by the attachment of polyubiquitin chains (Finley, 2009). The system relies on the concerted actions of three enzymes. In the first step, a ubiquitin-activating enzyme (known as E1) hydrolyses ATP and adenylates a ubiquitin molecule. The activated ubiquitin molecule is attached to the cysteine residue of the active site of the respective E1. Secondly this ubiquitin molecule is transferred to a ubiquitin-conjugating enzyme (E2). And finally, a ubiquitin ligase (E3) recognizes a protein for degradation and catalyses the transfer of ubiquitin from the E2 enzyme to the target protein (Figure 1. 4.).

Figure 1. 4.: Enzymatic cascade of the Ubiquitin Proteasome System.

The concerted action of three enzymes (E1, E2, E3) leads to the attachment of ubiquitin to lysine residues on proteins. These substrates are either targeted for degradation by the proteasome or deubiquitylating enzymes reverse the reaction (Varshavsky, 2012).

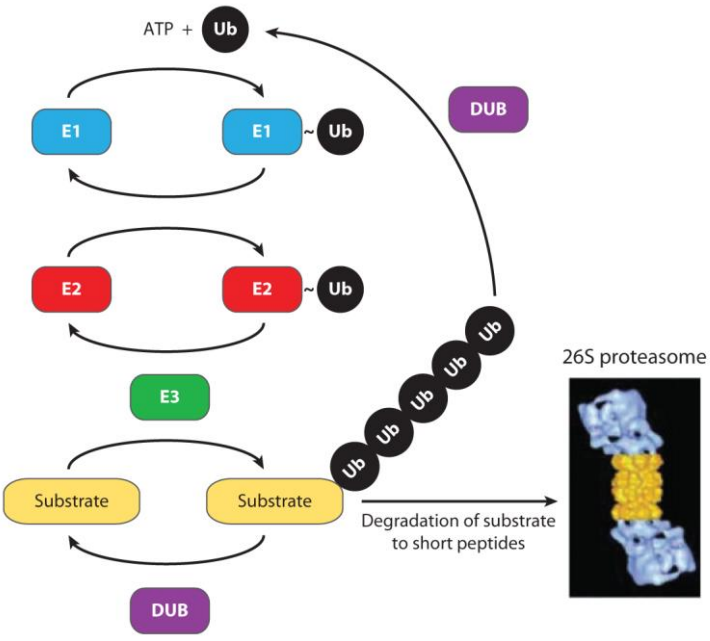

The human genome encodes for two E1 enzymes, more than 30 E2 enzymes and between 600 and 1000 E3 ligases (Deshaies and Joazeiro, 2009; van Wijk and Timmers, 2010). Therefore, this system acquires its specificity by the E3 ligases that recognize target proteins.

Once a target protein has been loaded with four ubiquitin monomers, the proteasome is able to recognize this protein. These chains are mainly recognized by the 19S proteasome “caps” that further process proteins for degradation into the 20S holoenzyme, in which proteolytic enzymes cleave proteins into peptides.

In many instances, ubiquitination is regulated by its removal through the actions of specific deubiquitylating enzymes (DUBs), some of which also play key roles in ubiquitin-precursor processing (Nishi et al., 2014). The combination of DUBs, ubiquitin ligases and the action of the proteasome regulates proteins and their concentrations within the cell cycle.

1. 5. 2. Proteasome in the nucleus

The nuclear function of the proteasome has been most prominently associated with transcriptional activation, as proteasomal subunits associate with transcriptionally active chromatin (Geng et al., 2012). At these sites the proteasome acts as a transcriptional modulator either by dislocating elongating complexes of RNA polymerase (Auld et al., 2006), by regulating transcription factor and cofactor levels when they are no longer required (Lafon et al., 2015; Lonard et al., 2000), by regulating their localization (Hoppe et al., 2000), the repression of cryptic transcription (Szutorisz et al., 2006) or by establishing an active histone modifications pattern at a promoter (Ezhkova and Tansey, 2004). In most cases the function seems to be dependent on the proteolytic activities but some data also suggest a non-proteolytic but more chaperone-like function of the proteasomal ATPases (Geng et al., 2012; Kaiser et al., 2000).

The connection of the UPS with DNA replication and chromatin maturation is somewhat less well-understood. Several findings suggest that the UPS has an impact on DNA replication and potentially chromatin maturation (Abbas et al., 2010; Centore et al., 2010; Saredi et al., 2016; Satheshkumar et al., 2009). For example, it has been shown that polyubiquitination plays a key role in disassembly of the replisome machinery (Maric et al., 2014; Moreno et al., 2014) suggesting a direct effect of the proteasome on replicating chromatin. These studies can be used as a starting point to further investigate the function of the proteasome during replication and chromatin assembly.

1. 6. Mass spectrometry

Mass spectrometry is a technique to determine the mass-to-charge ratio of ions to identify and quantify molecules in simple and complex mixtures. All mass spectrometers consist of an ion source, a mass analyser and an ion detector (Figure 1. 5.). These three parts vary between

different types of mass spectrometer according to the physical properties of the sample and the type of data acquired.

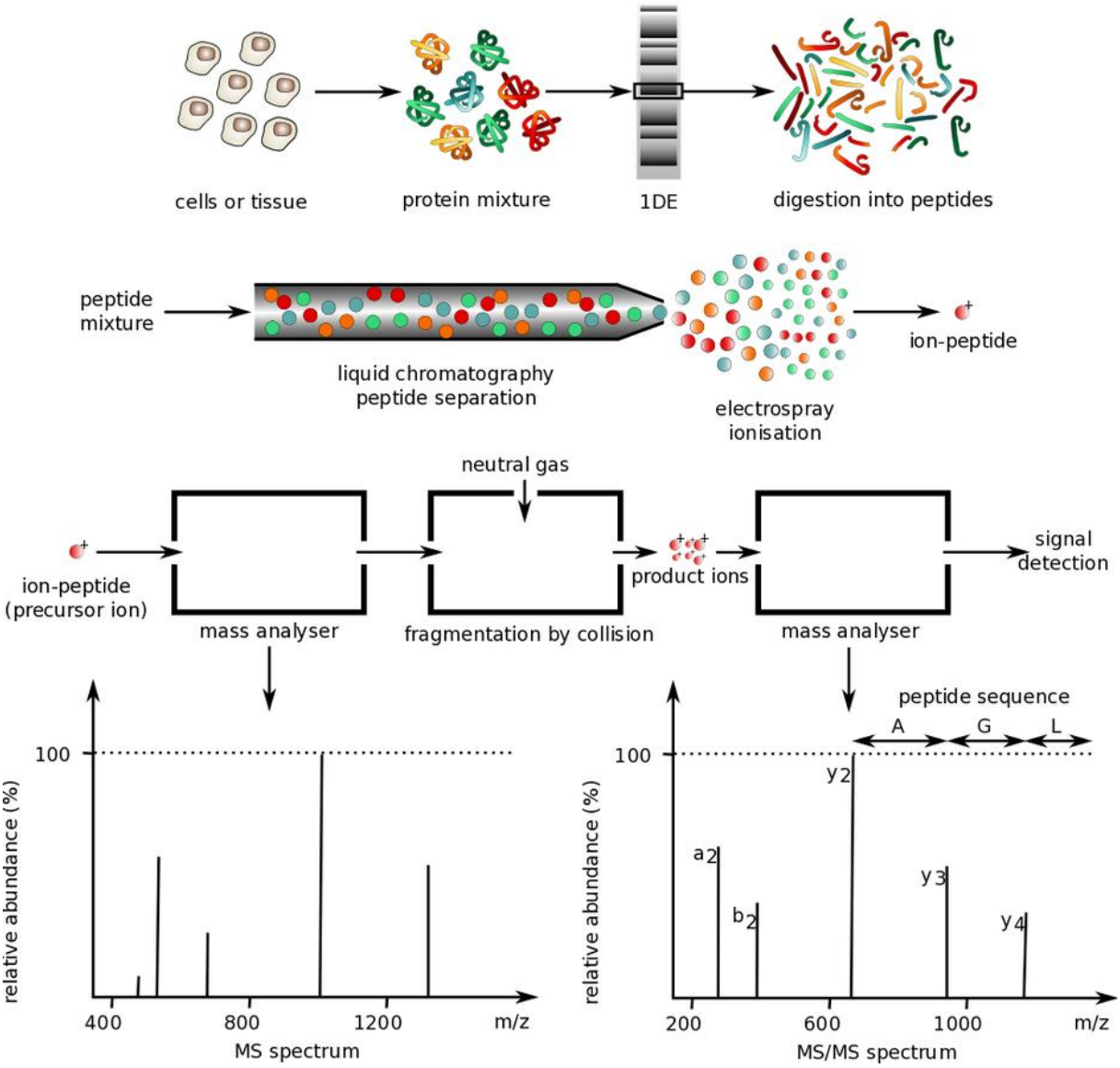

Figure 1. 5.: Workflow and analysis pathway in mass spectrometry.

Proteins are digested into peptides and separated over chromatographic devices. Then peptides are ionized and analysed by a mass spectrometer in the mass analyser (analysis of precursor ions in MS1) or after fragmentation in a second mass analyser (fragment ions in MS2). m/z: mass-to-charge ratio, y and a indicate the type of fragment ions (Hupe et al., 2012).

First, a sample is applied for MS analysis in liquid, gas or dried form and then vaporized and ionized within the ion source. The charged ions are accelerated by the mass analyser leading to paths of individual ions based on their mass and charge (m/z) (Figure 1. 5.). The acceleration of charged ions is mediated by an electric and/or magnetic field inside the mass analyser, which include most commonly time-of-flight (TOF), orbitraps, quadrupoles and ion traps with each having specific characteristics. In addition, mass analysers can be used to not only identify analytes in a sample but also to filter specific ions towards the detector.

Detectors within mass spectrometers are electron multipliers or microchannel plates. These devices emit a cascade of electrons once an ion has reached the detector. This amplification of signal leads to improved sensitivity of each measured event (Finehout and Lee, 2004).

1. 6. 1. Proteomics

Mass spectrometers have been heavily used in the last 15 years to perform proteomic studies. Proteomics describes the study of all proteins in a biological system at a given time point (Mallick and Kuster, 2010). The major fields of study have been the investigation of protein structure, function, folding and interaction (Aebersold and Mann, 2016). An emerging field in the past 10 years was the investigation of specific post-translational modifications throughout complex biological samples and to quantify proteins either in relative or absolute amounts (Alabert et al., 2015; Huang et al., 2015; Scharf et al., 2009). Finally, the field of proteomics developed further due to the improvements of sample preparation techniques for mass spectrometry.

An approach in which proteins are studied as intact entities by mass spectrometry is called “top-down” proteomics (Tran et al., 2011). In this way, the entire protein is analysed together meaning that modifications on the same molecule are measured in parallel in a comparable manner. However, alternative “bottom-up” proteomics has been developed and used much more extensively. In “bottom-up” proteomics, several techniques exist to prepare and analyse peptides derived from protein digestion. Each technique has a unique purpose and range of utility.

In “bottom-up” proteomics, proteins are extracted from the source material and digested by sequence specific enzymes as for example trypsin. This digestion leads to peptides of specific lengths that are applied to a mass spectrometer coupled to reverse-phase chromatography to separate peptides by their retention time. Once peptides elute at a specific point from a reverse-phase chromatography column, they enter the mass spectrometer as charged ions after electrospray ionization. In general, three main approaches to analyse peptides in a mass spectrometer are currently applied: Data-dependent acquisition proteomics (DDA), targeted proteomics and data-independent acquisition proteomics (DIA) (Figure 1. 6.).

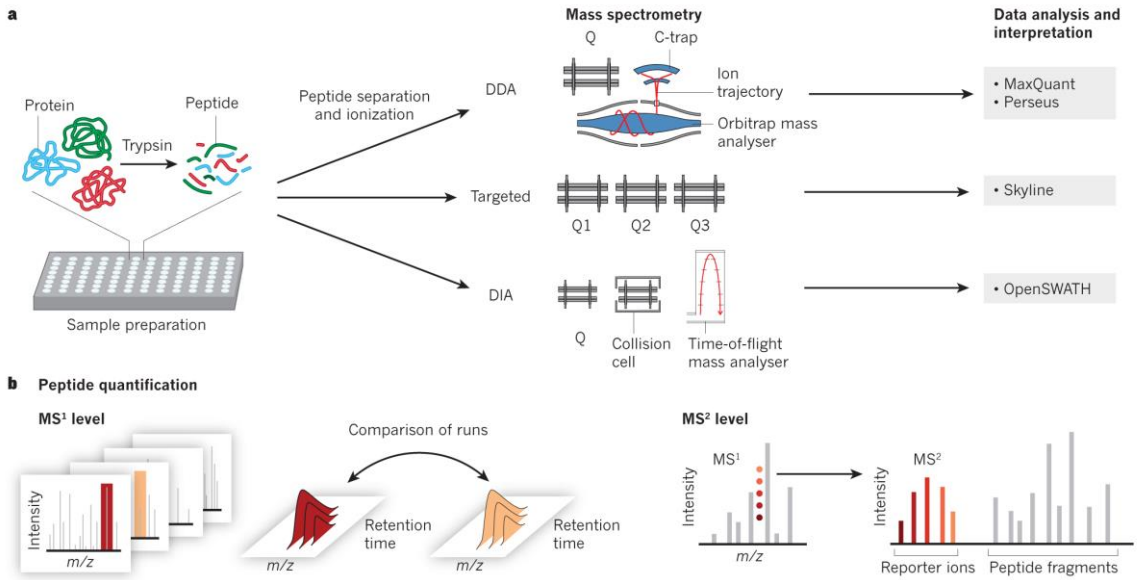

Figure 1. 6.: Bottom-up proteomics.

a: Proteins are digested with a sequence-specific enzyme into peptides to further analyse ionized peptides on a mass spectrometer in three different modes. Data-dependent acquisition collects a full spectrum of a peptide (MS1 level) and then acquires fragmentation peptide spectra of the most abundant precursor ions, here depicted with a quadrupole-orbitrap mass analyser. Widely used software is MaxQuant and Perseus. Targeted approaches use predefined information of a peptide to target a specific mass-to-charge ratio in the first quadrupole. Then the ion is fragmented and fragment ions are measured. This type of data is usually analysed with Skyline software. In data-independent acquisition, ranges of m/z values are selected and further fragmented and measured in time-of-flight mass analysers. The multiplexed data are aligned to spectral libraries using OpenSWATH or ProteinPilot.
b: Peptide quantification can be determined at the MS1 level by integrating the signal from peaks of the precursor ion. Peaks can be compared between runs. For MS2 quantification, intensities of unique fragment ions for a specific peptide are used (Aebersold and Mann, 2016).

1. 6. 1. 1. Shotgun/Data-dependent acquisition proteomics

Shotgun proteomics by means of DDA based methods have the purpose to achieve an unbiased and complete coverage of the proteome. Once the charged ions enter the mass spectrometer, the mass spectra of all ions species at the given time point (precursor ions) are recorded in the full scan modus (MS1 level). Simultaneously, the machine switches to the fragmentation modus to fragment as many of the acquired precursor ions into fragment ions. In typical “top N cycles” (N denotes the number of MS2 spectra that follow) an MS1 scan is followed by ca. 10-20 MS2 spectra.

1. 6. 1. 2. Targeted Proteomics

By definition, targeted proteomics uses prior information about specific proteins of interest to acquire mass spectra (Figure 1.5). In the setup of a triple quadrupole instrument, the first quadrupole filters for the expected precursor ion m/z ratio. In this step, the mass spectrum of the precursor ion can be measured. The second quadrupole functions as collision chamber to induce peptide fragmentation (dissociation). Finally, the third quadrupole functions as additional filter for expected fragment ion m/z ratios of the formerly selected precursor ion.

This can be even improved by multiplexing several fragment ions per peptide to increase selectivity better known as multiple reaction monitoring (MRM) (Picotti and Aebersold, 2012). Currently, Orbitrap instruments utilize the entire MS2 spectrum to record mass spectra, which is called parallel reaction monitoring (PRM) (Peterson et al., 2012).

1. 6. 1. 3. SWATH-MS/Data-independent acquisition proteomics

In data-independent data acquisition methods or SWATH standing for "Sequential window acquisition of all theoretical fragment ion spectra", entire ranges of precursor ions are fragmented at the same time (Gillet et al., 2012). To cover the full mass range between m/z 400-1250, the mass spectrometer sequentially acquires one full MS spectrum and about 40 CID-MS/MS spectra with isolation windows of m/z 25 during one cycle of roughly 3.5 s. This leads to a total fragmentation of all precursor ions detectable throughout the entire mass range and along the chromatographic elution period. The data analysis of these data is challenging since the resulting fragment ion spectra are highly multiplexed meaning that a fragment ion spectrum is difficult to relate to a specific precursor ion spectrum. Therefore, the information of peptide fragmentation is either gained by targeted signal extraction on the basis of previously acquired single-peptide fragmentation spectra (Peterson et al., 2012) or by the generation of "pseudo" fragment ion spectra constructed directly from the DIA data that are then subjected to classic database searching.

1. 7. Aims of the thesis

Chromatin assembly following DNA replication, DNA repair and gene transcription is critical for the maintenance of the genome and the epigenetic information.

Many of the individual factors involved in this assembly process have been characterized in detail with regards to their structure and function (De Koning et al., 2007; Hamiche and Shuaib, 2012; Hammond et al., 2017). It is well-appreciated that chromatin assembly is a highly regulated multi-step process involving synthesis, storage and nuclear transport of histones followed by their deposition onto DNA.

Despite its biological importance, the coordination of the individual steps and their dynamic properties are insufficiently described. This is mainly because it is difficult to fully describe and dissect the entire system *in vivo* making a functional analysis and a defined disturbance of the system almost impossible.

Therefore, this thesis was aimed to describe

- the order of chromatin assembly steps,
- the molecular mechanisms that coordinate the required cellular machinery in time
- the quality control of this assembly

To address these questions, our lab uses an *in vitro* system that resembles the formation of chromatin on double-stranded DNA (Becker and Wu, 1992). The biotinylated DNA is captured by magnetic beads upon various times of incubation with embryonic extracts prepared from preblastoderm *Drosophila melanogaster* embryos.
For the time-resolved quantitation of chromatin-bound proteins, the label-free quantitative SWATH-MS technology is used, which allows to precisely describe distinct aspects of chromatin assembly such as the appearance and disappearance of histone PTMs, the levels of histone chaperones, the activity of histone writers/erasers or the concentration of distinct DNA binding factors (Gillet et al., 2012). Another aim of this thesis was the addition of further time points of acquisition during *in vitro* chromatin assembly to increase resolution of protein binding kinetics.
In addition to this *in vitro* system combined with the SWATH-MS technique, NCC experiments in HeLa cells were performed to monitor chromatin assembly kinetics in an *in vivo* setup. The two datasets allowed a comparison between *in vitro* and *in vivo* systems and a verification of selected predictions based on *in vitro* assembly results and vice versa.

2. MATERIALS & METHODS

2. 1. Materials

Plasmids

Plasmid	Insert	Application	Remark
pBluescript (SK (-))	Empty vector	Bacterial expression	Provided by Philipp Korber
pAI61 (pBS SK (-))	13 repeats of the 5S rRNA gene of *L. variegatus*	Bacterial expression	(Eskeland et al., 2007)
4x 359 bp (pBS SK (-))	Containing 4 repeats of 359 repeats from D. melanogaster	Bacterial expression	(Völker-Albert et al., 2016)

Oligonucleotides

All oligonucleotides were ordered from Eurofins MWG Operon and designed manually or with the aid of different programs such as SnapGene, SerialCloner and CLC Workbench.

Name	Sequence (5'-3')	Restriction site added	Application/ Cloning method
M13 uni (-21)	TGTAAAACGACGGCCAGT	-	Sequencing of pBSK (-)
M13 rev (-29)	CAGGAAACAGCTATGACC	-	Sequencing of pBSK (-)
359 bp repeat for 51 0	CGGTCATCAAATCATTTATTTTGC	-	Amplification of 359 bp repeat unit from genomic DNA
359 bp repeat rev 51 9	CGAAATTTGGAAAAACAGACTCTG	-	Amplification of 359 bp repeat unit from genomic DNA
Gibson A FW	CCCCCCTCGAGGGTCGACGGTCATCAAATAATCATTTATTTTGC	SalI	Generation of 359 bp repeat fragments for multimerization via Gibson Cloning
Gibson D RV	GGAATTCGATATCAAGCTTGAAATTTGGAAAAACAGACTCTGC	HindIII	Generation of 359 bp repeat fragments for multimerization via Gibson Cloning
Gibson B FW	GACTACGAATTCATTGGGGGGTCATCAAATAATCATTTATTTTGC	EcoRI	Generation of 359 bp repeat fragments for multimerization via Gibson Cloning
Gibson B RV	CCCCAATGAATTCGTAGTCGAAATTTGGAAAAACAGACTCTGC	EcoRI	Generation of 359 bp repeat fragments for multimerization via Gibson Cloning
Gibson C FW	GATCATACTAGTGGCTAGGCGGTCATCAAATAATCATTTATTTTGC	SpeI	Generation of 359 bp repeat fragments for multimerization via Gibson Cloning

Gibson C RV	GCCTAGCCACTAG TATGATCGAAATT TGGAAAAACAGA CTCTGC	SpeI	Generation of 359 bp repeat fragments for multimerization via Gibson Cloning
FW359Seq	GGGATTTTGCCGA TTTCGGCC	-	Sequencing of pBSK (-)
RV359Seq	GCGAGGAAGCGG AAGAGCGC	-	Sequencing of pBSK (-)
359cc2HindIIIFW	CCCTCGAGAAGCT TCGGTCATCAAAT AATC	HindIII	Generation of 359 bp repeat fragments for multimerization via restriction cloning
359cc2EcoIRV	CGATATCGAATTC GAAATTTGGAAAA ACAGAC	EcoRI	Generation of 359 bp repeat fragments for multimerization via restriction cloning

Antibiotics

Name	Concentration of stock solution	Working concentration
Ampicillin	100mg/ml (1000x) in H_20	100µg/ml

Antibodies

Primary antibodies

Name	Supplier	Dilution
α PCNA	Abcam (ab29)	Western Blotting 1:1000 IF 1:500
α H3	Abcam (ab1791)	Western blotting 1:5000
α H4K5ac	Abcam (ab51997)	Western blotting 1:1000
α Acf1	In-house generated (Jain et al., 2015)	Western blotting 1:5

All dilutions in 1-5% BSA or 1-5% milk in PBS.

Secondary antibodies

Type	Supplier	Dilution
ECL antibodies	VWR	1:10000
Immunofluorescence antibodies	Jackson Immuno Research	1:500

All dilutions in 0.1% PBS-Tween.

Staining solutions

Type	Supplier	Dilution
Streptavidin Alexa Fluor 555 Conjugate	ThermoFisher Scientific (S32355)	IF 1:400
DAPI	Sigma (D-9542)	IF 1:500

All dilutions in 0.1% PBS-Tween /5% BSA.

Protease inhibitors and reducing agents

Name	Stock concentration	Dilution
Aprotinin	1 mg/ml in H_20	All 1:1000
Leupeptin	1 mg/ml in H_20	
Pepstatin	0.7 mg/ml in Ethanol	
PMSF	0.2 M in Isopropanol	
DTT	1 M in 10 mM sodium acetate pH 5.2	

Proteasome-, HDAC- and cell cycle- modulators

Name	Function	Stock concentration	Dilution
N-ethylmaleimide (NEM)	Irreversible inhibitor of deubiquitinases	100 mM in Ethanol	1:20
MG132	Blocking the proteolytic activity of the 26S proteasome	4 mM in DMSO	1:400
Trichostatin A (TSA)	Inhibition of Histone Deacetylases (HDACs) groups I, II and IV	1 mg/ml	1:66
Thymidine	Synchronization of cells in G1/early S-phase	20 mM in DMEM without pen/strep and FBS	1:10
2-Deoxycytidine hydrochloride	Release from G1/early S-phase block for cell cycle progression	24 mM in DMEM with pen/strep and FBS	1:1000

2. 2. Methods

2. 2. 1. Microbiology Methods

Plasmid transformation of *E.coli* bacteria

A maximum of 5 µl of plasmid DNA was added to 100 µl chemically competent cells which were thawn on ice. After 20 min incubation, the cell suspension was heat-shocked for 90 s at 42 °C in a water bath followed by incubation on ice for 2 min. All used plasmids carried an ampicillin resistance gene for selection. 900 µl of liquid Luria-Bertani (LB)-medium were added and the cells were incubated for 1 h in a shaking incubator at 37 °C at 750 rpm. Cells were then centrifuged for 3-5 min at 800 g, the supernatant was taken off leaving 100 µl for resuspension. 100 µl of the bacteria were plated on LB-Amp agar plates (ampicillin 100 µg/ml) and incubated o/n at 37 °C. (Method adapted from "plasmid transformation of *E.coli* bacteria" from PhD thesis, Miriam Pusch, 2013, page: 39).

Luria-Bertani medium

1.0% (w/v) Bacto-Tryptone
1.0% (w/v) NaCl
0.5% (w/v) Bacto-Yeast extract

Growing of bacteria and DNA extraction and purification of plasmid DNA

Single grown colonies were picked and inoculated into 5 ml liquid LB-medium containing the appropriate antibiotics. The cells were incubated o/n in a shaking incubator (Infors Multitron) at 37 °C, 140 rpm for DNA minipreparation. For DNA maxipreparation, 5 ml of grown bacteria in liquid LB-medium were transferred into 500 ml liquid LB-medium with antibiotics for incubation o/n in a shaking incubator at 37 °C, 140 rpm. The subsequent isolation of plasmid DNA was done using Qiagen Plasmid Kits/Macherey-Nagel Kits according to manufacturer's instructions.

2. 2. 2. Nucleic Acid Methods

Storage of DNA

DNA obtained from isolations and purifications was reconstituted in ddH_2O or 1x TE buffer and stored at -20 °C.

TE buffer

10 mM Tris pH 8.0
1 mM EDTA

DNA quantification

DNA concentration was quantified by measuring the absorbance at the wavelength of 260 nm using a NanoDrop ND-1000 UV spectrophotometer (Peqlab) or a DeNovix DS 11+ spectrophotometer (Biozym). Blank measurements were taken with the respective buffers the DNA was reconstituted in (see above).

Agarose gel electrophoresis

Agarose gel electrophoresis was performed to separate and distinguish DNA fragments obtained from restriction digests, MNase digestions, supercoiling assays or PCR reactions.
DNA fragments migrate with different behaviour according to size and conformation inside an agarose gel. Therefore, the percentage of agarose inside the gel needs to be adapted to the DNA fragments loaded onto the gel. The smaller the fragments for analysis, the higher the percentage of agarose was chosen. Agarose was weighed and dissolved in the appropriate volume of 1x TBE (90 mM Tris, 90 mM Boric acid, 2 mM EDTA) by boiling in the microwave until the solution was completely clear and no small floating particles were visible.
DNA samples were mixed with 5x loading dye (0.3% (w/v) Orange G, 5 mM EDTA, 50% (v/v) Glycerol) prior to loading onto the gel. To distinguish different fragment lengths, DNA ladders (1 kb, 100 bp, New England Biolabs (NEB)) were used as size standard. Electrophoresis was performed at 50-150 V as determined by the distance of the gel chamber electrodes (4-10 V/cm). Staining of DNA was either carried out by adding ethidium bromide to a final concentration of 1 µg/µl prior to pouring the solution into the gel tray or by staining the gel in ethidium bromide solution (1 µg/ml in TBE) after staining for 30 min followed by 15 min destaining in 1x TBE. Alternatively, DNA was stained with Midori Green Direct (Nippon Genetics) by mixing the DNA samples and DNA ladders with Midori Green Direct at 1:10 (dye:sample) dilution rate. Gels were analysed by radiation with UV light (254-366 nm) and documented by means of a Chemidoc Imaging Touch system (Biorad).
(Method adapted from “Agarose gel electrophoresis” from PhD thesis, Miriam Pusch, 2013, page: 35).

TBE buffer	**Orange G**
90 mM Tris	0.3% (w/v) Orange G
90 mM Boric acid	5 mM EDTA
2 mM EDTA	50% (v/v) glycerol

Restriction Digest

Buffer conditions and temperatures for restriction digests were used according to the manufacturer's instructions. Units of enzymes were calculated according to their unit definition. All restriction endonucleases were purchased from NEB. The reaction products were analysed by agarose gel electrophoresis.

DNA precipitation

In all cases, DNA was precipitated by a final concentration of 1 M NH_4SO_4 and adding 1.5 volumes of 100% ethanol. DNA containing samples were filled up with TE buffer and glycogen. After 2 hrs of incubation at -20 °C, samples were centrifuged at full speed for 1 h at 4 °C. Samples were washed with 70% ethanol and centrifuged for 30 min at 4 °C. Small leftover ethanol droplets were removed by a vacuum-device. Precipitated DNA was resuspended in TE buffer.

Polymerase chain reaction (PCR)

The Polymerase chain reaction was used to amplify DNA sequences or to modify inserts for cloning by adding overlapping sequences and restriction sites. PCR reactions were performed either with a Taq-polymerase or with the Phusion High Fidelity DNA polymerase. The Phusion Polymerase has in contrast to a Taq-polymerase a proof reading function and is therefore suited for longer sequences that have been used for further cloning steps. The following PCR conditions for respective enzymes were applied:

Table 2. 1.: Pipetting scheme protocol for standard PCR with Taq DNA polymerase.

Reaction component	Volume	Final concentration
10x standard Taq reaction buffer	5 µl	1x
dNTPs 10 mM	1 µl	200 µM
Forward primer 10 µM	2.5 µl	0.5 µM
Reverse primer 10 µM	2.5 µl	0.5 µM
DNA template	variable	<1000 ng
Taq DNA polymerase	0.25-0.5 µl	1.25-2.5 U
Nuclease free water	to 50 µl	-

Table. 2. 2.: Program for PCR with Taq DNA polymerase.

PCR step	Number of cycles	Temperature	Duration
Initial denaturation	1	95 °C	5 min
Denaturation	25-30	95 °C	30 s
Annealing		45-65 °C	30 s
Elongation		72 °C	1 kb/min
Final elongation	1	72 °C	5-10 min

Table 2. 3.: Pipetting scheme protocol for PCR with Phusion® High-Fidelity DNA polymerase.

Reaction component	Volume	Final concentration
5x Phusion HF or GC buffer	10 µl	1x
dNTPs 10 mM	1 µl	200 µM
Forward primer 10 µM	2.5 µl	0.5 µM
Reverse primer 10 µM	2.5 µl	0.5 µM
DNA template	variable	<250 ng
Phusion® DNA polymerase	0.5 µl	1.0 U
Nuclease free water	to 50 µl	-

Table 2. 4.: Program for PCR with Phusion® High-Fidelity DNA polymerase.

PCR step	Number of cycles	Temperature	Duration
Initial denaturation	1	98 °C	30 s
Denaturation	25-30	98 °C	10 s
Annealing		56-64 °C	30 s
Elongation		72 °C	4 kb/min
Final elongation	1	72 °C	5-10 min

Amplified fragments were analysed by agarose gel electrophoresis. Bands of interest for ligations were cut out of the gel and purified using a gel extraction kit (Qiagen) and sent to MWG for sequencing.

Plasmid construction and cloning

Vectors containing 359 bp repeats were generated by Gibson cloning, In-Fusion cloning and conventional restriction cloning.

Gibson cloning and In-Fusion cloning are based on homolog fragment ends and a single-tube enzymatic reaction. The difference is in the composition of the enzyme mix.

Gibson cloning relies on the single-tube isothermal assembly reaction featuring three different enzymatic activities that perform in the same buffer (Gibson et al., 2010; Gibson et al., 2009):

The exonuclease creates single-stranded 3´ overhangs that facilitate the annealing of fragments that share complementarity at one end (overlap region).

The proprietary DNA polymerase fills in gaps within each annealed fragment. The DNA ligase seals nicks in the assembled DNA.

In-Fusion cloning depends on the In-Fusion enzyme, which fuses DNA fragments e.g. PCR-generated sequences and linearized vectors, efficiently and precisely by recognizing a 15 bp overlap at their ends. This 15 bp overlap can be engineered by designing primers for amplification of the desired sequences.

For Gibson and In-Fusion cloning, primers were designed to amplify DNA fragments that have overlapping sequences of 15 bp length. These overlaps were utilised for cloning of the 359 bp repeat units into a pBluescript SK (-) vector and for additional multimerization of the repeat units. Overlapping sequences of one insert were complementary to the neighbouring insert and were thus inserted into the linearized backbone vector as arrays. Molar ratios were calculated by the length of vector and inserts and were chosen 1:1 or adjusted up to 1:3 depending on the number of fragments that were intended for insertion.

For Gibson cloning, 10 µl of self-prepared Gibson reagent mix (final concentration: 1.33x Gibson assembly buffer, 0.005 U/µl T5 exonuclease, 0.033 U/µl Phusion polymerase, 5.333 U/µl Taq ligase) was added to the DNA inserts and vector followed by 1 h incubation at 50 °C.

For In-Fusion cloning, 5x In-Fusion enzyme premix (Clontech) was applied in a 1:5 ratio to vector and inserts (total reaction volume: 5 µl) and incubated for 15 min at 50 °C.

In case of conventional restriction cloning, insertion fragments of interest were digested with same enzymes that have been used to open the vector to generate compatible ends. For ligation, T4 ligase buffer (NEB) and T4 ligase (NEB) was added in a ratio of 1:10 and 1:20 respectively to vector and inserts (total reaction volume: 20 µl) on ice and incubated for cohesive ends 10 min at room temperature. After heat inactivation for 10 min at 65 °C, 1-5 µl of the reaction were transformed to competent cells.

2. 2. 3. Tissue Culture Methods

Cultivation and passaging of cells

HeLa S3-spinner cells were cultivated in Dulbecco's Modified Eagle Medium (DMEM) supplemented with 10% FCS, 1x Pen/strep at 37 °C with 5% CO^2 and were maintained by diluting the culture every 24 hrs to 0.7x 10^5 cells/ml. Cells were grown in spinner flasks (Wheaton) with a stirring application (Thermo Scientific) for keeping the cells in suspension with 40 rotations/min.

Cryopreservation of cells

50 ml of cells with a concentration of 1x 10^6 cells/ml were collected and centrifuged at 300 g for 5 min. Cells were then resuspended in 10 ml freezing medium. 1 ml aliquots were frozen in cryovials stored in a freezing container (Fisher Scientific) with a cooling rate of 1 °C/min at -80 °C. The next day, cells were transferred to the -180 °C liquid nitrogen freezer.
Cells of 1 cryovial were thawn on ice and resuspended in fresh medium and sown in a 10-cm petri dish without surface treatment to prevent cell adhesion. After 3 hrs incubation, cells were centrifuged at 300 g for 5 min and resuspended in 15 ml fresh DMEM. To expand cells, every 24 hrs cells were splitted by half (7.5 ml to new 10 cm petri dish and all dishes were filled up to 15 ml again) until 32 dishes have been reached. All cells were collected and centrifuged at 300 g for 5 min and transferred to a spinner flask pre-cleaned with 1x PBS. Cells were transferred into half "fresh" DMEM and half "old" DMEM.
Freezing medium: 10% DMSO/FCS.

1x PBS

136 mM NaCl
2.7 mM KCl
4 mM Na_2HPO_4

Nascent Chromatin Capture

Synchronization of cells

1x10^6 HeLa S3 cells/ml were blocked for 17 hrs with a single thymidine block (2 mM thymidine in DMEM) in a total volume of 300 ml. A 1 ml fluorescence activated cell sorting **(**FACS) sample was taken from the culture and centrifuged for 5 min at 300 g. Cells for the FACS sample were dissolved in 1 ml PBS and vortexed while adding 2.7 ml ice-cold 100% ethanol.

Each FACS sample was stored at 4 °C until further processing. Next day, HeLa S3 cells growing in suspension were released from a single thymidine block for 3 hrs by washing the cells twice with PBS and resuspending in DMEM containing 24 µM deoxycytidine. Additional FACS samples before and after the release have been taken and processed as described above.

Biotin-dUTP labelling

For biotin-dUTP labelling, cells were centrifuged at 300 g for 6 min and washed with KBH buffer (50 mM KCl and 10 mM Hepes). Then cells were again centrifuged at 300 g for 6 min and incubated for 5 min in a hypotonic KBH buffer containing biotin-dUTP (10 nM biotin-dUTP, 10 mM Tris pH 8) (IBA technologies) and resuspended in fresh cell culture medium. For immunofluorescence labelling, 30 µl of cell suspension before and after biotin-dUTP labelling have been added to 500 µl PBS and stored on ice until further processing.

Fixation and nuclear extraction

NCC cells were fixed in 2% formaldehyde at RT on a shaker at 36 rpm after 15 min (nascent chromatin), or chased for 1 h or 4 hrs in fresh medium before fixation (medium/mature chromatin). Each time point, FACS samples and IF samples have been collected and processed as described above. Crosslinking was stopped after 15 min by adding glycine to a final concentration of 1% and incubating for 5 min at room temperature on a shaker at 36 rpm.
Cells were centrifuged for 10 min at 1000 g at 4 °C. From now on, all steps have been performed on ice/4 °C. The cell pellet was washed twice with cold PBS-PMSF (1 mM PMSF in 1x PBS). Next, cells were resuspended in ice-cold sucrose buffer (0.3 M sucrose, 10 mM Hepes-NaOH at pH 7.9, 1% Triton X-100 and 2 mM MgOAc) and centrifuged for 10 min at 1000 g. The cells were resuspended in sucrose buffer and nuclei were mechanically isolated by using a 15 ml dounce homogenizer with a ‘tight’ pestle. Dounced material was centrifuged for 10 min at 2500 g and cytoplasmic supernatant was discarded. The nuclear pellet was resuspended in ice-cold glycerol buffer (25% glycerol, 10 mM Hepes-NaOH at pH 7.9, 0.1 mM EDTA, 0.1 mM EGTA, 5 mM MgOAc) centrifuged for 10 min at 2500 g and then resuspended in one volume ice-cold glycerol buffer and snap-frozen in liquid nitrogen and stored at -80 °C until further use.

Preparation of chromatin

Chromatin was solubilized by sonication in a Diagenode Bioruptor at 4 °C in sonication buffer (10 mM Hepes-NaOH at pH 7.9, 100 mM NaCl, 2 mM EDTA at pH 8, 1 mM EGTA at pH 8, 0.2% SDS, 0.1% sodium sarkosyl and 1 mM phenylmethylsulphonylfluoride; Bioruptor setting: High, 28 cycles of 30 s sonication and 90 sec pause). Sonicated chromatin was centrifuged for 15 min at 5000 g at 4 °C.

Affinity purification of biotin-tagged chromatin

Solubilized chromatin was diluted 1:1 with dilution buffer (10 mM Hepes-NaOH at pH 7.9, 100 mM NaCl, 2 mM EDTA pH 8, 1 mM EGTA pH 8, 1 mM PMSF) to reduce SDS concentration. Biotinylated chromatin fragments were purified on streptavidin-coated magnetic beads (M280 Streptavidin beads; 50 µl beads per 100x 10^6cells) by two overnight end-over-end rotations at 4 °C and 5 stringent washes (10 mM Hepes-NaOH at pH 7.9, 100 mM NaCl, 2 mM EDTA at pH 8, 1 mM EGTA at pH 8, 0.1% SDS, and 1 mM phenylmethylsulphonyl-fluoride). Input material for Western blot or MS analysis was taken before addition of beads to chromatin. To release chromatin and reverse the crosslink, beads were boiled in 4x Laemmli sample buffer for 40 min at 100 °C, including a brief vortex and short spin every 10 min to prevent drying.

KBH buffer	**PBS-PMSF**	**Sucrose buffer**	**Glycerol buffer**
50 mM KCl	1 mM PMSF	0.3 M Sucrose	25% Glycerol
10 mM Hepes		10 mM Hepes-NaOH pH 7.9	10 mM Hepes-NaOH pH 7.9
		1% Triton X-100	0.1 mM EDTA pH 8
		2 mM MgoAc	0.1 mM EGTA pH 8
			5 mM MgOAc

Sonication buffer	**Dilution buffer**	**Wash buffer**
100 mM NaCl	100 mM NaCl	100 mM NaCl
10 mM Hepes-NaOH pH 7.9	10 mM Hepes-NaOH pH 7.9	10 mM Hepes-NaOH pH 7.9
2 mM EDTA pH 8	2 mM EDTA pH 8	2 mM EDTA pH 8
1 mM EGTA pH 8	1 mM EGTA pH 8	1 mM EGTA pH 8
0.2% SDS	1 mM PMSF	0.1% SDS
0.1% Sodium sarkosyl		1 mM PMSF
1 mM PMSF		

Fluorescence activated cell sorting

FACS samples from NCC experiments were kept at 4 °C up to one week and then diluted with 10 ml PBS containing 1% FBS. Cells were centrifuged for 4 min at 300g at 4 °C. Then the supernatant has been removed and the cell pellet was dissolved in 1 ml PBS containing 10 µg/ml propidium iodide (Sigma) and 20 µg/ml RNAse. The samples were mixed and transferred to a FACS tube using a filter to avoid cell aggregates to be measured by the FACS machine.

Samples were measured on the FACSCanto device. Cell appearance was measured with forward and side scatter (FSC/SSC) indicating cell size and granularity, respectively. Propidium iodide was measured in the PE channel. Per condition, 100.000 cell events were measured.

2. 2. 4. Protein Methods

SDS-Polyacrylamide-Gel electrophoresis

The denaturing SDS-Polyacrylamide-Gel electrophoresis (SDS-PAGE) is a method to separate proteins in an electrical field according to their electrophoretic mobility (Laemmli, 1970). The proteins are denatured by heat (95 °C) and DTT and/or β-mercaptoethanol and are covered with the anionic detergent SDS. By binding to the hydrophobic group of a protein it adds negative charge. Therefore, the speed of migration is based on the size of the proteins according to their size. Proteins were separated by gradient gels containing acrylamide in the range of 4-20% (Serva). Protein samples were mixed with 4x Laemmli sample buffer and denatured for 5 min at 95 °C before loading onto the gel. Protein markers (peqGOLD Protein Marker IV and V, Peqlab) were used to estimate the molecular weight of the proteins. Electrophoresis was performed at 25 mA per gel until the protein running front reached the lower edge of the gel. Afterwards gels were stained with Coomassie, silver or subjected to Western blotting.

SDS running buffer	**4x Laemmli sample buffer**
25 mM Tris	200 mM Tris pH 6.8
190 mM glycine	8% /w/v) SDS
0.1% (w/v) SDS	40% (v/v) glycerol
	0.2% (w/v) bromphenol blue
	4.2% (v/v) β-mercaptoethanol

Coomassie Staining

The loading pockets of the gel were removed and the gel was washed once with distilled water. Then the gel was submersed with InstantBlue solution (Expedeon) to cover the gel (ca. 20 ml) for 30-60 min until bands became visible. Gels were documented with Chemidoc Imaging Touch system (Biorad).
For mass spectrometry analysis, proteins of interest were cut out with a clean scalpel and stored in 0.2 ml tubes filled with 100 µl of ddH_20 at 4 °C until further analysis.

Silver staining

Silver staining was performed as described by Blum et al. (Blum et al., 1987).

Western blotting

SDS-PAGE of protein samples was performed as described above. The gel from SDS-PAGE was removed from the gel chamber and a PVDF membrane was prepared by incubation in methanol for 15 s using the BioRad "Wet Blot system", the gel was placed onto the membrane and sandwiched between gel-sized Whatman papers soaked in Western blot buffer in the following order starting at the negative power source:

Sponge
2 Whatman papers
SDS-gel
Nitrocellulose-membrane
2 Whatman papers
Sponge

The gel holder was inserted in the holder cassette and the gel transfer cell was filled with 1x Western Blot buffer and a cooling unit. The proteins were then transferred onto the membrane for 1 h (400 mA constant) in a cold room or o/n at 40 mA at 4 °C.
After the transfer, the PVDF membrane was adjusted to the size of the gel by cutting the overlapping end of the membrane. Then the membrane was blocked for 30 min at RT on a shaker with blocking solution 5% (w/v) milk in 1x PBS) in order to reduce the non-specific background. After blocking, the membrane was treated with an appropriate dilution of the primary antibody directed against the protein of interest in 5% TBS-T milk for 1hr at RT on a shaker. The membrane was washed three times (10 min each) with PBS/0.1% Tween and incubated for 45 min with horseradish peroxidase-coupled secondary antibody in 5% TBS-T milk. After three washes (5 min each with TBS-T) antigen-antibody complexes were detected

using the Amersham™ECL™Prime Western Blotting Detection Reagent Kit (GE Healthcare) according to the manufacturer's instructions (500 µl on each membrane).

1x PBS Tween	**Western blot buffer**
1x PBS	25 mM Tris
0.1% (v/v) Tween 20	192 mM glycine
	0.02% (w/v) SDS
	15% (v/v) methanol

2. 2. 5. Chromatin Methods

Preparation of Drosophila embryonic extract [DREX]

D*. melanogaster embryos were collected on agar trays with yeast paste 0-90 min after egg-laying. Using a brush and sieves with descending mesh size (0.71 mm, 0.355 mm, 0.125 mm), embryos were rinsed with cold tap water and allowed to settle into ice-cold embryo wash buffer to arrest further development. After five successive collections, the wash buffer was decanted and replaced with wash buffer at room temperature. For dechorionation of the embryos, the volume was adjusted to 200 ml and 60 ml of 13% hypochlorite solution was added. The embryos were stirred vigorously for 4 min on a magnetic stirrer, poured back into the collection sieve (0.125 mm), and rinsed with tap water for 5 min. Embryos were allowed to settle in 200 ml of wash buffer for about 3 min. Afterwards the supernatant containing the chorions was removed. Following two more settlings in 0.7% NaCl and in extract buffer at 4 °C, the embryos were settled in extract buffer in a 60-ml glass homogenizer on ice. The volume of the packed embryos was estimated before the supernatant was aspirated, leaving packed embryos and additional 2 ml buffer on top. Homogenization was performed with one stroke at 3,000 rpm and 10 strokes at 1,500 rpm with a pestle connected to a drill press. The homogenate was supplemented with $MgCl_2$ to a final $MgCl_2$ concentration of 5 mM. Nuclei were pelleted by centrifugation for 10 min at 10,000 rpm in a SS34 rotor. (Sorvall, Thermo-Fisher Scientific, Waltham, USA). The supernatant was centrifuged again for 2 hrs at 45.000 rpm in a chilled SW 56 rotor (Beckman-Coulter, Germany). The clear extract was isolated with a syringe, avoiding the top layer of lipids. Extract aliquots were frozen in liquid nitrogen. Protein concentration was determined by Nanodrop measurement and titration with chromatin assembly experiments.*

Embryo wash	**Extract buffer**
0.7% (w/v) NaCl	10 mM Hepes pH 7.6

0.05% (v/v) Triton X-100	10 mM KCl
	1.5 mM $MgCl_2$
	0.5 mM EGTA
	10% (v/v) glycerol
	1 mM DTT (add fresh)
	0.2 mM PSMF (add fresh)

Biotinylation of DNA

To obtain linearized and biotinylated DNA, plasmid DNA (pAI61; 4x 359 bp) containing oligomers of the sea urchin 5S rRNA positioning sequence was used. 500 µg plasmid DNA were linearized using the restriction enzyme SacI. Completion of the digest was analysed by agarose gel electrophoresis. Upon completion of the plasmid digestion, the restriction enzyme XbaI was added to the reaction and incubated for at least 3 hrs at 37 °C. Subsequently, the DNA was precipitated and purified, followed by incubation with 80 mM dCTP and dGTP, 3 mM biotinylated dUTP and dATP and the Klenow Polymerase. To purify DNA from excessive nucleotides and enzyme, G50 Sepharose columns (Roche) were used according to the manufacturers protocol. Finally, DNA concentration was measured and adjusted to 200 ng/ul.

Chromatin assembly on immobilized DNA

4 µg DNA was immobilized onto 120 µl M280 paramagnetic streptavidin beads (Invitrogen) in EX100 buffer (10 mM Hepes [pH 7.6], 100 mM NaCl, 1.5 mM MgCl2, 0.5 mM EGTA, 10 % [vol/vol] glycerol, 0.2 mM PMSF, 1 mM DTT) for 1 h. Beads were extensively washed and blocked with BSA for 30 min (1.75 g/l) in EX100. After another washing step in EX-NP40 (10 mM Hepes pH 7.6, 1.5 mM $MgCl_2$, 0.5 mM EGTA, 10 % (v/v) Glycerol, 0.05 % NP-40), 60 µl of DNA immobilized beads were resuspended in a total volume of 240 µl containing 45 µl DREX and an ATP regenerating system (3 mM ATP, 30 mM creatine phosphate, 10 µg creatine kinase/ml, 3 mM MgCl2, and 1 mM DTT) and EX100. To study the influence of protein acetylation, TSA was added to a final concentration of 50 µM as indicated. For proteasome inhibition experiments, the respective concentration of MG132 and NEM was added to the reaction. For time-resolved studies, the reaction was incubated at 26 °C for 15 min, 1 h and 4 hrs, respectively. After two stringent wash steps with EX200, beads were resuspended in elution buffer (EX100 with 0.5 U/µl MNase and 2 mM $CaCl_2$). The supernatant after 10 min of MNase-mediated elution was subjected to mass spectrometry based protein quantitation.

1 M Dynawash	2 M Dynawash	EX 100 (200)
10 mM Tris HCl pH 8	10 mM Tris HCl pH 8	10 mM Hepes pH 7.6
1 mM EDTA	1 mM EDTA	100 (200) mM NaCl
1 M NaCl	2 M NaCl	1.5 mM $MgCl_2$
		0.5 mM EGTA
		10% (v/v) glycerol
		1 mM DTT (add fresh)
		0.2 mM PSMF (add fresh)

EX-NP-40	McNap	Elution buffer
10 mM Hepes pH 7.6	3 mM ATP	In EX 100
1.5 mM $MgCl_2$	30 mM creatine phosphate	0.5 U/µl MNase
0.5 mM EGTA	10 µg creatine kinase/ml	2 mM $CaCl_2$
10% (v/v) glycerol	3 mM $MgCl_2$	
0.05% (v/v) NP-40	1 mM DTT	

Chromatin accessibility assay by Micrococcal nuclease digestion

Chromatin from 2 µg circular DNA assembled for 15 min, 1 h or 4 hrs at 26 °C was mixed with EX100 containing 5 mM $CaCl_2$ and 1 Becker unit/µl of MNase (Sigma). After incubation at room temperature for 30 s and 90 s, respectively, a 110 µl fraction of the digestion was stopped by adding 40 µl MNase stop solution (2.5 % N-Lauroylsarcosine, 100 mM EDTA pH 8.0). The suspension was subjected to RNase A and proteinase K treatment and precipitated DNA was separated with a 1.3 % agarose gel. A 100-bp ladder (Invitrogen) was used as a size marker.

Analysis of nucleosome assembly by supercoiling assay

Supercoiled plasmid (1 µg) was incubated under standard conditions at 26 °C with 2 mg Drosophila extract in the presence of 6.5 mM $MgCl_2$. After various times, 40 µl aliquots were removed from the reaction and assembly was stopped by the addition of 10 µl stop mix. The suspension was subjected to RNase A and proteinase K treatment and precipitated DNA was separated with a 1.3% agarose gel. A 100 bp ladder (Invitrogen) was used as a size marker.

2. 2. 6. Mass spectrometry methods

Preparation of MS samples for proteomics analysis

Assembled chromatin was subjected to mass spectrometry analysis. 10% of the chromatin-bound proteins were separated on a 4-20% gradient SDS-PAGE and analysed by silver staining (Blum et al.). 90% of the chromatin-bound proteins were subjected to MS sample preparation. Proteins were denatured in 3 M Urea, 1 M Thiourea and 25 mM DTT for 2 hrs at 20 °C followed by an incubation for 30 min in a dark place with a final concentration of 25 mM iodoacetamide at 20 °C to carbamidomethylate sulfhydryl groups of free cysteines. Subsequently, DTT was added to a final concentration of 50 mM and incubated for 30 min at 20 °C. The samples were diluted with 100 mM ammonium bicarbonate to lower the urea concentration below 1 M for tryptic cleavage with 200 ng of trypsin (Promega) in 50 mM ammonium bicarbonate. Digestion was completed after 14 hrs at 25 °C. 10% of the tryptic peptide mixture were acidified using trifluoroacetic acid (TFA) and desalted using C18 stage tips prior to mass spectrometry analyses and redissolved in 0.2% TFA (Rappsilber et al., 2007). The resulting liquid, containing the digested peptides, was dried and redissolved in 17 µl of 0.2% TFA and stored at –20 ºC until further processing.

Proteomic analysis via LC-MS/MS on Orbitrap mass spectrometer

The peptide mixture resulting from tryptic cleavage was injected onto an Ultimate 3000 HPLC system equipped with a C18 trapping column (C18 PepMap, 5 mm x 0.3 mm x 5 µm, 100 Å) and an analytical column (C18RP Reposil-Pur AQ, 120 mm x 0.075 mm x 2.4 µm, 120 Å, Dr. Maisch, Germany) packed into an ESI-emitter tip (New Objective, USA). First, the peptide mixture was desalted on the trapping column for 7 min at a flow rate of 25 ul/min (0.1% FA). For peptide separation a linear gradient from 5-40% B (HPLC solvents A: 0.1% FA, B: 80% ACN, 0.1% FA) was applied over a time of 120 min. The HPLC was online coupled to an LTQ Orbitrap XL mass spectrometer (Thermo-Fisher Scientific, USA).

The mass spectrometer was operated in DDA-mode employing a duty cycle of one survey scan in the orbitrap at 60,000 resolution followed by up to 6 tandem MS scans in the ion trap. Precursors were selected when they had a minimal intensity of 10,000 counts and a charge state of 2+ or higher. Previously analysed precursors were excluded for 20 seconds within a mass window of -1.5 to + 3.5 Da.

Proteomic analysis via LC-MS/MS on Q-TOF mass spectrometer

Samples were injected into an Ultimate 3000 HPLC system (Thermo Fisher Scientific). For nano-reversed-phase separation of tryptic peptide mixtures before MS analysis, peptides were desalted on a trapping column (5 x 0.3 mm inner diameter; packed with C18 PepMap100, 5 µm particle size, 100 Å pore diameter, Thermo-Fisher Scientific). The loading pump flow of 0.1% formic acid (FA) was set to 25 µl/minute with a washing time of 10 min under isocratic conditions. Samples were separated on an analytical column (150 x 0.075 mm inner diameter; packed with C18RP Reposil-Pur AQ, 2.4 µm particle size, 100 Å pore diameter, Dr. Maisch) using a linear gradient from 4% to 40% B in 170 min with a gradient flow of 270 nl/minute. Solvents for sample separation were A 0.1% FA in water and B: 80% ACN, 0.1% FA in water. The HPLC was directly coupled to the 6600 TripleTOF mass spectrometer using a nano-ESI source (both Sciex). A data-dependent method was selected for MS detection and fragmentation of eluting peptides comprising one survey scan for 225 ms from 300 to 1800 m/z and up to 40 tandem MS scans for putative precursors (100-1800 m/z). Precursors were selected according to their intensity. Previously fragmented precursors were excluded from reanalysis for 30 seconds.

SWATH data acquisition on Q-TOF mass spectrometer

Peptides from tryptic digestion were resuspended in 10 ul 0.1% TFA and injected into a Ultimate 3000 nano-chromatography system equipped with trapping column (C18 AcclaimPepMap, 5 x 0.2 mm, 5 µm 100 Å) and a separation column (C18RP Reposil-Pur AQ, 150 x 0.075 mm x 2.4 µm, 100 Å, Dr. Maisch, Germany) poured into a nano-ESI emitter tip (New Objective, Woburn MA). After washing for 10 min on the precolumn with 0.05% TFA, peptides were separated by a linear gradient from 4% to 40 % B (solvent A 0.1% FA in water, solvent B 80% ACN, 0.1% FA in water) for 150 min at a flow rate of 270 nl/min. Eluting peptides were detected on a 6600 Triple TOF quadrupol-TOF hybrid mass spectrometer (Sciex, Framingham, MA). First, a mixture of all conditions was run in data-dependent mode to generate an ion library for the data-independent SWATH measurements and optimize the isolation window distribution over the mass range for SWATH data acquisition. Data-dependent acquisition consisted of a survey scan and up to 40 tandem MS scans for precursors with charge 2-5 and more than 200 cps abundance. Rolling collision energy was set to generate peptide fragments. The overall cycle time for the DDA experiment was 2.676 seconds. Previously analysed precursors were excluded from repeated fragmentation for 30 seconds employing a mass window of 20 ppm around the precursor mass.

MS data with data-independent SWATH acquisition were generated using the same HPLC conditions as used for the generation of the ion library. Based on the distribution of the m/z values of identified peptides in the ion library, the mass range from 300-1200 m/z was split into 40 SWATH mass windows. First, precursors were monitored from 300-1500 m/z in a survey scan of 50 ms, followed by the SWATH data acquisition for 65 ms/mass windows, resulting in an overall cycle time of 2.7 seconds. The fragmentation energy was adjusted to fragment 2+ charged ions in the center of the mass window and a collision energy spread over 7 units was allowed.

Sample preparation for histone modification analysis by MS

Nuclear-enriched fractions were separated by SDS-PAGE, stained with Coomassie (Brilliant blue G-250) and protein bands in the molecular weight range of histones (15-23 kDa) were excised as single band. Gel slices were destained in 50% acetonitrile/ 50 nM ammonium bicarbonate. Lysine residues were chemically modified by propionylation for 30 min at RT with 2.5% propionic anhydride (Sigma) in ammonium bicarbonate, pH 7.5 to prevent tryptic cleavage. This step added a propionyl group only to unmodified and monomethylated lysines, whereas lysines with other side chain modification will not obtain an additional propionyl-group. A set of 30 precursors of heavy SILAC-R10 labelled standard peptides, (spiketides) coding for common histone modifications was added prior to tryptic digestion. Spiketide abundance was used to normalize for different sample amounts. Proteins were then digested with 200 ng of trypsin (Promega) in 50 mM ammonium bicarbonate overnight and the supernatant was desalted by carbon Top-Tips (Glygen) according to the manufacturer's instructions.

Histone modification analysis on LC-MS/MS on Q-TOF mass spectrometer

Following carbon stage tip, the dried peptides were resuspended in 5 µl of 0.1% TFA and the complete sample was directly injected onto the reversed-phase separation column (C18RP Reposil-Pur AQ, 120 x 0.075 mm x 2.4 µm, 100 Å, Dr. Maisch, Germany) of an Ultimate 3000 nano-chromatography system (Thermo-Fisher, San Jose, CA). A separation gradient from 5% B to 30% B (solvent A 0.1% FA in water, solvent B 80% ACN, 0.1% FA in water) over 32 min was applied to separate the histone peptides at a flow rate of 325 nl/min. Since the column was poured into the nano-ESI emitter tip, peptides were directly analysed by mass spectrometry using a TripleTOF 6600 quadrupol-TOF mass spectrometer (Sciex, Framingham, MA). A targeted MS/MS method was selected for detection and quantitation of N-terminal peptides of histone 3.1 and histone 4 with specific modifications. The first scan monitored the abundance

of the precursor ion for 225 ms, the MRM scans for individual modifications were acquired for 35 ms per precursor. The overall cycle time was 2.05 seconds.

2. 2. 7. Software Methods

Data analysis of data-dependent LC-MS experiments

DDA-MS data recorded on the LTQ Orbitrap mass spectrometer were processed with MaxQuant (version 1.2.2.5) using standard settings with the additional options LFQ and iBAQ (log fit) selected. Data were searched against a combined forward/reversed database (special amino acids: KR) including common contaminants for false-discovery rate filtering of peptide and protein identifications. The mass deviation for the precursor mass was set 20 ppm; fragment ions were matched within 0.5 Da mass accuracy. Fixed modifications of cysteine (Carbamidomethyl (C)) were included as well as variable modifications by oxidation of methionine and acetylation (Acetyl (Protein N-term); Oxidation (M)). Matches were filtered setting false peptide and protein (PSM FDR and protein FDR) hits to 1%. The minimum peptide length was allowed to be 6 amino acids, the minimum score for modified peptides was set to 40. For protein identification, one non-unique razor peptide was required, whereas protein quantitation was only performed if at least 2 razor peptides were associated with the protein hit. Prior to statistical analysis in Perseus, protein hits associated with the reversed database or common contaminants were filtered in the protein.groups.txt file.
Data-dependent experiments performed on the Q-TOF mass spectrometer were analysed in MaxQuant (version 1.5.1.2) using the Andromeda search engine and the same flybase database as for Orbitrap data. The settings for database search were as follows: fixed modification carbamidomethyl (C), variable modification oxidation (M) and acetyl (protein N-term); Δmass = 20 ppm for precursors, Δmass = 50 ppm for TOF fragment ions. Peptide hits required a minimum length of 7 amino acids and a minimum score of 20 for unmodified and 40 for modified peptides. Resulting protein hits were FDR filtered for 1% false discoveries on the PSM level and up to 5% false protein hits. Settings for protein identification and quantitation were identical as for orbitrap data (see above).

Data analysis of histone modifications

Peptide fragment masses of heavy and light peptide variants were calculated in silico using GPMAW 5.0 software (GPMAW3) and applied to filter the MRM data for abundance of specific modifications using MultiQuant software (Sciex Framingham, version 3.0). Peptides with

similar precursor masses containing either trimethylation or acetylation of K were distinguished based on the mass accuracy of the instrument and the difference in retention time. PTM-data analysis was performed with PeakView software (version 2.1, ABSciex) by using doubly and triply charged peptide masses for extracted ion chromatograms (XICs). XICs were checked manually and values were exported to Excel for further calculations. Standard deviation of the mean was used for error bar calculation. The mass spectrometry raw data are deposited to the ProteomeXchangeConsortium with the data set identifier submission number PXD002537 and PXD003445.

Software packages

Perseus software version 1.5.1.6 has been used to process proteomic MS data. Volcano-, heatmap- and kinetic-plots have been created via Perseus (Tyanova et al., 2016) after statistical testing and filtering for valid values. Default settings were used for analysis in Perseus.
Imputation of missing values from a standard deviation was done in the Perseus software. Therefore, the distribution was optimized to simulate a typical abundance region that the missing values would have if they had been measured. Imputation was done with following parameters. 0.3 Width: defines the width of the Gaussian distribution relative to the standard deviation of measured values. In this case, 0.3 means that the width of the distribution used for drawing random numbers is one third of the standard deviation of the data. 1.8 Down shift: specifies the amount by which the distribution used for the random numbers is shifted downwards. 1.8 is the unit of the standard deviation of the valid data. The replacement of missing values was applied to each expression column separately.
Skyline software version 3.6 has been applied for PTM-data analysis by using doubly and triply charged peptide masses for extracted ion chromatograms (XICs). XICs were checked manually and peptide ratio results were exported as .csv file for further calculations.
BioMart algorithm from Ensemble was used for genomic species comparisons: (http://www.ensembl.org/biomart/martview). First the human Ensemble Gene 89 database was chosen. Then the dataset "Human genes (GRCh38.p10) was selected. Next, filters were applied: The "MULTI SPECIES COMPARISONS" box was opened and the "Homolog filters" option was ticked and "Orthologous Fruitfly Genes" from the drop-down menu were chosen. Then, "Attributes" in the left menu were clicked and "Homologs" were selected. The "Fruitfly Orthologs" box was opened and data of interest were selected (e.g. gene ID and the orthology type). Finally the "Results" button was confirmed to choose the favorite type of output file. All

subsequent analyses were done in Excel and with Knime. Flybase annotation were retrieved from www.flybase.org: /Tools/Retrieve Convert Tools/Upload-Convert IDs.

Knime software version 2.9.4 was used to combine several excel sheets into one final excel sheet. Therefore, original excel sheets have been transformed into .txt files and uploaded within KNIME. Then the full outer join modus has been selected for combining excel sheets after having chosen the combination parameters. By using the CSV Writer modus, .csv files have been generated containing combined excel sheet data.

Image Lab software version 5.2.1 has been used to analyse and visualize SDS-PAGE gels and DNA agarose gels. Gels were documented with the Chemidoc Imaging Touch system (Biorad) and data were imported into the Image Lab Software Suite. Cropping, adjustment and annotation of gels has been done with the respective tools. Raw and modified data have been saved.

FlowJo software (version 8.8.7) was applied for the analysis of FACS data. Raw files were imported into the FlowJo software. Gating the cells was performed by selecting areas of cell counting events. Therefore, cells were separated from debris by a plot of FSC versus SSC. Single cells were obtained by plotting PE-A (area) versus PE-W (width). Living cells were selected and histograms depicting PE-A and % of Max were generated and exported as .pdf files.

Fiji software version 1.0 from ImageJA1.45b package has been used to process pictures from the Axiovert microscope. Pictures have been uploaded into Fiji as .zvi files and cropped, and converted into .tiff files. Additionally, pictures were transformed from the RGB modus to be able to insert scale bars and adjust the contrast.

2. 2. 8. Immunohistochemical methods

Immunostaining of HeLa S3-spinner cells

Cells from NCC experiments diluted in 500 µl PBS were applied in a specialized module to the Cytospin centrifuge (Thermo Scientific) to bring the cells from suspension onto a microscope slide. Cells were centrifuged for 500 g for 10 min until all volume has been applied onto the microscopic slide. The microscopic slides were incubated for 5 min at RT to allow the cells to settle. Then, cells were washed in CSK buffer for 5 min at RT in a Coplin Jar. Next, cells were incubated for 5 min at RT in CSK buffer with Triton for permeabilization. Cells were washed twice with PBS and fixed in PBS/2% formaldehyde for 15 min at RT followed by two PBS washes for 5 min each.

Before blocking cells in PBS-Tween/5% BSA for 20 min, cells were incubated for 15 min in ice cold 100% methanol at -20 °C and then washed with PBS for 5 min. Slides were allowed to dry and then cells were incubated with 50 µl of primary antibody diluted in PBS-Tween/5% BSA. Slides were mounted and incubated overnight in a wet chamber in the dark at 4 °C. On the following day, slides were washed twice with PBS to remove the mounting glass. Then, cells were washed three times in PBS-Tween and incubated with the secondary antibody for 1 h at RT in a dark place followed by two washes in PBS. Cells were DAPI stained by applying a PBS-Tween/5% BSA solution with 0.2 µg/ml DAPI to the cells for 4 min at RT. Then cells were washed again in PBS and mounted with 5 µl Vectashield (Vector Laboratories), covered with a coverslip and sealed with nail polish. Slides were stored at 4 °C.

CSK buffer (Triton)

10 mM Pipes pH7
100 mM NaCl
300 mM Sucrose
3 mM $MgCl_2$
(0.5% (v/v) Triton X-100)

Microscopy

All slides were analysed using the Axiovert 200M epifluorescence microscope (Zeiss). Images were taken with the 60x objective and were kept using the Axiovision 4.7 software (Zeiss). Editing of pictures was done using Adobe CS5 Photoshop and Illustrator as well as Fiji software version 1.0.

3. RESULTS

3. 1. *In vitro* chromatin assembly

To investigate the kinetics of the chromatin-associated proteome during assembly, an *in vitro* chromatin assembly system was chosen. This system is based on the immobilization of repetitive DNA sequences onto paramagnetic-streptavidin beads (Figure 3. 1. A). Initially a DNA sequence derived from the *Lytechinus variegatus* (sea urchin) 5S rRNA gene was used for this reconstitution assay. This sequence consists of an array of nucleosomal positioning sequences in a backbone of a pBluescript (SK-) vector (Hansen et al., 1991). Cleavage sites of the linearized vector were filled up with dCTP, dGTP and biotinylated dATP and dUTP. Due to the Klenow enzyme reactivity during incorporation, only one end of the DNA was biotinylated and immobilized onto magnetic streptavidin beads.

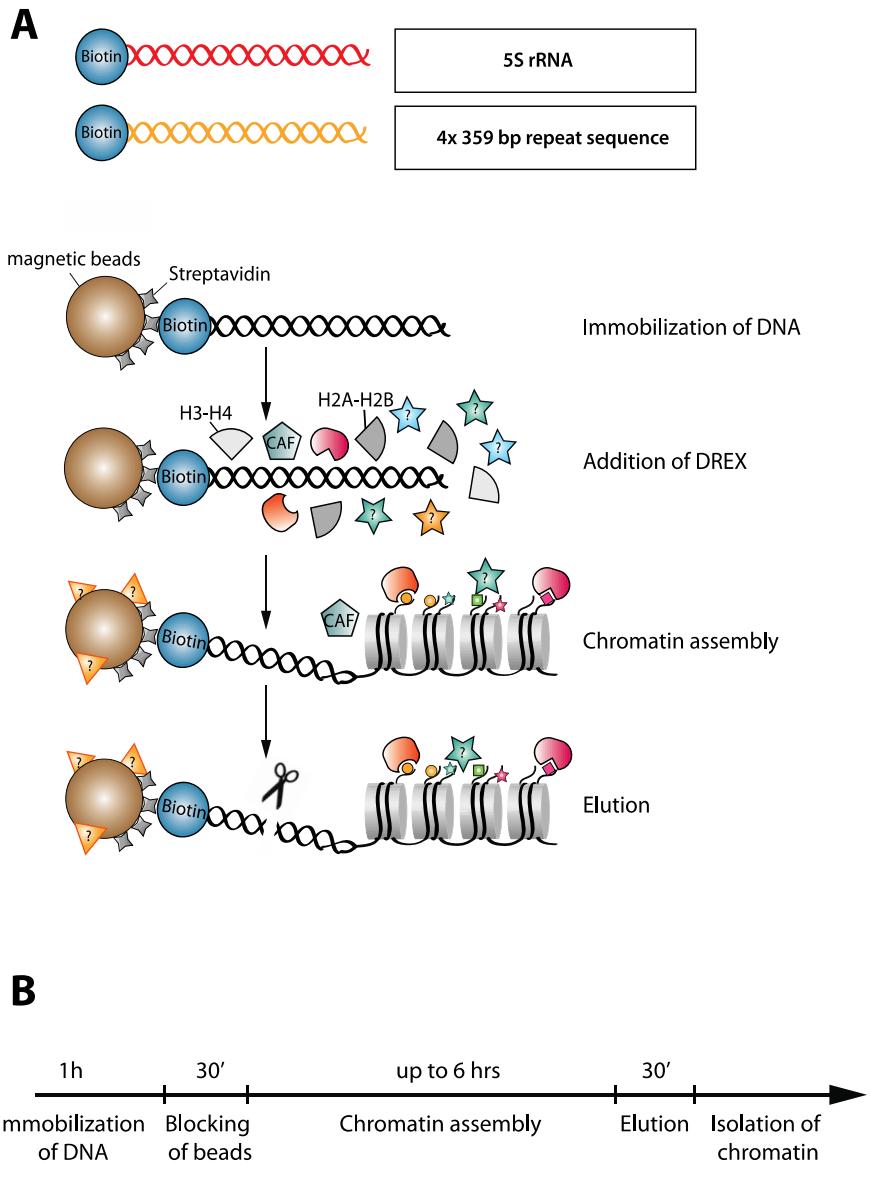

Figure 3. 1.: Workflow of DREX mediated chromatin assembly.

A: 5S rRNA or 4x 359 bp linearized and biotinylated DNA sequences were immobilized on streptavidin-coated paramagnetic beads. Incubation with Drosophila embryonic extract (DREX) led to chromatin assembly. The assembly was stopped in regular time intervals to investigate DNA structure as well as protein composition. Chromatin was washed and eluted by MNase digestion for further analysis.
B: Timeline indicates the duration of experiments

Beads-DNA conjugates were incubated in BSA to block the binding capacity before the addition of *a well-characterized S-150 chromatin-assembly extract prepared from early Drosophila embryos (DREX) (Becker and Wu, 1992). It has been shown that this protein extract is able to assemble large DNA fragments into an ordered array that closely resembles the chromatin structure seen in early embryos with regards to nucleosome spacing (Blank et al., 1997) and histone modifications (Bonaldi T. et al., 2004; Scharf et al., 2009).* To determine the quality of the extract after preparation, varying amounts of extract were incubated with 2 µg of DNA. For all prepared extracts, 40 – 60 µl of extract per reaction showed best assembly reactions (Figure 3. 2. A).

Since this *in vitro* system relies on the usage of magnetic beads, chromatin assembly can be stopped at any given time point by magnetic purification of the beads and subsequent MNase digestion. MNase-digested chromatin showed distinct patterns after 15 min, 1 h and 4 hrs of assembly arguing for a gradual maturation of chromatin (Figure 3. 1. B). With respect to the MNase digestion pattern, *in vitro* formed chromatin showed increased regularity with increasing time. In this assay, up to 5 regularly spaced nucleosomes were detected in the respective DNA template after 4 hrs of chromatin assembly (Figure 3. 2. C, left panel: 5S rRNA).

With respect to the intensity of protein bands on a silver stained gel, no major differences of the assembled chromatin between all three time points were observed (Figure 3. 2. B). To distinguish chromatin-binding proteins from proteins that bind to the beads non-specifically, beads without immobilized DNA were incubated with extract as "beads-only" control. Comparing both conditions indicated a significant protein binding dependency on the immobilized DNA for all three time points (Figure 3. 2. B). Another quality control of this assembly system was the wash with a 200 mM salt solution after the assembly of chromatin to reduce any unspecific binding of proteins. Furthermore, chromatin was digested with MNase to mildly elute the assembled chromatin from the beads therefore reducing any background binding proteins *since proteins that interact unspecifically with the beads are not released (Mellacheruvu et al., 2013).*

3. 1. 1. DNA sequence dependency of *in vitro* assembled chromatin

To test whether the underlying DNA sequence has any effect on chromatin assembly, a plasmid containing a repeated 359 bp sequence from *Drosophila melanogaster* was used for assembly. The 359 bp sequence is the most abundant satellite repeat found in the *Drosophila melanogaster* genome (Brutlag, 1980). Moreover, the 359 bp repeat sequence is an interesting candidate for

studying heterochromatin-associated sequences since it is predominately located at the centromere of the *Drosophila melanogaster* X chromosome. In contrast to that, some variants of the sequence are interspersed in pericentromeric regions of the autosomes 2 and 3 (Usakin et al., 2007). However, 359 bp repeat-related sequences are not only present in heterochromatic regions but also partly in euchromatin as it was shown for X-linked as well as for chromosome 2- and 3-linked variants.

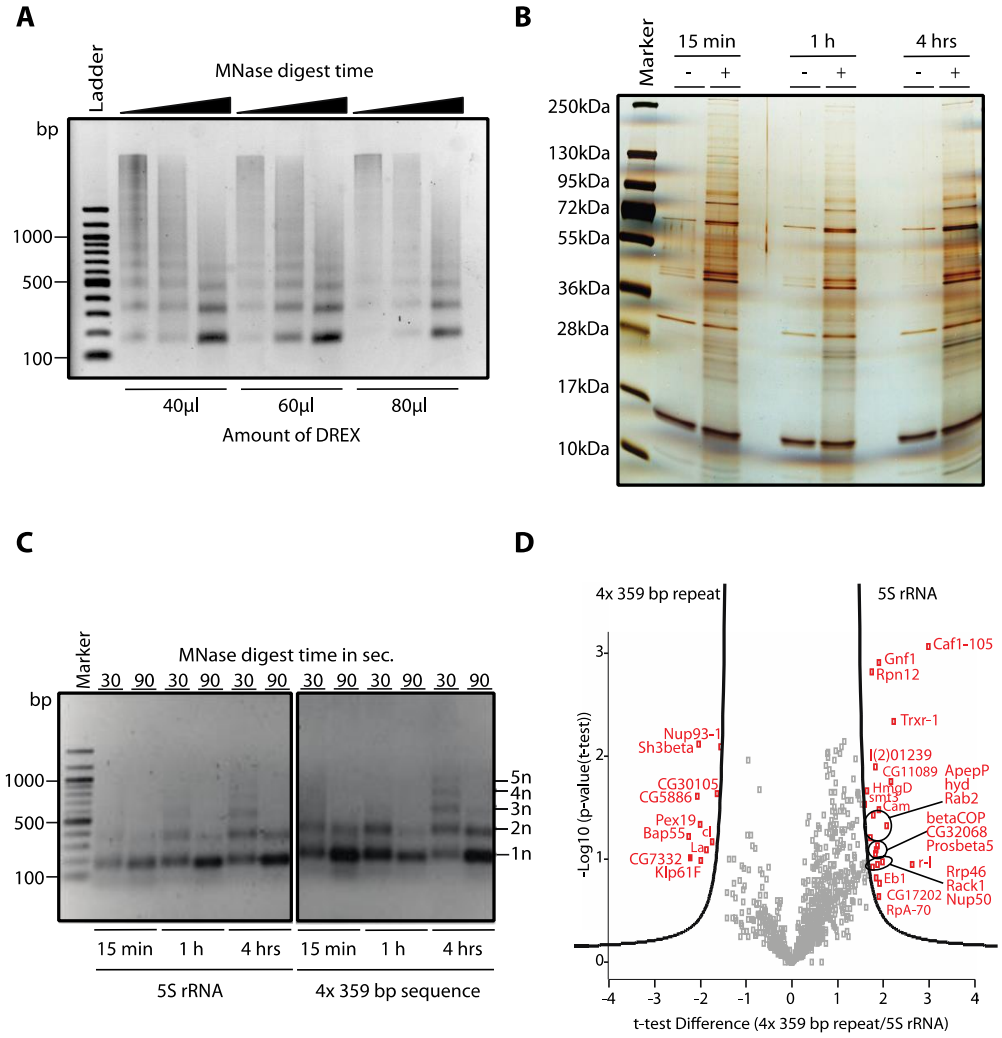

Figure 3. 2.: Chromatin assembly analysis and sequence dependency comparison.

A: Two micrograms of DNA were reconstituted into chromatin by an incubation for 6 hrs at 26 °C with different amounts of Drosophila embryo extract. It was digested with MNase for 30 s, 90 s, or 240 s. Ladder: 100 bp DNA.
B: SDS-Page of assembled chromatin. Beads with (+) and without (-) immobilized DNA were incubated for 15 min, 1 h and 4 hrs at 26 °C with 45 µl of DREX. DNA was cleaved from beads by MNase digestion for 10 min at 26 °C. 10% of each sample was loaded onto a 4-20% gradient gel and proteins were visualized by silver staining.
C: Two micrograms of either 5S rRNA or 4x 359 bp sequence DNA were incubated for 15 min, 1 h and 4 hrs at 26 °C with 40 µl DREX and digested with MNase for 30 s or 90 s. Marker: 100 bp DNA.
D: Identification of specific DNA binding proteins by a two-sample, FDR-corrected t-test of the mean averages of 5S rRNA and 359-repeat binding proteins (threshold: P=0.5 (FDR from permutation) and s0=2). Red illustrated proteins show significant binding onto an indicated DNA sequence. Circles are used to illustrate protein names.

MNase-digested chromatin using both sequences showed no differences in terms of MNase digestion patterns and number of regularly spaced nucleosomes (Figure 3. 2. C). With respect to protein binding, *most of the proteins assembled on chromatin independent of the underlying DNA sequence as we only observed a small number of proteins that showed differential binding between the 5S rRNA repeat and the repeated 359 bp sequence from D. melanogaster* (Figure 3. 2. D). It could well be that the early extract did not differentiate between different DNA sequences since no major differences in the proteome were observed when using various DNA sequences for assembly.

All further experiments relied on the usage of the 5S rRNA sequence to describe *in vitro* chromatin assembly kinetics.

3. 2. Data-dependent MS acquisition of *in vitro* assembled chromatin

Chromatin-bound proteins as well as proteins from DREX were digested with the protease trypsin and the resulting peptides were analysed with a 2 hrs LC-MS gradient on an Orbitrap XL mass spectrometer operated in data-dependent acquisition mode. All presented data are based on three biological replicates. Each replicate was performed with an individually collected DREX extract.

For subsequent analysis of proteomic data, the MaxQuant analysis suite combined with the search engine Andromeda was used. The MaxQuant software provided LFQ values that have been used to quantify proteins indicating their abundances at a given time point (Figure 3. 3. A).

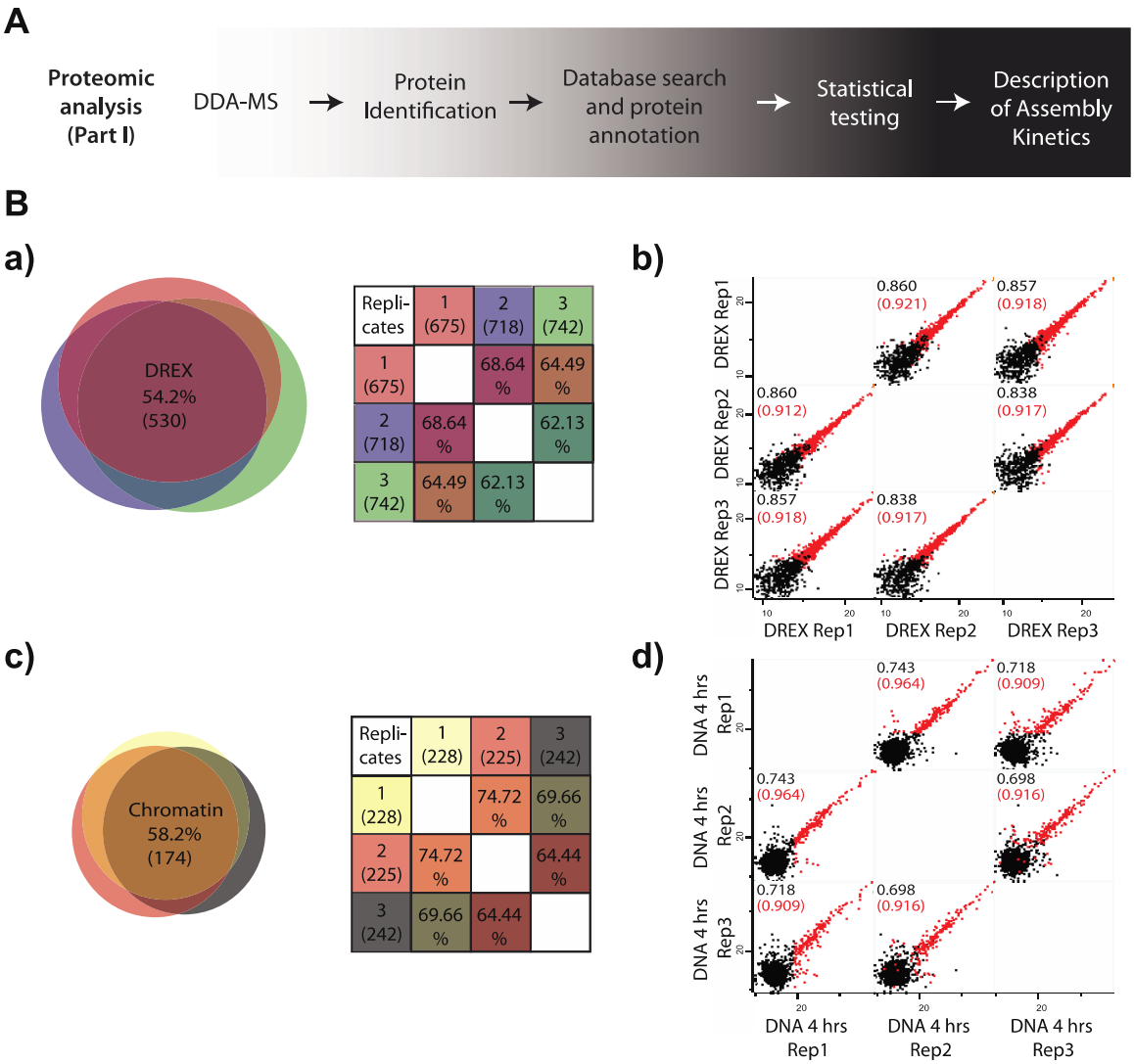

Figure 3. 3.: Data-dependent acquisition of chromatin assembly.

A: Workflow of proteomic analysis for DDA-MS mode.
B: Venn diagram with respective table showing the overlap of proteins identified by DDA-MS.
a) Overlap of proteins in three biological replicates of DREX with replicate 1 (675 proteins), replicate 2 (718 proteins) and replicate 3 (742 proteins). Over 54% (530 proteins) have been identified in all DREX samples.
b) Multi-scatter plots showing the correlation of replicates after imputation of missing values for DREX samples. Red dots show correlation of proteins identified in all three replicates. Black dots display the correlation of proteins identified at least once per dataset and after imputation of missing values. Black and embraced red numbers indicate the coefficient of determination in R^2.
c) Overlap of proteins of three 4 hrs assembly reactions with replicate 1 (228 proteins), replicate 2 (225 proteins) and replicate 3 (242 proteins). Over 58% (313 proteins) are identical in the chromatin samples.
d) Multi-scatter plots showing the correlation of replicates after imputation of missing values for chromatin samples as described in Figure 3. 3. B, panel (b).

In total, 977 proteins have been identified in three biological replicates of the assembly extract. Out of the 977 proteins, 530 proteins were present in all three biological replicates (54.2%) (Figure 3. 3. B, panel a)). All other proteins have been identified once or twice within all three biological replicates (Figure 3. 3. B, panel b)). To overcome this "missing-data" problem from data-dependent acquisition, data were imputed from a normal distribution (see section 2.2.7.: Software Methods/Software Packages/Perseus).

In general, it was observed that most intense proteins were highly correlating between all three replicates whereas proteins of low intensities were identified in only one or two out of three biological replicates (Figure 3. 3. B, panel b)).

When analysing the proteins bound to chromatin after 4 hrs, we identified a total of 299 proteins using the OrbitrapXL with 174 (58.2%) being present in all three replicates (Figure 3. 3. B, panel c)).

Similar to what has been observed for proteins detected in the DREX measurements, most intense proteins in assembled chromatin correlated best between all three biological replicates (red data points Figure 3. 3. B, panels b) and d)). Proteins with missing data points in one or two biological replicates had the tendency to be of low intensity even in the replicate in which they have been identified.

3. 3. Data-independent MS acquisition of *in vitro* assembled chromatin

Since data-dependent acquisition deals with the problem of missing values, a label-free SWATH-MS based quantitation approach was chosen for the analysis of kinetics of chromatin assembly. In contrast to data-dependent acquisition, in which a specific precursor ion is selected for fragmentation, data-independent acquisition and especially SWATH-MS fragments everything within a mass window of m/z 25 to acquire a single CID fragment ion spectrum. To cover the full mass range between m/z 400-1250, the mass spectrometer sequentially acquires one full MS spectrum and about 40 CID-MS/MS spectra with isolation windows of m/z 25 during one cycle of roughly 3.5 s. This leads to a total fragmentation of all precursor ions detectable throughout the entire mass range and along the chromatographic elution period. The data analysis of these data is challenging since the resulting fragment ion spectra are highly multiplexed meaning that a fragment ion spectrum is difficult to relate to a specific precursor ion spectrum.

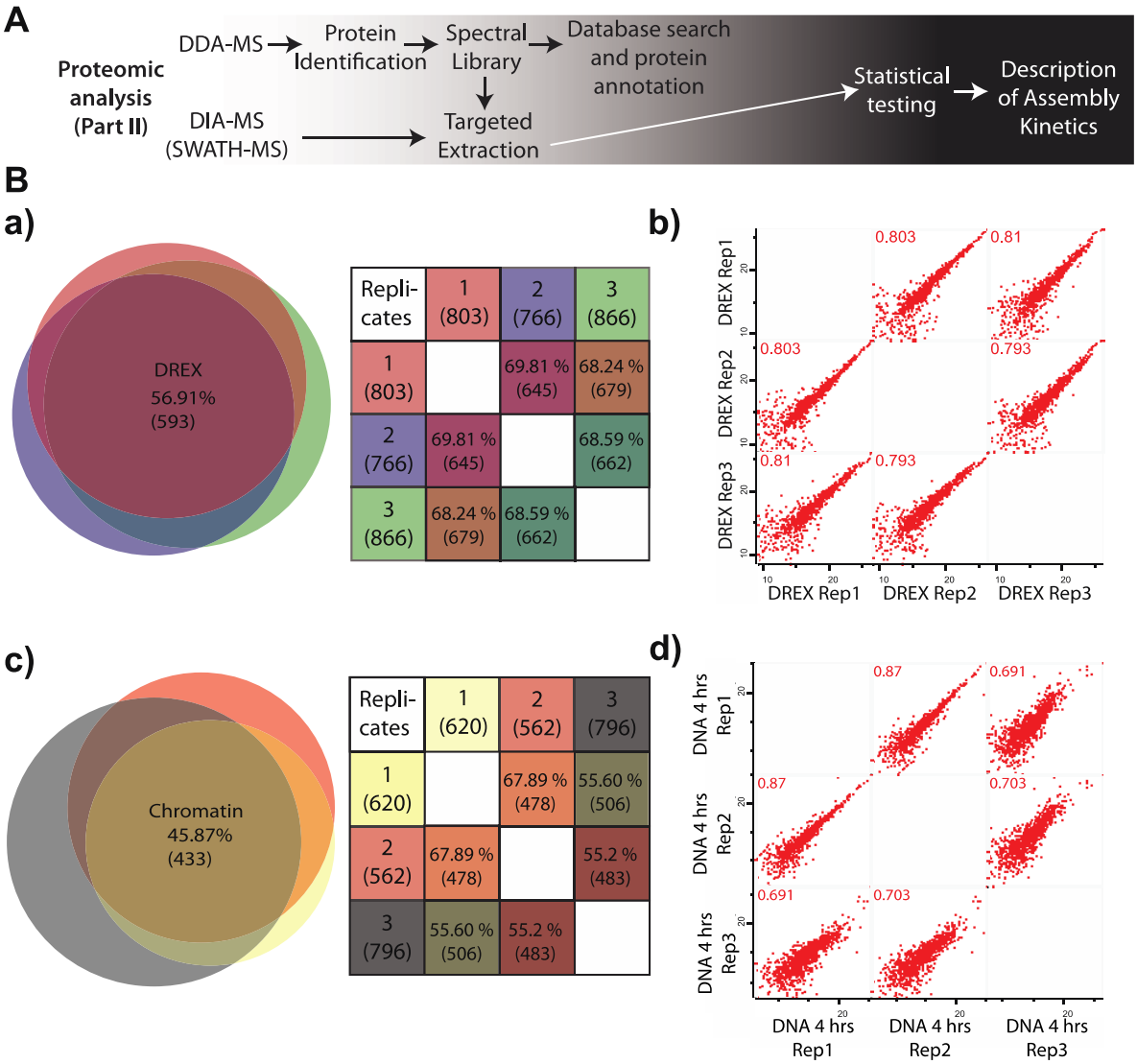

Figure 3. 4.: Data-dependent acquisition of chromatin assembly for library generation and quantitation with data-independent acquisition.

A: Workflow of proteomic analysis for DIA-MS mode (SWATH-MS).
B: Venn diagram with respective table showing the overlap of proteins identified by DDA-MS.
a) Overlap of proteins in three biological replicates of DREX with replicate 1 (803 proteins), replicate 2 (766 proteins) and replicate 3 (866 proteins). Over 56% (593 proteins) have been identified in all DREX samples.
b) Multi-scatter plots showing the correlation of three replicates for DREX samples acquired in DIA-MS mode. All proteins have been identified in all three biological replicates indicated by red colour of the dots as described in Figure 3. 3. B, panel b).
c) Overlap of proteins of three 4 hrs assembly reactions with replicate 1 (620 proteins), replicate 2 (562 proteins and replicate 3 (796 proteins). Over 45% (433 proteins) are identical in the chromatin samples.
d) Multi-scatter plots showing the correlation of three replicates for 4 hrs assembled chromatin samples acquired in DIA-MS mode.

Therefore, SWATH-MS data analysis relies on the generation of spectral libraries that can be used to identify and quantify fragment ion spectra. Such a library has been generated by measuring three replicates of the DREX extract as well as three replicates of 4 hrs assembled chromatin by measuring in a data-dependent acquisition run using a Top 25 fragmentation scheme. First, the spectral library was used to adjust the SWATH window size. All 40 windows covering the entire mass range for fragmentation of precursor ions were adjusted to the

distribution of tryptic peptides. Second, the spectral library was subsequently used to match with the SWATH-MS measurements for identification and quantification of proteins (Figure 3. 4. A).

When analysing the data-dependent acquisition runs for library generation, 1050 proteins in the DREX and 943 proteins associated with 4 hrs assembled chromatin were identified with an overlap of 56.9% or 45.87% respectively (Figure 3. 4. B, panel a) and c)).

For targeted extraction of the SWATH files in combination with the spectral library, all runs were calibrated according to their calibration time. This calibration grounds on the use *of ten conserved peptides that were distributed over the entire LC gradient. Finally, we could quantify 1024 proteins in the SWATH runs performed on triplicate samples of chromatin assemblies after 15, 60 and 240 minutes.*

Since quantification in data-independent acquisition is based on MS/MS data and by the alignment to a spectral library, all 1024 proteins have been found in all three biological replicates at all three time points (Figure 3. 4. B, panel b) and d)). With this "complete" data set, the kinetics of chromatin assembly were further investigated to describe binding behaviour over time.

3. 4. Kinetics of *in vitro* assembled chromatin

Despite the fact that we selectively eluted the assembled chromatin using a digestion with micrococcal nuclease, which shows a relatively low background (Figure 3. 2. B) *we still identified and quantified proteins that were eluted from the beads in the absence of chromatin.*

For the analysis of chromatin-specific proteins, a two-sample t-test comparing chromatin over "beads-only" control experiments revealed 480 significantly enriched proteins (red dots in Figure 3. 5. A).

It was possible to describe clusters of proteins according to their binding kinetics by means of Euclidean clustering of replicate-averaged Log2(x)-transformed SWATH intensities for each time point (Figure 3. 5. B and D). First, 104 proteins had high intensities at the beginning of chromatin assembly and their intensities dropped over time. Therefore, they were called "early binders" (Figure 3. 5. D). Such proteins are well-described to play roles in DNA replication (PCNA) and in histone deposition (Caf-180 and Caf-105). PCNA as a clamp loader protein had high abundances at 15 min of assembly compared to 4 hrs of assembly. Orthogonal Western blot experiments confirmed MS results and illustrated also that PCNA binding peaks at 1 h (Figure 3. 5. C).

Caf-180 and Caf-105 have been shown to interact with PCNA and were both early binding proteins. The third subunit of the CAF complex had also a positive ratio but according to the classification for early binding proteins to have higher ratios than "1", it was classified as constant binding protein. Nevertheless these data confirm former studies that showed the requirement of two largest subunits of CAF (Caf-180 and Caf-105) for efficient *in vitro* chromatin assembly (Kaufman et al., 1995; Tyler et al., 2001).

Additionally, the Drosophila ortholog of Rfc1, named Gnf-1, was also found as an early binder together with all its subunits (Rfc3, Rfc4, Rfc38) (Figure 3. 5. D). Another complex that has been found to be early binding is the FACT complex (dre4 and ssrp-1) (Figure 3. 5. D). A similar binding behaviour has been observed for Acf1 as part of the CHRAC complex. The other subunits of this complex, namely Chrac-14 and Iswi were also found as early binding proteins. In total, the majority of early binding proteins is associated with well-described functions in DNA replication, chromatin remodelling and nucleosome deposition.

The abundance of the canonical histone H3 did not change over time shown by MS data as well as Western blot experiments (Figure 3. 5. C and D). H3 belonged to the largest cluster (775 proteins) of constant binding proteins that had similar intensities over all three time points of chromatin assembly. Also, the other canonical histones were constant binding proteins. Presumably, their constant binding reflects the fact that once a nucleosome is incorporated into the DNA, it stays bound to the DNA. Additionally, some of the Minichromosome complex subunits were constant binding proteins (Mcm3 and 6). Other replication-associated complexes were also found as constant binding proteins as for example DNA polymerase α (subunits 180, 73 and 50). DNA polymerase α has been shown to interact with Mcm3 strengthening the validity of this dataset.

Finally, proteins with higher intensities after 4 hrs of chromatin assembly than compared to 15 min assembly were found as well (146 proteins). In general, those proteins are well-known DNA repair factors such as Ku80 and Irbp (Ku70) (Figure 3. 5. D). Both proteins interact with each other and had higher intensities after 4 hrs of chromatin assembly. Alternatively, it could be that they accumulated since the ratio of 15 min divided by 4 hrs does not distinguish between accumulation and higher abundance at a single time point. Additionally, late binding proteins were also Rpa3, 2 and 70, all subunits of the RPA heterotrimer. These proteins have been reported to be involved in DNA replication as well as in homologous recombination (HR) and non-homologous end-joining (NHEJ) due to their much higher affinity towards single-stranded DNA than RNA or double-stranded DNA (Chen and Wold, 2014).

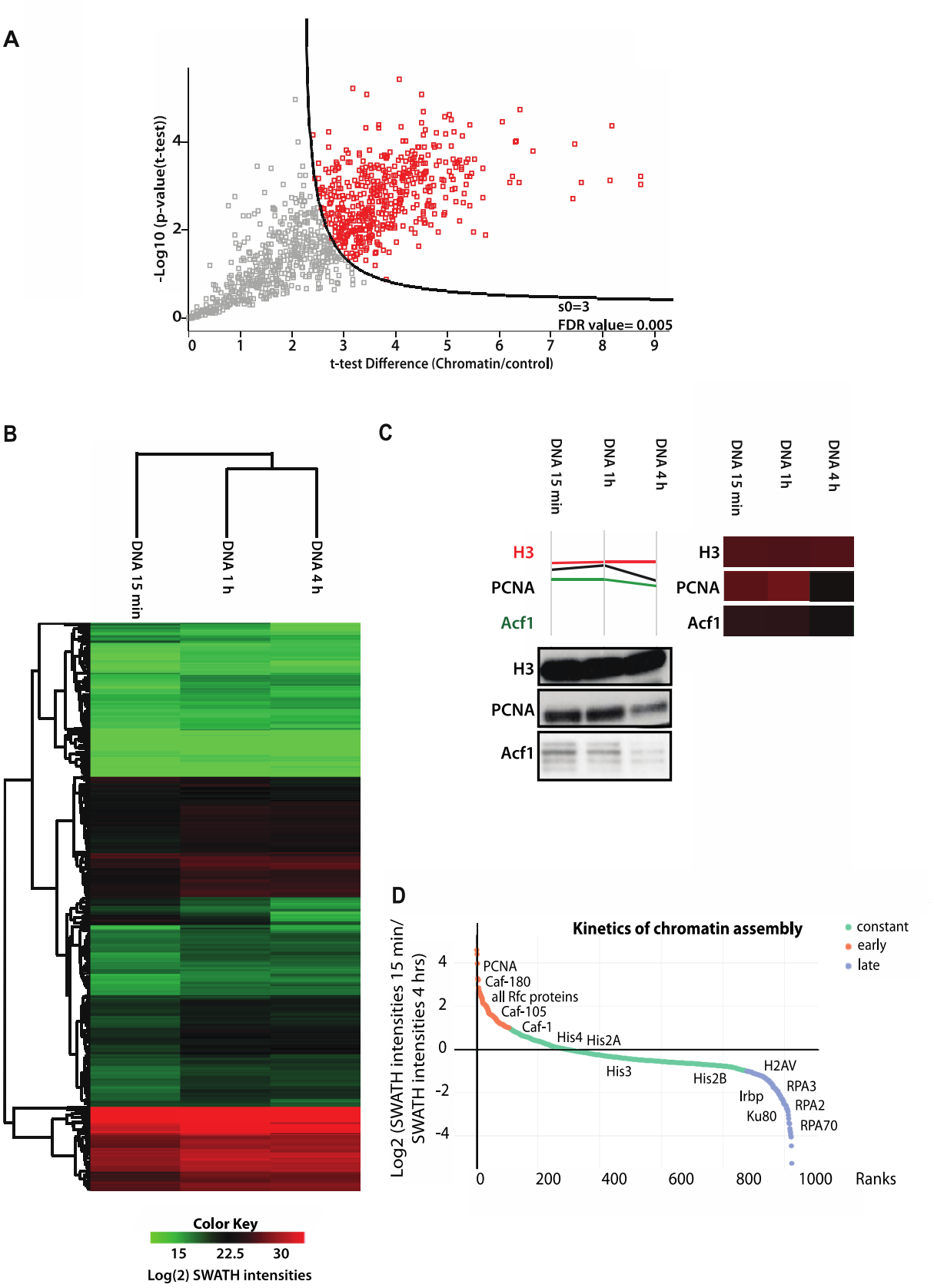

Figure 3. 5.: Kinetics of chromatin assembly.

A: Identification of chromatin-specific binding proteins by a two-sample, FDR-corrected t-test of the mean averages of SWATH intensities of beads-only control experiments versus chromatin assembly experiments (threshold: p = 0.005 (FDR from permutation) and s0 = 3). Red dots illustrate chromatin-specific proteins (480 proteins).

B: Heatmap illustrating Log2(x)-transformed median-averaged SWATH intensities from three replicates after Euclidean clustering. Rows indicate proteins; columns represent different conditions of chromatin assembly. Red and green colours indicate SWATH intensities.
C: Time-resolved kinetics for H3, proliferating cell nuclear antigen (PCNA) and ATP-dependent chromatin assembly factor 1 (Acf1). Plots illustrate the Log2(x)-transformed SWATH intensities in each assembly condition for 15 min, 1 h and 4 hrs. Each line illustrates the binding behaviour of a single protein. Enlarged heatmap rows illustrate the kinetics of specified factors as described in legend Figure 3. 5. B. Western blot of all three proteins in chromatin assembly experiments for 15 min, 1 h and 4 hrs.
D: Waterfall plot illustrates Log(2)-transformed quotient of median-averaged replicates after 15 min SWATH intensity divided by its respective 4 hrs SWATH intensity for each single protein. Proteins were sorted from largest to smallest quotient and plotted with a scatter graph tool. 104 proteins (orange) showed higher values than 1.0 and could be identified as early binding proteins. 774 proteins (green) had a quotient value between 1.0 and -1.0 and did not change between 15 min and 4 hrs. 146 late binding proteins (blue) had negative values below -1.0. They were enriched after 4 hrs. Examples of proteins are spotted in the waterfall plot.

3. 5. *In vivo* assembled chromatin analysis with Nascent Chromatin Capture

To investigate whether the *in vitro* system resembles physiological conditions regarding replication fork speed, protein abundance and interplay of factors, this study was complemented with *in vivo* chromatin capture experiments combined with quantitative mass spectrometry. NCC is a biochemical approach to isolate newly synthesized DNA for quantitative proteomics to investigate proteins associated with DNA replication and chromatin maturation (Alabert et al., 2014). The system relies on the synchronization of HeLa S3-spinner cells until all cells are blocked in G2/S-phase transition (Figure 3. 6.). Subsequently, cells were released from the single thymidine block to progress for another 3 hrs in cell cycle. Then biotin-dUTP was introduced by a short hypotonic shift without affecting S-phase progression or triggering DNA damage (Alabert et al., 2014).

DNA synthesis and its assembly into chromatin can be either investigated in nascent chromatin immediately after the biotin-dUTP pulse or in chromatin that has been allowed to mature for longer times (Figure 3. 6.). Nascent chromatin (15 min) and mature chromatin (2 hrs) was compared by means of different techniques to adjust the protocol setup and to minimize sample number (Figure 3. 7.). For the proteomic analysis of this study, chromatin has been chased after pulse labelling for 15 min, 1 h and 4 hrs to have comparable time points with regards to the *in vitro* chromatin assembly system.

In NCC, proteins were crosslinked to DNA and nuclear extracts were generated. During sonication, crosslinked-chromatin was sheared into 2-3 kb fragments and purified via streptavidin beads (Figure 3. 6.). Stringent washing steps reduced unspecific binding proteins. Upon extensive washing, beads were boiled in buffers with high concentrations of detergents to elute proteins from the beads. Finally, proteins were prepared for proteomic analysis similar to the *in vitro* assembled chromatin.

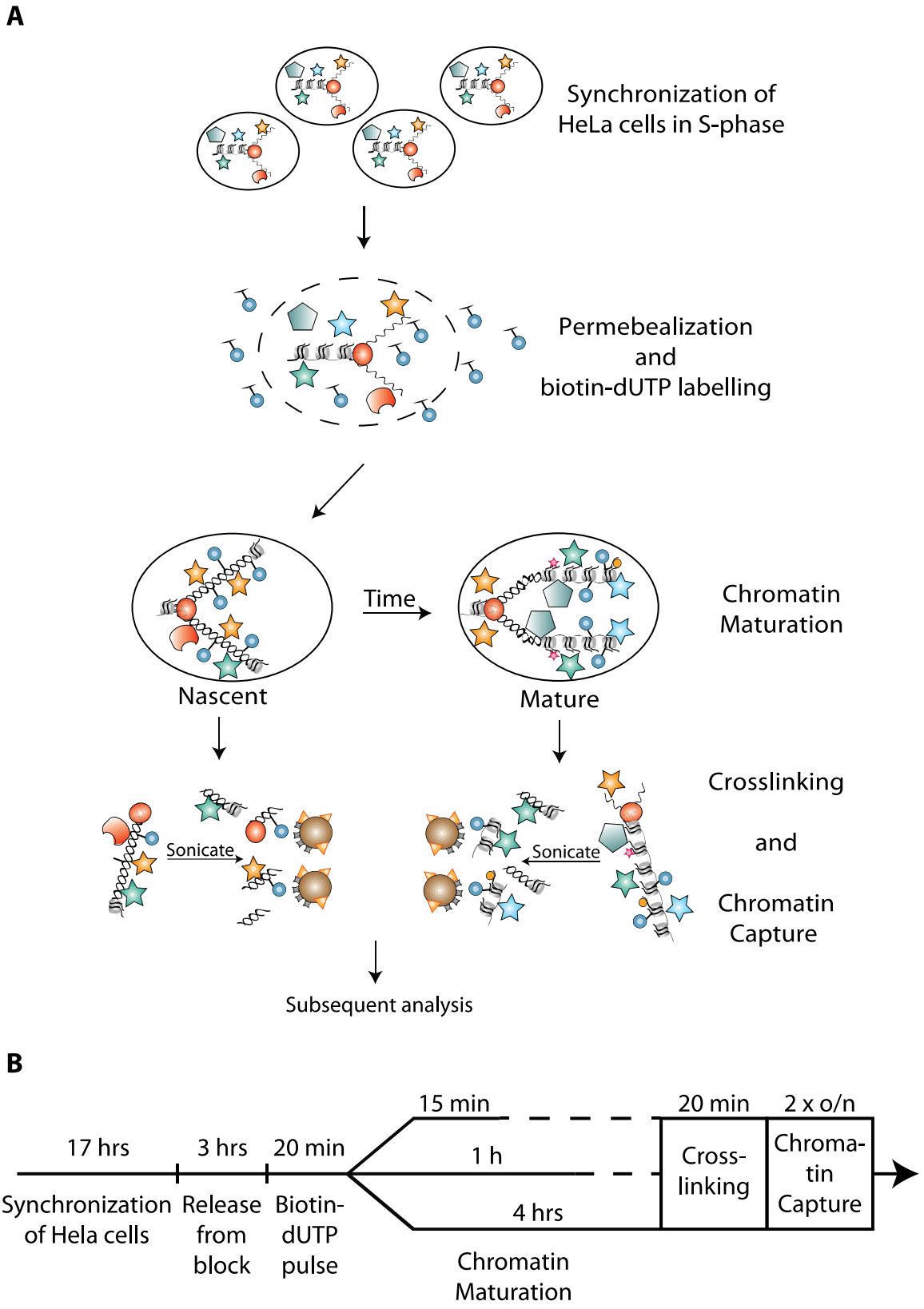

Figure 3. 6.: Nascent chromatin capture workflow.

A: HeLa S3-spinner cells were synchronized in spinner cultures with a single thymidine block. 3 hrs after release, chromatin got tagged with biotin-dUTP. Chromatin maturation was stopped in regular intervals before crosslinking. Nuclear extracts were prepared and chromatin was sonicated to create fragment of 2-3 kb. Biotinylated chromatin fragments were purified on paramagnetic streptavidin-coated beads by two o/n incubations, washed extensively and analysed using SWATH-MS.
B: Timeline indicates the duration of experiments.

The FACS analysis during NCC experiments showed, that the majority of cells were blocked and proceeded synchronically in the cell cycle after release from thymidine block (Figure 3. 7. A). Additionally, nascent and mature chromatin was distinguished according to the FACS profile of the cells. Western blot experiments showed that PCNA as replication fork component was always enriched in the nascent chromatin pulldown but did not show any signal in the mature chromatin pulldown (Figure 3. 7. B). In contrast, H3 was detected in both pulldown experiments because it was incorporated as part of the nucleosome in newly synthesized DNA and still bound to DNA in mature chromatin (Figure 3. 7. B). Both observations confirm previous data in literature and are in agreement with the *in vitro* data described above.

Moreover, H4K5ac was enriched in nascent chromatin (Figure 3. 7. B). This histone modification mark has been shown to label newly replicated chromatin until acetylation is removed shortly after replication as nascent chromatin matures into a nuclease-resistant state (Annunziato and Seale, 1983; Benson et al., 2006; Scharf et al., 2009; Sirbu et al., 2011). Here, it has been confirmed that NCC reflects these observations.

Furthermore, immunofluorescence pictures confirmed the labelling of newly synthesized DNA with biotin-dUTP in NCC experiments. Before biotin-dUTP pulse labelling, cells showed PCNA foci because these cells were in mid-S-phase during DNA replication (Figure 3. 7. C). Before biotin-dUTP pulse labelling, biotin-dUTP staining did not colocalise with PCNA foci. Any biotin signal detected in these cells resembled physiological biotin levels inside the cells. Upon biotin-dUTP pulse labelling and immediate collection of cells (nascent), PCNA signals and biotin-dUTP staining colocalised and biotin-dUTP levels were increased. Cells that were collected 2 hrs after biotin-dUTP labelling (mature) still showed increased biotin-dUTP staining compared to the state before biotin-dUTP labelling but with a much-dispersed pattern. To investigate the efficiency of biotin-dUTP pulse labelling, 100 cells per condition were counted in three biological replicates. Figure 3. 7. D illustrates that more than 70% of all cells in “nascent” condition showed biotin-dUTP incorporation. In NCC experiments with “mature” chromatin, 65% of all cells still showed positive biotin-dUTP signals. These results showed that NCC experiments labelled the majority of cells in a cell suspension.

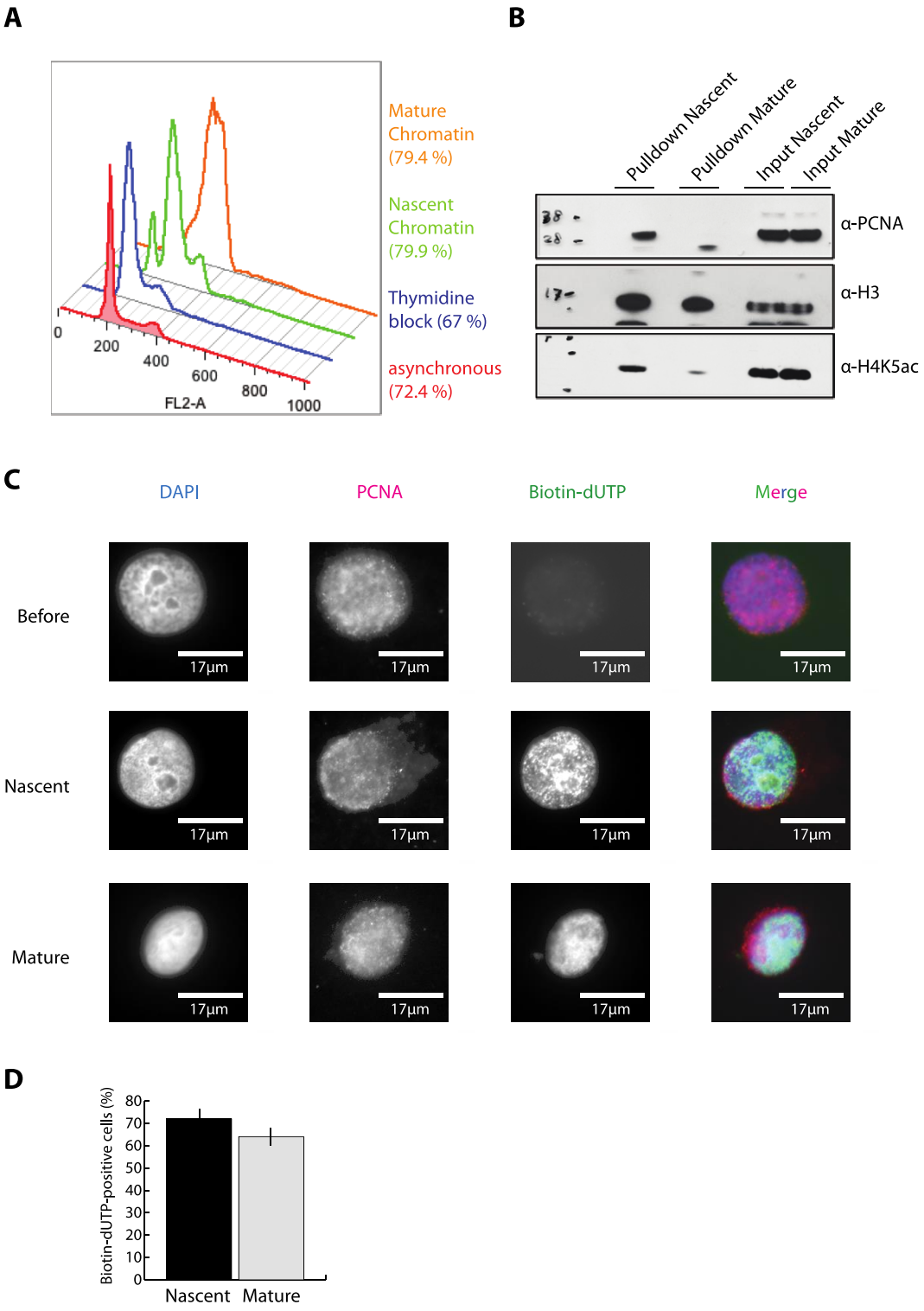

Figure 3. 7.: Validation of NCC experimental workflow.

A: Analysis of cell cycle profiles of propidium iodide stained cells. 100.000 HeLa S3-spinner cells were counted. Manual selection (indicated by %) of cells was used for histogram plotting counts of cells versus FL2-A (total cell fluorescence).
B: Western Blot of indicated proteins or histone modifications. Input sample was taken before purification over magnetic-streptavidin beads. Pulldown samples were fractions of purified proteins bound to magnetic beads from nascent or mature chromatin.
C: Incorporation and overlap of biotin-dUTP with PCNA was tested with either a specific antibody against PCNA or with a streptavidin Alexa Flour 555 Conjugate. Scale bar is 17 µm.
D: Cells were scored according to their biotin-signal with 100 cells counted in total per time point of chromatin assembly. Error bars illustrate error of the mean (n=3).

3. 6. Data-independent MS acquisition of *in vivo* assembled chromatin

Using NCC experiments combined with SILAC based quantitative proteomics, Alabert and colleagues identified approximately 3996 proteins bound to chromatin immediately after or 2 hrs past assembly *in vivo* (Alabert et al., 2014). As the quantification was based on classical shotgun proteomics (DDA-MS), statistically solid quantification requiring at least 3 valid values could only be performed on 2125 out of the 3996 proteins.

To circumvent the missing-data problem, the SWATH-MS technology was chosen to quantify proteins in a label-free and reproducible setting. Therefore, a spectral library was generated based on DDA-MS runs from multiple time points of NCC experiments in addition to human cell lysates. In total, this library contains 4487 proteins and was used for quantification of SWATH-MS experiments.

NCC experiments were performed for 15 min, 1 h and 4 hrs after biotin-dUTP pulse of HeLa S3-spinner cells. These time points were chosen in analogy to the former acquired *in vitro* experiments. Considering a replication fork progression of 1-2 kb min^{-1} *in vivo*, 15 min of labelling marks 15-30 kb of DNA behind each replication fork which equals 4-5% of the total genome.

All *in vivo* experiments were performed in 4 biological replicates and the final data set contains 2487 proteins quantified reproducibly in all replicates.

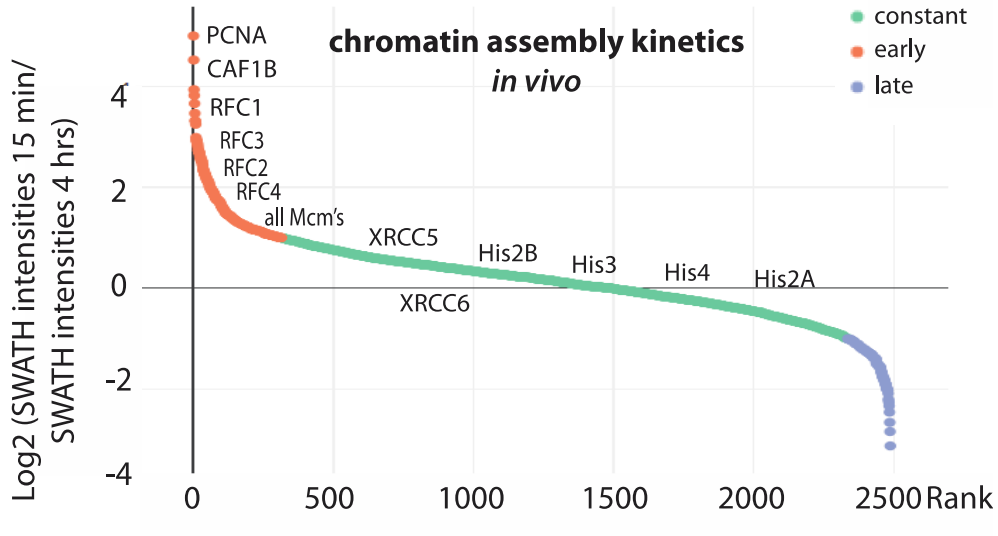

Figure 3. 8.: Chromatin assembly kinetics *in vivo*.

Waterfall plot illustrating ratios of SWATH intensities of 15 min assembly divided by SWATH intensities of 4 hrs assembled chromatin. Proteins were ranked and plotted. Proteins with Log2(x) values higher than "1" were categorised as "early", whereas proteins with Log2(x) values below "-1" were categorised as "late". Proteins with ratios between Log2(x) "1" and "-1" were classified as constant binders indicated by a colour code as seen in the legend.

In general, the dataset contains many replication-associated proteins arguing that active human replication forks were successfully isolated. Among the quantified proteins in the dataset were all Mcm proteins, Cdc45 and Gins3 as part of the CMG complex. Moreover, the clamp loader complex subunits, PCNA and the RFC proteins were quantified as well as many polymerases (Polδ 1, 2, 3 and Polα 1, 2). Furthermore, factors of the fork stability complex as Rpa1, 2, 3 and Timeless and Tipin together with Okazaki fragment processing proteins such as DNA ligase1 and Fen1 were identified and quantified.

Figure 3. 8. illustrates a waterfall plot that shows the Log2(x) ratio of each protein derived from its intensity after 15 min chromatin assembly divided by the intensity after 4 hrs chromatin assembly. According to this ratio, each protein was ranked with ranks from 1 to 2487. The protein with the most positive ratio received the rank 1 and the protein with the most negative ratio received the rank 2487. Using this ranking method, proteins with positive ratios were plotted in the upper left part of the waterfall plot whereas proteins with negative ratios are found in the lower right quadrant of the plot.

The majority of proteins had the tendency to bind early because almost 1500 proteins showed positive ratios. Among the top ranked proteins are PCNA, CAF, RFCc proteins and all Mcm proteins that all belong to the group of early binding proteins (314 proteins, 13%). This observation confirmed the purification of replication forks within nascent chromatin. Furthermore, these data are similar to *in vitro* data, in which PCNA, CAF and RFC proteins were also found as early binding proteins.

Proteins present in chromatin assembled for 15 min as well as for 4 hrs were the histone proteins and DNA repair factors (Xrcc5 and Xrcc6). Some of the DNA repair factors have also been associated with replication-independent repair processes. The class of constant binding proteins was by far the largest with 2012 proteins in total (81%).

Proteins that either bound late or accumulated over time were proteins classified as cytoskeletal proteins and RNA associated proteins as for example: Vimentin, RNA phosphatases or tubulin. The late binding proteins contributed only 6% to the entire dataset.

3. 7. Comparison of *in vitro and in vivo* chromatin assembly

The two assembly systems used, relied on different experimental setups, cell organisms and many other parameters. It was therefore difficult to compare each single protein kinetic. However, a comparison of the two methods could give insights into conservation of proteins between both systems. Additionally, differences and similarities between protein networks could be compared.

NCC experiments were performed in a human cell line (HeLa) whereas *in vitro* experiments were based on an embryonic Drosophila extract. To identify the Drosophila proteins that contained a unique human ortholog, the BioMart algorithm was applied (Kustatscher et al., 2014).

The *in vitro* assay revealed 1024 proteins to be involved in chromatin assembly in total. 472 proteins out of the 1024 proteins had a clear ortholog in the human proteome and 374 of them (79%) were also detected in the NCC dataset.

Focusing on 480 proteins in the *in vitro* system that assembled specifically onto chromatin when compared by a two-sided t-test to the negative control, 216 proteins (out of 480) had a clear ortholog in the human proteome and 184 of them (85%) were also detected as chromatin-associated during NCC experiments.

Furthermore, the similarity in binding kinetics was compared between *in vitro* and *in vivo* experiments. Especially early binding proteins involved in chromatin assembly were very comparable in context of binding properties. Factors such as RFC proteins, the CAF complex and some subunits of the FACT complex had positive ratios indicating higher chromatin binding at 15 min of assembly compared to 4 hrs (Figure 3. 9.). Moreover, most of these factors showed very similar ratios confirming the high similarity between *in vitro* and *in vivo* experiments (Figure 3. 9.). The fact, that these proteins showed early binding in both experimental assays argues for a similar function and activity during chromatin assembly and reveals a high evolutionary conservation of chromatin assembly mechanisms across species.

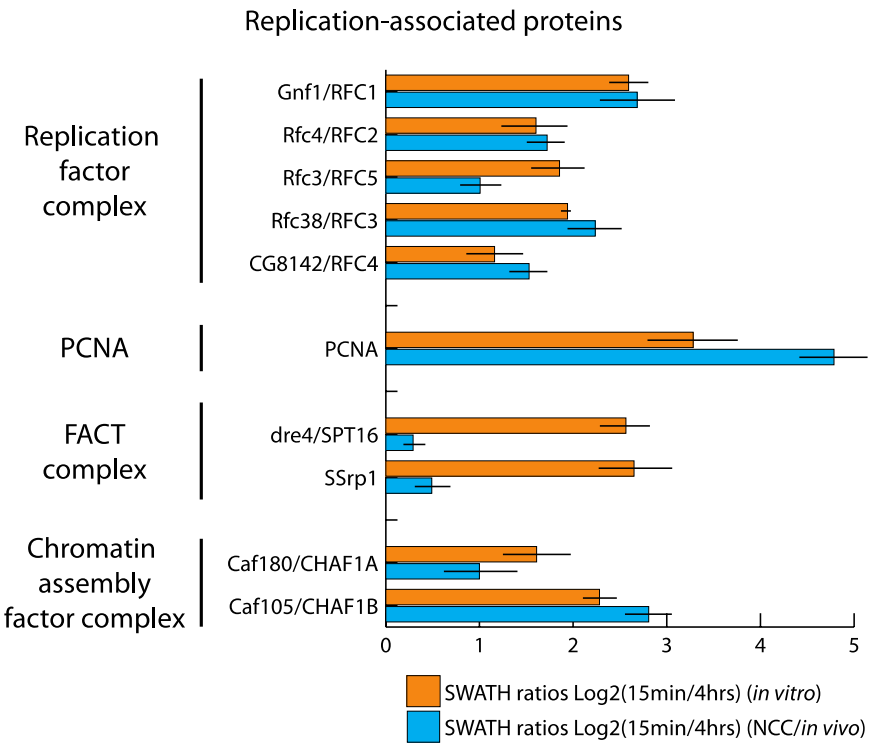

Figure 3. 9.: Comparison of binding kinetics *in vitro* and *in vivo*.

Mean-averaged replicate Log2(x) SWATH intensity of 15 min assembly was divided by the respective 4 hrs SWATH intensity of each indicated protein from *in vitro* and *in vivo* experiments. Depicted are fly protein names and respective human protein names. Error bars represent standard error of the mean, n=3.

Finally, multi-scatter plots depicting all three biological replicates in both experimental conditions allowed a correlation of all quantified proteins. Grey dots illustrate that proteins in all replicates correlated well with overall correlation coefficients between 0.7 to 0.9 *in vitro* and *in vivo* (Figure 3. 10.).

Interestingly, the majority of factors that were described as minimal set of replisome components (Kurat et al., 2017) (red dots) correlated extremely well between all replicates and these factors also belonged to the class of most abundant proteins within each replicate underlining the power of both systems to study replication factors.

Surprisingly, the proteasome subunits were equally well-correlating between all three biological replicates in comparison to the replication factors in both experimental conditions. Moreover, the proteasome subunits have also been detected as some of the most abundant proteins in both chromatin assembly assays (blue dots in Figure 3. 10).

Recent studies showed that polyubiquitination plays a key role in disassembly of the replisome machinery (Maric et al., 2014; Moreno et al., 2014; Moreno and Gambus, 2015) suggesting a direct effect of the proteasome within replicating chromatin *in vitro*. Therefore, the role of the proteasome during chromatin assembly was further investigated by means of *in vitro* experiments.

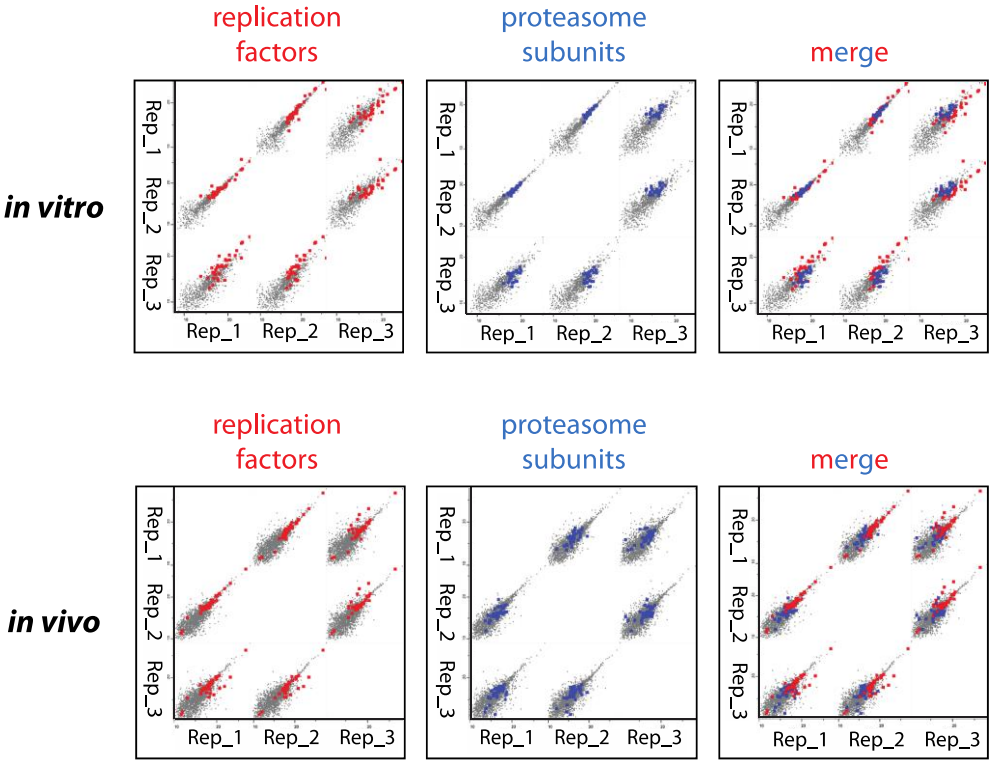

Figure 3. 10.: Correlation comparison between experimental approaches.

Three biological replicates (Rep) of 1 h assembled chromatin were multi-scatter plotted in both experimental conditions. Red dots illustrate replication-associated proteins described by (Kurat et al., 2017). Blue dots depict all detected proteasome subunits. Merged multi-scatter plots show both classes of proteins.

3. 8. Investigation of chromatin assembly upon chromatin decondensation

Among the two experimental setups, the *in vitro* reconstitution system allows a quick and easy manipulation of assembly conditions for functional studies. First, this system was chosen to test the effect of an inhibitor of which previous *in vitro* results have been reported (Scharf et al., 2009). Therefore, the addition of the broad HDAC inhibitor Trichostatin A (TSA) was tested. It has been shown that the presence of TSA *during replication-coupled chromatin assembly in vivo results in a failure to establish repressive chromatin (Wong et al., 1998) and a broadening of replication initiation areas (Kemp et al., 2005) suggesting that it results in a more open chromatin structure. To get a better insight into the effect of TSA on chromatin assembly, we performed a time-resolved analysis of protein assembled to chromatin in vitro in the absence or presence of TSA. We verified the efficiency of the TSA treatment on the acetylation levels by measuring the acetylation of H4 in the absence or presence of TSA* (Figure 1, Appendix). *It is worth mentioning that the presence of TSA does not result in a histone hyperacetylation, which is usually observed in tissue culture cells but induces a moderate increase in the acetylation due to a failure to efficiently remove the acetylation pattern present on histones before assembly (Scharf et al., 2009). The reason for this is unclear but it is probably due to a general lack of site specific histone acetyltransferases in early embryos (Bonaldi T. et al., 2004).*

Nevertheless, we observed a substantial change in the proteomic composition of chromatin assembled in the presence of TSA. To detect all proteins affected by TSA treatment, we quantified the changes of all proteins rather than only focusing on the ones that were significantly enriched on chromatin. An unsupervised clustering revealed a clear difference between chromatin assembled in the absence or the presence of TSA (Figure 3. 11. A). *We found 131, 224 and 270 proteins being enriched on chromatin upon TSA treatment and 195, 71 and 121 being reduced after 15, 60 and 240 minutes respectively* (Figure 3. 11. B).

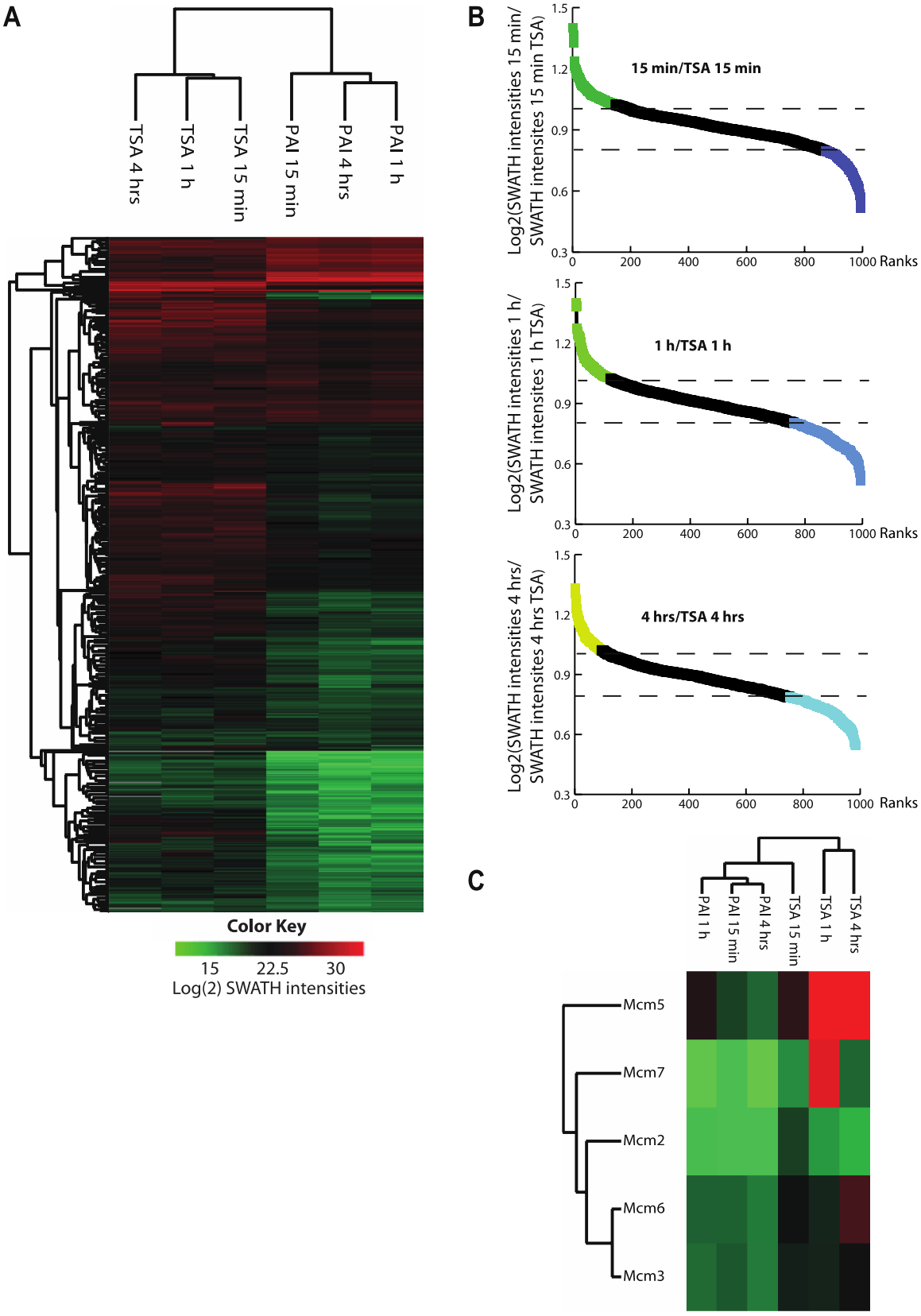

Figure 3. 11.: Challenge of chromatin assembly by means of chromatin decondensation.

A: Heatmap illustrating Log2(x)-transformed median-averaged SWATH intensities from three replicates after Euclidean clustering. Rows indicate proteins, columns represent different conditions of chromatin assembly for unperturbed assembly and TSA treated chromatin assembly for different time points. Red and green colours indicate SWATH intensities. (PAI: indicates assembly with 5S rRNA sequence without TSA treatment; TSA: indicates assembly with 5S rRNA sequence with TSA treatment).

B: Waterfall plots illustrate change between unperturbed assembly and TSA treated assembly. For each of the three time points, Log2(x)-transformed median-averaged unperturbed assembly replicates were divided by respective TSA treated assembly replicates. Proteins were sorted from largest to smallest quotient and plotted with a scatter graph tool. Proteins with values higher than 1 were regarded as enriched in unperturbed chromatin assembly. Proteins with values lower than 0.8 were regarded as enriched upon chromatin decondensation. GO term analysis of enriched proteins is depicted in Table 1, Appendix (Huang da et al., 2009a, b).
C: Heatmap illustrating Log2(x)-transformed median-averaged SWATH intensities from three replicates after Euclidean clustering. Rows indicate Mcm proteins, columns represent different conditions of chromatin assembly for unperturbed assembly and TSA treated chromatin assembly for different time points. Red and green colours indicate SWATH intensities (Völker-Albert et al., 2016).

A GO term analysis of the assembled chromatin in the presence of TSA suggested that the TSA treatment results in an increased association of factors that interact non-specifically with chromatin in comparison to the assembly reaction that is unperturbed (Table 1, Appendix), *which suggested a more open and hence more error prone chromatin assembly. Alternatively, the higher degree of non-specific binding could also be caused by a hyperacetylation and concomitant regulation of the multiple chaperones we found to be associated with in vitro assembled chromatin and whose job it may be to remove unwanted protein associations. We also found an increased binding of all subunits of the MCM helicase complex to chromatin that is treated with TSA* (Figure 3. 11. C), *which is interesting in light of earlier findings that show a general broadening of DNA replication and a more widespread binding of MCMs to replication origins in vivo when cells were treated with TSA (Kemp et al., 2005).*

3. 9. Inhibition of proteasome during *in vitro* assembled chromatin

3. 9. 1. Proteasome inhibition changes chromatin assembly proteomics

Chromatin (re-)assembly occurs after processes like DNA replication, transcription and repair for which the DNA was made accessible. During these processes, DNA becomes accessible and can bind non-specifically to a multitude of proteins that have a low to moderate affinity to DNA. If this accessibility of chromatin is enhanced by HDAC inhibitor treatment, even more unspecific protein binding could be observed *in vitro* (see paragraph above) and *in vivo* (Alabert et al., 2014; Sirbu et al., 2012). Moreover, the interference with chromatin assembly by stalling replication forks results in a disturbed inheritance of histone marks bearing the danger of losing epigenetic information (Jasencakova et al., 2010).
It is therefore fair to assume that quality control mechanisms exist, which prevent, recognise and correct errors during chromatin assembly. As the proteomic composition of newly assembled chromatin *in vitro* and *in vivo* revealed the proteasome as one of the most abundant

and best correlating complex, the *in vitro* system was used to investigate the effects of proteasome inhibition on chromatin assembly.

To do this, chromatin assembly experiments were performed in the presence of two UPS-system inhibitors. MG132 is a peptide aldehyde, which effectively blocks the proteolytic activity of the 26S proteasome complex, being a potent inhibitor of its chymotrypsin-like activity (Lee and Goldberg, 1998). Additionally, NEM is an irreversible inhibitor of deubiquitinases UCHL5 and USP14, which are localized in the 19S regulatory particle. Together, the addition of both inhibitors led to an effective block of the UPS-system. Since MG132 was dissolved in DMSO and NEM was dissolved in EtOH, all "unperturbed" samples have been supplemented with the respective amounts of DMSO and EtOH.

First, it can be observed that there was a low background binding of proteins to the "beads-only" control, in which no DNA has been immobilized to the beads (Figure 3. 12. A). Upon addition of proteasome inhibitors, more proteins bound to beads carrying immobilized DNA. Especially after 4 hrs of assembly in the presence of inhibitors, the chromatin was completely occupied with proteins. These results were verified by SWATH-MS analysis.

Chromatin was assembled within three biological replicates for the time of 15 min, 1 h and 4 hrs either in the presence or the absence of proteasome inhibitors. All samples were subjected to SWATH-MS analysis. By means of unsupervised Euclidean clustering of all quantified proteins, the heatmap clustering resembled the results of the silver stained gel (Figure 3. 12. B).

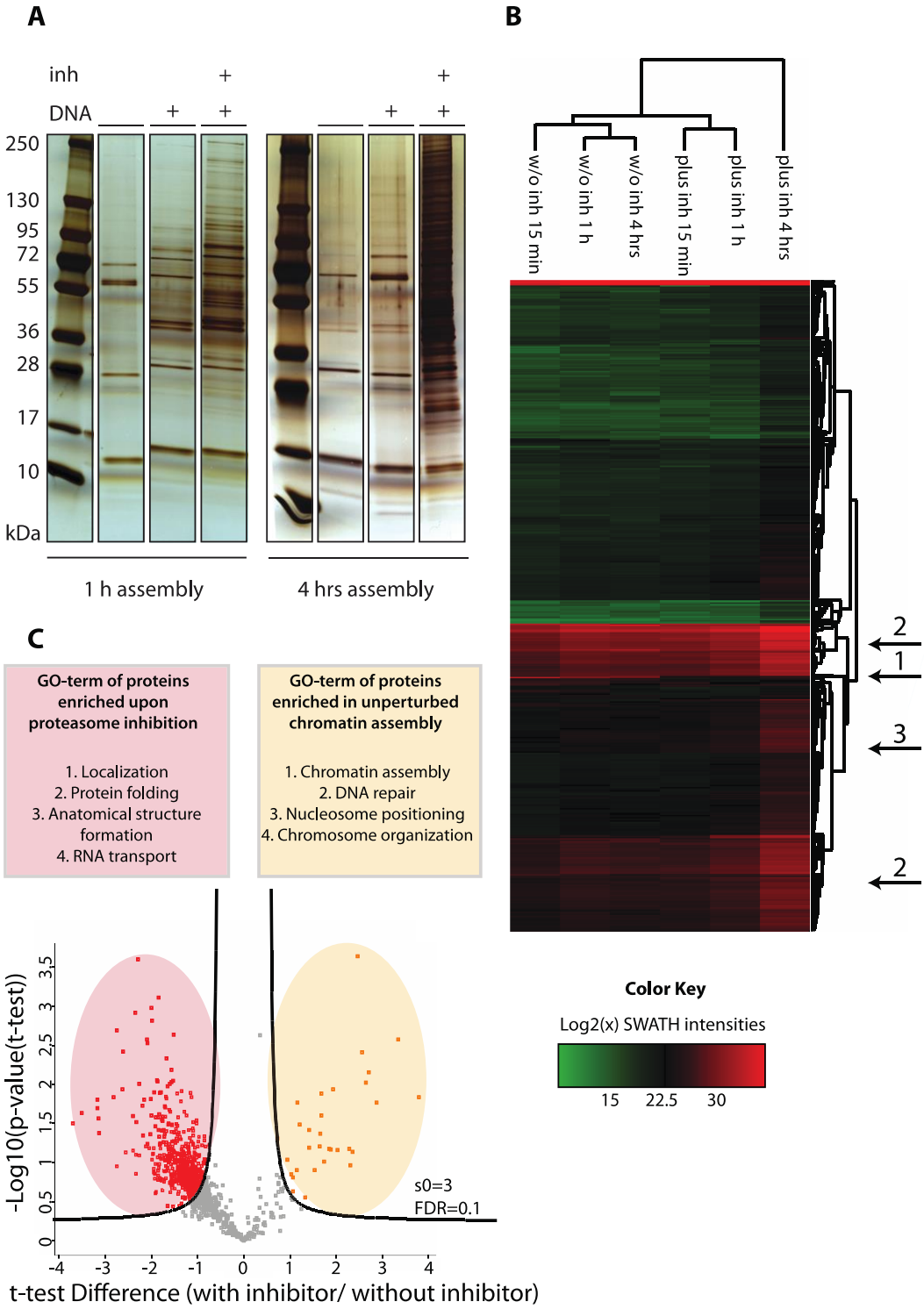

Figure 3. 12.: Proteomic analysis of proteasome-inhibited chromatin.

A: Representative silver gel lanes are shown of assembled chromatin for 1 h and 4 hrs. Negative controls were beads incubated with DREX without immobilized DNA. Beads with immobilized DNA and MG132/NEM are indicated with "+" symbols in "inh" line.
B: Euclidean clustering of mean-averaged Log2(x) SWATH intensities of three biological replicates of assembled chromatin for three time points. The addition of proteasome inhibitors is indicated by the addition "plus", whereas "w/o" means "without inhibitor treatment. Numbered arrows indicate clusters of proteins.
C: Volcano plot illustrating the results of a two-sample t-test comparing samples from unperturbed chromatin assembly to proteasome-inhibited chromatin assembly. Red dots show significant enriched proteins upon proteasome-inhibited chromatin assembly. Orange dots depict proteins enriched in unperturbed chromatin assembly. For GO-term analysis of respective proteins the open software "GO term finder" (Boyle et al., 2004) was used (threshold: p = 0.1 (FDR from permutation) and s0 = 3).

The heatmap clustered according to the inhibitor treatment and not primarily according to the time points. Therefore, it can be concluded that the inhibition of the proteasome changed the protein composition of chromatin at each observed time point.

It is worth mentioning that the 4 hrs assembled chromatin upon proteasome inhibition clustered separately (cluster tree of “plus inh 4 hrs” is separated from other trees) and was not related with the other time points upon proteasome inhibition. As observed in silver stain gel analysis, much more proteins were bound to chromatin after 4 hrs compared to 1 h of assembly upon proteasome inhibition. A very small subset of proteins that was bound to chromatin in unperturbed experiments was repelled from chromatin upon proteasome inhibition (Figure 3. 12. B, indicated with arrow 1). Some of the proteins that were bound to chromatin during unperturbed assembly showed higher abundances after proteasome inhibition (Figure 3. 12. B, indicated by arrow 2). Additionally, some proteins were only bound to chromatin upon proteasome inhibition (Figure 3. 12. B, indicated by arrow 3).

To investigate protein categories that specifically bound to chromatin when the inhibitor was present, a two-sample t-test revealed a high number of proteins being significantly enriched to chromatin upon proteasome inhibition. Similar to results from TSA inhibitor experiments, GO-term analysis annotated these proteins with functions for “localization”, “protein folding”, “anatomical structure formation” and “RNA transport”. These terms did not reflect expected GO-terms during chromatin assembly. However, proteins specifically enriched in unperturbed experiments showed GO-terms describing functions during chromatin assembly such as: “chromatin assembly”, nucleosome positioning”, “DNA repair” or “chromosome organization”. This list of proteins also contained proteins as ISWI subunits, CAF subunits, RPA and RFC proteins as well as PCNA.

This observation supports a hypothesis in which the proteasome functions as a quality control system to ensure proper chromatin assembly. As soon as the proteasome is inhibited, unspecific proteins can bind and occupy chromatin.

To understand the regulation of proteins by the proteasome during chromatin assembly, protein binding kinetics in both experimental conditions were compared.

3. 9. 2. Changes of protein binding kinetics during chromatin assembly upon proteasome inhibition

To investigate the proteasome-mediated regulation of protein binding to chromatin, kinetics of protein association during the time course of chromatin assembly were measured. As described previously, early, constant and late binding proteins could be discriminated according to their SWATH Log2(x) ratios after 15 min assembly divided by 4 hrs assembly.

Figure 3. 13. shows two waterfall plots, in which the upper waterfall plot illustrates binding kinetics of unperturbed chromatin assembly and the lower visualizes binding kinetics upon proteasome inhibition.

In both waterfall plots, the labelling of “early”, “constant” and “late” binding proteins is identical to the classification established in Figure 3. 5. D, based on unperturbed experimental conditions. Proteins were classified as “early” with a Log2(x) ratio higher than “1”. Constant binding proteins were classified with Log2(x) ratios between “1” and “-1”. Late binding proteins had Log2(x) ratios below “-1”.

Upon proteasome inhibition, much more proteins showed negative Log2(x) ratios. Moreover, some of the formerly early binding proteins became constant or even late binding. Examples are PCNA and subunits of the RFC complex. In contrast, formerly late binding proteins such as RPA and other DNA repair factors were found with positive ratios higher than 1.0 meaning that they would be classified as early binding upon proteasome inhibition.

In the case of the histones, some variants stayed as constant binders as for example H2A and H2B but others as H3 and H4 became early binding. This difference in the kinetics could be also observed for other DNA replication and chromatin assembly factors like the largest subunits of CAF.

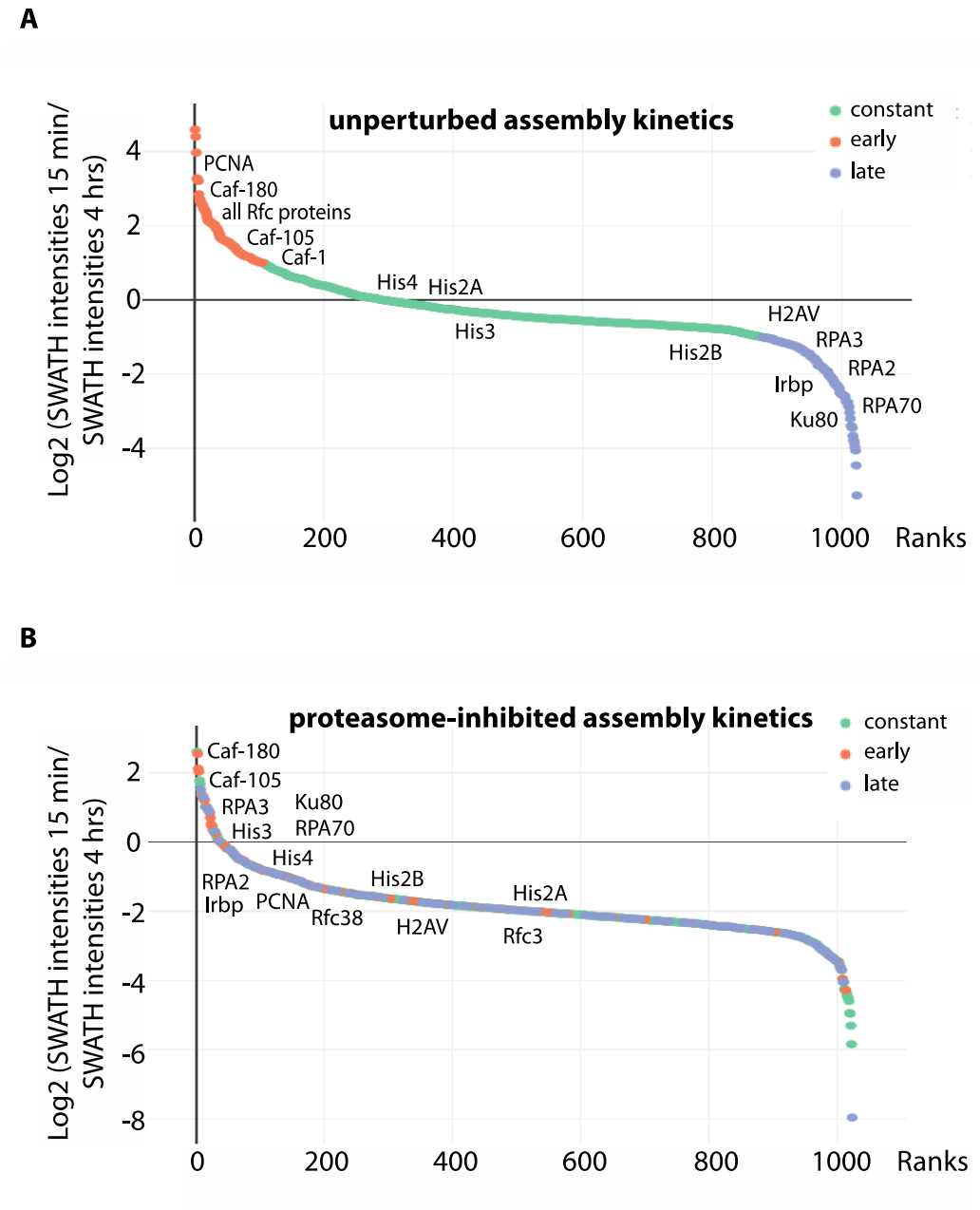

Figure 3. 13.: Change of binding kinetics upon proteasome inhibition.

A: Figure 3. 5. D, for comparison displayed here again.
B: Waterfall plot generated as in Figure 3. 5. D using SWATH intensities upon proteasome inhibition. Proteins of interest are depicted. Early, constant and late binding classification was used from unperturbed experiments.

Taken together, proteasome inhibition changed the overall protein binding kinetics during chromatin assembly. In particular, it influenced binding of chromatin assembly factors. Some factors became constant binding proteins, others became even earlier binding proteins compared to their former binding kinetics.

These proteomic results raised questions whether any protein kinetic changes upon proteasome inhibition influence DNA topology and/or the incorporation of nucleosomes. Therefore, additional biochemical assays were performed.

3. 10. Chromatin reprogramming influenced by proteasome inhibition

Protein binding to DNA can change DNA topology and chromatin composition. Many mechanisms can lead to an altered DNA topology, either by chromatin remodelling, exchange of histone variants, transcriptional regulation, DNA repair and many others. Therefore, it was of special interest, whether the topology and accessibility of chromatin changes upon proteasome inhibition.

To assess chromatin formation, a supercoiling assay in the presence and absence of proteasome inhibitors was performed. In general, a supercoiling assay visualizes the incorporation of nucleosomes in a DNA molecule. Furthermore, this assays also provides information about the DNA topology and the change of DNA topology upon nucleosome incorporation. This assay was based on the incubation of circular plasmid DNA (1 µg) with 2 mg Drosophila extract in the presence of 6.5 mM $MgCl_2$ under standard conditions at 26 °C. After various time points, 40 µl aliquots were removed from the reaction and assembly was stopped by the addition of 10 µl stop mix. The suspension was subjected to RNase A and proteinase K treatment and precipitated DNA was separated on a 1.3% agarose gel. A 100 bp ladder was used as a size marker.

Migration position corresponding to relaxed DNA (rel), nicked DNA (nc) and supercoiled DNA (sc) are indicated (Figure 3. 14.). The slow migration form or relaxed DNA at early time raised from the action of topoisomerases in the extract that relaxed the initially negatively supercoiled plasmid (0’ min). Progressive supercoiling was detected with the appearance of topological intermediates and an accumulation of fast migrating forms corresponding to the position of fully supercoiled DNA in the absence of proteasome inhibitor. Upon proteasome inhibition, overall similar progressive supercoiling occurred, however topological intermediates and fully supercoiled DNA were detected at earlier time points than compared to the unperturbed reaction.

These observations would argue for a faster chromatin assembly at early time points and a quicker recruitment of chromatin assembly factors to chromatin upon proteasome inhibition.

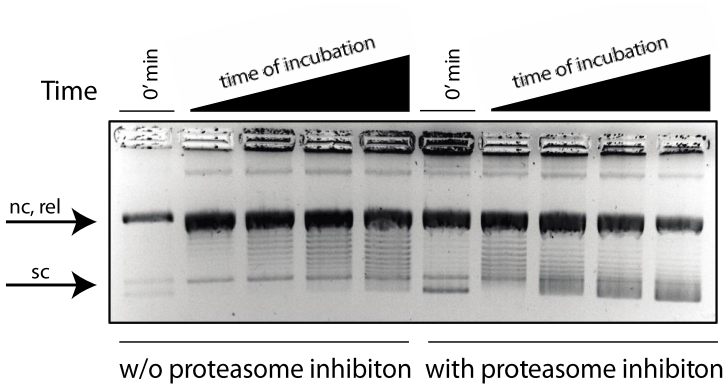

Figure 3. 14.: Supercoiling assay.

Circular DNA was incubated with Drosophila extract and the reaction was stopped at time points 0 min, 10 min, 30 min, 60 min and 120 min. Nicked (nc), relaxed (rel) and supercoiled (sc) DNA is indicated. Reactions were performed in the presence or absence of proteasome inhibitor (w/o: without).

In summary, the proteasome seems to be involved in chromatin assembly with effects on DNA topology and altered protein binding kinetics upon proteasome inhibition. To investigate these effects further, the *in vitro* reconstitution system was used and combined with MNase digestion experiments, macroscopic and microscopic analyses.

Linearized and biotinylated DNA was immobilized on streptavidin-coated, paramagnetic beads and incubated with Drosophila embryo extract with or without proteasome inhibitors. Additionally, 2 µg of DNA were reconstituted into chromatin by an incubation for indicated times at 26 °C with 40 µl of Drosophila embryo extract with and without proteasome inhibitors (Figure 3. 15.). This reconstitution was then digested with MNase for 30 s, 90 s and 240 s. Parts of this reconstitution were investigated with a microscope.

At the start of assembly, beads were suspended in solution with Drosophila extract and showed a uniformly brown suspension. After 15 min of chromatin assembly, small aggregates became visible upon proteasome inhibition (Figure 3. 15., panel "microscopic analysis"). After 180 min of assembly more pronounced effects of aggregate formation became visible in the microscopic analysis. Aggregates formed larger structures and grew also in number.

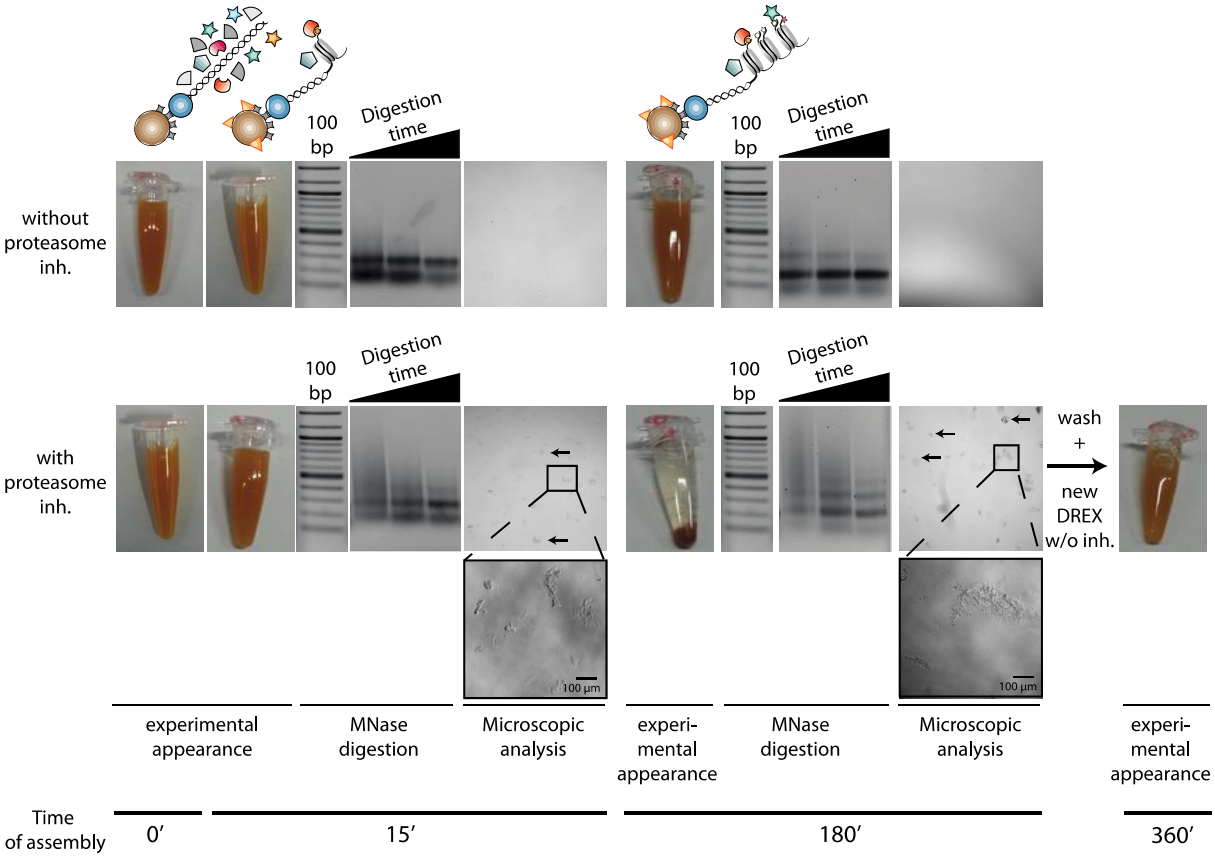

Figure 3. 15.: Chromatin reprogramming.

Time of assembly indicates the duration of chromatin assembly *in vitro*. The experimental appearance shows how the suspension within each tube looked like throughout the experiment. "MNase digestion" illustrates the MNase digestion pattern of chromatin assembled for indicated time points. Three lanes show results of MNase digestion for 30 s, 90 s and 240 s respectively. Microscopic analysis shows two magnifications of *in vitro* assembled chromatin for indicated time points. Arrows indicate aggregates in solution at a magnification of 4x. Zoom pictures show structures at magnification of 20x with light microscopy in Brightfield modus. Scale bars indicate the equivalent length of 100 µm.

Furthermore, the paramagnetic beads formed no longer a smooth suspension after 180 min of chromatin assembly and a phase separation effect was observed (Figure 3. 15., lower panel: "experimental appearance"). Upon proteasome inhibition, the MNase digestion pattern showed longer arrays of regularly spaced nucleosomes after 180 min of assembly when compared to an untreated reaction (Figure 3. 15., "MNase digestion").

This aggregation was reversible as the aggregated beads formed a smooth suspension upon removal of the inhibitors and resuspension in fresh embryonic extract. Presumably, the different MNase digestion patterns upon proteasome inhibition were due to this change in conformation, as the MNase enzyme might be partially inhibited to access the DNA. Similar effects have been observed (Schubert et al., 2012).

All observed effects were DNA-dependent. Figure 3.16. shows results from experiments with "only-beads" controls highlighting that aggregation only occurred in the presence of

proteasome inhibitors and immobilized DNA. All other control experiments did not show any aggregation verifying that DMSO and EtOH addition did not cause aggregation.

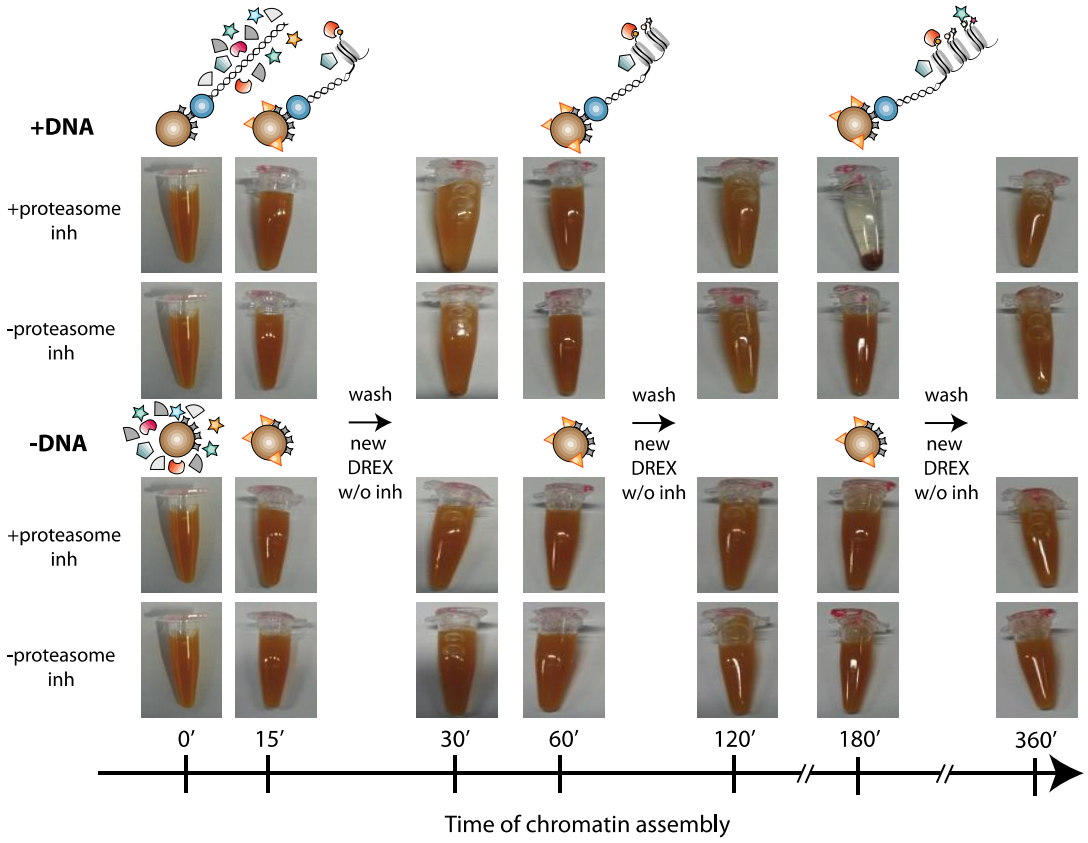

Figure 3. 16.: Bead-aggregation is DNA-dependent.

Time of assembly indicates the duration of chromatin assembly *in vitro*. Beads were either immobilized with DNA or without DNA indicated as (+DNA) or (-DNA). Each condition was then incubated with proteasome inhibitors (+proteasome inhibitors) or with respective amounts of DMSO and EtOH (-proteasome inhibitors). Chromatin was assembled for 15 min, 60 min and 180 min. At each time point, pictures were taken and beads were washed twice with Ex200. Then new DREX without inhibitors was added for the same amount of time for assembly than before (w/o: without), (inh: inhibitor).

4. DISCUSSION

4. 1. Complementary techniques for the investigation of chromatin assembly

The combination of an *in vitro* chromatin reconstitution assay, *in vivo* nascent chromatin capture and mass spectrometry techniques is a powerful approach to investigate the kinetics of chromatin assembly. The results of this thesis show that the advancement of experimental techniques such as NCC and the subsequent proteomic approach with DIA methods provide new avenues for the investigation of replication-dependent chromatin assembly. The first part of this chapter discusses technical aspects of the applied systems and future directions for chromatin assembly analysis.

4. 2. Reproducibility and validation of assembled chromatin

Mass spectrometry as a highly sensitive and precise technology can reveal experimental variations in sample preparation as well as within a mass spectrometer. Therefore, it is important to control for the comparability between experimental setups and between the settings of the mass spectrometer. One strategy to measure any variation within sample preparation is the application of biological and technical replicates. By comparing biological replicates, biological variability within the experiment can be determined. Technical experiments can reveal differences in handling and performance between each set of experiments.

The present study started with the exploration of the kinetics of chromatin assembly within three biological replicates. By measuring the proteome of crude extracts on the mass spectrometer in DDA-MS mode, all three replicates showed an overlap of 54.2%. The proteome of chromatin that was assembled by means of *Drosophila melanogaster* extracts showed similarity in 58.2% of all proteins between all three biological replicates. These percentages can be explained by the fact that all biological replicates have been performed with individually collected Drosophila extracts. These values are in line with comparable studies using proteomics to investigate proteins at replication forks. NCC experiments analysed with DDA-MS identified 3995 proteins in total (Alabert et al., 2014). Of these almost 4000 proteins, 53.2% (2125 proteins) were detected in all three replicates. The application of click-chemistry based EdU (5-ethynyl-2’-deoxyuridine)-labelling of nascent chromatin combined with mass spectrometry (iPOND) showed an overlap of only 18.4% between three biological replicates out of a total number of 1223 proteins identified (Lopez-Contreras et al., 2013).

This means, that our analysis of *in vitro* assembled chromatin by means of DDA-MS is comparable with similar chromatin assembly studies in terms of reproducibility. Nevertheless, it symbolises that DDA-MS suffers from a problem of missing values that need to be imputed to make statistically valid statements about protein association.

4. 3. Critical assessment of mass spectrometry approaches

Traditionally, shotgun proteomic approaches target stochastically the top N ions (N=10-20) at each time point of the analysis for fragmentation and further post-analysis peptide identification. Despite major improvements to increase the number of identified peptides and the reproducibility of these identifications, this approach shows low reproducibility between biological methods, which is often due to instrumental limitations and results in a maximal overlap between two replicates of approximately 60% of proteins.

Quantification of proteins is either based on the number of peptides belonging to a certain protein (spectral counting) or the intensity of a peptide ion over retention time (intensity based quantification). In both cases, only peptides that are fragmented can be afterwards quantified. Therefore, DDA methods present an inherent tendency to lose quantitative information, hence limiting the statistical power of the experiment as described in the paragraph above.

Among the strategies that have been proposed to overcome this problem is the bioinformatic feature within the MaxQuant software tool to "match identifications between runs" (Cox and Mann, 2008; Tyanova et al., 2016). To still identify features in a run with insufficient information, MS/MS and sequence information can be obtained from another run by matching within tight mass and retention time windows. Therefore, both runs are aligned according to their retention times and then the identification(s) are transferred from the run containing the necessary information to the run with insufficient information (see also Figure 1. 6. panel b). This alignment is based on very robust retention times in all runs that need to be compared. In addition, this feature relies on the identification of a peptide in at least one run and is still more a comparison than a clear identification.

To circumvent this issue, targeted approaches have been developed where particular signature peptides of a given protein are repeatedly selected for fragmentation irrespectively of their abundance. The fragmented peptides are then quantified by measuring the intensity of selected fragment ions that are generated when fragmenting a particular ion. This strategy, which is called selected reaction monitoring (SRM), allows the precise and reproducible quantification of up to several 100 proteins over a large dynamic range even in very complex mixtures (Picotti et al., 2009). However, the number of peptides and proteins that can be measured is limited by

the duty cycle of the mass spectrometer. The duty cycle is the proportion of time during a device or system is usefully operated. In terms of mass spectrometry, the duty cycle describes the percentage of time in which a particular ion is getting through the quadrupole and reaching the detector (Canas et al., 2006).

Recently, DIA techniques as SWATH-MS or PRM (Gillet et al., 2012; Peterson et al., 2012) have been developed that allow a precise and reproducible quantification of several thousand proteins in a single analysis run. This is achieved by fragmentation of all ions during an LC-MS run by selecting defined mass windows of fragmentation and a fast cycling through the whole mass range. Similar to the SRM methods, the resulting fragment ions can then be used for quantification. The short duty cycle of a QTOF instrument allows a reliable quantification due to a high number of MS/MS data points over a chromatographic peak. Moreover, as all ions are fragmented, SWATH analyses essentially generate a digital footprint that can be analysed and quantified in retrospect. Nevertheless, DIA is limited to a dynamic range of 4-5 orders of magnitude and it requires the *a priori* construction of fragment ion spectra libraries for the query peptides to deconvolve these peptides from the DIA data (Aebersold and Mann, 2016; Rosenbeger et al., 2014; Röst et al., 2014; Tsou et al., 2015).

Future applications will include hybrid methods of DDA and DIA as well as completely new methods. For instance, recently it has become possible to store several precursor ions in parallel in a trapped-ion mobility device, which can then be followed by serial fragmentation known as "parallel accumulation-serial fragmentation (PASEF) (Meier et al., 2015). This method promises to increase the speed and sensitivity of fragmentation several folds.

Additionally, it has been shown by comparing 'peptide-centric' query tools to 'data-centric' approaches, that bioinformatic tools will further improve quantification in label-free quantification (Navarro et al., 2016). In the special case of SWATH-MS, some tools use tandem MS (MS/MS) libraries to extract groups of signals that reliably represent a specific peptide together with statistical methods to distinguish true from false matches. Alternatively, DIA-Umpire assembles 'pseudo'-MS/MS spectra that can be identified and quantified with conventional database-searching and protein-interference tools without an assay library (Tsou et al., 2015). All in all, further usage and increasing experience of SWATH-MS will show, which analysis tools are best-suited for which kind of experiments.

Finally, the quantification of multiple proteins by SWATH-MS relies on stable retention times of individual proteins. In this study, peptide prefractionation for a subsequent MS analysis (LC-MS/MS) was exclusively done on nano LC systems using columns with an inner diameter of 75 µm. Although this set up offers the highest possible sensitivity, it suffers from poor retention

time stability and long separation times. Future studies could use micro LC systems that offer higher flow rates, shorter separation times and more stable retention times to shorten the measurement time required.

4. 4. Exploration of sample preparation methods

At the beginning of this study, several sample preparation protocols were tested to evaluate best conditions for subsequent MS analysis. Classical sample preparation uses an in-gel digestion protocol (Lu and Zhu, 2005; Shevchenko et al., 1996). For this method, proteins are first separated using SDS-PAGE to reduce the complexity of the proteome. The gel lane is then cut into pieces and the proteins in these gel slices are digested with trypsin within the gel. The resulting peptides are then extracted from gel pieces and analysed using LC-MS/MS. An advantage of in-gel digestion is the analysis of the protein amount in a sample via the Coomassie staining before further procedures. However, the in-gel digestion is relatively time consuming, SDS contamination of MS samples needs to be tidily controlled and in the specific case of this work, the yield of in-gel digestion was low.

In contrast to in-gel digestion, proteins can be also prepared for MS analysis by means of in-solution digestion (Washburn et al., 2001). In this case, chaotropic reagents like urea and thiourea are used to denature proteins to make them more accessible for protease digestion. All further steps are performed in the same tube to reduce any protein/peptide loss. A critical step in this protocol is the digestion by trypsin because the denaturating agent needs to be diluted to a concentration in which enzymes are functional to digest proteins into peptides. Experiments throughout this work showed, that this relatively quick protocol revealed best results in terms of identification and quantification.

The more recently developed method of ‘filter-aided sample preparation’ (FASP) (Manza et al., 2005; Wisniewski et al., 2009), combines advantages of both above-described methods. Samples are solubilised in SDS and further processed in an ultrafiltration device to remove detergents and other reagents. This approach combines many advantages of a time-reduced protocol, SDS solubilisation and filter-assisted cleaning. Nevertheless, elution and subsequent quantification did not reach same levels as in-solution digestion in this study. Therefore, all MS samples have been prepared by means of in-solution digestion.

Recently, new approaches have been shown to develop sample preparation further in terms of time and quality. On the one hand, pipette tip based methods (Kulak et al., 2014) have been shown to massively improve sample preparation by shortening and simplifying current protocols. Sample preparation kits combine lysis, denaturation, reduction and alkylation in one

step. These kits also reduce the time required for protease digestion to one hour. Finally, the peptide purification results in a ready-to-measure sample in reproducible quality. On the other hand 'Gel-assisted sample preparation' (GASP) is based on copolymerization of proteins with acrylamide facilitating denaturation, reduction, quantitative cysteine alkylation and matrix formation (Fischer and Kessler, 2015). This method combines advantages of in-solution and filter based methods being a further development towards sample preparation.

4. 5. DNA sequence dependency of chromatin assembly

The proteomic analysis of *in vitro* assembled chromatin depends on many parameters such as assembly time, washing conditions and the type of immobilized DNA within this assay. To study the contribution of particular sequences to chromatin assembly, two DNA sequences have been compared in this work. Data gathered from the DNA sequence containing bacterial vector DNA and repeats of the 5S rRNA nucleosome positioning sequence were related to those from a plasmid containing repetitive heterochromatic DNA (four copies of the 359 bp repeat from *Drosophila melanogaster*).

The current understanding comprehends that heterochromatin formation is – with some exceptions to point centromeres of budding yeast – independent of the underlying DNA sequence (Furuyama and Biggins, 2007; Grewal and Jia, 2007).

Because no major differences in the proteome were observed when using the two DNA sequences for assembly, it can be concluded that the early extract does not differentiate between different DNA sequences. However, a small subset of proteins was significantly enriched during the assembly of the 5S rRNA repeat sequence compared to the plasmid containing repetitive heterochromatin sequences. These proteins like Gnf-1, Caf-105 and Rpa70 have well-described functions during DNA replication. In addition, some proteasome subunits (Rpn12, Prosbeta5) were also significantly enriched to the 5S rRNA repeat sequence. Since only single subunits of replication- and degradation complexes were enriched to the 5S rRNA repeat sequence, it must be further investigated whether these subunits are functional and their association biologically relevant.

In contrast, proteins binding preferentially to the heterochromatic sequences harbour cytoskeletal functions within a cell (Bap55, Nup93-1, Klp61F). Other enriched proteins on the heterochromatic sequence have unknown functions and their detection could be a starting point for further experiments to elucidate their working mechanism.

The fact that no major differences in the proteome were observed when using the two DNA sequences for assembly may be due to the embryonic Drosophila extract and its potential to

form heterochromatin. It could be that the composition of the DREX may not allow full maturation of heterochromatin: In early stages of development, nuclei of the syncytial embryo divide every 9 min (Becker and Wu, 1992). Considering an average time of 20 min, which is required for the full maturation of chromatin after DNA synthesis (Worcel et al., 1978) chromatin may not reach a fully mature state during early development. Although maternally provided, the pool of factors hence may, in a developmental context, not be suited to constitute functional heterochromatin. Although *in vitro* chromatin reconstitution was performed for up to 4 hrs, it could well be that other cellular processes like DNA repair, replication and cellular division require all resources of the extract with the result that heterochromatin formation is diminished. In addition, it could be assumed that heterochromatin formation depends on *in vivo*-like circumstances and is not able to be achieved in an *in vitro* setup based on Drosophila extracts.

Connected with that, it is conceivable that the *in vitro* assembled chromatin on the 359 bp repeats harbours certain proteins, which can facilitate heterochromatin formation only at specific developmental time points. The phenomenon of heterochromatin spreading functions in a hierarchical manner and involves self-promoting feedback loops. Factors involved in these processes are SUV39H1, HP1 and CAF that have been found to bind to both sequences. However, further investigations are needed to confirm their function and their subsequent effect on the underlying DNA sequence. Those experiments would rely on the incubation with nuclear extracts from more mature embryos (0-12 hrs) with chromatin that was either preassembled using early embryo extracts (0-1.5 hrs) or by salt dialysis using purely recombinant histones or histones derived from Drosophila embryos.

4. 6. A detailed proteomic analysis of chromatin assembly

As shown in this work, the combination of label-free proteomics with a well-described *in vitro* chromatin assembly system enabled a comprehensive quantitative analysis of the proteome of *in vitro* assembled chromatin. The subsequent comparison of these *in vitro* data with label-free proteomics of *in vivo* assembled chromatin showed that the *in vitro* system resembled many aspects of replication-dependent chromatin synthesis *in vivo* and can therefore be used to dissect key regulatory steps in chromatin assembly. Functional studies by means of inhibitor treatment and the temporal kinetics in both systems describe the kinetics and maturation process of chromatin assembly at an unprecedented depth. The second part of this chapter focuses on a discussion of biological aspects and their implication for future experiments.

4. 7. Comparison *in vitro* and *in vivo*

4. 7. 1. Proteomic coverage between *D. melanogaster* and *H. sapiens*

The use of a deep high-quality ion library generated from the chromatin assembly extract and the chromatin-bound factors enabled us to determine the kinetic of chromatin binding for 480 proteins highly enriched in chromatin. Due to the fact that the in vitro extract is prepared from Drosophila and the nascent chromatin capture has been performed in human cells, the orthologous proteins between *Drosophila melanogaster* and *Homo sapiens* needed to be determined firstly. By using the BioMart tool from the Ensemble software, it was possible to retrieve all orthologous genes between both organisms to find 116161 orthologous genes between *Drosophila melanogaster* and *Homo sapiens* (see section 2.2.7.: Software Methods/Software Packages/BioMart). This number contains “many2many”, “one2many”, and “one2one” orthologous genes. Orthologs are pairs of genes that started diverging by speciation. In this case, “many2many” describes an entry in the genome database that has more than one ortholog in *Drosophila melanogaster* and the orthologous entries have more than one ortholog in H*omo sapiens*. This implies that the gene was duplicated at least twice: In the lineage of Drosophilae as well as in humans. “One2many” orthologous genes have more than one ortholog in H*omo sapiens* but all orthologous entries have only one ortholog in *Drosophila melanogaster*. “One2one” orthologous genes are genes with exactly one ortholog between both species. Interested only in the “one2one” genes left 3171 genes that have been aligned to 13440 human proteins using the Uniprot database with ENSG annotation and 6056 fly proteins with FBgn annotation using the Flybase database.

The *in vitro* assay revealed 1025 proteins to be involved in chromatin assembly in total. 472 proteins out of the 1025 proteins had a clear ortholog in the human proteome and 374 of them (79%) were also detected in the NCC dataset.

Previous analysis focused on 480 proteins in the *in vitro* system that specifically assembled onto chromatin when compared to the negative control by a two-sided t-test. 216 proteins (out of 480) that specifically assembled onto chromatin had a clear "one2one" ortholog in the human proteome and 184 of them (85%) were also detected as chromatin-associated during nascent chromatin capture.

This supports the hypothesis that the general pathways for chromatin assembly are conserved among different eukaryotes. It is even more obvious comparing proteins from the crude extract to proteins enriched in chromatin assembly. The percentage of similarity increases and strengthens the idea that replication-coupled chromatin assembly is conserved among species.

4. 7. 2. Conservation of replication-coupled chromatin assembly

DNA as one of the most evolutionary conserved molecules needs to be replicated and segregated to assure proper cell division and growth. Any defect in DNA replication results in genomic instability and furthermore to premature aging and cancer. Therefore, it is plausible that factors involved in replication-dependent chromatin assembly are highly conserved. Some factors described in this thesis, such as PCNA and CAF show very similar behaviour between both investigated chromatin assembly systems, which proves earlier work by the Stillman group. They demonstrated that the CAF complex is composed of the three subunits (p48, p60 and p150) that are evolutionary conserved from yeast to humans. CAF preferentially deposits acetylated H3-H4 molecules onto replicated DNA (Kaufman et al., 1995; Kaufman et al., 1997; Verreault et al., 1996). In addition, it has been shown that the two largest subunits of the CAF complex (p150 and p60 in *Homo sapiens* and p180 and p105 in Drosophila) are required for efficient chromatin assembly *in vitro* in Drosophila and human systems (Kaufman et al., 1995; Tyler et al., 2001).

PCNA as a DNA polymerase processivity factor interacts with the largest CAF subunit, Caf-150 in human cells (Shibahara and Stillman, 1999) in chromatin reconstitution assays based on Xenopus egg extracts (Moggs et al., 2000) and in yeast co-immunoprecipitations (Krawitz et al., 2002; Zhang et al., 2000). Both factors (CAF and PCNA) bind to replication origins in an interdependent manner, suggesting that both factors rely on reciprocal action to fulfil their function during DNA replication-dependent chromatin assembly (Krawitz et al., 2002; Moggs et al., 2000).

4. 8. Compendium of *in vitro* and *in vivo* binding kinetics

Interestingly, not only the identity of the bound proteins is conserved but also their dynamics of binding. For example, multiple components of the replication machinery like the RFC clamp loading complex, PCNA, the single strand binding complex RPA, members of the MCM helicase complex and the subunits of chromatin assembly factor CAF1 were enriched at early time points of the assembly reaction, which is consistent with their enrichment in nascent over mature chromatin shown by NCC data. The possibility to perform measurements of all chromatin-associated proteins at three time points using SWATH based quantitation enabled the inclusion of an intermediate measurement of assembly (1 h) rather than only comparing nascent and mature chromatin. This dissection of the binding kinetics verifies earlier in vitro findings that the clamp loader complex first binds to the DNA and facilitates PCNA loading and then dissociates from the template upon loading of the sliding clamp leaving PCNA-bound to the template to stabilize the polymerase. So far, this loading event has only been characterised upon reconstitution in a highly purified system (Gomes et al., 2001; Hedglin et al., 2013). The fact that we observed a transient peak of PCNA at the intermediate time point during in vitro chromatin, which decreased substantially at late chromatin assembly resembling nascent chromatin findings (Alabert et al., 2014), suggests that this loading process is indeed occurring during chromatin assembly.

Nevertheless, this study compares two systems that are based on different organisms. Even though only orthologous proteins can be compared with this approach, many other parameters need to be considered.

The *in vitro* chromatin assembly is based on an extract from Drosophila preblastoderm embryos whereas NCC is performed in fully differentiated human cell lines. This means that developmental differences and programs could lead to variation of results comparing both systems. For example, the length of a cell cycle in differentiated HeLa cells usually lasts 24 hrs whereas the syncytial division of Drosophila embryos occurs every 9 min. Therefore, protein kinetics, protein complex formation and control mechanisms could differ a lot.

Moreover, the *in vitro* reconstitution assay was performed in a test tube to incubate the extract with immobilized DNA. Although initial experiments tested for best assembly conditions, it is difficult to resemble *in vivo* settings within the *in vitro* system in terms of dilution and other parameters. Especially the concentration of specific factors can vary between both systems and can alter binding behaviour and the formation of protein complexes.

Furthermore, the actual template for chromatin assembly differs between both systems. In the *in vitro* system, single-end-immobilized and unfolded double-stranded DNA was used for the

assembly of chromatin. In contrast, synchronized HeLa cells contained chromatin that replicated upon helicase opening. With respect to the accessibility of the DNA and the dimensions at the respective template, contrary results could be anticipated while comparing both experimental systems. In addition, the recruitment of factors for single-end-immobilized DNA could lead to higher affinity for DNA repair factors compared to the physiological condition during DNA replication in HeLa cells.

Finally, different binding kinetics of some replication-associated proteins between both systems could be caused by different replication speed in both experimental systems. It was shown that the majority of replication forks in various human cell lines travel between 1 and 2 kb min^{-1}, with an average of 1.5 kb min^{-1} (Conti et al., 2007; Hodgson et al., 2007). The rate for proper replication in chromatin *in vitro* has been determined to be 1.4 kb min^{-1}, which is very similar to *in vivo* rates (Kurat et al., 2017). This rate is highly dependent on the interplay between the replisome and FACT associated protein Nhp6, INO80 or Isw1a and lysine acetyltransferases (Kurat et al., 2017). In any case, the reconstituted replication rates *in vitro* resemble *in vivo* rates but are measured in conditions that do not resemble the Drosophila extract.

In summary, a plethora of parameters differ between both experimental systems and can explain variations in results. But especially with the knowledge of all possible differences, it is impressive to observe high similarities between protein binding kinetics. In particular, protein binding kinetics of chromatin-associated proteins show high similarities arguing for a strong conservation of these pathways between both species. Finally, it proves that both systems can be used to investigate chromatin assembly mechanisms.

4. 9. Inhibitor treatment effects during chromatin assembly

4. 9. 1. Inhibition of Histone deacetylases by Trichostatin A (TSA)

The fact that we found much more factors with no apparent chromatin function associated with chromatin upon TSA treatment suggests that chaperones may be required to prevent such proteins from binding to accessible (i.e. TSA treated) chromatin or remove mis-localised factors. This hypothesis would fit to previous findings that the formation of regularly spaced chromatin in vitro is entirely dependent on the presence of ATP (Becker and Wu, 1992; Bulger et al., 1995), which is a substrate of all nucleosome remodelling factors but also of the Hsp and TriC/CCT chaperones. Alternatively, chaperones might function in the remodelling of chromatin-bound multi-subunit complexes. This hypothesis is supported by findings showing

that molecular chaperones are responsible for the rapid exchange of hormone receptors during oscillating transcription (McNally et al., 2000; Stavreva et al., 2004).

To test whether we are able to investigate quantitative changes in the assembly kinetics of specific chromatin factors upon a challenge of the system, we added the broad histone deacetylase inhibitor TSA to a reaction and repeated the quantitative proteomic analysis of the bound proteins. We have shown in the past that TSA treatment results in a moderate increase of histone acetylation on assembled chromatin in contrast to what is observed in tissue culture cells where TSA treatment results in a strong hyperacetylation of histones (Bantscheff et al., 2011; Choudhary et al., 2009; Turner et al., 1989). During in vitro assembly, the histones are deposited in a preacetylated form, which will not get deacetylated when TSA is present (Scharf et al., 2009). TSA treatment has been shown to prevent the formation of transcriptionally repressed chromatin (Wong et al., 1998) in Xenopus oocytes and lead to an altered pattern of DNA replication origin activity in human tissue culture cells (Kemp et al., 2005). The exact mechanism of how TSA mediates these effects has so far remained unclear. Our finding that all MCM proteins, which are key regulators of eukaryotic replication having an increased binding to chromatin when TSA is present, provides a potential explanation for this finding. However, it remains to be determined whether this is an indirect effect of a more open chromatin structure or a direct effect that is mediated by MCM acetylation (Choudhary et al., 2009).

4. 10. Proteasome during chromatin assembly

4. 10. 1. Cellular and nuclear localization of the proteasome

The comprehensive quantitative analysis of *in vitro* and *in vivo* assembled chromatin revealed that some of the most abundant proteins within both systems belong to the proteasome (Figure 3. 10.). These data support findings reported in literature about the nuclear localization of the proteasome:

The nucleoplasm as well as the cytoplasm contains three distinct but functionally related proteasome particles (19S, 20S and 26S), which co-exist in equilibrium of assembled and disassembled subunits (Fabre et al., 2013; Hölzl et al., 2000; Kleinschmidt and Franke, 1982; Udvardy, 1993). The separation of the 26S proteasome into the 19S and 20S subcomplexes is ATP-dependent and it has been shown that re-addition of ATP to the 19S and 20S particles in cell extracts leads to the reformation of the 26S proteasome (Kleinschmidt and Franke, 1982). Presumably other factors are involved in this re-assembly but further experiments should test the specific proteins involved in this mechanism. Moreover, future experiments could test the

effect of ATP during chromatin assembly on proteasome activity. It would be interesting if inhibited proteasomes within the extract can be reactivated by the addition of ATP. But since ATP-utilizing chromatin remodelling enzymes have been shown to regulate chromatin (Becker and Horz, 2002; Clapier et al., 2017; Ito et al., 1997; Maier et al., 2008), it will be challenging to differentiate between ATP effects of ATP-dependent remodelling enzymes and the proteasome during chromatin assembly. Therefore, the addition of purified proteasome upon proteasome inhibition in the *in vitro* assay could give new insights into the reversibility of observed effects.

4. 10. 2. Functions of proteasome inside chromatin

Recent work on the UPS system factors and especially on the proteasome has revealed many effects on chromatin and its associated proteins. Quantitative proteomics data from this thesis confirm that all subunits of the proteasome were very abundant in all biological replicates. Furthermore, all proteasomal subunits highly correlated with DNA replication factors in both experimental datasets (Figure 3. 10., results), supporting earlier findings that chromatin-associated processes such as transcription, DNA repair and DNA replication are regulated by the action of the UPS system (Auld et al., 2006; Hoppe et al., 2000; Lafon et al., 2015; Lonard et al., 2000; Szutorisz et al., 2006).

Interestingly, recent studies showed that polyubiquitylation plays a key role in disassembly of the replisome machinery (Maric et al., 2014; Moreno et al., 2014). In both model systems (frog and yeast), one subunit of the replicative helicase (Mcm7) has been found polyubiquitylated with K48 linked chains upon replication fork termination. Further studies in Xenopus egg extracts have identified $CRL2^{Lrr1}$ as an E3 ubiquitin ligase that specifically attaches ubiquitin to Mcm7 (Dewar et al., 2017). This ubiquitylation is then followed by dissolution of the replicative helicase (CMG complex), which is dependent on the activity of the protein segregase, Cdc48/p97/VCP. The segregase is a homohexameric ring-shaped ATPase, which can recognise proteins modified with K48 linked ubiquitin chains and remodel them in an ATP-dependent manner (Peters et al., 1990; Rouiller et al., 2002). These factors have been also shown to be recruited to chromatin during assembly in the current work further supporting the power of the Drosophila *in vitro* assembly system as well as NCC *in vivo* experiments.

Taken together the above described points, it becomes clear that the proteasome has a pronounced function during chromatin organization and that it is an integral part for proper chromatin assembly. Therefore, the inhibition of the proteasome during *in vitro* chromatin assembly was a subsequent step in this work to elucidate the effects of the proteasome action

within chromatin maturation. Any inhibitor experiments in an *in vivo* setting are much more challenging since it is very difficult to separate indirect from direct effects due to the fact that the UPS is a major contributor to the degradation of cyclins and cdk regulators and hence has a major impact on the cell cycle (Bassermann et al., 2014).

4. 10. 3. *In vitro* inhibitor studies

To investigate any effects of the proteasome during chromatin assembly, proteasomes were inhibited with two inhibitors. MG132 is a peptide aldehyde, which effectively blocks the proteolytic activity of the 26S proteasome complex, being a potent inhibitor of the chymotryptic-like site (Lee and Goldberg, 1998). Additionally, NEM is an irreversible inhibitor of deubiquitinases UCHL5 and USP14, which are localized in the 19S regulatory particle. Future experiments should investigate additional inhibitors during chromatin assembly. For example, another widely used inhibitor is lactacystein discovered as the first non-peptidic proteasome inhibitor. It was shown that this inhibitor modifies the amino-terminal threonine of specific catalytic subunits of the proteasome to inhibit their function specifically (Gastaldello et al., 2008; Ni et al., 2008).

4. 10. 4. Effects of proteasome inhibition onto protein binding kinetics

The addition of proteasome inhibitors during *in vitro* chromatin assembly experiments showed effects on the binding kinetics of almost all proteins. Formerly early binding proteins became constant or even late binding proteins (PCNA, RFC complex subunits). These proteins could be putative targets of the UPS systems because the respective protein binding kinetics were altered upon proteasome inhibition.

A similar mechanism could explain the fact that formerly late binding proteins were found as early binding proteins upon proteasome inhibition (RPA, Ku80 and Irbp). These proteins could be constantly degraded by the proteasome during early assembly time points in unperturbed experiments. Once the proteasome was inhibited, these proteins were found as early binding proteins because of the lack of proteasomal regulation.

In contrast, the subunits of the CAF complex showed an irregular binding kinetic upon proteasome inhibition. The largest subunits Caf-180 and Caf-105 remained as an early binding protein upon inhibition whereas Caf-1 (smallest subunit) became a protein with negative ratio. In line with these findings, histone proteins 3 and 4 also became proteins with higher ranks whereas H2A and H2B were almost unchanged.

In general, chromatin-specific proteins tended to associate earlier to chromatin upon proteasome inhibition than compared to unperturbed experiments. However, this observation can be also based on the "ranking method".

For this method, Log2(x) ratios of each protein derived from its intensity after 15 min chromatin assembly divided by the intensity after 4 hrs chromatin assembly were ranked. The protein with the most positive ratio received the rank 1 and the protein with the most negative ratio received the rank N (N stands for the number of quantified proteins). Due to the ranking, there will be always proteins with high ranks independently of their actual ratios. In this work, Caf-180 and Caf-105 did still have high ranks upon proteasome inhibition but the overall ratio was lower upon proteasome inhibition than compared to unperturbed experiments.

In the presence of proteasome inhibitors, the majority of proteins accumulated to chromatin over time shown with silver gel and proteomic data. The accumulation led to higher values of respective proteins after 4 hrs of chromatin assembly and reduced the 15 min/4 hrs Log2(x) ratio of these proteins for the ranking method. Therefore, a general trend of reduced protein ratios became visible. But chromatin-specific proteins showed still highest ranks since they were presumably proteasome independent.

4. 10. 5. Non-proteolytic actions of the proteasome

In most cases, the function of the proteasome harbours proteolytic activities but other published data also suggest a non-proteolytic but more chaperone-like function of the proteasomal ATPases (Geng et al., 2012; Kaiser et al., 2000).

During the non-proteolytic action, the proteasome shields proteins from aggregation and refolds them back into the native state. As soon as proteins are not folded correctly, the proteasome will target them for degradation according to a "better safe than sorry"-principle, because aggregation or the accumulation of misfolded proteins leads to disorders such as cystic fibrosis. In cystic fibrosis, protein aggregates are sequestered into large aggregates called "aggresomes" (Johnston et al., 1998) because the cell's degradation capacity is over exceeded (Kopito and Sitia, 2000). These aggresomes are insoluble structures that are highly dependent on the action of cytoskeletal proteins that transport aggregated proteins to the aggresomes (Garcia-Mata et al., 1999). Purified aggresomes have been described to contain intermediate filament proteins like vimentin (Johnston 1998), proteasomal subunits (Garcia-Mata, 1999) and protein chaperones such as Hsp70/Hsp90. In particular vimentin and other filament proteins like actin and tubulin are necessary for aggresome formation to form a cage-like structure surrounding the aggresome for its stabilization (Johnston et al., 1998). In recent years, it became clear that

aggresomes contain a significant proportion of functional proteins and in addition it was observed that accumulation of misfolded proteins in aggresomes is a characteristic feature of many disorders (Corchero, 2016).

Examples of such proteins are the CFTR protein (fibrosis transmembrane conductance regulator) involved in cystic fibrosis (Johnston et al., 1998), the ALS-associated protein FUS forming liquid compartments *in vivo* and *in vitro* (Patel et al., 2015) and the chaperone and stress response protein Hsp70 with connections to Parkinson's disease (Ardley et al., 2004; Mishra et al., 2009).

Further evidence of massive chaperone activity during chromatin assembly is also given by the fact that many constant binding proteins and protein complexes involved in protein folding were identified such as *the TriC/CCT complex (Tcp1, TCPeta, TCPzeta, CG7033, CG8258, CCT5 and CCTgamma) or Hsp60 and Hsp70, being stably bound to chromatin during assembly. This binding of chaperone factors suggests that chromatin assembly is associated with extensive and continuous protein folding and refolding events. Although TriC/CCT has been suggested to be mainly involved in the folding of newly translated proteins (Dunn et al., 2001), there is increasing evidence that it has additional functions such as the prevention of the aggregation of poly-Q proteins (Shahmoradian et al., 2013) or the formation of macromolecular protein complexes in the nucleus (Doerks et al., 2002; Freund et al., 2014). The TriC/CCT complex can also be observed on nascent and mature chromatin in-vivo (Alabert et al., 2014) and in interphase chromatin (Kustatscher et al., 2014), which also supports its integral role in chromatin dynamics and metabolism. The function of these chaperones in chromatin has so far been enigmatic and no clear function was assigned to them.*

4. 11. Towards a model for proteasome action during chromatin assembly

4. 11. 1. The proteasome functions as protein-chaperone

One possible mode of action of the proteasome during chromatin assembly could be a chaperone-like function for low-complexity proteins that lack a well-defined 3D structure and are often named intrinsically disordered proteins (Uversky, 2002). Nowadays it becomes clear that theses unstructured domains of proteins are functional and often help in binding to biological targets or for the assembly of macromolecular arrays (Dyson and Wright, 2005). Molecular chaperones can facilitate the folding of unstructured proteins (Dyson and Wright, 2005). One of these chaperone molecules is also the proteasome.

The observation that aggresome formation is DNA-dependent supports the idea that functional unstructured domains of proteins are used to interact with the DNA. But once proteasome activity is reduced and chaperone activity is decreased, proteins aggregate at the DNA over time.

When analysing all chromatin-associated orthologous proteins during chromatin assembly *in vitro* and *in vivo* with a program for the prediction of unstructured regions from amino acid sequences (SLIDER: Super-fast predictor of proteins with Long Intrinsically Disordered regions) (Peng et al., 2014), the majority of proteins (70%) has scores higher than 0.5 (SLIDER score between 0 and 1 (the higher the more likely a protein has long disorder segment)).

One example is the Cul4B E3-ligase with a slider score of 0.8429. This E3 ligase could be regulated in a chaperone-like mechanism by the proteasome and as soon as the proteasome is inhibited, the protein is unfolded and not able to bind to PCNA. Therefore, it might bind with unfolded domains to the DNA and associates to chromatin unspecifically. This could explain its change in kinetics from a formerly constant binding proteins towards a late binding protein upon proteasome inhibition.

Surprisingly, ubiquitin, as a marker protein during degradation cascades, is not found in any experiment that has been performed. The fact that no ubiquitin is found during MS analysis could be due to a low abundance of ubiquitin. In general, this would argue for mainly non-proteolytic function of the UPS system during chromatin assembly. This is in line with the observation that many chaperone proteins are found in the assembly extract and protein aggregation occurs upon proteasome inhibition.

Additionally, it has been described that chaperones itself contain unfolded regions with which they bind to misfolded proteins and RNA molecules, such that they function as recognition elements and/or help in the loosening and unfolding of kinetically-trapped folding intermediates (Tompa and Csermely, 2004).

The interaction of proteins with other proteins and RNA requires a bimodal binding modus involving conformational changes (Leulliot and Varani, 2001; Williamson, 2000). This modus has been mainly observed for ribosomal proteins (Ban et al., 2000), the transcriptional antitermination protein N (Mogridge et al., 1998) and the HIV-1 REV protein (Battiste et al., 1996). In addition, proteins binding to RNA and interacting with other proteins are also described in dosage compensation. Dosage compensation describes the global activation of genes on the male X chromosome. The complex responsible for this up-regulation, MSL-DCC, consists of male-specific-lethal (MSL) proteins and two long, non-coding roX RNAs. One MSL

subunit of the complex, the RNA helicase MLE, incorporates roX into functional DCC (Maenner et al., 2013).

Another RNA-binding protein with bimodal functions is FUS. FUS contains intrinsically disordered domains and is prone to form aggresomes associated with the neurodegenerative disease ALS (Amyotrophic lateral sclerosis) (Patel et al., 2015). The FUS protein is also a RNA chaperone binding to folded RNA cognate intermediates to support RNA folding and biogenesis (Lagier-Tourenne et al., 2012; Wang et al., 2008).

Earlier work in our laboratory described a couple of factors that are recruited to chromatin by RNA to regulate higher order chromatin structures. The Drosophila decondensation factor Df31 binds to RNA and localizes to euchromatic regions. The decondensation factor is an intrinsically disordered protein that binds to snoRNAs that are known as RNA chaperones. This DF31-mediated linkage of RNAs and chromatin forms a RNA-chromatin network resulting in the establishment of open chromatin domains (Schubert et al., 2012).

All in all, the proteasome could function as a chaperone and our results implicate that the proteasome together with other abundant chaperones such as Hsp70 and the TriC/CCT complex supports major protein refolding during chromatin assembly *in vitro* as well as *in vivo*. Especially the aggregation of proteins in the absence of functional proteasome argues for a chaperone activity. But the proteasome is also well-known for its degradation activity that can have many influences during chromatin assembly.

4. 11. 2. The proteasome functions as protein degradation machine

Another mechanism by which the UPS system could regulate chromatin assembly is via degradation. The UPS system is a major regulator of proteins whose concentration must vary with time and alterations in the state of the cell cycle by means of degradation (Varshavsky, 2012). This role could be executed by the proteasome during chromatin assembly. The accumulation of proteins on chromatin over time upon proteasome inhibition would support this idea. But it is still not known whether the proteasome degrades proteins according to their concentration or whether the interaction with DNA is necessary for this action.

Instead of a chaperoning activity of the proteasome, the results of DNA-dependent aggregation could be also explained by the degradation function of the proteasome. Proteins bind to DNA and change their conformation. Upon conformational changes they are able to be ubiquitylated and targeted by the proteasome for degradation (Ulrich, 2014). According to this hypothesis, an alternative mechanism for the regulation of PCNA and Cul4B by the proteasome could be proposed. Cul4B regulates PCNA for degradation as soon as it binds DNA. Then PCNA is

degraded and appears therefore as early binding protein. Once the proteasome is inhibited, PCNA is not degraded anymore and becomes a constant binding protein having still a low positive ratio. The fact that it is only occurring at DNA could be due to a conformational change upon DNA binding of PCNA.

To investigate this idea further, proteins in the assembly system were checked to be ubiquitinated or not. The analysis of ubiquitinated proteins via a MaxQuant search for modified peptides with a GlyGly modification revealed that mainly chromatin unspecific proteins were identified (Table 2, Appendix). These findings support the role of the proteasome as degradation machinery of unspecific interactors during chromatin assembly.

An additional assumption that would support a working model for a role of proteasomal degradation during chromatin assembly is the presence of proteins containing specific degrons that serve as docking platforms for proteasome action.

Ubiquitin is a 76-residue protein that mediates proteolysis to proteins containing primary degradation signals, called degrons. Therefore, all analysed peptides have been searched for a so-called PIP-degron (PCNA-Interacting Protein motif) that has been shown to facilitate protein-protein interaction but also degradation of respective proteins (Arias and Walter, 2006; Varshavsky, 1991). The degron describes a sequence of 8 amino acids in which the first amino acid needs to be Glutamine (Q). The second and third amino acid can be any possible amino acid in any possible combination. The fourth amino acid needs to be hydrophobic (L, I, M, V) but without any given order. This is followed again by two amino acids of all possible amino acids. Seventh and eighth amino acids need to be an aromatic amino acid (F, Y or W) but without any special order resulting in the following order Q-x-x-h-x-x-a-a.

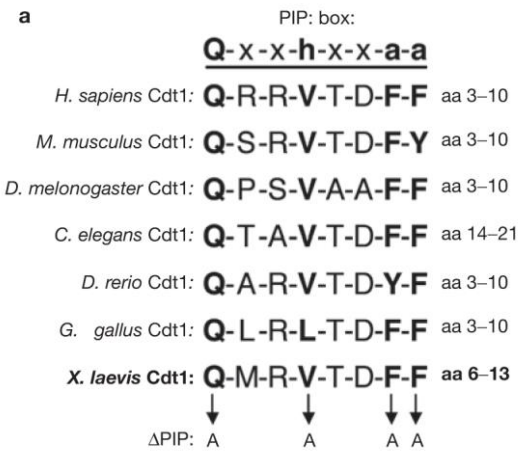

Figure 4. 1.: Proliferating cell nuclear antigen (PCNA)-interacting protein (PIP) box motif.

a) In the sequence "h" represents a hydrophobic amino acid (typically L, I or M), "a" an aromatic (F or Y) and "x" any amino acid. aa: amino acid (Arias and Walter, 2006).

Searching amongst all identified peptides, we found 460 redundant peptides containing the above-described degron and 71 unique proteins with the PIP degron. Interestingly, many well-described chromatin- and replication-associated proteins are in this list of proteins such as PCNA, Acf1, Caf-180, Mcm5, Orc1, DNA polymerase δ. Furthermore, proteins with well-described chaperone function as Hsp70 and Tcp1 are also in this list as well as some factors of the UPS system such as Usp7, Rpn9, Rpn13 and Prosbeta3.
Some of these factors (Orc1, Mcm5 and DNA polymerase δ) show changes in binding kinetics upon proteasome inhibition. They become late binding proteins upon proteasome inhibition arguing for regulation by the proteasome in unperturbed circumstances.

4. 11. 3. The proteasome as quality control during chromatin assembly

The above-discussed results in combination with published data argue for a quality control function of the proteasome during chromatin assembly. Here, a model for the action of the proteasome during chromatin assembly is presented.
The data from TSA treatment have shown that open chromatin is accessible for many factors with specific and unspecific binding affinities. In this model, specific chromatin assembly factors would only bind to chromatin at early time points due to the action of the proteasome during chromatin assembly (Figure 4. 2.). With this regard, the proteasome would act as a quality machine that regulates the proper binding. During chromatin maturation, the proteasome could also function in a proteolytic and non-proteolytic manner to either support the folding of proteins but also to degrade proteins from chromatin lacking specific functions during chromatin assembly. In addition, chromatin assembly factors such as PCNA and Caf-180 would act as binding platforms for additional early chromatin assembly factor by means of their PIP degron. This degron might be used for their subsequent degradation after elementary chromatin assembly steps have been fulfilled to make space for late binding proteins to facilitate further chromatin maturation. The proteasome would further regulate the binding and folding of proteins in a network of many RNA binding proteins that help to maintain an open chromatin structure (Schubert et al., 2012). Once the proteasome is disturbed during chromatin assembly, unspecific binding proteins and formerly constant or late binding proteins would associate to open chromatin and the chromatin assembly process would be altered. Furthermore, the open structure of chromatin could be inhibited and proteins aggregate together with DNA.

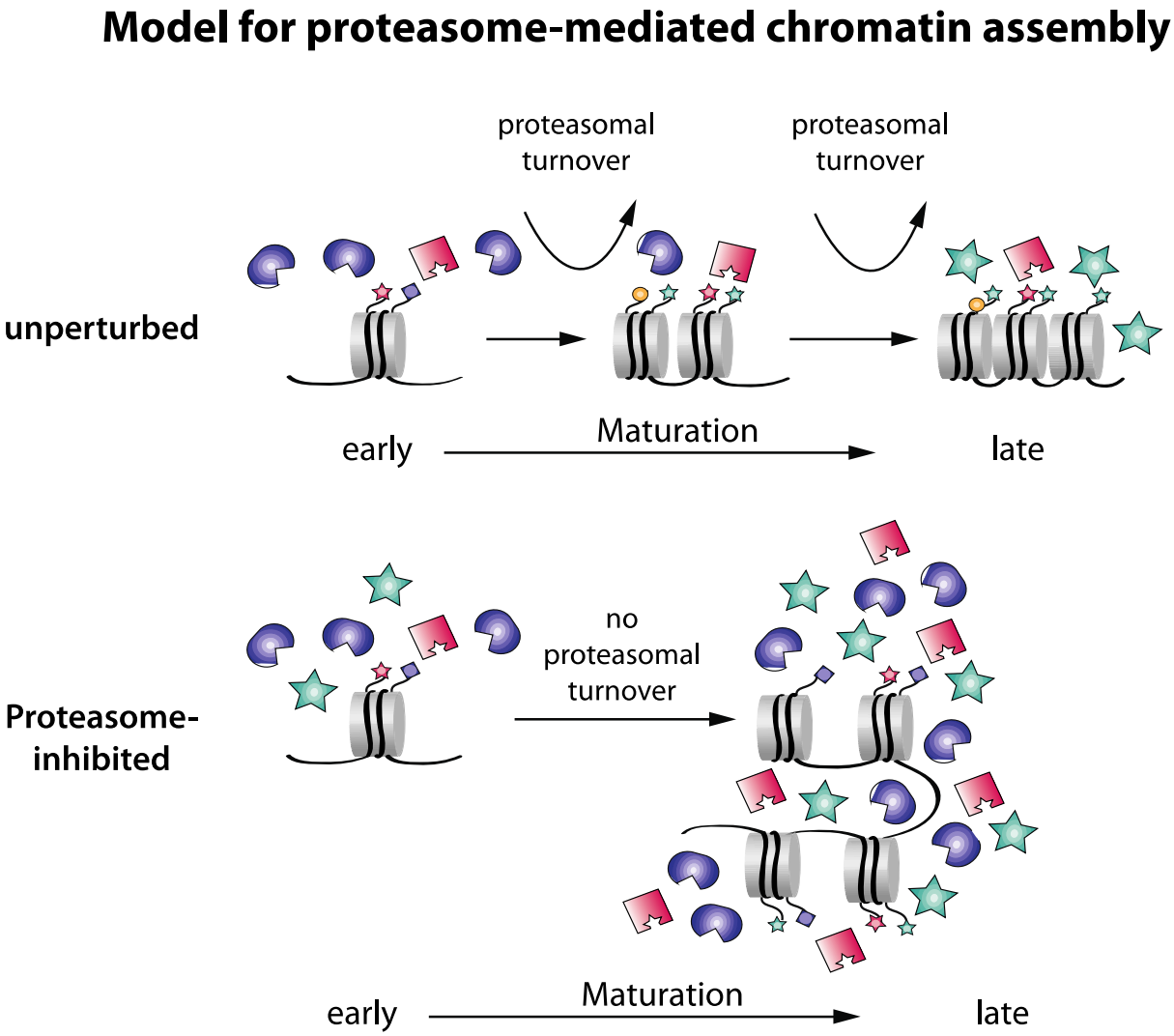

Figure 4. 2.: Quality control model for proteasome action during chromatin assembly.

In unperturbed chromatin assembly, the proteasome might chaperone and degrade proteins at chromatin to facilitate protein turnover to drive chromatin maturation. When the proteasome is inhibited, specific and unspecific proteins could bind to chromatin and accumulate into aggresomes.

Moreover, the model argues for a role of the proteasome during chromatin assembly because chromatin maturation induces higher order structure and this leads to less space for binding. Once there is less space, it must be tidily controlled which proteins get access to chromatin to further help maturation. As soon as this “access control” would be disturbed, many proteins could bind to chromatin and accumulate. In the extreme case, chromatin precipitates and aggregates are formed. The addition of new proteasome can rescue this effect. Therefore, the proteasome could recognize the necessity of proteins for chromatin maturation.

4. 12. Perspectives

Both, *in vitro* and *in vivo* systems can also be used to investigate the establishment of histone modifications. The *in vitro* system has been used to quantify histone modifications at early assembled chromatin and it was shown that new histones become monomethylated at H4K20 upon their deposition thereby facilitating a removal of the predeposition acetyl marks on the H4 molecule (Scharf et al., 2009b). As most of the H4 molecules are dimethylated at H4K20 when bound to DNA, the proportionally lower degree of H4K20 methylation in newly replicated chromatin allows the cellular machinery to distinguish newly synthesized chromatin in G2-phase from chromatin after mitosis (Saredi et al., 2016). These findings suggest that a deep proteomic investigation and histone modification analysis can reveal further mechanisms that ensure the maintenance of chromatin structure and hence epigenetic information.

Furthermore, the *in vivo* system was used to systematically study histone modification establishment. These experiments revealed two basic principles for histone PTM propagation: In mode 1, new histones acquire PTMs to become identical to the parental histones within one cell cycle whereas in mode 2, the propagation relies on progressive modification of both new and parental histones (H3K9me3 and H3K27me3) (Alabert et al., 2015).

Combining *in vitro* and *in vivo* systems, the effects of histone modifications can be investigated upon inhibitor studies. These insights into PTM establishment and propagation can further help to understand processes during chromatin assembly.

In addition, it would be interesting to measure chromatin assembly proteomics at more time points. With a better resolution of time during chromatin assembly, the binding kinetics gets more exact and single complex kinetics can be investigated in more detail.

Finally, the usage of the CRISPR-Cas technology in combination with NCC experiments can elucidate the contribution of specific factors during chromatin assembly. For example, NCC experiments with cells lacking proteins that set histone modifications required for chromatin maturation could be performed. The observed effects can further contribute to the understanding of the different steps of chromatin assembly. With regards to proteasome studies, it could be interesting to knock-out putative targets of the proteasome to investigate their function during chromatin assembly.

REFERENCES

Aebersold, R., and Mann, M. (2016). Mass-spectrometric exploration of proteome structure and function. Nature *537*, 347-355.

Alabert, C., Barth, T.K., Reveron-Gomez, N., Sidoli, S., Schmidt, A., Jensen, O.N., Imhof, A., and Groth, A. (2015). Two distinct modes for propagation of histone PTMs across the cell cycle. In Genes & development, pp. 585-590.

Alabert, C., Bukowski-Wills, J.C., Lee, S.B., Kustatscher, G., Nakamura, K., de Lima Alves, F., Menard, P., Mejlvang, J., Rappsilber, J., and Groth, A. (2014). Nascent chromatin capture proteomics determines chromatin dynamics during DNA replication and identifies unknown fork components. In Nature Cell Biology, pp. 281-293.

Alvarez, F., Munoz, F., Schilcher, P., Imhof, A., Almouzni, G., and Loyola, A. (2011). Sequential establishment of marks on soluble histones H3 and H4. In The Journal of Biological Chemistry, pp. 17714-17721.

Annunziato, A.T., and Seale, R.L. (1983). Histone deacetylation is required for the maturation of newly replicated chromatin. Journal of Biological Chemistry *258*, 12675-12684.

Ardley, H.C., Scott, G.B., Rose, S.A., Tan, N.G., and Robinson, P.A. (2004). UCH-L1 aggresome formation in response to proteasome impairment indicates a role in inclusion formation in Parkinson's disease. J Neurochem *90*, 379-391.

Arents, G., and Moudrianakis, E.N. (1995). The histone fold: a ubiquitous architectural motif utilized in DNA compaction and protein dimerization. In Proc Natl Acad Sci U S A, pp. 11170-11174.

Arias, E.E., and Walter, J.C. (2006). PCNA functions as a molecular platform to trigger Cdt1 destruction and prevent re-replication. In Nature cell biology, pp. 84-90.

Auld, K.L., Brown, C.R., Casolari, J.M., Komili, S., and Silver, P.A. (2006). Genomic association of the proteasome demonstrates overlapping gene regulatory activity with transcription factor substrates. Molecular Cell *21*, 861-871.

Avvakumov, N., Nourani, A., and Cote, J. (2011). Histone chaperones: modulators of chromatin marks. Molecular Cell *41*, 502-514.

Ban, N., Nissen, P., Hansen, J., Moore, P.B., and Steitz, T.A. (2000). The complete atomic structure of the large ribosomal subunit at the 2.4 Å resolution. Science *289*, 905-920.

Bannister, A.J., and Kouzarides, T. (2011). Regulation of chromatin by histone modifications. In Nature (Nature), pp. 381-395.

Bantscheff, M., Hopf, C., Savitski, M.M., Dittmann, A., Grandi, P., Michon, A.M., Schlegl, J., Abraham, Y., Becher, I., Bergamini, G., *et al.* (2011). Chemoproteomics profiling of HDAC inhibitors reveals selective targeting of HDAC complexes. Nat Biotechnol *29*, 255-265.

Barth, T.K., and Imhof, A. (2010). Fast signals and slow marks: the dynamics of histone modifications. In Trends Biochem Sci, pp. 618-626.

Bassermann, F., Eichner, R., and Pagano, M. (2014). The ubiquitin proteasome system - implications for cell cycle control and the targeted treatment of cancer. Biochimica et biophysica acta *1843*, 150-162.

Battiste, J.L., Mao, H., Rao, S., Tan, R., Muhandiram, D.R., Kay, L.E., Frankel, A.L., and Williamson, J.R. (1996). Alpha helix-RNA major groove recognition in an HIV-1 REV peptide-RRE RNA complex. Science *273*, 1547-1551.

Becker, P., and Wu, C. (1992). Cell-free system for assembly of transcriptionally repressed chromatin from Drosophila embryos. In Molecular and Cellular Biology, pp. 2241-2249.

Becker, P.B., and Horz, W. (2002). ATP-dependent nucleosome remodeling. Annual review of biochemistry *71*, 247-273.

Bedford, M.T., and Clarke, S.G. (2009). Protein Arginine Methylation in Mammals: Who, What, and Why. In Molecular Cell, pp. 1-13.

Benson, L.J., Gu, Y., Yakovleva, T., Tong, K., Barrows, C., Strack, C.L., Cook, R.G., Mizzen, C.A., and Annunziato, A.T. (2006). Modifications of H3 and H4 during chromatin replication, nucleosome assembly, and histone exchange. In The Journal of Biological Chemistry, pp. 9287-9296.

Blank, T.A., Sandaltzopoulos, R., and Becker, P.B. (1997). Biochemical analysis of chromatin structure and function using Drosophila embryo extracts. Methods *12*, 28-35.

Blum, H., Beier, H., and Gross, H.J. (1987). Improved silver staining of plant proteins, RNA and DNA in polyacrylamide gels. In Electrophoresis, pp. 93-99.

Bonaldi T., Imhof, A., and Regula, J.T. (2004). A combination of different mass spectroscopic techniques for the analysis of dynamic changes of histone modifications. Proteomics, 1382-1396.

Boyle, E.I., Weng, S., Gollub, J., Jin, H., Botstein, D., Cherry, J.M., and Sherlock, G. (2004). GO:TermFinder--open source software for accessing Gene Ontology information and finding significantly enriched Gene Ontology terms associated with a list of genes. Bioinformatics *20*, 3710-3715.

Brooks, P., Fuertes, G., Murray, R.Z., Bose, S., Knecht, E., Rechsteiner, M.C., Hendil, K.B., Tanaka, K., Dyson, J., and Rivett, J. (2000). Subcellular localization of proteasomes and their regulatory complexes in mammalian cells. In Biochemical Journal, pp. 155-161.

Brutlag, D.L. (1980). Molecular arrangement and evolution of heterochromatic DNA. Annual review of genetics *14*, 121-144.

Bulger, M., Ito, T., Kamakaka, R., and Kadonaga, J.T. (1995). Assembly of regularly spaced nucleosome arrays by Drosophila chromatin assembly factor I and a 56-kDa histone binding protein. In Proc Natl Acad Sci U S A, pp. 11726-11730.

Buschbeck, M., and Hake, S.B. (2017). Variants of core histones and their roles in cell fate decisions, development and cancer. Nat Rev Mol Cell Biol *18*, 299-314.

Canas, B., Lopez-Ferrer, D., Ramos-Fernandez, A., Camafeita, E., and Calvo, E. (2006). Mass spectrometry technologies for proteomics. Brief Funct Genomic Proteomic *4*, 295-320.

Chen, R., and Wold, M.S. (2014). Replication protein A: single-stranded DNA's first responder: dynamic DNA-interactions allow replication protein A to direct single-strand DNA intermediates into different pathways for synthesis or repair. Bioessays *36*, 1156-1161.

Choudhary, C., Kumar, C., Gnad, F., Nielsen, M.L., Rehman, M., Walther, T.C., Olsen, J.V., and Mann, M. (2009). Lysine acetylation targets protein complexes and co-regulates major cellular functions. Science *325*, 834-840.

Clapier, C.R., Iwasa, J., Cairns, B.R., and Peterson, C.L. (2017). Mechanisms of action and regulation of ATP-dependent chromatin-remodelling complexes. Nat Rev Mol Cell Biol.

Conti, C., Sacca, B., Herrick, J., Lalou, C., Pommier, Y., and Bensimon, A. (2007). Replication fork velocities at adjacent replication origins are coordinately modified during DNA replication in human cells. Molecular Biology of the Cell *18*, 3059-3067.

Corchero, J.L. (2016). Eukaryotic aggresomes: from a model of conformational diseases to an emerging type of immobilized biocatalyzers. In Appl Microbiol Biotechnol, pp. 559-569.

Cox, J., and Mann, M. (2008). MaxQuant enables high peptide identification rates, individualized p.p.b.-range mass accuracies and proteome-wide protein quantification. Nat Biotechnol *26*, 1367-1372.

De Koning, L., Corpet, A., Haber, J.E., and Almouzni, G. (2007). Histone chaperones: an escort network regulating histone traffic. In Nat Struct Biol, pp. 997-1007.

Deshaies, R.J., and Joazeiro, C.A. (2009). RING domain E3 ubiquitin ligases. Annual review of biochemistry *78*, 399-434.

Dewar, J.M., Low, E., Mann, M., Raschle, M., and Walter, J.C. (2017). CRL2Lrr1 promotes unloading of the vertebrate replisome from chromatin during replication termination. Genes & development *31*, 275-290.

Doerks, T., Copley, R.R., Schultz, J., Ponting, C.P., and Bork, P. (2002). Systematic identification of novel protein domain families associated with nuclear functions. Genome research *12*, 47-56.

Dungrawala, H., Rose, K.L., Bhat, K.P., Mohni, K.N., Glick, G.G., Couch, F.B., and Cortez, D. (2015). The replication checkpoint prevents two types of fork collapse without regulating replisome stability. Molecular Cell *59*, 998-1010.

Dunn, A.Y., Melville, M.W., and Frydman, J. (2001). Review: cellular substrates of the eukaryotic chaperonin TRiC/CCT. J Struct Biol *135*, 176-184.

Dyson, H.J., and Wright, P.E. (2005). Intrinsically unstructured proteins and their functions. In Nat Rev Mol Cell Biol, pp. 197-208.

Elgin, S.C. (1996). Heterochromatin and gene regulation in Drosophila. In Curr Opin Genet Dev, pp. 193-202.

Eskeland, R., Eberharter, A., and Imhof, A. (2007). HP1 binding to chromatin methylated at H3K9 is enhanced by auxiliary factors. Mol Cell Biol *27*, 453-465.

Ezhkova, E., and Tansey, W.P. (2004). Proteasomal ATPases link ubiquitylation of histone H2B to methylation of HistoneH3. Molecular Cell *13*, 435-442.

Fabre, B., Lambour, T., Delobel, J., Amalric, F., Monsarrat, B., Burlet-Schiltz, O., and Bousquet-Dubouch, M.P. (2013). Subcellular distribution and dynamics of active proteasome complexes unraveled by a workflow combining in vivo complex cross-linking and quantitative proteomics. Molecular and Cellular Proteomics *12*, 687-699.

Finehout, E.J., and Lee, K.H. (2004). An introduction to mass spectrometry applications in biological research. Biochemistry and Molecular Biology Education *32*, 93-100.

Finley, D. (2009). Recognition and processing of ubiquitin-protein conjugates by the proteasome. In Annu Rev Biochem, pp. 477-513.

Fischer, R., and Kessler, B.M. (2015). Gel-aided sample preparation (GASP)- A simplified method for gel-assisted proteomic sample generation from protein extracts and intact cells. Proteomics *15*, 1224-1229.

Fischle, W., Wang, Y., and Allis, C.D. (2003). Histone and chromatin cross-talk. In Current opinion in cell biology, pp. 172-183.

Freund, A., Zhong, F.L., Venteicher, A.S., Meng, Z., Veenstra, T.D., Frydman, J., and Artandi, S.E. (2014). Proteostatic control of telomerase function through TRiC-mediated folding of TCAB1. Cell *159*, 1389-1403.

Furuyama, S., and Biggins, S. (2007). Centromere identity is specified by a single centromeric nucleosome in budding yeast. Proc Natl Acad Sci U S A *104*, 14706-14711.

Furuyama, T., Codomo, C.A., and Henikoff, S. (2013). Reconstitution of hemisomes on budding yeast centromeric DNA. Nucleic acids research *41*, 5769-5783.

Garcia-Mata, R., Bebök, Z., Sorscher, E.J., and Sztul, E.S. (1999). Characterization and dynamics of aggresome formation by cytosolic GFP-chimera. The Journal of Cell Biology *146*, 1239-1254.

Gastaldello, S., D'Angelo, S., Franzoso, S., Fanin, M., Angelini, C., Betto, R., and Sandona, D. (2008). Inhibition of proteasome activity promotes the correct localization of disease-causing alpha-sarcoglycan mutants in HEK-293 cells constitutively expressing beta-, gamma-, and delta-sarcoglycan. Am J Pathol *173*, 170-181.

Geng, F., Wenzel, S., and Tansey, W.P. (2012). Ubiquitin and proteasomes in transcription. In Annu Rev Biochem, pp. 177-201.

Gibson, D.G., Smith, H.O., Hutchison, C.A., 3rd, Venter, J.C., and Merryman, C. (2010). Chemical synthesis of the mouse mitochondrial genome. Nature methods *7*, 901-903.

Gibson, D.G., Young, L., Chuang, R.Y., Venter, J.C., Hutchison, C.A., 3rd, and Smith, H.O. (2009). Enzymatic assembly of DNA molecules up to several hundred kilobases. Nature methods *6*, 343-345.

Gillespie, P.J., Gambus, A., and Blow, J.J. (2012). Preparation and use of Xenopus egg extracts to study DNA replication and chromatin associated proteins. Methods *57*, 203-213.

Gillet, L.C., Navarro, P., Tate, S., Rost, H.L., Selevsek, N., Reiter, L., Bonner, R., and Aebersold, R. (2012). Targeted data extraction of the MS/MS spectra generated by data-independent acquisition: a new concept for consistent and accurate proteome analysis. In Molecular and Cellular Proteomics, pp. O111 016717.

Gomes, X.V., Schmidt, S.L., and Burgers, P.M. (2001). ATP utilization by yeast replication factor C. II. Multiple stepwise ATP binding events are required to load proliferating cell nuclear antigen onto primed DNA. Jornal of Biological Chemistry *276*, 34776-34783.

Goto, H., Yasui, Y., Nigg, E.A., and Inagaki, M. (2002). Aurora-B phosphorylates Histone H3 at serine28 with regard to the mitotic chromosome condensation. In Genes to Cells, pp. 1-7.

Grewal, S.I.S., and Elgin, S.C. (2002). Heterochromatin: new possibilities for the inheritance of structure. In Curr Opin Genet Dev, pp. 178-187.

Grewal, S.I.S., and Jia, S. (2007). Heterochromatin revisited. In Nat Rev Genet, pp. 35-46.

Guglielmi, B., La Rochelle, N., and Tjian, R. (2013). Gene-specific transcriptional mechanisms at the histone gene cluster revealed by single-cell imaging. Molecular Cell *51*, 480-492.

Hamiche, A., and Shuaib, M. (2012). Chaperoning the histone H3 family. Biochimica et Biophysica Acta (BBA) - Gene Regulatory Mechanisms *1819*, 230-237.

Hammond, C.M., Stromme, C.B., Huang, H., Patel, D.J., and Groth, A. (2017). Histone chaperone networks shaping chromatin function. Nat Rev Mol Cell Biol *18*, 141-158.

Han, J., Zhou, H., Li, Z., Xu, R.M., and Zhang, Z. (2007). Acetylation of lysine 56 of histone H3 catalyzed by RTT109 and regulated by ASF1 is required for replisome integrity. Journal of Biological Chemistry *282*, 28587-28596.

Hansen, J.C. (2002). Conformational Dynamics of the Chromatin Fiber in Solution: Determinants, Mechanisms, and Functions. In Annu Rev Biophys Biomol Struct, pp. 361-392.

Hansen, J.C., Van Holde, K.E., and Lohr, D. (1991). The mechanism of nucleosome assembly onto oligomers of the sea urchin 5 S DNA positioning sequence. Journal of Biological Chemistry *266*, 4276-4282.

Hashimoto, Y., Puddu, F., and Costanzo, V. (2011). RAD51- and MRE11-dependent reassembly of uncoupled CMG helicase complex at collapsed replication forks. Nat Struct Biol *19*, 17-24.

Hebbes, T.R., Clayton, A.L., Thorne, A.W., and Crane-Robinson, C. (1994). Core histone hyperacetlation co-maps with generalized DNase I sensitivity in the chicken beta-globin chromosomal domain. EMBO Journal *13*, 1823-1830.

Hedglin, M., Perumal, S.K., Hu, Z., and Benkovic, S. (2013). Stepwise assemby of the human replicative polymerase holoenzyme. eLife *2*, 1-20.

Heitz, E. (1935). Chromosomenstruktur und Gene. In Mol Gen Genet, pp. 402-447.

Hodgson, B., Calzada, A., and Labib, K. (2007). Mrc1 and Tof1 regulate DNA replication forks in different ways during normal S phase. Molecular Biology of the Cell *18*, 3894-3902.

Hölzl, H.K.B., Kellermann, J., Seemüller, E., Sümegi, M., A, U., Medalia, O., Sperling, J., Müller, S., Engel, A., and Baumeister, W. (2000). The regulatory complex of Drosophila melanogaster 26S Proteasomes: Subunit composition and localization of a deubiquitylating enzyme. In The Journal of Cell Biology, pp. 119-129.

Hoppe, T., Matuschewski, K., Rape, M., Schlenker, S., Ulrich, H.D., and Jentsch, S. (2000). Activation of a membrane-bound transcription factor by regulated Ubiquitin/Proteasome-depenendent processing. Cell *102*, 577-586.

Huang da, W., Sherman, B.T., and Lempicki, R.A. (2009a). Bioinformatics enrichment tools: paths toward the comprehensive functional analysis of large gene lists. Nucleic acids research *37*, 1-13.

Huang da, W., Sherman, B.T., and Lempicki, R.A. (2009b). Systematic and integrative analysis of large gene lists using DAVID bioinformatics resources. Nature protocols *4*, 44-57.

Huang, H., Lin, S., Garcia, B.A., and Zhao, Y. (2015). Quantitative proteomic analysis of histone modifications. Chem Rev *115*, 2376-2418.

Hupe, P., Barillot, E., Calzone, L., Vert, J.-P., and Zoinovyev, A. (2012). Mathematical & Computational Biology,. In Computational Systems Biology of Cancer (Chapman & Hall/CRC).

Ito, T., Bulger, M., Pazin, M.J., Kobayashi, R., and Kadonaga, J.T. (1997). ACF, an ISWI-containing and ATP-utilizing chromatin assembly and remodeling factor. Cell *90*, 145-155.

Jain, D., Baldi, S., Zabel, A., Straub, T., and Becker, P.B. (2015). Active promoters give rise to false positive 'Phantom Peaks' in ChIP-seq experiments. Nucleic acids research *43*, 6959-6968.

Jasencakova, Z., Scharf, A.N.D., Ask, K., Corpet, A., Imhof, A., Almouzni, G., and Groth, A. (2010). Replication stress interferes with histone recycling and predeposition marking of new histones. In Molecular Cell, pp. 736-743.

Johnston, J.A., Ward, C.L., and Kopito, R.R. (1998). Aggresome: A Cellular Response to Misfolded Proteins. In The Journal of Cell Biology, pp. 1883-1898.

Kaiser, P., Flick, K., Wittenberg, C., and Reed, S., I., (2000). Regulation of Transcription by Ubiquitination without proteolysis: Cdc34/SCF(Met30)-mediated inactivation of the transcription factor Met4. Cell *102*, 303-314.

Kamakaka, R., Bulger, M., and Kadonaga, J.T. (1993). Potentiation of RNA polymerase II transcription by Gal4-VP16 during but not after DNA replication and chromatin assembly. In Genes & development, pp. 1779-1795.

Kaufman, P.D., Kobayashi, R., Kessler, N., and Stillman, B. (1995). The p150 and p60 subunits pf chromatin assembly factor-1: A molecular link between newly synthesized histones and DNA replication. Cell *81*, 1105-1114.

Kaufman, P.D., Kobayashi, R., and Stillman, B. (1997). Ultraviolet radiation sensitivity and reduction of telomeric silencing in Saccharomyces cerevisiae cells lacking chromatin assembly factor-1. Genes & development *11*, 345-357.

Kemp, M.G., Ghosh, M., Liu, G., and Leffak, M. (2005). The histone deacetylase inhibitor trichostatin A alters the pattern of DNA replication origin activity in human cells. Nucleic acids research *33*, 325-336.

Kim, J.A., and Haber, J.E. (2009). Chromatin assembly factors Asf1 and CAF-1 have overlapping roles in deactivating the DNA damage checkpoint when DNA repair is complete. Proc Natl Acad Sci U S A *106*, 1151-1156.

Kimura, H., and Cook, P.R. (2001). Kinetics of core histones in living human cells: little exchange of H3 and H4 and some rapid exchange of H2B. The Journal of Cell Biology *153*, 1341-1353.

Kleinschmidt, J.A., and Franke, W.W. (1982). Soluble acidic complexes containing histones H3 and H4 in nuclei of Xenopus laevis oocytes. In Cell, pp. 799-809.

Kliszak, A.E., Rainey, M.D., Harhen, B., Boisvert, F.M., and Santocanale, C. (2011). DNA mediated chromatin pull-down for the study of chromatin replication. In Sci Rep.

Knoch, T.A., Wachsmuth, M., Kepper, N., Lesnussa, M., Abuseiris, A., Imam, A.M.A., Kolovos, P., Zuin, J., Kockx, C.E.M., Brouwer, R.W.W., *et al.* (2016). The detailed 3D multi-loop aggregate/rosette chromatin architecture and functional dynamic organization of the human and mouse genomes. In Epigenetics and Chromatin (BioMed Central), pp. 1-22.

Kopito, R.R., and Sitia, R. (2000). Aggresomes and Russel bodies, Symptoms of cellular indigestion? EMBO reports *1*, 225-231.

Krajewski, W., and Becker, P., B., (1998). Reconstitution of hyperacetylated DNase I-sensitive chromatin characterized by high conformational flexibility of nucleosomal DNA. Proc Natl Acad Sci U S A *95*, 1540-1545.

Krawitz, D.C., Kama, T., and Kaufman, P.D. (2002). Chromatin assembly factor I mutants defective for PCNA binding require Asf1/Hir proteins for silencing. Molecular and Cellular Biology *22*, 614-625.

Kulak, N.A., Pichler, G., Paron, I., Nagaraj, N., and Mann, M. (2014). Minimal, encapsulated proteomic-sample processing applied to copy-number estimation in eukaryotic cells. Nature methods *11*, 319-324.

Kurat, C.F., Yeeles, J.T.P., Patel, H., Early, A., and Diffley, J.F.X. (2017). Chromatin controls DNA replication origin selection, lagging-strand synthesis, and replication fork rates. In Molecular Cell, pp. 117-130.

Kustatscher, G., Hegarat, N., Wills, K.L.H., Furlan, C., Bukowski-Wills, J.C., Hochegger, H., and Rappsilber, J. (2014). Proteomics of a fuzzy organelle: interphase chromatin. In EMBO Journal, pp. 648-664.

Ladoux, B., Quivy, J.-P., Doyle, P., du Roure, O., Almouzni, G., and Viovy, J.L. (2000). Fast kinetics of chromatin assembly revealed by single-molecule videomicroscopy and scanning force microscopy. In Proc Natl Acad Sci U S A, pp. 14251-14256.

Laemmli, U., K., (1970). Cleavage of structural proteins during the Assembly of the Head of Bacteriophage T4. Nature *227*, 680-685.

Lafon, A., Taranum, S., Pietrocola, F., Dingli, F., Loew, D., Brahma, S., Bartholomew, B., and Papamichos-Chronakis, M. (2015). INO80 chromatin remodeler facilitates release of RNA polymerase II from chromatin for ubiquitin-mediated proteasomal degradation. Molecular Cell *60*, 784-796.

Lagier-Tourenne, C., Polymenidou, M., Hutt, K.R., Vu, A.Q., Baughn, M., Huelga, S.C., Clutario, K.M., Ling, S.C., Liang, T.Y., Mazur, C., *et al.* (2012). Divergent roles of ALS-linked proteins FUS/TLS and TDP-43 intersect in processing long pre-mRNAs. Nat Neurosci *15*, 1488-1497.

Laskey, R.A., Honda, B.M., Mills, A.D., and Finch, J.T. (1978). Nucleosomes are assembled by an acidic protein which binds histones and transfers them to DNA. In Nature, pp. 416-420.

Lee, D.H., and Goldberg, A.L. (1998). Proteasome inhibitors: valuable new tools for cell biologists. Trends in cell biology *8*, 397-403.

Leulliot, N., and Varani, G. (2001). Current topics in RNA-protein recognition: Control of specificity and biological function through induced fit and conformational capture. Biochemistry *40*, 7947-7956.

Levenson, J.M., and Sweatt, J.D. (2005). Epigenetic mechanisms in memory formation. In Nat Rev Neurosci, pp. 108-118.

Li, Q., Zhou, H., Wurtele, H., Davies, B., Horazdovsky, B., Verreault, A., and Zhang, Z. (2008). Acetylation of histone H3 Lysine 56 regulates replication-coupled nucleosome assembly. In Cell, pp. 244-255.

Liu, Y., Huang, H., Zhou, B.O., Wang, S.S., Hu, Y., Li, X., Liu, J., Zang, J., Niu, L., Wu, J., *et al.* (2010). Structural analysis of Rtt106p reveals a DNA binding role required for heterochromatin silencing. Journal of Biological Chemistry *285*, 4251-4262.

Lohe, A.R., Hilliker, A.J., and Roberts, P.A. (1993). Mapping simple repeated DNA sequences in heterochromatin of Drosophila melanogaster. In Genetics, pp. 1149-1174.

Lonard, D., M.,, Nawaz, Z., Smith, C., L.,, and O'Malley, B., o., (2000). The 26S Proteasome is required for estrogen receptor-alpha and coactivator turnover and for efficient estrogen receptor-alpha transactivation. Molecular Cell *5*, 939-948.

Lopez-Contreras, A.J., Ruppen, I., Nieto-Soler, M., Murga, M., Rodriguez-Acebes, S., Remeseiro, S., Rodrigo-Perez, S., Rojas, A.M., Mendez, J., Munoz, J., *et al.* (2013). A proteomic characterization of factors enriched at nascent DNA molecules. Cell reports *3*, 1105-1116.

Loyola, A., Bonaldi, T., Roche, D., Imhof, A., and Almouzni, G. (2006). PTMs on H3 variants before chromatin assembly potentiate their final epigenetic state. In Molecular Cell, pp. 309-316.

Lu, X., and Zhu, H. (2005). Tube-Gel digestion. Molecular and Cellular Proteomics *4*, 1948-1958.

Luger K., Mäder A. W., Richmond R. K., Sargent D. F., and J., R.T. (1997). Crystal structure of the nucleosome core particle at 2.8A resolution. In Nature, pp. 251-260.

Ma, X., Wu, J., Altheim, B.A., Schultz, M.C., and Grunstein, M. (1998). Deposition-related sites K5/K12 in histone H4 are not required for nucleosome deposition in yeast. Proc Natl Acad Sci U S A *95*, 6693-6698.

Maenner, S., Muller, M., Frohlich, J., Langer, D., and Becker, P.B. (2013). ATP-dependent roX RNA remodeling by the helicase maleless enables specific association of MSL proteins. Molecular Cell *51*, 174-184.

Maeshima, K., Rogge, R., Tamura, S., Joti, Y., Hikima, T., Szerlong, H., Krause, C., Herman, J., Seidel, E., DeLuca, J., *et al.* (2016). Nucleosomal arrays self-assemble into supramolecular globular structures lacking 30-nm fibers. In EMBO Journal.

Maier, V.K., Chioda, M., and Becker, P.B. (2008). ATP-dependent chromatosome remodeling. Biol Chem *389*, 345-352.

Mallick, P., and Kuster, B. (2010). Proteomics: a pragmatic perspective. Nat Biotechnol *28*, 695-709.

Manza, L.L., Stamer, S.L., Ham, A.L., Codreanu, S.G., and Liebler, D.C. (2005). Sample preparation and digestion for proteomic analysis using spin filters. Proteomics *5*, 1742-1745.

Maric, M., Maculins, T., De Piccoli, G., and Labib, K. (2014). Cdc48 and a ubiquitin ligase drive disassembly of the CMG helicase at the end of DNA replication. In Science, pp. 1253596.

Marx, V. (2012). Epigenetics: Reading the second genomic code. Nature *491*, 143-147.

Mattiroli, F., Gu, Y., Balsbaugh, J.L., Ahn, N.G., and Luger, K. (2017a). The Cac2 subunit is essential for productive histone binding and nucleosome assembly in CAF-1. Sci Rep *7*, 46274.

Mattiroli, F., Gu, Y., Yadav, T., Balsbaugh, J.L., Harris, M.R., Findlay, E.S., Liu, Y., Radebaugh, C.A., Stargell, L.A., Ahn, N.G., *et al.* (2017b). DNA-mediated association of two histone-bound CAF-complexes drives tetrasome assembly in the wake of DNA replication. eLife *10.7554/eLife.22799*.

McNally, J.G., Müller, W.G., Walker, D., Wolford, R., and Hager, G.L. (2000). The glucocorticoid receptor: rapid exchange with regulatory sites in living cells. Science *287*, 1262-1265.

Meier, F., Beck, S., Grassl, N., Lubeck, M., Park, M.A., Raether, O., and Mann, M. (2015). Parallel accumulation-serial fragmentation (PASEF): multiplying sequencing speed and sensitivity by synchronized scans in a trapped ion mobility device. J Proteome Res *14*, 5378-5387.

Mellacheruvu, D., Wright, Z., Couzens, A.L., Lambert, J.P., St-Denis, N.A., Li, T., Miteva, Y.V., Hauri, S., Sardiu, M.E., Low, T.Y., *et al.* (2013). The CRAPome: a contaminant repository for affinity purification-mass spectrometry data. Nature methods *10*, 730-736.

Mishra, A., Godavarthi, S.K., Maheshwari, M., Goswami, A., and Jana, N.R. (2009). The ubiquitin ligase E6-AP is induced and recruited to aggresomes in response to proteasome inhibition and may be involved in the ubiquitination of Hsp70-bound misfolded proteins. Journal of Biolical Chemistry *284*, 10537-10545.

Moggs, J.G., Grandi, P., Quivy, J.-P., Jonsson, Z.O., Hübscher, U., Becker, P.B., and Almouzni, G. (2000). A CAF-1-PCNA-mediated chromatin assembly pathway triggered by sensing DNA damage. In Molecular and Cellular Biology, pp. 1206-1218.

Mogridge, J., Legault, P., Li, M., Van Oene, M.D., Kay, L.E., and Greenblatt, J. (1998). Independent ligand-indced folding of the RNA-binding domain and two functionally distinct antitermination regions in the Phage lambda N protein. Molecular Cell *1*, 265-275.

Moreno, S., Bailey, R., Campion, N., Herron, S., and Gambus, A. (2014). Polyubiquitylation drives replisome dissasembly at the termination of DNA replication. In Science, pp. 477-482.

Moreno, S.P., and Gambus, A. (2015). Regulation of Unperturbed DNA Replication by Ubiquitylation. In Genes, pp. 451-468.

Mosammaparast, N., Ewart, C.S., and Pemberton, L.F. (2002). A role for nucleosome assembly protein 1 in the nuclear transport of histone H2A and H2B. EMBO Journal *21*, 6527-6538.

Mueller-Planitz, F., Klinker, H., Ludwigsen, J., and Becker, P.B. (2013). The ATPase domain of ISWI is an autonomous nucleosome remodeling machine. Nat Struct Biol *20*, 82-89.

Narlikar, G.J., Sundaramoorthy, R., and Owen-Hughes, T. (2013). Mechanisms and functions of ATP-dependent chromatin-remodeling enzymes. Cell *154*, 490-503.

Navarro, P., Kuharev, J., Gillet, L.C., Bernhardt, O.M., MacLean, B., Rost, H.L., Tate, S.A., Tsou, C.C., Reiter, L., Distler, U., *et al.* (2016). A multicenter study benchmarks software tools for label-free proteome quantification. Nat Biotechnol *34*, 1130-1136.

Newport, J., and Kirschner, M. (1982). A Major Developmental Transition in Early Xenopus Embryos: I. Characterization and Timing of Cellular Chnages at the Midblastula Stage. Cell *30*, 675-686.

Ng, S.S., Yue, W.W., Oppermann, U., and Klose, R.J. (2008). Dynamic protein methylation in chromatin biology. In Cell Mol Life Sci, pp. 407-422.

Ni, X.G., Zhou, L., Wang, G.Q., Liu, S.M., Bai, X.F., Liu, F., Peppelenbosch, M.P., and Zhao, P. (2008). The ubiquitin-proteasome pathway mediates gelsolin protein downregulation in pancreatic cancer. Molecular Medicine *14*, 582-589.

Nishi, R., Wijnhoven, P., le Sage, C., Tjeertes, J., Galanty, Y., Forment, J.V., Clague, M.J., Urbe, S., and Jackson, S.P. (2014). Systematic characterization of deubiquitylating enzymes for roles in maintaining genome integrity. In Nature Cell Biology.

Patel, A., Lee, H.O., Jawerth, L., Maharana, S., Jahnel, M., Hein, M.Y., Stoynov, S., Mahamid, J., Saha, S., Franzmann, T.M., *et al.* (2015). A Liquid-to-Solid Phase Transition of the ALS Protein FUS Accelerated by Disease Mutation. Cell *162*, 1066-1077.

Pedersen, M.T., and Helin, K. (2010). Histone demethylases in development and disease. Trends in cell biology *20*, 662-671.

Peng, Z., Mizianty, M.J., and Kurgan, L. (2014). Genome-scale prediction of proteins with long intrinsically disordered regions. Proteins *82*, 145-158.

Peters, J., Franke, W., and Kleinschmidt, J. (1994). Distinct 19S and 20S subcomplexes of the 26S Proteasome and their distribution in the nuecleus and the cytoplasm. In The Journal of Biological Chemistry, pp. 7709-7718.

Peters, J.M., Walsh, M.J., and Franke, W.W. (1990). An abundant and ubiquitous homo-oligomeric ring-shaped ATPase particle related to the putative vesicle fusion proteins Sec18p and NSF. In EMBO Journal, pp. 1757-1767.

Peterson, A.C., Russell, J.D., Bailey, D.J., Westphall, M.S., and Coon, M.S. (2012). Parallel reaction monitoring for high resolution and high mass accuracy quantitative, targeted proteomics. In Molecular and Cellular Proteomics, pp. 1475-1488.

Picotti, P., and Aebersold, R. (2012). Selected reaction monitoring–based proteomics: workflows, potential, pitfalls and future directions. In Nature methods, pp. 555-566.

Picotti, P., Bodenmiller, B., Mueller, L.N., Domon, B., and Aebersold, R. (2009). Full dynamic range proteome analysis of S. cerevisiae by targeted proteomics. Cell *138*, 795-806.

Polo, S.E., Roche, D., and Almouzni, G. (2006). New histone incorporation marks sites of UV repair in human cells. Cell *127*, 481-493.

Postberg, J., Alexandrova, O., Cremer, T., and Lipps, H.J. (2005). Exploiting nuclear duality of ciliates to analyse topological requirements for DNA replication and transcription. Journal of cell science *118*, 3973-3983.

Rappsilber, J., Mann, M., and Ishihama, Y. (2007). Protocol for micro-purification, enrichment, pre-fractionation and storage of peptides for proteomics using StageTips. In Nature protocols, pp. 1896-1906.

Raschle, M., Smeenk, G., Hansen, R.K., Temu, T., Oka, Y., Hein, M.Y., Nagaraj, N., Long, D.T., Walter, J.C., Hofmann, K., *et al.* (2015). DNA repair. Proteomics reveals dynamic assembly of repair complexes during bypass of DNA cross-links. In Science, pp. 1253671.

Ray-Gallet, D., Woolfe, A., Vassias, I., Pellentz, C., Lacoste, N., Puri, A., Schultz, D.C., Pchelintsev, N.A., Adams, P.D., Jansen, L.E., *et al.* (2011). Dynamics of histone H3 deposition in vivo reveal a nucleosome gap-filling mechanism for H3.3 to maintain chromatin integrity. Molecular Cell *44*, 928-941.

Rhee, H.S., Bataille, A.R., Zhang, L., and Pugh, B.F. (2014). Subnucleosomal structures and nucleosome asymmetry across a genome. Cell *159*, 1377-1388.

Rosenbeger, G., Koh, C.C., Guo, T., Röst, H.L., Kouvonen, P., Collins, B.C., Heusel, M., Liu, Y., Caron, E., Vichalkovski, A., *et al.* (2014). A repository of assays to quantify 10,000 human proteins by SWATH-MS. Scientific Data *1*.

Röst, H.L., Rosenberger, G., Navarro, P., Gillet, L., Miladinovic, S.M., Schubert, O.T., Wolski, W., Collins, B.C., Malmstrom, J., Malmstrom, L., *et al.* (2014). OpenSWATH enables automated, targeted analysis of data-independent acquisition MS data. Nat Biotechnol *32*, 219-223.

Rouiller, I., DeLaBarre, B., May, A.P., Weis, W.I., Brunger, A.T., Milligan, R.A., and Wilson-Kubalek, E.M. (2002). Conformational changes of the multifunction p97 AAA ATPase during its ATPase cycle. In Nat Struct Biol, pp. 950-957.

Sauer, P., Timm, J., Liu, D., Sitbon, D., Boeri-Erba, E., Velours, C., Mücke, N., Langowksi, J., Ochsenbein, F., Almouzni, G., *et al.* (2017). Insights into the molecular architecture and histone H3-H4 deposition mechanism of yeast Chromatin assembly factor 1. eLife *10.7554/eLife.23474*.

Scharf, A.N., Meier, K., Seitz, V., Kremmer, E., Brehm, A., and Imhof, A. (2009). Monomethylation of lysine 20 on histone H4 facilitates chromatin maturation. In Molecular and Cellular Biology, pp. 57-67.

Scholes, T., D., , Banerjee, M., Bowen, B., and Curcio, M., j., (2001). Multiple regulators of Ty1 transposition in Saccharomyces cerevisiae have conserved roles in genome maintenance. Genetics *159*, 1449-1465.

Schubert, T., Pusch, M.C., Diermeier, S., Benes, V., Kremmer, E., Imhof, A., and Langst, G. (2012). Df31 protein and snoRNAs maintain accessible higher-order structures of chromatin. In Molecular Cell, pp. 434-444.

Selth, L., and Svejstrup, J.Q. (2007). Vps75, a new yeast member of the NAP histone chaperone family. Journal of Biological Chemistry *282*, 12358-12362.

Shahmoradian, A.H., MGalaz-Montoya, J.G., Schmid, M.F., Cong, Y., Ma, B., Spiess, C., Frydman, J., Ludtke, S.J., and Chiu, W. (2013). TRiC's tricks inhibit huntingtin aggregation. eLife *2*, 1-17.

Shevchenko, A., Wilm, M., Vorm, O., and Mann, M. (1996). Mass Spectrometric Sequencing of proteins from silver-stained Polyacrylamide gels. Analytical Chemistry *68*, 850-858.

Shi, Y., Lan, F., Matson, C., Mulligan, P., Whetstine, J.R., Cole, P.A., Casero, R.A., and Shi, Y. (2004). Histone demethylation mediated by the nuclear amine oxidase homolog LSD1. In Cell, pp. 941-953.

Shibahara, K., and Stillman, B. (1999). Replication-dependent marking of DNA by PCNA facilitates CAF-1-coupled inheritance of chromatin. In Cell, pp. 575-585.

Shimamura, A., and Worcel, A. (1989). The assembly of regularly spaced nucleosomes in the xenopus oocyte S-150 extract is accompanied by deacetylation of histone H4. In Journal of Biological Chemistry, pp. 14524-14530.

Shopland, L.S., Lynch, C.R., Peterson, K.A., Thornton, K., Kepper, N., Hase, J., Stein, S., Vincent, S., Molloy, K.R., Kreth, G., *et al.* (2006). Folding and organization of a contiguous chromosome region according to the gene distribution pattern in primary genomic sequence. J Cell Biol *174*, 27-38.

Sirbu, B.M., Couch, F.B., and Cortez, D. (2012). Monitoring the spatiotemporal dynamics of proteins at replication forks and in assembled chromatin using isolation of proteins on nascent DNA. In Nat Protoc, pp. 594-605.

Sirbu, B.M., Couch, F.B., Feigerle, J.T., Bhaskara, S., Hiebert, S.W., and Cortez, D. (2011). Analysis of protein dynamics at active, stalled, and collapsed replication forks. Genes & development *25*, 1320-1327.

Sirbu, B.M., McDonald, W.H., Dungrawala, H., Badu-Nkansah, A., Kavanaugh, G.M., Chen, Y., Tabb, D.L., and Cortez, D. (2013). Identification of proteins at active, stalled, and collapsed replication forks using isolation of proteins on nascent DNA (iPOND) coupled with mass spectrometry. In The Journal of Biological Chemistry, pp. 31458-31467.

Smith, D.J., and Whitehouse, I. (2012). Intrinsic coupling of lagging-strand synthesis to chromatin assembly. In Nature, pp. 434-438.

Smith, P.A., Jackson, V., and Chalkley, R. (1984). Two-stage maturation process for newly replicated chromatin. In Biochemistry, pp. 1576-1581.

Solovei, I., Kreysing, M., Lanctot, C., Kosem, S., Peichl, L., Cremer, T., Guck, J., and Joffe, B. (2009). Nuclear architecture of rod photoreceptor cells adapts to vision in mammalian evolution. Cell *137*, 356-368.

Stavreva, D.A., Muller, W.G., Hager, G.L., Smith, C.L., and McNally, J.G. (2004). Rapid glucocorticoid receptor exchange at a promoter is coupled to transcription and regulated by chaperones and proteasomes. Molecular and Cellular Biology *24*, 2682-2697.

Stevens, T.S., Lando, D., Basu, S., Atkinson, L.P., Cao, Y., Lee, S.F., Leeb, M., Wohlfahrt, K.J., Boucher, W., O'Shaughnessy-Kriwan, A., *et al.* (2017). 3D structures of individual mammalian genomes studied by single-cell Hi-C. Nature *544*, 59-64.

Strahl, B.D., and Allis, C.D. (2000). The language of covalent histone modifications. In Nature, pp. 41-45.

Su, D., Hu, Q., Li, Q., Thompson, J.R., Cui, G., Fazly, A., Davies, B.A., Botuyan, M.V., Zhang, Z., and Mer, G. (2012). Structural basis for recognition of H3K56-acetylated histone H3-H4 by the chaperone Rtt106. In Nature, pp. 104-107.

Szutorisz, H., Georgiou, A., Tora, L., and Dillon, N. (2006). The proteasome restricts permissive transcription at tissue-specific gene loci in embryonic stem cells. Cell *127*, 1375-1388.

Tagami, H., Ray-Gallet, D., Almouzni, G., and Nakatani, Y. (2004). Histone H3.1 and H3.3 complexes mediate nucleosome assembly pathways dependent or independent of DNA synthesis. In Cell, pp. 51-61.

Tan, M., Luo, H., Lee, S., Jin, F., Yang, J.S., Montellier, E., Buchou, T., Cheng, Z., Rousseaux, S., Rajagopal, N., *et al.* (2011). Identification of 67 histone marks and histone lysine crotonylation as a new type of histone modification. Cell *146*, 1016-1028.

Tompa, P., and Csermely, P. (2004). The role of structural disorder in the function of RNA and protein chaperones. FASEB J *18*, 1169-1175.

Tran, J.C., Zamdborg, L., Ahlf, D.R., Lee, J.E., Catherman, A.D., Durbin, K.R., Tipton, J.D., Vellaichamy, A., Kellie, J.F., Li, M., *et al.* (2011). Mapping intact protein isoforms in discovery mode using top-down proteomics. In Nature, pp. 254-258.

Tsou, C.C., Avtonomov, D., Larsen, B., Tucholska, M., Choi, H., Gingras, A.C., and Nesvizhskii, A.I. (2015). DIA-Umpire: comprehensive computational framework for data-independent acquisition proteomics. Nature methods *12*, 258-264, 257 p following 264.

Tsunaka, Y., Fujiwara, Y., Oyama, T., Hirose, S., and Morikawa, K. (2016). Integrated molecular mechanism directing nucleosome reorganization by human FACT. In Genes & development, pp. 673-686.

Turner, B.M., O'Neill, L.P., and Allan, I.M. (1989). Histone H4 acetylation in human cells. Frequency of acetylation at different sites defined by immunolabeling with site-specific antibodies. FEBS Letters *253*, 141-145.

Tyanova, S., Temu, T., Sinitcyn, P., Carlson, A., Hein, M.Y., Geiger, T., Mann, M., and Cox, J. (2016). The Perseus computational platform for comperehensive analysis of (prote)omics data. Nature methods *13*, 731-740.

Tyler, J.K., Collins, K.A., Prasad-Sinha, J., Amiott, E., Bulger, M., Harte, P.J., Kobayashi, R., and Kadonaga, J.T. (2001). Interaction between the Drosophila CAF-1 and ASF1 chromatin assembly factors. Molecular and Cellular Biology *21*, 6574-6584.

Udvardy, A. (1993). Purification and characterization of a multiprotein component of the Drosophila 26S (1500kDa) Proteolytic Complex. In The Journal of Biological Chemistry, pp. 9055-9062.

Ulrich, H.D. (2014). Two-way communications between ubiquitin-like modifiers and DNA. Nat Struct Biol *21*, 317-324.

Usakin, L., Abad, J., Vagin, V.V., de Pablos, B., Villasante, A., and Gvozdev, V.A. (2007). Transcription of the 1.688 satellite DNA family is under the control of RNA interference machinery in Drosophila melanogaster ovaries. Genetics *176*, 1343-1349.

Uversky, V.N. (2002). Natively unfolded proteins: a point where biology waits for physics. Protein Sci *11*, 739-756.

Van Holde, K.E. (1989). Chromatin. In Springer Series in Molecular Biology.

van Wijk, S.J., and Timmers, H.T. (2010). The family of ubiquitin-conjugating enzymes (E2s): deciding between life and death of proteins. FASEB J *24*, 981-993.

Varga-Weisz, P. (2001). ATP-dependent chromatin remodeling factors: Nucleosome shufflers with many missions. Oncogene *20*, 3076-3085.

Varshavsky, A. (1991). Naming a targeting signal. Cell *64*, 13-15.

Varshavsky, A. (2012). The Ubiquitin System, an Immense Realm. In Annual review of biochemistry, pp. 167-176.

Venkatesh, S., and Workman, J.L. (2015). Histone exchange, chromatin structure and the regulation of transcription. Nat Rev Mol Cell Biol *16*, 178-189.

Verreault, A., Kaufman, P.D., Kobayashi, R., and Stillman, B. (1996). Nucleosome assembly by a complex of CAF-1 and acetylated histones H3/H4. Cell *87*, 95-104.

Völker-Albert, M.C., Pusch, M.C., Fedisch, A., Schilcher, P., Schmidt, A., and Imhof, A. (2016). A quantitative proteomic analysis of in vitro assembled chromatin. In Molecular and Cellular Proteomics, pp. 945-959.

Wachsmuth, M., Knoch, T.A., and Rippe, K. (2016). Dynamic properties of independent chromatin domains measured by correlation spectroscopy in living cells. In Epigenetics and Chromatin (BioMed Central), pp. 1-20.

Wagner, G., Bancaud, A., Quivy, J.-P., Clapier, C., Almouzni, G., and Viovy, J.L. (2005). Compaction kinetics on single DNAs: purified nucleosome reconstitution systems versus crude extract. In Biophys J, pp. 3647-3659.

Wang, X., Arai, S., Song, X., Reichart, D., Du, K., Pascual, G., Tempst, P., Rosenfeld, M.G., Glass, C.K., and Kurokawa, R. (2008). Induced ncRNAs allosterically modify RNA-binding proteins in cis to inhibit transcription. Nature *454*, 126-130.

Washburn, M.P., Wolters, D., and Yates, J., R., (2001). Large-scale analysis of the yeast proteome by multidimensional protein identification technology. Nat Biotechnol *19*, 242-247.

Williamson, J.R. (2000). Induced fit in RNA-protein recognition. Nat Struct Biol *7*, 834-837.

Winkler, D.D., Zhou, H., Dar, M.A., Zhang, Z., and Luger, K. (2012). Yeast CAF-1 assembles histone (H3-H4)2 tetramers prior to DNA deposition. In Nucleic acids research, pp. 10139-10149.

Wisniewski, J.R., Zougman, A., Nagaraj, N., and Mann, M. (2009). Universal sample preparation method for proteome analysis. Nature methods *6*, 359-362.

Wong, J., Patterton, D., Imhof, A., Guschin, D., Shi, Y.B., and Wolffe, A.P. (1998). Distinct requirements for chromatin assembly in transcriptional repression by thyroid hormone receptor and histone deacetylase. EMBO Journal *17*, 520-534.

Worcel, A., Han, S., and Wong, M.L. (1978). Assembly of newly replicated chromatin. In Cell, pp. 969-977.

Yadav, T., and Whitehouse, I. (2016). Replication-Coupled Nucleosome Assembly and Positioning by ATP-Dependent Chromatin-Remodeling Enzymes. In Cell reports, pp. 715-723.

Zhang, H., Gan, H., Wang, Z., Lee, J.H., Zhou, H., Ordog, T., Wold, M.S., Ljungman, M., and Zhang, Z. (2017). RPA Interacts with HIRA and Regulates H3.3 Deposition at Gene Regulatory Elements in Mammalian Cells. Molecular Cell *65*, 272-284.

Zhang, Z., Shibahara, K., and Stillman, B. (2000). PCNA connects DNA replication to epigenetic inheritance in yeast. Nature *408*, 221-225.

Zhu, Q., Wani, G., Arab, H.H., El-Mahdy, M.A., Ray, A., and Wani, A.A. (2009). Chromatin restoration following nucleotide excision repair involves the incorporation of ubiquitinated H2A at damaged genomic sites. DNA Repair (Amst) *8*, 262-273.

Zink, L.M., and Hake, S.B. (2016). Histone variants: nuclear function and disease. In Curr Opin Genet Dev, pp. 82-89.

ABBREVIATIONS

°C	Degree Celsius
µ	Micro
3D	3 dimensions
A	Ampere
Å	*Ångström*
a, y, b ions	Type of fragment ion
Ac	Acetylation
Acetyl CoA	Acetyl coenzyme A
Acf1	ATP-dependent chromatin assembly factor
ACN	Acetonitrile
al.	Altera
ASF1	Anti-silencing function 1
ATP	Adenosintriphosphate
ATRX	ATP dependent X-linked helicase
bp	Base pair
BSA	Bovine serum albumin
C	Centi
C18	Octadecyl carbon chain
ca.	Circa
CAF	Chromatin assembly factor
CAS	CRISPR-associated protein 9
Cdc48	Cell division cycle 48
CFTR	Cystic fibrosis transmembrane conductance regulator)
CHRAC	Chromatin accessibility complex
CID	Collision-induced dissociation
CMG helicase	Cdc45-Mcm-GINS complex
Cps	Counts per seconds
CRISPR	Clustered regulatory interspaced short palindromic repeats
$CRL2^{LRR1}$	Cullin 2-RING ubiquitin ligase/leucine-rich repeat protein-1
CSK buffer	Cytoskeletal buffer
Csm3	Chromosome segregation in meiosis protein 3
.csv	Comma-separated values
Cul4B	Cullin 4B
Da	Dalton
DAPI	4’, 6-Diamidin-2-phenylindol
DAXX	Death domain-associated protein
dCTP, dGTP, dUTP, dATP	Deoxy Cytidine, Guanosine, Uridine, Adenosine triphosphate
DDA	Data-dependent acquisition
ddH_2O	Double-distilled water

Df31	Decondensation factor 31
DIA	Data-independent acquisition
Dm-ChP	DNA-mediated chromatin pull-down
DMEM	Dulbecco's modified eagle medium
DMSO	Dimethyl sulfoxide
DNA	Deoxyribonucleic acid
DNMT1	DNA methyltransferase 1
dNTP	Deoxy nucleotide triphosphate
DREX	Drosophila embryonic extract
DSB	Double strand break
DTT	1,4-Dithiothreitol
DUB	Deubiquitinating enzyme
E.coli	*Escherichia coli*
e.g.	Exempli gratia: for example
E1/E2/E3 enzyme	Ubiquitin activating protein 1/2/3
ECL	Enhanced chemiluminescence
EDTA	Ethylenediaminetetraacetic acid
EdU	5-Ethynyl-2'-deoxyuridine
EGTA	Ethylene glycol-bis-tetra acetic acid
ENSG	Ensemble gene
Esco2	Establishment of sister chromatid cohesion N-acetyltransferase 2
ESI	Electrospray ionization
EtOH	Ethanol
FA	Fluoroacetic acid
FACS	Fluorescence-activated cell sorting
FACT	Facilitates chromatin transcription
FASP	Filter-aided sample preparation
FBgn	Flybase gene
FBS	Fetal bovine serum
FCS	Fetal calf serum
FDR	False discovery rate
FEN1	Flap endonuclease 1
FSC/SSC	Forward scatter/Sideward scatter
FW	Forward
G	Gram
g/RCF	Relative centrifugal force
G1/G2 phase	Gap phase
GASP	Gel-assisted sample preparation
Gcn5	Histone acetyltransferase 5
GINS	Go, Ichi, Nii and San; five, one, two and three in Japanese

GlyGly	Glycine-Glycine
Gnf	Germ line transcription factor
GO	Gene ontology
h/hrs	Hour/hours
H1, H3, H2A, H2B, H4	Histones
HAT	Histone-acetyltransferase
HDAC	Histone deacetylase
Hela S3 cells	Henrietta Lacks S3 cells
HF	High fidelity
HIRA	Histone cell cycle regulator
HMT	Histone methyltransferase
HP1	Heterochromatin protein 1
HPLC	High performance liquid chromatography
HR	Homologous recombination
Hsp	Heat shock protein
IAA	Iodoacetamide
iBAQ	Intensity based absolute quantification
IF	Immunofluorescence
Inh	inhibitor
iPOND	Isolation of proteins on nascent DNA
Irbp	Inverted repeat binding protein
Iswi	Imitation switch
JMJD2	Jumonji domain 2
K5/K12	Lysine 5/12
Kb	Kilobase
KBH	Krebs-bicarbonate-Hepes buffer
L	Litre
LB	Luria-Bertani
LC-MS/MS	Liquid chromatography mass spectrometry
LFQ	Label-free quantitation
Log	Logarithm
LSD1	Lysine specific demethylase 1
LTQ	Linear trap quadrupole
M	Meter
M	Milli
M	Molar
m/z	Mass-to-charge ratio
Mcm	Mini-chromosome maintenance
Me	Methylation
Min	Minute/minutes
MNase	Micrococcal nuclease

Mrc1	Mannose receptor, C type 1
MRM	Multiple reaction monitoring
MS	Mass spectrometry
MS1/2	Mass spectrum 1/2
N	Nano
Nap1	Nucleosome assembly protein
Nc	Nicked
NCC	Nascent chromatin capture
NEM	N-Ethylmaleimide
NHEJ	Non-homologous end joining
NP-40	Nonyl phenoxypolyethoxylethanol
o/n	Over night
Orc	Origin recognition complex
PASEF	Parallel accumulation-serial fragmentation
PBS	Phosphate buffered saline
PCNA	Proliferating cell nuclear antigen
PCR	Polymerase chain reaction
Pen/strep	Penicillin/Streptomycin
pH	Potential of hydrogen
PhD	Doctor of Philosophy
PI	Propidium iodide
PIP	PCNA-interacting protein motif
PMSF	Phenylmethylsulphonylfluoride
Ppm	Parts per million
PRM	Parallel reaction monitoring
PSM	Peptide spectra matches
PTM	Post-translational modification
PVDF	Polyvinylidene fluoride
Q	Quadrupole
Q-TOF	Quadrupole-time-of-flight
R^2	Coefficient of determination
Rel	Relaxed
Rep	Replicate
Rfc	Replication factor
RNA	Ribonucleic acid
RNA pol II	RNA polymerase II
RPA	Replication protein A
Rpm	Revolutions per minute
Rpn	Proteasome regulatory particle, Non-ATPase-like
rRNA	Ribosomal RNA
RT	Room temperature

Rtt106/Rtt109	Regulator of Ty1 transposition 106/109
RV	Reverse
SAM	S-adenosyl methionine
Sc	Supercoiled
SDS	Sodium dodecyl sulphate
SDS-PAGE	SDS-Polyacrylamide gel electrophoresis
SILAC	Stable isotope labelling by amino acids in cell culture
SK (bluescript)	SacI and KpnI cloning sites
SLIDER	Super-fast predictor of proteins with long intrinsically disordered regions
SMC	Structural maintenance of chromosomes
S-phase	Synthesis-phase
SRM	Selected reaction monitoring
SUV39H1	Suppressor of variegation 3-9 homologue 1
SWATH	Sequential window acquisition of all theoretical fragment ion spectra
TBE	Tris-borate-EDTA buffer
TBS-buffer	Tris buffered saline
TCP-1	T-complex protein 1
TE-buffer	Tris-EDTA buffer
TFA	Trifluoroacetic acid
Tip60	HIV-1 Tat interactive protein, 60kDa
TOF	Time-of-flight
TriC/CCT	TCP-1 Ring complex/chaperoning containing TCP-1
TSA	Trichostatin A
Txt	Text file
U	Unit
Ub	Ubiquitination
UCHL5	Ubiquitin carboxyl-terminal hydrolase isozyme L
UHRF1	Ubiquitin like with PHD and RING finger domains 1
UPS	Ubiquitin Proteasome-System
USP14	Ubiquitin specific peptidase 14
UV	Ultraviolet light
V	Volt
v/v	Volume per volume
Vcp	Valosin-containing protein
w/v	Weight per volume
XIC	Extracted ion chromatogram
XRCC	X-ray repair cross-complementing protein
Zvi file	Zeiss vision image

APPENDIX

Table 1: Functional Annotation Clustering for factors enriched or repelled upon TSA.

GO-term analysis of 15 min unperturbed assembly

Enrichment Score: 9.22

Term	Count	PValue	FDR
mitotic spindle organization	25	3.80E-13	6.01E-10
microtubule cytoskeleton organization	29	3.47E-12	5.49E-09
mitotic cell cycle	28	1.36E-09	2.15E-06
cell cycle process	32	6.80E-08	1.08E-04

Enrichment Score: 6.2

Term	Count	PValue	FDR
atp-binding	31	7.92E-10	9.74E-07
nucleotide binding	53	2.67E-08	3.60E-05
ATPase activity	24	5.61E-07	7.57E-04
ribonucleotide binding	41	1.68E-06	0.002265

Enrichment Score: 5.04

Term	Count	PValue	FDR
glycolysis	8	2.90E-08	3.56E-05
gluconeogenesis	5	1.32E-06	0.001627
binding site:Substrate	6	0.016564	19.71693
sequence variant	12	0.087857	70.15314

Enrichment Score: 4.94

Term	Count	PValue	FDR
DNA packaging	13	3.84E-09	6.07E-06
nucleosome organization	11	9.58E-09	1.52E-05
chromatin assembly	9	3.71E-07	5.86E-04
nucleosome assembly	8	1.12E-06	0.001774

GO-term analysis of 15 min TSA treated assembly

Enrichment Score: 2.12

Term	Count	PValue	FDR
cytoplasm	14	1.63E-04	0.186748
alternative splicing	13	0.010174	11.04422
splice variant	13	0.256158	97.44797

Enrichment Score: 1.85

Term	Count	PValue	FDR
cell division	10	2.03E-04	0.309723
septin ring	3	9.74E-04	1.215431
cell cortex part	4	0.021168	23.53893
cell cycle	12	0.043918	49.58396

Enrichment Score: 1.76

Term	Count	PValue	FDR
cell cortex	6	0.002667	3.294388
organelle localization	4	0.039664	46.05263
organelle localization	4	0.049507	53.89628

Enrichment Score: 1.75

Term	Count	PValue	FDR
nuclear envelope	8	1.04E-04	0.131005
endomembrane system	10	0.001763	2.189531
nuclear pore	5	0.002557	3.161166
pore complex	5	0.003245	3.994777

GO-term analysis of 1 h unperturbed assembly

Enrichment Score: 9.28

Term	Count	PValue	FDR
microtubule cytoskeleton organization	29	2.47E-14	3.87E-11
mitotic spindle organization	23	4.60E-13	7.20E-10
mitotic cell cycle	26	4.97E-10	7.78E-07
M phase	27	4.20E-08	6.58E-05

Enrichment Score: 4.80

Term	Count	PValue	FDR
Chaperonin Cpn60/TCP-1	7	9.96E-09	1.37E-05
protein folding	14	3.95E-08	6.18E-05
Chaperone	8	3.84E-06	0.004638
GO:0016887~ATPase activity	14	0.007046	8.940187

Enrichment Score: 3.62

Term	Count	PValue	FDR
nucleotide-binding	30	3.63E-09	4.39E-06
atp-binding	23	6.76E-07	8.17E-04
ATPase activity, coupled	13	0.00604	7.709858
ATPase activity	14	0.007046	8.940187

Enrichment Score: 3.61

Term	Count	PValue	FDR
proteasome	11	4.55E-11	5.50E-08
proteasome complex	12	1.87E-08	2.29E-05
Proteasome, subunit alpha/beta	7	8.97E-07	0.001234
proteasome core complex	7	8.17E-06	0.010008

GO-term analysis of 1 h TSA treated assembly

Enrichment Score: 2.59

Term	Count	PValue	FDR
ligase	12	1.91E-04	0.233314
ligase activity	10	9.84E-04	1.314718
acid-amino acid ligase activity	9	0.001069	1.427017
small conjugating protein ligase activity	7	0.005496	7.1377

Enrichment Score: 2.08

Term	Count	PValue	FDR
cytoskeleton	10	8.61E-06	0.010528
cytoskeleton organization	23	3.30E-05	0.052609
cytoskeletal part	17	3.56E-04	0.464948
mitosis	10	0.001368	2.159029

Enrichment Score: 2.03

Term	Count	PValue	FDR
Transcription factor CBF/NF-Y	4	2.14E-04	0.302006
Histone-fold	4	0.008696	11.5976
sequence-specific DNA binding	6	0.407632	99.91201

Enrichment Score: 1.98

Term	Count	PValue	FDR
nuclear envelope	10	8.09E-05	0.10594
nuclear pore	7	3.54E-04	0.462561
pore complex	7	5.06E-04	0.660863
organelle envelope	13	0.064149	58.0273

GO-term analysis of 4 h unperturbed assembly

Enrichment Score: 7.66

Term	Count	PValue	FDR
microtubule cytoskeleton organization	22	1.76E-10	2.72E-07
cytoskeleton organization	26	8.11E-10	1.25E-06
mitotic spindle organization	17	3.52E-09	5.44E-06
mitotic cell cycle	22	5.03E-09	7.78E-06

Enrichment Score: 3.43

Term	Count	PValue	FDR
glycolysis	7	6.80E-08	8.09E-05
gluconeogenesis	4	2.69E-05	0.032023
binding site:Substrate	4	0.095377	71.81538
sequence variant	8	0.24148	96.95562

Enrichment Score: 2.73

Term	Count	PValue	FDR
protein folding	10	1.79E-05	0.027585
Chaperone	6	2.00E-04	0.23782
Chaperonin Cpn60/TCP-1	4	3.78E-04	0.49338
unfolded protein binding	6	0.003623	4.63903

Enrichment Score: 2.73

Term	Count	PValue	FDR
proteasome	8	1.48E-07	1.76E-04
proteasome complex	9	5.23E-06	0.006187
Proteasome, subunit alpha/beta	6	7.74E-06	0.010139
ubl conjugation pathway	3	0.232195	95.68984

GO-term analysis of 4 h TSA treated assembly

Enrichment Score: 4.07

Term	Count	PValue	FDR
chromosome	23	2.24E-05	0.029437
chromosomal part	20	2.99E-05	0.039307
non-membrane-bounded organelle	44	2.71E-04	0.356303
non-membrane-bounded organelle	44	2.71E-04	0.356303

Enrichment Score: 3.01

Term	Count	PValue	FDR
DNA metabolic process	17	5.77E-05	0.092643
DNA repair	10	6.16E-04	0.98601
cellular response to stress	13	8.41E-04	1.343486
response to DNA damage stimulus	10	0.001459	2.318664

Enrichment Score: 2.24

Term	Count	PValue	FDR
translational initiation	8	2.72E-04	0.43593
translation initiation factor activity	8	3.37E-04	0.457158
protein biosynthesis	8	0.001828	2.213803
Initiation factor	4	0.027596	28.99392

Enrichment Score: 2.18

Term	Count	PValue	FDR
cytoskeleton	10	4.34E-05	0.053145
cell cycle	10	7.91E-05	0.096712
microtubule cytoskeleton organization	15	0.010139	15.10588
spindle organization	12	0.01656	23.53692

Table 1, Appendix: Coloured Proteins with Log2(x) values in Fig. 3. 11B were processed with the Functional Annotation Tool from DAVID Bioinformatics Resources 6.7, NIAID/NIH. FBgn numbers were uploaded as list and used for the search for GO-terms of biological processes according to the *Drosophila melanogaster* background with a threshold of 2 counts and an EASE of 0.1. Table shows GO-terms with highest enrichment scores for proteins enriched or repelled upon TSA treatment for samples after all three time points of assembly.

Figure 1: Histone modification analysis upon TSA treatment.

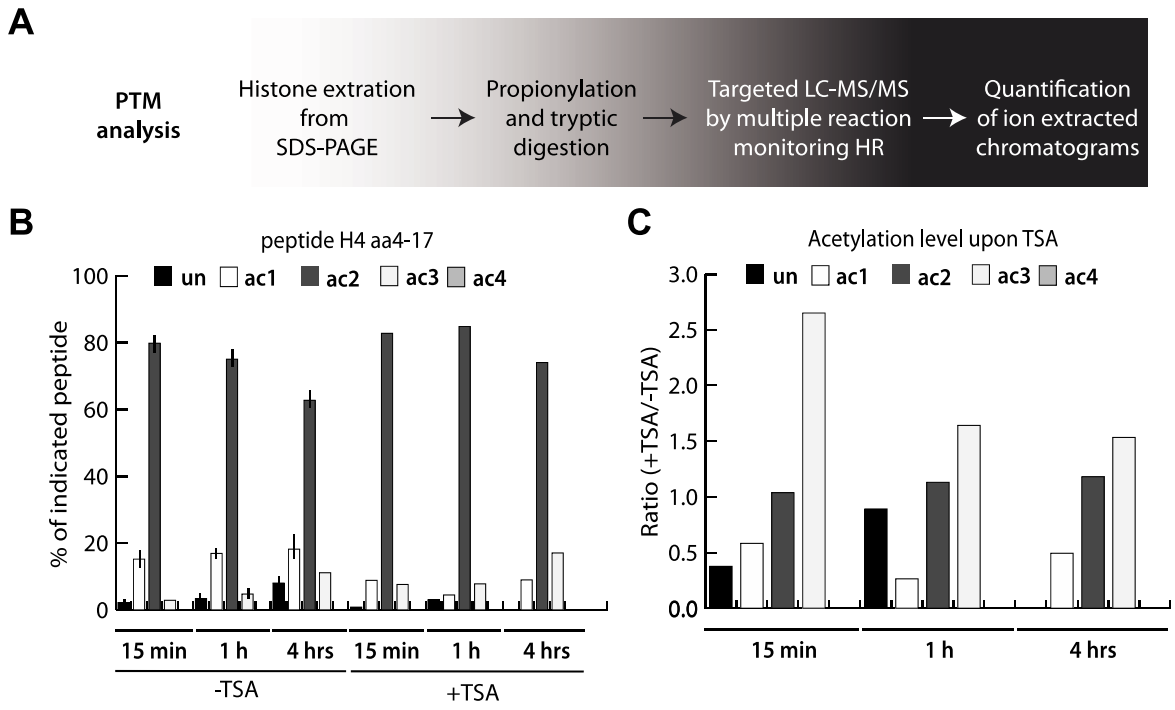

Figure 1, Appendix: A: Workflow of PTM analysis by MRM-HR analysis (see section 2.2.6.: Mass spectrometry methods/Histone modification analysis on LC-MS/MS on Q-TOF mass spectrometer). **B:** Quantification of MRM-HR data for histone peptide H4 aa4-17. unmod, unmodified; ac, acetylation; me, methylation; TSA, Trichostatin A. (see section 2.2.7.: Software Methods/Data analysis of histone modifications). **C:** Ratio of acetylation levels on peptide H4 aa4-17 comparing treatment and no-treatment in the time course of 15 min, 1 h and 4 hrs.

Table 2: Identified Peptides with GlyGly(k) modifications *in vitro* and *in vivo*.

***In vitro* identified peptides with GlyGly(K) modification**

Flybase Protein	Protein Name	Sequence Window	Modified Sequence
FBpp0071216	Lim1-PA	DSQAENKSPDDAN	_GDSQAENK(gl)SPDDANGSK_
FBpp0072752	osm-1-PA	VDNYTGKKQTIIS	_IIIVDNYTGK(gl)K(gl)_
FBpp0075096	CG9951-PA	VQIDGEKIKNVIT	_EIEVQIDGEK(gl)_
FBpp0075754	CG5642-PA	FNDINRKIKNINI	_FNDINRK(gl)_
FBpp0077420	CG9961-PA	DNKKKVKADPAKV	_KVK(gl)ADPAK_
FBpp0077690	Lsp1beta-PA	DYEMWMKMTMYEK	_FDYEM(ox)WM(ox)K(gl)M(ox)TM(ox)YEK(gl)_
FBpp0078469	katanin-60-PA	YRGESEKMVRIIF	_GESEK(gl)M(ox)VRIIFEM(ox)AR_
FBpp0079682	Lip4-PA	VHEFIPKNEFISM	_IIGVHEFIPK(gl)_
FBpp0079976	PICK1-PA	FFFEEDKMGMTVS	_(ac)M(ox)ITDTEDDFFFEEDK(gl)M(ox)GM(ox)TVSTNAVVITK(gl)_
FBpp0081012	CG8671-PA	GMAFMMKKKKYKF	_MTIIGPSAPGM(ox)AFM(ox)M(ox)K(gl)K(gl)_
FBpp0082056	CG5196-PA	KKCEGYKAPRSHH	_KCEGYK(gl)APR_
FBpp0082173	CG11668-PA	GQIIEIKRISQHP	_GQIIEIK(gl)R_
FBpp0082175	Hsc70-2-PA	KIEVEFKGERKRF	_IEVEFK(gl)GER_
FBpp0082205	CG8630-PA	VVMFQKKMYFVVM	_K(gl)M(ox)YFVVM(ox)PICCFAIPM(ox)IFPYYVM(ox)GSSIR_
FBpp0082485	CG3987-PA	IAEDQIKNNTIVV	_(ac)M(ox)AHSM(ox)IKIGM(ox)M(ox)CGIIHIITFGVIAEDQIK(gl)_
FBpp0083145	Cyp12a4-PA	MSMPGGKYKNMEI	_INM(ox)WAISM(ox)K(gl)M(ox)SM(ox)PGGK(gl)_
FBpp0084150	vig2-PB	EPAKAPKAPKSKS	_KPEPAK(gl)APK(gl)_
FBpp0085859	Dp1-PC	TSVWGPKN_____	_NITAPNTQSQEDFPHFAAGGAPVASTPITSVWGPK(gl)_
FBpp0086114	EDTP-PA	IMVENRKIKYFMA	_K(gl)IK(gl)YFM(ox)AVSSSEK_
FBpp0111524	Pvf3-PA	KAKMVQKRRIHYN	_MVQK(gl)RR_
FBpp0111545	Rgk2-PA	KEKREKKATASKM	_K(gl)ATASKMK(gl)_
FBpp0288417	Ir25a-PB	NKRQIEKIKEKWW	_QIEK(gl)IKEK_
FBpp0291066	CG30410-PB	VVASCAKHFIVVA	_HMVIIKGGGGCIIQEKVVASCAK(gl)_
FBpp0291508	CG14967-PB	AEQMGSKRAKRDV	_IYGNICGAEQMGSK(gl)R_

***In vivo* identified peptides with GlyGly(K) modification**

Ensemble Protein	Protein name	Sequence window	GlyGly(K) Probabilities
ENSP00000396320	SCN4A_HUMAN	KKKLGGKDIFMTEEQKKYYNAMKKLGSKKPQ	DIFMTEEQK(1)
ENSP00000390667	DLDH_HUMAN	ASRGIEMSEVRLNLDKMMEQKSTAVKALTGG	LNLDK(0.98)MMEQK(0.02)
ENSP00000220058	FMT_HUMAN	IMQIRPKRFDVGPILKQETVPVPPKSTAKEL	FDVGPILK(1)
ENSP00000385990	FAKD2_HUMAN	MLTTLKPFGSVSVESKMNNKAGSFFWNLRQF	PFGSVSVESK(1)
ENSP00000241704	COPA_HUMAN	LSFLYLITGNLEKLRKMMKIAEIRKDMSGHY	K(1)MMK(1)IAEIR
ENSP00000258198	DC1L2_HUMAN	ESLQKWASVLREHIDKMKIPPEKMRELERKF	EHIDK(0.828)MK(0.172)IPPEK
ENSP00000261606	MYOM1_HUMAN	KLVDEAFKELMMEVCKKIALSATDLKIQSTA	ELMMEVCK(0.976)K(0.024)
ENSP00000262435	SMUF2_HUMAN	ELIICGLGKIDVNDWKVNTRLKHCTPDSNIV	IDVNDWK(0.998)VNTRLK(0.002)
ENSP00000263674	ARHGH_HUMAN	FLRQEMVIEVKAIGGKKDRSLFLFTDLIVCT	AIGGK(0.5)K(0.5)DR
ENSP00000393722	E41L5_HUMAN	LFFWPKITRLDFKKNKLTLVVVEDDDQGKEQ	LDFK(1)K(1)NK(1)
ENSP00000382350	TINF2_HUMAN	RNLGSPTQVISKPESKEEHAIYTADLAMGTR	PESK(1)EEHAIYTADLAMGTR
ENSP00000345230	TPM4_HUMAN	_____MDAIKKKMQMLKLDKENAIDR;	K(1)K(1)MQMLK
ENSP00000354322	GON4L_HUMAN	LPSGSQSAKPVSQPRKSTQPDVCASPQEKPL	PVSQPRK(1)
ENSP00000385659	RS27A_HUMAN	VKLAVLKYYKVDENGKISRLRRECPSDECGA	VDENGK(1)ISR
ENSP00000378710	F135B_HUMAN	ELGLPGGKLDFLMSEKNQMDTFADFDTMTDR	LDFLMSEK(1)
ENSP00000347255	SCN8A_HUMAN	LFIGVIIDNFNQQKKKFGGQDIFMTEEQKKY	K(0.22)K(0.78)FGGQDIFMTEEQK
ENSP00000328494	KI21B_HUMAN	RLKKKEVRQRRKSPEKEAFKKRAKLQQENSE	SPEK(1)EAFK
ENSP00000299314	GNPTA_HUMAN	LKELQQVREQMEEEQKAMREILGKNTTEPTK	EQMEEEQK(1)AMR
ENSP00000300035	PAF15_HUMAN	VPGTYRKVVAARAPRKVLGSSTSATNSTSVS	K(1)VLGSSTSATNSTSVSSR
ENSP00000388560	7B2_HUMAN	PGLGKWNKKLLYEKMKGGERRKRRSVNPYLQ	LLYEK(1)MK(1)GGER
ENSP00000357373	TPD53_HUMAN	QVLSAKERHLVEIKQKLGMNLMNELKQNFSK	QK(1)LGMNLMNELK
ENSP00000306678	ANKK1_HUMAN	ALRSRKQGIMSFLEGKEPSVATLGGSKPGAE	QGIMSFLEGK(1)
ENSP00000321000	CE152_HUMAN	QQLEKEWQSKLDQTIKAMKKKTLDCGSQTDQ	LDQTIK(1)AMK(1)
ENSP00000380180	H2B1C_HUMAN	ELAKHAVSEGTKAVTKYTSSK_____	AVTK(1)YTSSK
ENSP00000395368	G3V0I5_HUMAN	WRLKGSLSRGDWYKTKEILLKGPDWILGEIK	TK(1)EILLK
ENSP00000339063	EF1A1_HUMAN	FLKSGDAAIVDMVPGKPMCVESFSDYPPLGR	SGDAAIVDMVPGK(1)PMCVESFSDYPPLGR
ENSP00000349634	ZGPAT_HUMAN	GWEVHTRGIGSRLLTKMGYEFGKGLGRHAEG	LLTK(0.994)MGYEFGK(0.006)
ENSP00000343221	LRC69_HUMAN	LSGGKNTKIITLNGKKMTKMPSALGKLPGLK	IITLNGK(0.359)K(0.641)
ENSP00000348089	ERCC6_HUMAN	KSEAKEQSNDDYVLEKLFKKSVGVHSVMKHD	SEAK(1)EQSNDDYVLEK(1)
ENSP00000352185	PHF2_HUMAN	GLAAAAAKLSQQEEQKSKKKKSAKRKLTPNT	LSQQEEQK(1)SK(1)K(1)
ENSP00000353518	ANS1A_HUMAN	_____MGKEQELLEAARTGHLPA	GK(1)EQELLEAAR
ENSP00000356822	ADCYA_HUMAN	VAIWYARLQEWDNFYKFSNRAKNLLPRRTMT	LQEWDNFYK(0.833)FSNRAK(0.167)
ENSP00000392131	A2A3P3_HUMAN	LQEALIDTEKKLEEIKKQCQDKETQLICQKK	LEEIK(0.999)K(0.999)QCQDK(0.002)
ENSP00000358596	DUS5_HUMAN	_____MKVTSLDGRQLRKMLRK	K(1)VTSLDGR
ENSP00000360069	ZN831_HUMAN	AEKPWDAKAPEGRLRKCESTDSGYLSRSDSA	LRK(1)CESTDSGYLSR
ENSP00000361818	SDC4_HUMAN	IPERAGSGSQVPTEPKKLEENEVIPKRISPV	AGSGSQVPTEPK(0.823)K(0.177)
ENSP00000367851	CY24B_HUMAN	TKVVTHPFKTIELQMKKKGFKMEVGQYIFVK	TIELQMK(0.495)K(0.495)K(0.01)
ENSP00000381568	E9PB39_HUMAN	IPRSFLRSNHKKQMQKLVKAAKDGTKDGLER	SNHK(1)K(1)QMQK(1)
ENSP00000390546	H7BZN6_HUMAN	GPVTGSASRGPARGPKGMVIRSTVWLGFPNF	GPK(1)GMVIR
ENSP00000419325	SUCB2_HUMAN	LKVPLVVRLEGTFMEKKGSYMHIKQETGNSN	LEGTFMEK(0.964)K(0.036)

List 1: Kinetics of unperturbed chromatin assembly.

Name	Flybase gene identifier	Log2 (Median (15min/4hrs))	Name	Flybase gene identifier	Log2 (Median (15min/4hrs))
CG42593-PC	FBgn0260970	4.59710476	CG42232-PB	FBgn0250754	1.64679525
mod(mdg4)-PF	FBgn0002781	4.405093798	CG4069-PA	FBgn0036301	1.626599001
RanBP3-PA	FBgn0039110	3.973212716	Caf1-105-PA	FBgn0033526	1.614809546
PCNA-PB	FBgn0005655	3.281504949	HmgD-PD	FBgn0004362	1.613252666
hang-PD	FBgn0026575	3.24123152	RfC4-PA	FBgn0260985	1.603191232
Bap55-PA	FBgn0025716	3.207883189	CG4951-PB	FBgn0039563	1.602540108
CG10565-PB	FBgn0037051	2.849433183	Aprt-PD	FBgn0000109	1.592627045
GAPsec-PA	FBgn0035916	2.734499543	Etl1-PA	FBgn0032157	1.591343348
Ssrp-PA	FBgn0010278	2.650280085	wde-PB	FBgn0027499	1.5654209
CG6950-PD	FBgn0037955	2.649107245	cin-PA	FBgn0000316	1.557730198
Gnf1-PA	FBgn0004913	2.59225791	Bet3-PA	FBgn0260859	1.556608129
dre4-PB	FBgn0002183	2.564451503	Acf1-PA	FBgn0027620	1.534865764
Mlf-PC	FBgn0034051	2.553629785	SMC2-PA	FBgn0027783	1.52190871
CG9485-PF	FBgn0034618	2.46492676	Aats-arg-PA	FBgn0027093	1.514691342
ArfGAP1-PB	FBgn0020655	2.462555957	CG14036-PA	FBgn0031677	1.498703229
hyd-PB	FBgn0002431	2.425859845	wupA-PA	FBgn0004028	1.471453777
Dsor1-PB	FBgn0010269	2.384812789	CG6195-PA	FBgn0038723	1.464650886
CG13690-PA	FBgn0031252	2.373245836	CG8243-PA	FBgn0033349	1.453414407
Caf1-180-PB	FBgn0030054	2.281723088	Aats-glupro-PA	FBgn0005674	1.451811614
borr-PB	FBgn0032105	2.199839591	Cap-G-PF	FBgn0259876	1.435424738
CSN8-PB	FBgn0261437	2.140651091	mtd-PU	FBgn0013576	1.411815286
CG17209-PC	FBgn0030687	2.135994273	Aats-asp-PC	FBgn0002069	1.373994882
HmgZ-PD	FBgn0010228	2.109799805	ash2-PC	FBgn0000139	1.359511396
Rpd3-PA	FBgn0015805	2.099802947	gw-PJ	FBgn0051992	1.352473018
Parp-PB	FBgn0010247	2.090926931	Tap42-PA	FBgn0051852	1.314873737
Ote-PA	FBgn0266420	2.084105319	Aats-lys-PA	FBgn0027084	1.306353825
Orc1-PA	FBgn0022772	2.067508154	nbs-PE	FBgn0261530	1.28721259
Aats-ile-PD	FBgn0027086	2.05235669	RpS15-PB	FBgn0034138	1.267955035
barr-PC	FBgn0014127	2.037924217	CstF-64-PA	FBgn0027841	1.262717826
Rrp46-PA	FBgn0037815	2.033902095	MBD-R2-PB	FBgn0038016	1.247699459
CG18004-PB	FBgn0033566	2.019921698	Rpi-PC	FBgn0050410	1.243343949
lola-PD	FBgn0005630	2.010325379	SH3PX1-PA	FBgn0040475	1.241384213
Dpy-30L1-PA	FBgn0032293	1.941092265	Rox8-PH	FBgn0005649	1.214845918
RfC38-PB	FBgn0028700	1.940029787	Iswi-PC	FBgn0011604	1.208538011
Rad9-PB	FBgn0025807	1.923440081	Klp3A-PB	FBgn0011606	1.198172682
SmD1-PA	FBgn0261933	1.88415834	bigmax-PA	FBgn0039509	1.182091781
RfC3-PA	FBgn0032244	1.854482351	osa-PE	FBgn0261885	1.179943388
Arpc2-PB	FBgn0032859	1.7766489	FANCI-PA	FBgn0033354	1.178159014
Snr1-PA	FBgn0011715	1.776118139	mor-PA	FBgn0002783	1.173274683
CG30185-PA	FBgn0050185	1.671031727	Abp1-PA	FBgn0036372	1.169871094
CG33123-PB	FBgn0053123	1.667256265	fon-PC	FBgn0032773	1.168506821
CG9914-PB	FBgn0030737	1.662688196	CG8142-PA	FBgn0030871	1.16069826

Name	Flybase gene identifier	Log2 (Median (15min/4hrs))	Name	Flybase gene identifier	Log2 (Median (15min/4hrs))
CG8235-PA	FBgn0033351	1.160499717	Rab5-PI	FBgn0014010	0.781012935
Max-PD	FBgn0017578	1.155685774	egg-PA	FBgn0086908	0.776361973
Cap-D2-PA	FBgn0039680	1.134427096	Chd64-PB	FBgn0035499	0.770397419
CG15100-PA	FBgn0034401	1.131396214	Fen1-PA	FBgn0025832	0.7693874
MEP-1-PG	FBgn0035357	1.107451378	BigH1-PA	FBgn0038252	0.749942471
mre11-PA	FBgn0020270	1.090924701	lig-PK	FBgn0020279	0.746215214
rad50-PD	FBgn0034728	1.080069231	Rab35-PD	FBgn0031090	0.74240326
CG5098-PC	FBgn0034300	1.071532669	CG14110-PA	FBgn0036352	0.741987932
CG12129-PA	FBgn0033475	1.070347892	CG41099-PE	FBgn0039955	0.736894719
CG12304-PA	FBgn0036515	1.06593213	Chrac-16-PB	FBgn0043001	0.731394469
CG6045-PA	FBgn0038349	1.056398668	CG7339-PB	FBgn0036188	0.716221585
CG13142-PC	FBgn0032251	1.052404562	CG15717-PE	FBgn0030451	0.715466982
gkt-PA	FBgn0260817	1.043981554	eIF-3p66-PB	FBgn0040227	0.684056587
Chrac-14-PB	FBgn0043002	1.040427318	mago-PA	FBgn0002736	0.675385839
Prp19-PA	FBgn0261119	1.024314821	CG4300-PC	FBgn0036272	0.671247529
RanGAP-PB	FBgn0003346	1.023561451	Nup93-2-PA	FBgn0038274	0.669375647
CSN7-PA	FBgn0028836	1.021766745	sqh-PE	FBgn0003514	0.647496372
Rrp1-PA	FBgn0004584	1.015412034	Nsun2-PA	FBgn0026079	0.636240977
CG2982-PC	FBgn0266570	1.012161852	nesd-PA	FBgn0032848	0.635880998
Aats-gln-PA	FBgn0027090	1.005764856	vih-PA	FBgn0264848	0.634765281
Top2-PB	FBgn0003732	1.003683516	mbo-PA	FBgn0026207	0.632618347
Srp9-PA	FBgn0035827	0.999983934	CG32164-PB	FBgn0042177	0.623337724
Caf1-PA	FBgn0263979	0.993052199	sle-PB	FBgn0037810	0.619903531
CG1646-PB	FBgn0039600	0.989422618	Rrp4-PB	FBgn0034879	0.618398632
RhoGDI-PB	FBgn0036921	0.971244306	CG30122-PD	FBgn0050122	0.611843652
Dlc90F-PA	FBgn0024432	0.962195074	Trn-PD	FBgn0024921	0.608202786
RpLP1-PB	FBgn0002593	0.936401058	mod-PC	FBgn0002780	0.60771461
FK506-bp1-PA	FBgn0013269	0.932680423	Drep-2-PC	FBgn0028408	0.606225143
lola-PR	FBgn0005630	0.92376655	CG2918-PB	FBgn0023529	0.59274072
eIF5B-PF	FBgn0026259	0.914778382	Cp190-PB	FBgn0000283	0.587759684
CG33156-PF	FBgn0053156	0.901729785	tefu-PB	FBgn0045035	0.58548266
CG14309-PA	FBgn0038611	0.901700707	Hrb27C-PH	FBgn0004838	0.58216853
lolal-PH	FBgn0022238	0.897371018	Cul4-PB	FBgn0033260	0.577143183
asp-PA	FBgn0000140	0.886050196	Arf79F-PJ	FBgn0010348	0.575737578
CG15047-PA	FBgn0030938	0.856237375	CG1703-PB	FBgn0030321	0.575730333
Mi-2-PD	FBgn0262519	0.849118978	Ice-PA	FBgn0019972	0.571237224
PI31-PF	FBgn0033669	0.847743618	Bx42-PB	FBgn0004856	0.570164574
pnut-PA	FBgn0013726	0.839894726	Got2-PA	FBgn0001125	0.566365288
glu-PA	FBgn0015391	0.8255136	Dsp1-PG	FBgn0011764	0.55777954
Sip1-PA	FBgn0010620	0.823540346	Dis3-PB	FBgn0039183	0.548762627
eIF2B-delta-PD	FBgn0034858	0.817086771	CG3731-PB	FBgn0038271	0.548665877
CG12173-PA	FBgn0037305	0.807576979	yps-PA	FBgn0022959	0.539506116
CG2924-PE	FBgn0023528	0.800964653	Nup98-96-PD	FBgn0039120	0.531143238
Tal-PA	FBgn0023477	0.799579754	CG17266-PB	FBgn0033089	0.526778142
Rae1-PA	FBgn0034646	0.79692142	Incenp-PB	FBgn0260991	0.518578859

Name	Flybase gene identifier	Log2 (Median (15min/4hrs))
CG7656-PF	FBgn0036516	0.51465004
Hrb87F-PE	FBgn0004237	0.502439202
DNApol-delta-PA	FBgn0263600	0.499450921
Srp54k-PA	FBgn0010747	0.495981121
CkIIbeta-PE	FBgn0000259	0.478274641
Nacalpha-PD	FBgn0086904	0.468969749
Msh6-PA	FBgn0036486	0.467287416
RpL22-PA	FBgn0015288	0.456393281
CG8386-PA	FBgn0034061	0.45533762
nero-PA	FBgn0261479	0.43939695
eIF-2gamma-PD	FBgn0263740	0.438932055
TfIIS-PB	FBgn0010422	0.43622137
eIF-2alpha-PB	FBgn0261609	0.436221153
Cp36-PA	FBgn0000359	0.436118297
dec-1-PB	FBgn0000427	0.429596987
Atx2-PB	FBgn0041188	0.416123005
Stam-PA	FBgn0027363	0.411118736
Smn-PB	FBgn0036641	0.41069944
Rpb8-PA	FBgn0037121	0.408878784
CG11164-PB	FBgn0030507	0.407228598
CG12018-PA	FBgn0027903	0.406874609
CG16712-PB	FBgn0031561	0.397922891
PHGPx-PD	FBgn0035438	0.395030003
lap-PF	FBgn0086372	0.393956822
bif-PD	FBgn0014133	0.392234999
RpS25-PB	FBgn0086472	0.391904241
Ama-PC	FBgn0000071	0.387035853
Ccs-PC	FBgn0010531	0.385933873
eIF3-S8-PB	FBgn0034258	0.379248454
CG11107-PB	FBgn0033160	0.371878058
endos-PF	FBgn0061515	0.366794948
Akap200-PG	FBgn0027932	0.362503948
Ubqn-PB	FBgn0031057	0.360509743
Map205-PB	FBgn0002645	0.357648989
fax-PC	FBgn0014163	0.353002691
Mapmodulin	FBgn0034282	0.352788615
Su(var)205-PB	FBgn0003607	0.335849216
mahj-PB	FBgn0034641	0.335677257
pont-PA	FBgn0040078	0.33480649
ALiX-PA	FBgn0086346	0.333230268
PPP4R2r-PC	FBgn0030208	0.317300901
UK114-PB	FBgn0086691	0.312068239
lqfR-PD	FBgn0261279	0.302693754
msd5-PA	FBgn0035210	0.301239919
PpD3-PC	FBgn0005777	0.296022087
spel1-PF	FBgn0015546	0.295150951
CanB2-PB	FBgn0015614	0.292104993
Bruce-PC	FBgn0266717	0.291759982
enc-PH	FBgn0004875	0.264669593
spag-PA	FBgn0015544	0.264165477
cpa-PA	FBgn0034577	0.260993812
rept-PC	FBgn0040075	0.255900838
vib-PC	FBgn0262468	0.254816621
CG11444-PB	FBgn0029715	0.24874719
heph-PZ	FBgn0011224	0.243785607
Pen-PA	FBgn0011823	0.237997922
baf-PB	FBgn0031977	0.237548625
CG8149-PA	FBgn0037700	0.236643201
CG14207-PD	FBgn0031037	0.232180573
His4r-PD	FBgn0013981	0.23118341
RpS10b-PE	FBgn0261593	0.229224536
l(2)k14710-PB	FBgn0021847	0.219954754
DNA-ligI-PA	FBgn0262619	0.214597553
Hrb98DE-PF	FBgn0001215	0.194935316
RpLP2-PA	FBgn0003274	0.184553609
dj-1beta-PA	FBgn0039802	0.176277303
SA-PA	FBgn0020616	0.174995848
Hmg-2-PA	FBgn0026582	0.17220111
Swip-1-PB	FBgn0032731	0.167351759
CG1640-PB	FBgn0030478	0.16246949
Nup50-PA	FBgn0033264	0.15707335
Gl-PA	FBgn0001108	0.156319005
Npl4-PD	FBgn0039348	0.151193128
Atg7-PA	FBgn0034366	0.150700378
Alg-2-PC	FBgn0086378	0.1394135
deltaCOP-PA	FBgn0028969	0.133539982
woc-PE	FBgn0010328	0.1304399
Nup43-PA	FBgn0038609	0.118770477
ndl-PA	FBgn0002926	0.113952199
btz-PD	FBgn0045862	0.113740424
RpS18-PA	FBgn0010411	0.112890223
CG2046-PA	FBgn0037378	0.111831799
smid-PA	FBgn0016983	0.106748723
swm-PB	FBgn0002044	0.101742735
D1-PD	FBgn0000412	0.098104341
AGO2-PC	FBgn0087035	0.097735184
Pp1-87B-PA	FBgn0004103	0.097325985
CLIP-190-PB	FBgn0020503	0.095108771
tyf-PM	FBgn0026083	0.086910582

Name	Flybase gene identifier	Log2 (Median (15min/4hrs))
alphaSnap-PA	FBgn0250791	0.082515967
Lis-1-PG	FBgn0015754	0.080696944
nonA-PD	FBgn0004227	0.078974596
CG6028-PA	FBgn0038924	0.076570928
Mlc-c-PA	FBgn0004687	0.073699442
Fs(2)Ket-PE	FBgn0262743	0.069499483
jar-PL	FBgn0011225	0.068118811
Nup154-PD	FBgn0021761	0.066026014
Jupiter-PC	FBgn0051363	0.065858677
Nplp2-PB	FBgn0040813	0.064607337
CG3689-PC	FBgn0035987	0.05733012
RanBPM-PF	FBgn0262114	0.054591106
sqd-PB	FBgn0263396	0.052119441
CG6543-PB	FBgn0033879	0.051732039
Tm2-PG	FBgn0004117	0.048502749
trsn-PA	FBgn0033528	0.046655443
Smc5-PH	FBgn0052438	0.042748369
bl-PF	FBgn0015907	0.040337894
Nup358-PA	FBgn0039302	0.036977506
l(2)06496-PB	FBgn0010622	0.036675757
CG13217-PA	FBgn0033590	0.028303596
Rack1-PD	FBgn0020618	0.022806364
CTPsyn-PC	FBgn0266452	0.012224725
l(2)09851-PB	FBgn0022288	0.011049927
Lsd-2-PA	FBgn0030608	0.008720697
Fer1HCH-PI	FBgn0015222	0.00761743
csw-PB	FBgn0000382	0.005297609
tws-PI	FBgn0004889	0.00327918
CG14352-PA	FBgn0031351	0.001268396
tral-PC	FBgn0041775	-0.003247066
pix-PB	FBgn0086706	-0.007861099
CG32066-PB	FBgn0052066	-0.008567906
Set-PA	FBgn0014879	-0.012799165
gammaCOP	FBgn0028968	-0.014306671
CG10222-PB	FBgn0036356	-0.014546953
CG10635-PA	FBgn0035603	-0.015267286
CG7182-PB	FBgn0035878	-0.018554016
CG9330-PA	FBgn0036888	-0.02160793
lost-PA	FBgn0263594	-0.024497602
CkIIalpha-PG	FBgn0264492	-0.024511603
vig2-PB	FBgn0046214	-0.028752379
TFAM-PA	FBgn0038805	-0.033700026
AP-1gamma-PI	FBgn0030089	-0.037916426
B52-PO	FBgn0004587	-0.039840628
Edc3-PB	FBgn0036735	-0.039972094
CG30118-PA	FBgn0050118	-0.041374299
Tango7-PB	FBgn0033902	-0.046326786
Rbp2-PE	FBgn0262734	-0.046554081
BicC-PB	FBgn0000182	-0.047023097
CSN3-PA	FBgn0027055	-0.052630055
La-PA	FBgn0011638	-0.056259849
wmd-PB	FBgn0034876	-0.058054693
Rrp40-PB	FBgn0260648	-0.058805399
cathD-PA	FBgn0029093	-0.061916036
Mhc-PU	FBgn0264695	-0.064279053
CG17737-PA	FBgn0035423	-0.068571166
SmD2-PA	FBgn0261789	-0.071576316
bic-PB	FBgn0000181	-0.07193602
und-PC	FBgn0025117	-0.074784783
tacc-PI	FBgn0026620	-0.078862075
His3.3B-PE	FBgn0004828	-0.083190206
Pp4-19C-PH	FBgn0023177	-0.084271383
Rfabg-PD	FBgn0087002	-0.087795087
CG3760-PC	FBgn0022343	-0.093096185
ebi-PA	FBgn0263933	-0.093675417
Rho1-PG	FBgn0014020	-0.097338177
kay-PF	FBgn0001297	-0.097995717
l(3)72Ab-PA	FBgn0263599	-0.100854889
CG5171-PD	FBgn0031907	-0.102499724
CG7332-PB	FBgn0030973	-0.102549705
Mcm2-PA	FBgn0014861	-0.103153995
EfTuM-PB	FBgn0024556	-0.103937698
lds-PA	FBgn0002542	-0.114605427
His2A:CG33865-PA	FBgn0053865	-0.114808845
Rab2-PB	FBgn0014009	-0.114884128
CG2852-PD	FBgn0034753	-0.116228104
Klp10A-PF	FBgn0030268	-0.119868647
CG7945-PA	FBgn0036505	-0.122946513
CG15439-PA	FBgn0031606	-0.125345305
zip-PD	FBgn0265434	-0.125535606
poe-PB	FBgn0011230	-0.125687455
Pp2B-14D-PC	FBgn0011826	-0.132148135
CG8636-PA	FBgn0029629	-0.136597432
sgg-PH	FBgn0003371	-0.137188687
Cand1-PB	FBgn0027568	-0.139604896
Hus1-like-PB	FBgn0026417	-0.140081009
Su(var)3-7-PA	FBgn0003598	-0.140564981
Prx2540-1-PA	FBgn0033520	-0.142587209
CG5174-PP	FBgn0034345	-0.142965903

Name	Flybase gene identifier	Log2 (Median (15min/4hrs))
AP-2alpha-PA	FBgn0264855	-0.149104463
Su(var)2-10	FBgn0003612	-0.14920935
His3:CG33866	FBgn0053866	-0.149398602
RpS8-PG	FBgn0039713	-0.152775754
CG7261-PA	FBgn0027509	-0.156352514
hoip-PB	FBgn0015393	-0.157138369
CG9286-PA	FBgn0038183	-0.158273054
Irp-1B-PA	FBgn0024957	-0.162664599
DhpD-PA	FBgn0261436	-0.164677361
DNApol-alpha180-PA	FBgn0259113	-0.174812329
CG4646-PB	FBgn0033810	-0.1769813
Arpc3A-PE	FBgn0038369	-0.180866213
Ssb-c31a-PA	FBgn0015299	-0.182662762
Cdk7-PA	FBgn0263237	-0.184629172
SF2-PB	FBgn0040284	-0.184753636
CG6907-PB	FBgn0031711	-0.188746081
eIF-4B-PB	FBgn0020660	-0.190940824
bel-PA	FBgn0263231	-0.193561527
Khc-PA	FBgn0001308	-0.194562489
GstS1-PC	FBgn0010226	-0.199090191
Rpn5-PA	FBgn0028690	-0.203727821
msps-PC	FBgn0027948	-0.205649998
Fib-PA	FBgn0003062	-0.207935044
Sap47-PE	FBgn0013334	-0.20981808
betaCOP-PA	FBgn0008635	-0.212526771
CG3448-PB	FBgn0035996	-0.215264136
nocte-PD	FBgn0261710	-0.216840826
Ts-PB	FBgn0024920	-0.220313024
Trip1-PA	FBgn0015834	-0.222715112
CG11334-PC	FBgn0039849	-0.232046616
shi-PP	FBgn0003392	-0.233572829
eRF1-PH	FBgn0036974	-0.235189999
alphaTub84B	FBgn0003884	-0.235457481
Karybeta3-PB	FBgn0087013	-0.236746722
janA-PA	FBgn0001280	-0.239238117
Art3-PB	FBgn0038306	-0.241601984
Usp7-PC	FBgn0030366	-0.24210644
Act88F-PA	FBgn0000047	-0.242227485
eIF3-S9-PA	FBgn0034237	-0.245359886
Moe-PK	FBgn0011661	-0.245697955
alphaTub67C	FBgn0087040	-0.247144956
RnrS-PA	FBgn0011704	-0.2473568
Grip84-PE	FBgn0026430	-0.247378926
CG3430-PA	FBgn0031875	-0.252615317
CG1943-PD	FBgn0037468	-0.253156663
Droj2-PE	FBgn0038145	-0.25315817
CG5642-PA	FBgn0036258	-0.255002415
Act42A-PA	FBgn0000043	-0.255803835
shrb-PA	FBgn0086656	-0.25597946
wdb-PE	FBgn0027492	-0.261069773
AMPdeam-PJ	FBgn0052626	-0.26448137
CG9281-PD	FBgn0030672	-0.266235477
CG30499-PB	FBgn0050499	-0.269954142
CtBP-PG	FBgn0020496	-0.271287694
Hsc70-3-PE	FBgn0001218	-0.271337909
x16-PB	FBgn0028554	-0.276847017
EloB-PA	FBgn0023212	-0.280595893
cact-PE	FBgn0000250	-0.283070641
CG3523-PA	FBgn0027571	-0.288916929
Sec13-PB	FBgn0024509	-0.289479985
CG10289-PC	FBgn0035688	-0.291952878
aub-PA	FBgn0000146	-0.292172118
Sgt1-PA	FBgn0265101	-0.29741753
Arp1-PA	FBgn0011745	-0.302164757
Drp1-PB	FBgn0026479	-0.303221186
dpa-PB	FBgn0015929	-0.303339648
LM408-PB	FBgn0027611	-0.304777351
CG7834-PB	FBgn0039697	-0.304819787
CG17202-PA	FBgn0038043	-0.306197751
CG4365-PC	FBgn0037024	-0.306409878
Prp8-PA	FBgn0033688	-0.309762147
polo-PB	FBgn0003124	-0.316627254
ben-PE	FBgn0000173	-0.317792305
CG1218-PA	FBgn0037377	-0.318496729
fit-PA	FBgn0038914	-0.319391746
Argk-PA	FBgn0000116	-0.319448802
Gclc-PD	FBgn0040319	-0.320859859
tsu-PA	FBgn0033378	-0.321727012
CG2246-PG	FBgn0039790	-0.32426695
CG8209-PA	FBgn0035830	-0.325155991
stai-PC	FBgn0266521	-0.327814192
Nup58-PA	FBgn0038722	-0.328253989
Txl-PA	FBgn0035631	-0.329508592
betaTub56D	FBgn0003887	-0.331632988
pAbp-PB	FBgn0265297	-0.332437052
Cul2-PB	FBgn0032956	-0.333208515
CG18067-PB	FBgn0034512	-0.341342024
me31B-PA	FBgn0004419	-0.342692541
mbf1-PE	FBgn0262732	-0.342930231

Name	Flybase gene identifier	Log2 (Median (15min/4hrs))
rhea-PH	FBgn0260442	-0.344545192
Arpc4-PA	FBgn0031781	-0.345821612
Top3alpha-PA	FBgn0040268	-0.346790463
CG10184-PA	FBgn0039094	-0.348563829
Ran-PD	FBgn0020255	-0.349320044
Snx6-PB	FBgn0032005	-0.349358911
bnb-PD	FBgn0001090	-0.349676073
CG17746-PB	FBgn0035425	-0.353008388
EF2-PD	FBgn0000559	-0.354131363
CG8858-PA	FBgn0033698	-0.354828183
Fim-PA	FBgn0024238	-0.355501253
CG1890-PA	FBgn0039869	-0.358319859
Ald-PM	FBgn0000064	-0.359104067
CG5792-PA	FBgn0032455	-0.360413352
PP2A-B'-PQ	FBgn0042693	-0.361341203
CG10254-PC	FBgn0027512	-0.362731623
CG1440-PD	FBgn0030038	-0.363262837
Mcm7-PA	FBgn0020633	-0.363861127
DNApol-alpha73-PC	FBgn0005696	-0.365783548
Df31-PF	FBgn0022893	-0.368961153
mask-PE	FBgn0043884	-0.369092084
Clc-PD	FBgn0024814	-0.378837705
rin-PG	FBgn0015778	-0.38094735
smt3-PA	FBgn0264922	-0.382841303
CG10638-PD	FBgn0036290	-0.383246196
Mcm3-PB	FBgn0024332	-0.383251502
Zwilch-PA	FBgn0061476	-0.388089993
mgr-PA	FBgn0264694	-0.388673913
Nup107-PA	FBgn0027868	-0.39092507
Cdc37-PA	FBgn0011573	-0.394608126
dod-PA	FBgn0015379	-0.394701096
CG1707-PA	FBgn0033162	-0.395797026
CG31075-PB	FBgn0051075	-0.396667738
CG9328-PA	FBgn0032886	-0.398605964
p47-PA	FBgn0033179	-0.398740583
VhaSFD-PB	FBgn0027779	-0.399971464
CG11858-PA	FBgn0039305	-0.400048733
Rab11-PB	FBgn0015790	-0.403655091
Amph-PA	FBgn0027356	-0.40865309
RpS17-PB	FBgn0005533	-0.409491972
CG6664-PE	FBgn0036685	-0.409523675
p38b-PA	FBgn0024846	-0.414038333
Aats-gly-PC	FBgn0027088	-0.414661332
REG-PB	FBgn0029133	-0.414681831
Ars2-PE	FBgn0033062	-0.415291433
CG1749-PA	FBgn0030305	-0.415977301
CG3909-PA	FBgn0027524	-0.418034241
l(3)01239-PB	FBgn0010741	-0.418837125
Prosalpha2-PA	FBgn0086134	-0.421418496
Mtpalpha-PA	FBgn0028479	-0.421793628
fs(1)N-PA	FBgn0004650	-0.424506008
CG6767-PI	FBgn0036030	-0.42460521
Prosalpha7-PA	FBgn0023175	-0.428170784
Plap-PC	FBgn0024314	-0.430410613
eIF-5A-PA	FBgn0034967	-0.439120265
CG2091-PA	FBgn0037372	-0.439202833
coro-PG	FBgn0265935	-0.439662363
ATPCL-PF	FBgn0020236	-0.440178045
14-3-3epsilon-PC	FBgn0020238	-0.44130243
TBCB-PA	FBgn0034451	-0.441648779
GstE6-PA	FBgn0063494	-0.444318197
CG4408-PB	FBgn0039073	-0.444357949
Cam-PE	FBgn0000253	-0.44605785
CG5126-PA	FBgn0031320	-0.447742616
CG14715-PA	FBgn0037930	-0.447999789
epsilonCOP-PA	FBgn0027496	-0.44858981
flr-PA	FBgn0260049	-0.452622148
sta-PF	FBgn0003517	-0.456357217
Cys-PA	FBgn0004629	-0.456451795
TppII-PD	FBgn0020370	-0.45747382
Bacc-PD	FBgn0031453	-0.457868381
Vinc-PC	FBgn0004397	-0.458948135
CG10863-PA	FBgn0027552	-0.463755273
CG9135-PD	FBgn0031769	-0.464459052
CG2034-PB	FBgn0015359	-0.464467116
Mcm6-PA	FBgn0025815	-0.465645253
CG32068-PB	FBgn0052068	-0.465989881
CG17259-PB	FBgn0031497	-0.466948583
CG13364-PA	FBgn0026879	-0.467986234
14-3-3zeta-PL	FBgn0004907	-0.469143864
Aats-tyr-PA	FBgn0027080	-0.47266535
emb-PA	FBgn0020497	-0.473491808
Act57B-PA	FBgn0000044	-0.473798927
SmE-PA	FBgn0261790	-0.475922673
chic-PF	FBgn0000308	-0.477654218
eIF4G-PC	FBgn0023213	-0.478548348
Gapdh2-PC	FBgn0001092	-0.479259732
CG5384-PB	FBgn0032216	-0.480059723

Name	Flybase gene identifier	Log2 (Median (15min/4hrs))
CG10038-PA	FBgn0038013	-0.482449126
Sec24CD-PC	FBgn0262126	-0.48312679
Prosbeta1-PA	FBgn0010590	-0.48438924
Tudor-SN-PB	FBgn0035121	-0.485171374
Yp1-PB	FBgn0004045	-0.487090875
CG16817-PB	FBgn0037728	-0.488472441
Mtap-PC	FBgn0034215	-0.488957807
cib-PE	FBgn0026084	-0.490026425
TER94-PA	FBgn0261014	-0.490036215
CG5412-PA	FBgn0038806	-0.493091347
SmD3-PA	FBgn0023167	-0.494071974
Rpn1-PA	FBgn0028695	-0.495534542
cdc2c-PC	FBgn0004107	-0.496617709
Vha26-PC	FBgn0015324	-0.497014077
CG1416-PC	FBgn0032961	-0.497264233
CG17904-PA	FBgn0032597	-0.497444799
CG2004-PG	FBgn0030060	-0.502465736
Updo-PA	FBgn0033428	-0.503460467
CG2025-PA	FBgn0030344	-0.503552487
Prosalpha5-PB	FBgn0016697	-0.506608526
Reps-PB	FBgn0032341	-0.508446468
Nedd8-PB	FBgn0032725	-0.510828327
CG8184-PG	FBgn0030674	-0.512009155
Aps-PC	FBgn0036111	-0.512851924
regucalcin-PD	FBgn0030362	-0.513446676
CrebB-PF	FBgn0265784	-0.513931647
Pglym78-PC	FBgn0014869	-0.514561709
Ntf-2-PE	FBgn0031145	-0.515203046
CG10306-PA	FBgn0034654	-0.516632195
GstE12-PD	FBgn0027590	-0.517547464
faf-PC	FBgn0005632	-0.517873963
vlc-PI	FBgn0259978	-0.519158186
Nmt-PA	FBgn0020392	-0.519184845
CSN5-PB	FBgn0027053	-0.519823681
CG9436-PA	FBgn0033101	-0.519985705
CG11395-PB	FBgn0034200	-0.520691711
CG4752-PA	FBgn0034733	-0.521727295
CG7048-PB	FBgn0038976	-0.521867824
eIF-1A-PC	FBgn0026250	-0.522029717
ERp60-PA	FBgn0033663	-0.522104832
CG7789-PA	FBgn0039698	-0.522807408
CG8036-PC	FBgn0037607	-0.523973714
DNApol-alpha50-PA	FBgn0011762	-0.524276162
Cas-PA	FBgn0022213	-0.52498136
Tm1-PO	FBgn0003721	-0.525296268
Rpt1-PA	FBgn0028687	-0.525389992
Aats-asn-PB	FBgn0086443	-0.526656748
Srp68-PA	FBgn0035947	-0.526861508
ade5-PA	FBgn0020513	-0.529433112
Arp2-PC	FBgn0011742	-0.530810663
Act5C-PE	FBgn0000042	-0.531161152
Rcc1-PC	FBgn0002638	-0.531408715
Hsp27-PB	FBgn0001226	-0.53173792
CG10802-PA	FBgn0029664	-0.53274564
Dp1-PH	FBgn0027835	-0.534517176
Uch-PB	FBgn0010288	-0.53559718
Yp2-PB	FBgn0005391	-0.537158058
CG9674-PD	FBgn0036663	-0.537267734
sn-PG	FBgn0003447	-0.538414758
CG30105-PA	FBgn0050105	-0.538814349
Vps29-PA	FBgn0031310	-0.539362437
Sec23-PF	FBgn0262125	-0.544520479
UGP-PE	FBgn0035978	-0.544994459
CG3609-PC	FBgn0031418	-0.54977291
CG32473-PC	FBgn0052473	-0.550294362
26-29-p-PA	FBgn0250848	-0.550515878
Gdi-PC	FBgn0004868	-0.55198178
Hel25E-PB	FBgn0014189	-0.552839144
blw-PA	FBgn0011211	-0.553230552
Pxt-PB	FBgn0261987	-0.553699684
Rpn8-PB	FBgn0002787	-0.55484379
Hsp83-PB	FBgn0001233	-0.55646234
CG2862-PC	FBgn0031459	-0.556522175
CG8223-PA	FBgn0037624	-0.556929842
CG7770-PB	FBgn0036918	-0.558355489
CG17337-PA	FBgn0259979	-0.56066867
CG9853-PC	FBgn0086605	-0.562727321
alph-PC	FBgn0086361	-0.563158713
CG6617-PA	FBgn0030944	-0.564259267
CG3226-PA	FBgn0029882	-0.564854203
Rpn2-PC	FBgn0028692	-0.564863298
CG11267-PA	FBgn0036334	-0.566031261
Prosalpha6-PB	FBgn0250843	-0.568636425
Gs1l-PA	FBgn0019982	-0.572091001
Fmr1-PG	FBgn0028734	-0.574799393
cnn-PL	FBgn0013765	-0.575066489
HBS1-PB	FBgn0042712	-0.575177383
Vha55-PC	FBgn0005671	-0.575468686
Crc-PB	FBgn0005585	-0.577586831

Name	Flybase gene identifier	Log2 (Median (15min/4hrs))	Name	Flybase gene identifier	Log2 (Median (15min/4hrs))
NC2alpha-PA	FBgn0034650	-0.577959921	Idh-PK	FBgn0001248	-0.619269343
Pgd-PB	FBgn0004654	-0.582319371	Rpn3-PB	FBgn0261396	-0.620304664
Eb1-PG	FBgn0027066	-0.583662461	CG2051-PA	FBgn0037376	-0.621291709
eIF-4a-PF	FBgn0001942	-0.58505738	eEF1delta-PA	FBgn0032198	-0.621549208
dUTPase-PA	FBgn0250837	-0.585546924	Sep2-PA	FBgn0014029	-0.622929483
CG2200-PB	FBgn0030447	-0.58633341	Eno-PD	FBgn0000579	-0.623364352
vas-PC	FBgn0262526	-0.587160617	msk-PA	FBgn0026252	-0.623372197
Yp3-PB	FBgn0004047	-0.587280433	Ef1beta-PC	FBgn0028737	-0.623432505
eIF5-PG	FBgn0030719	-0.587298679	Aats-ala-PB	FBgn0027094	-0.62854563
Prosbeta4-PB	FBgn0032596	-0.588720376	Tcp-1zeta-PA	FBgn0027329	-0.628871009
CG4603-PC	FBgn0035593	-0.589588377	Aats-thr-PD	FBgn0027081	-0.631050311
Pdi-PE	FBgn0014002	-0.5916837	clu-PA	FBgn0034087	-0.631921827
CG9705-PC	FBgn0036661	-0.593568005	CoRest-PI	FBgn0261573	-0.63194472
CG6693-PB	FBgn0037878	-0.593850755	AGBE-PA	FBgn0053138	-0.634400806
CG1532-PB	FBgn0031143	-0.594976551	Sptr-PA	FBgn0014032	-0.634754745
FKBP59-PB	FBgn0029174	-0.595691159	eEF1delta-PB	FBgn0032198	-0.637416847
Tctp-PA	FBgn0037874	-0.595844814	Synj-PC	FBgn0034691	-0.637491384
Vha13-PB	FBgn0026753	-0.596210174	Mp20-PC	FBgn0002789	-0.637746186
Hex-A-PA	FBgn0001186	-0.597409503	pzg-PB	FBgn0259785	-0.639804666
CG12321-PA	FBgn0038577	-0.599789066	Pfk-PA	FBgn0003071	-0.640110199
Prosbeta6-PA	FBgn0002284	-0.600954087	CG40045-PD	FBgn0058045	-0.640417114
T-cp1-PA	FBgn0003676	-0.602459938	CG1236-PA	FBgn0037370	-0.641105012
nudC-PB	FBgn0021768	-0.60285648	Mdh1-PB	FBgn0262782	-0.641664801
Aos1-PA	FBgn0029512	-0.603142819	Dek-PE	FBgn0026533	-0.643088649
CG15735-PA	FBgn0030364	-0.603967086	Ranbp9-PD	FBgn0037894	-0.643620966
CG32495-PH	FBgn0052495	-0.605067608	Adk2-PA	FBgn0022708	-0.643799965
Dlic-PD	FBgn0030276	-0.605317451	SpdS-PC	FBgn0037723	-0.645402193
CG30382-PB	FBgn0050382	-0.606014599	Mcm5-PA	FBgn0017577	-0.646333511
GstO2-PA	FBgn0035906	-0.606080953	scu-PA	FBgn0021765	-0.646582491
Tsf1-PC	FBgn0022355	-0.606674232	sw-PK	FBgn0003654	-0.647080446
Dph5-PA	FBgn0024558	-0.608045412	CG8498-PB	FBgn0031992	-0.64840284
Pgi-PC	FBgn0003074	-0.608924811	Cbs-PC	FBgn0031148	-0.648624034
Jafrac1-PE	FBgn0040309	-0.609170146	Hop-PA	FBgn0024352	-0.64877124
rngo-PB	FBgn0030753	-0.609672721	Prosbeta2-PA	FBgn0023174	-0.650557996
pod1-PG	FBgn0029903	-0.609746345	Hsc70-4-PG	FBgn0266599	-0.651167964
SC35-PD	FBgn0265298	-0.611749312	CG31673-PB	FBgn0051673	-0.651479635
Hsc70Cb-PI	FBgn0026418	-0.612045638	Aats-his-PA	FBgn0027087	-0.653259196
BubR1-PA	FBgn0263855	-0.613174898	capt-PB	FBgn0261458	-0.653765816
Pgm-PA	FBgn0003076	-0.614364969	Inos-PA	FBgn0025885	-0.654038634
Nlp-PB	FBgn0016685	-0.615189279	Prosalpha4-PA	FBgn0004066	-0.654473214
CG17768-PB	FBgn0032240	-0.615565328	CG6287-PA	FBgn0032350	-0.655509238
CG4199-PI	FBgn0025628	-0.616438935	glob1-PF	FBgn0027657	-0.655648439
PDCD-5-PA	FBgn0036580	-0.618307127	Capr-PB	FBgn0042134	-0.656049743
pic-PA	FBgn0260962	-0.61884379	Cp1-PC	FBgn0013770	-0.65632255
Sod-PA	FBgn0003462	-0.618994278	Arpc1-PA	FBgn0001961	-0.657731497

Name	Flybase gene identifier	Log2 (Median (15min/4hrs))
DppIII-PC	FBgn0037580	-0.657989493
Cyp1-PA	FBgn0004432	-0.658061812
Got1-PB	FBgn0001124	-0.66041494
Prat-PB	FBgn0004901	-0.66206575
Fdh-PA	FBgn0011768	-0.663323338
eIF-2beta-PA	FBgn0004926	-0.665194787
Aats-cys-PA	FBgn0027091	-0.665431973
Paf-AHalpha-PB	FBgn0025809	-0.668230655
CG11089-PB	FBgn0039241	-0.6692128
grsm-PF	FBgn0040493	-0.67491181
fabp-PB	FBgn0037913	-0.675066756
CHORD-PA	FBgn0029503	-0.675128626
tsr-PA	FBgn0011726	-0.676734252
Klc-PC	FBgn0010235	-0.677274488
Prosbeta3-PA	FBgn0026380	-0.677628211
CG42813-PA	FBgn0261995	-0.678219119
CG5355-PA	FBgn0032242	-0.678578874
Prosbeta7-PB	FBgn0250746	-0.682971553
CG11980-PC	FBgn0037652	-0.683206779
CG12279-PA	FBgn0038080	-0.68333135
CG14434-PC	FBgn0029915	-0.68388267
Rpn9-PA	FBgn0028691	-0.685791732
CG4390-PA	FBgn0038771	-0.68661288
Adh-PI	FBgn0000055	-0.688342083
GstO2-PB	FBgn0035906	-0.693124225
Dip-B-PD	FBgn0000454	-0.695806116
CG31549-PB	FBgn0051549	-0.695839068
cana-PA	FBgn0040233	-0.697148821
CG4968-PA	FBgn0032214	-0.699964841
Tcp-1eta-PA	FBgn0037632	-0.700700873
CG8258-PA	FBgn0033342	-0.700964238
CG2767-PA	FBgn0037537	-0.703682125
CG10576-PD	FBgn0035630	-0.70475125
Ef1gamma-PD	FBgn0029176	-0.704759091
Cctgamma-PD	FBgn0015019	-0.705385395
Uba2-PA	FBgn0029113	-0.705565704
CG18190-PB	FBgn0034403	-0.707131033
Trx-2-PA	FBgn0040070	-0.708440503
RnrL-PA	FBgn0011703	-0.708486245
Sh3beta-PE	FBgn0035772	-0.708553879
CG7911-PB	FBgn0039735	-0.708649458
NAT1-PD	FBgn0010488	-0.709183206
Prx5-PB	FBgn0038570	-0.7096707
ade3-PC	FBgn0000053	-0.709671584
Rpb5-PB	FBgn0033571	-0.710123508
Sep1-PA	FBgn0011710	-0.71182462
GstD1-PB	FBgn0001149	-0.712376684
Aats-val-PA	FBgn0027079	-0.713006203
Zpr1-PA	FBgn0030096	-0.713082607
Rala-PC	FBgn0015286	-0.715991359
Cypl-PA	FBgn0035141	-0.717398994
HIP-R-PD	FBgn0029676	-0.717856045
FK506-bp2-PA	FBgn0013954	-0.719364795
Gapdh1-PB	FBgn0001091	-0.720894639
Ahcy13-PC	FBgn0014455	-0.721329377
CG12082-PB	FBgn0035402	-0.721860035
gammaTub37C-PB	FBgn0010097	-0.722280457
CHIP-PA	FBgn0027052	-0.724167771
CSN4-PB	FBgn0027054	-0.724196722
RpS27A-PA	FBgn0003942	-0.724876855
Lig4-PA	FBgn0030506	-0.724939599
CG9184-PB	FBgn0035208	-0.729495899
Uev1A-PC	FBgn0035601	-0.731172321
UbcD4-PC	FBgn0015321	-0.731569411
Uba1-PA	FBgn0023143	-0.732242854
CG5525-PA	FBgn0032444	-0.733852708
dalao-PA	FBgn0030093	-0.734192103
GlyP-PB	FBgn0004507	-0.73446493
CG5941-PB	FBgn0029833	-0.735359722
CG7322-PC	FBgn0030968	-0.740385387
ras-PE	FBgn0003204	-0.741248741
Pp2A-29B-PC	FBgn0260439	-0.741804104
CG12171-PA	FBgn0037354	-0.742793181
Gpdh-PF	FBgn0001128	-0.743480904
CG18815-PE	FBgn0042138	-0.743848792
ade2-PC	FBgn0000052	-0.745142861
Rpt6-PA	FBgn0020369	-0.746433854
CIAPIN1-PA	FBgn0001977	-0.748062543
Gip-PA	FBgn0011770	-0.748230664
Dak1-PA	FBgn0028833	-0.748839169
AdenoK-PC	FBgn0036337	-0.74904724
pch2-PB	FBgn0051453	-0.749953557
mst-PB	FBgn0020272	-0.750119418
CG7054-PA	FBgn0038972	-0.751267887
Rad23-PC	FBgn0026777	-0.753792377
awd-PD	FBgn0000150	-0.754285587
Dmn-PA	FBgn0021825	-0.755871513
lic-PA	FBgn0261524	-0.761301309

Name	Flybase gene identifier	Log2 (Median (15min/4hrs))
mts-PC	FBgn0004177	-0.763301727
CG6084-PD	FBgn0086254	-0.763964493
Mdh2-PA	FBgn0262559	-0.76609278
CG7737-PB	FBgn0033584	-0.767846866
CG7966-PA	FBgn0038115	-0.769648635
LSm3-PB	FBgn0051184	-0.770809224
CG31472-PB	FBgn0051472	-0.771215999
Vha68-2-PF	FBgn0263598	-0.772973679
Adam-PB	FBgn0027619	-0.77307117
ncd-PB	FBgn0002924	-0.774057759
unc-45-PA	FBgn0010812	-0.77473179
CG10777-PC	FBgn0029979	-0.77496026
Chc-PG	FBgn0000319	-0.775850531
Art4-PB	FBgn0037770	-0.776123993
CG9471-PB	FBgn0037749	-0.777355063
Tpi-PA	FBgn0086355	-0.780941795
Psa-PE	FBgn0261243	-0.782051388
AdSS-PA	FBgn0027493	-0.78398262
Pgk-PE	FBgn0250906	-0.784535487
Uch-L5-PB	FBgn0011327	-0.790254275
CG3011-PA	FBgn0029823	-0.790424972
CG1354-PE	FBgn0030151	-0.793513278
ApepP-PB	FBgn0026150	-0.795107447
AdSL-PA	FBgn0038467	-0.798622668
CG7546-PE	FBgn0035793	-0.800220987
Amun-PL	FBgn0030328	-0.800441492
lwr-PD	FBgn0010602	-0.800721909
rump-PA	FBgn0260010	-0.802169037
cdc2-PA	FBgn0004106	-0.802409379
CG10602-PE	FBgn0032721	-0.802753183
Ef1alpha48D-PE	FBgn0000556	-0.805702847
Nap1-PC	FBgn0015268	-0.809188223
kra-PE	FBgn0250753	-0.812001897
Aats-trp-PB	FBgn0010803	-0.820815343
Mal-B2-PD	FBgn0032382	-0.822364214
Nurf-38-PA	FBgn0016687	-0.831959086
for-PI	FBgn0000721	-0.832335268
eIF-4E-PI	FBgn0015218	-0.839256513
Rpt3-PB	FBgn0028686	-0.839735568
CG7033-PA	FBgn0030086	-0.840180903
Gga-PB	FBgn0030141	-0.841878286
CG9796-PA	FBgn0038149	-0.842239961
Cct5-PA	FBgn0010621	-0.845687044
Rpt2-PB	FBgn0015282	-0.850632494
Trxr-1-PA	FBgn0020653	-0.855427969
Sgt-PB	FBgn0032640	-0.856933613
Rpn12-PA	FBgn0028693	-0.859256308
Rpt4-PB	FBgn0028685	-0.867783696
GstE13-PB	FBgn0033381	-0.881957563
AnxB10-PA	FBgn0000084	-0.882766452
r-PE	FBgn0003189	-0.889939349
Arpc5-PB	FBgn0031437	-0.89551888
PyK-PA	FBgn0003178	-0.898525136
CG9149-PA	FBgn0035203	-0.898649161
NC2beta-PA	FBgn0028926	-0.898798027
cup-PC	FBgn0000392	-0.902341417
CG11899-PA	FBgn0014427	-0.903096578
Acon-PF	FBgn0010100	-0.918343402
Cul3-PF	FBgn0261268	-0.92201448
CG33722-PE	FBgn0064126	-0.923872548
CG13090-PC	FBgn0032054	-0.926212713
CG8031-PA	FBgn0038110	-0.928027913
Elf-PD	FBgn0020443	-0.932472951
Nup153-PC	FBgn0061200	-0.933015431
bur-PC	FBgn0000239	-0.93797953
Rpn11-PA	FBgn0028694	-0.951697097
l(1)G0255-PA	FBgn0028336	-0.95258675
CG6180-PA	FBgn0032453	-0.954828222
IM10-PC	FBgn0033835	-0.957181115
CG6523-PA	FBgn0032509	-0.959960582
Prosalpha3-PA	FBgn0261394	-0.96457379
CG8892-PE	FBgn0031664	-0.965872894
Rab1-PA	FBgn0016700	-0.967607858
Bre1-PB	FBgn0086694	-0.968428751
cl-PC	FBgn0000318	-0.96852015
DnaJ-1-PB	FBgn0263106	-0.973990921
Lam-PD	FBgn0002525	-0.981238661
CG17333-PA	FBgn0030239	-0.986596563
EndoGI-PC	FBgn0028515	-0.987349253
S6k-PB	FBgn0015806	-0.997127966
Vha44-PB	FBgn0262511	-0.998371285
Rpn6-PC	FBgn0028689	-1.005321994
IntS11-PA	FBgn0039691	-1.007282247
Prosbeta5-PA	FBgn0029134	-1.009393362
beta'COP-PA	FBgn0025724	-1.012993263
poly-PB	FBgn0086371	-1.016233439
Mtor-PB	FBgn0013756	-1.019075358
CG10418-PA	FBgn0036277	-1.0197434
sds22-PA	FBgn0028992	-1.021994154

Name	Flybase gene identifier	Log2 (Median (15min/4hrs))
CG5706-PA	FBgn0039175	-1.024134686
CG9934-PB	FBgn0032467	-1.024605216
Arp3-PB	FBgn0262716	-1.033537395
CG5757-PB	FBgn0034299	-1.034996585
Mlc2-PA	FBgn0002773	-1.040035454
CG8525-PD	FBgn0033735	-1.041881177
Psi-PC	FBgn0014870	-1.04321415
AP-1-2beta-PA	FBgn0010380	-1.044062533
CG3800-PB	FBgn0034802	-1.048564116
Eip55E-PB	FBgn0000566	-1.059207513
Hsp23-PB	FBgn0001224	-1.067767508
CG10417-PB	FBgn0033021	-1.091063758
CG8003-PB	FBgn0036096	-1.09420049
Su(fu)-PA	FBgn0005355	-1.100588987
LSm7-PC	FBgn0261068	-1.103810265
r-l-PA	FBgn0003257	-1.106383431
Galk-PD	FBgn0263199	-1.113152161
Sec31-PB	FBgn0033339	-1.114720116
Nup93-1-PA	FBgn0027537	-1.115038542
CG5205-PA	FBgn0038344	-1.121117939
gro-PI	FBgn0001139	-1.12252891
CG3756-PA	FBgn0031657	-1.133268476
Ptpa-PA	FBgn0016698	-1.137719053
up-PJ	FBgn0004169	-1.14515101
CG30496-PA	FBgn0050496	-1.151933072
Nat1-PB	FBgn0031020	-1.154375196
mub-PH	FBgn0262737	-1.156516927
Hsp60-PB	FBgn0015245	-1.160931413
CG5721-PA	FBgn0034315	-1.163124022
Hsp26-PB	FBgn0001225	-1.164354425
GlyS-PA	FBgn0266064	-1.174714155
CG1578-PC	FBgn0030336	-1.176572716
Gp93-PA	FBgn0039562	-1.184642844
eIF2B-alpha-PA	FBgn0039726	-1.189248223
CG11984-PI	FBgn0037655	-1.192431952
eIF6-PA	FBgn0034915	-1.195699822
Snx1-PA	FBgn0031534	-1.211831228
CG1910-PA	FBgn0022349	-1.212330753
yl-PB	FBgn0004649	-1.215947197
Rpn7-PA	FBgn0028688	-1.22085405
Actn-PJ	FBgn0000667	-1.226141293
Rpt5-PA	FBgn0028684	-1.230652101
CG34455-PC	FBgn0085484	-1.234029604
Pect-PE	FBgn0032482	-1.242339997
His2B:CG33910-PA	FBgn0053910	-1.254962982
Vha14-1-PA	FBgn0262512	-1.260075619
eff-PC	FBgn0011217	-1.261827918
primo-1-PB	FBgn0040077	-1.273812438
Dhc64C-PA	FBgn0261797	-1.274922686
Grip71-PA	FBgn0032705	-1.308891744
Glycogenin-PE	FBgn0265191	-1.311610977
CG2263-PA	FBgn0030007	-1.319390745
GM130-PA	FBgn0034697	-1.319901355
CG12702-PC	FBgn0031070	-1.328956826
casp-PC	FBgn0034068	-1.338981043
CG4593-PB	FBgn0029929	-1.358397885
Srp72-PA	FBgn0038810	-1.359072265
His2Av-PB	FBgn0001197	-1.391892649
SelD-PA	FBgn0261270	-1.408816485
CG7787-PA	FBgn0032020	-1.412944211
Pmm45A-PA	FBgn0033377	-1.426197896
Bub3-PB	FBgn0025457	-1.428779086
CG2976-PB	FBgn0031633	-1.430042257
Rpn10-PB	FBgn0015283	-1.430872305
Irbp-PA	FBgn0011774	-1.448632518
dgt4-PC	FBgn0026085	-1.451497279
RecQ4-PA	FBgn0040290	-1.509073999
Gint3-PE	FBgn0034372	-1.515054651
Ku80-PA	FBgn0041627	-1.524142345
Nup205-PA	FBgn0031078	-1.546528831
viaf-PA	FBgn0036237	-1.550311819
CG6726-PC	FBgn0039049	-1.556417307
CG3511-PB	FBgn0035027	-1.57421408
CG1240-PA	FBgn0035370	-1.578797472
Oga-PA	FBgn0038870	-1.632855841
nclb-PA	FBgn0263510	-1.640940061
Mbs-PO	FBgn0005536	-1.646739091
CG5290-PA	FBgn0036772	-1.662411795
Dhpr-PC	FBgn0035964	-1.758541366
psidin-PA	FBgn0243511	-1.760689213
Ssdp-PD	FBgn0011481	-1.769601151
Aldh-PB	FBgn0012036	-1.769647922
CG10527-PA	FBgn0034583	-1.776580415
UbcD10-PA	FBgn0026316	-1.791852523
Nup62-PB	FBgn0034118	-1.799700225
Gel-PK	FBgn0010225	-1.809247237
Gs1-PD	FBgn0001142	-1.821059348
Vha36-1-PA	FBgn0022097	-1.871174363

Name	Flybase gene identifier	Log2 (Median (15min/4hrs))	Name	Flybase gene identifier	Log2 (Median (15min/4hrs))
CG7519-PB	FBgn0037087	-1.876415034	muskelin-PA	FBgn0033757	-2.530019687
CG5568-PA	FBgn0035641	-1.899474046	Tm1-PA	FBgn0003721	-2.539457214
CG14476-PD	FBgn0027588	-1.90158792	RpA-70-PA	FBgn0010173	-2.559318643
eIF3-S10-PD	FBgn0037249	-1.911175761	Det-PA	FBgn0264291	-2.572365404
Atg8a-PA	FBgn0052672	-1.916494017	CG3223-PA	FBgn0037538	-2.576399979
CG15141-PA	FBgn0032635	-1.933366258	RpII140-PB	FBgn0262955	-2.584701621
CG9391-PC	FBgn0037063	-1.997398031	CG2990-PC	FBgn0030170	-2.617484736
ATPsyn-beta-PD	FBgn0010217	-2.031218297	His1:CG33864-PA	FBgn0053864	-2.725428668
mtSSB-PA	FBgn0010438	-2.03654751	APP-BP1-PB	FBgn0261112	-2.725875112
CG31098-PA	FBgn0051098	-2.063990614	msi-PH	FBgn0011666	-2.756181519
CG9515-PB	FBgn0032077	-2.0915001	iPLA2-VIA-PA	FBgn0036053	-2.761296902
Prx6005-PA	FBgn0031479	-2.110163846	yip2-PA	FBgn0040064	-2.84755586
GstE11-PB	FBgn0034354	-2.120331854	Not1-PE	FBgn0085436	-2.883215087
CG6745-PA	FBgn0035901	-2.140876198	GstO1-PA	FBgn0035907	-3.040467388
CG1550-PA	FBgn0033225	-2.182210512	UbcD2-PD	FBgn0015320	-3.198355614
Art1-PA	FBgn0037834	-2.21711843	CG18586-PC	FBgn0035642	-3.391481308
ArfGAP3-PH	FBgn0037182	-2.26220935	twf-PA	FBgn0038206	-3.418541811
alphaCOP-PA	FBgn0025725	-2.267227136	GstE1-PA	FBgn0034335	-3.444147459
CG11148-PH	FBgn0039936	-2.279876908	Pex19-PC	FBgn0032407	-3.659363454
RPA3-PB	FBgn0266421	-2.290125503	Hrs-PC	FBgn0031450	-3.775367058
RPA2-PB	FBgn0032906	-2.334990614	Vps37B-PC	FBgn0037299	-3.849041895
porin-PE	FBgn0004363	-2.352081279	Mes4-PB	FBgn0034726	-3.964451614
dgt6-PA	FBgn0039638	-2.352346699	CG3704-PA	FBgn0040346	-4.056336404
mad2-PA	FBgn0035640	-2.397107533	RpIII128-PA	FBgn0004463	-4.460871571
ric8a-PB	FBgn0028292	-2.500386766	cpb-PB	FBgn0011570	-5.268636883
nst-PA	FBgn0036298	-2.5088221			

List 2: Kinetics of proteasome-inhibited chromatin assembly.

Name	FBgn	Log2 (Median (15min/4 hrs))
CG14352-PA	FBgn0031351	2.606117848
Top2-PB	FBgn0003732	2.541050101
Caf1-180-PB	FBgn0030054	2.112499657
mod(mdg4)-PF	FBgn0002781	2.029508172
eIF3-S9-PA	FBgn0034237	1.778044002
enc-PH	FBgn0004875	1.665387229
RpIII128-PA	FBgn0004463	1.511426392
Hmg-2-PA	FBgn0026582	1.382786578
bigmax-PA	FBgn0039509	1.330977198
Caf1-105-PA	FBgn0033526	1.305417388
RPA2-PB	FBgn0032906	1.290760515
CG14110-PA	FBgn0036352	1.215324619
CG42593-PC	FBgn0260970	1.203553442
NC2beta-PA	FBgn0028926	1.021387152
CG7339-PB	FBgn0036188	1.015489339
Rrp1-PA	FBgn0004584	1.007614466
RpA-70-PA	FBgn0010173	0.978931057
Rab5-PI	FBgn0014010	0.947569062
Sap47-PE	FBgn0013334	0.914034423
RPA3-PB	FBgn0266421	0.874392229
CG42232-PB	FBgn0250754	0.84126862
Parp-PB	FBgn0010247	0.699004491
HmgD-PD	FBgn0004362	0.51346122
Iswi-PC	FBgn0011604	0.462593571
woc-PE	FBgn0010328	0.450727998
Acf1-PA	FBgn0027620	0.350366469
NC2alpha-PA	FBgn0034650	0.313010346
Actn-PJ	FBgn0000667	0.308371776
CG6045-PA	FBgn0038349	0.293434412
CG17209-PC	FBgn0030687	0.247687791
Incenp-PB	FBgn0260991	0.188326405
SA-PA	FBgn0020616	0.176333869
Lig4-PA	FBgn0030506	0.111140681
Rab35-PD	FBgn0031090	0.058256176
barr-PC	FBgn0014127	0.031619927
ArfGAP3-PH	FBgn0037182	0.023036943
TFAM-PA	FBgn0038805	0.015601843
D1-PD	FBgn0000412	-0.003539475
CG13217-PA	FBgn0033590	-0.016780229
HmgZ-PD	FBgn0010228	-0.040408198
SmD2-PA	FBgn0261789	-0.064813114
MEP-1-PG	FBgn0035357	-0.069014848
glu-PA	FBgn0015391	-0.076013828
hang-PD	FBgn0026575	-0.092827763
Rpb5-PB	FBgn0033571	-0.105960081
Dsp1-PG	FBgn0011764	-0.150581502
CG15439-PA	FBgn0031606	-0.177201727
Cap-D2-PA	FBgn0039680	-0.190728907
Rab2-PB	FBgn0014009	-0.202299597
CrebB-PF	FBgn0265784	-0.209052705
Ku80-PA	FBgn0041627	-0.214129653
Max-PD	FBgn0017578	-0.21672945
APP-BP1-PB	FBgn0261112	-0.223973628
CG5941-PB	FBgn0029833	-0.241354178
Rpd3-PA	FBgn0015805	-0.26467033
lds-PA	FBgn0002542	-0.298355281
dalao-PA	FBgn0030093	-0.306181572
FK506-bp1-PA	FBgn0013269	-0.331374509
Irbp-PA	FBgn0011774	-0.355644078
CG17266-PB	FBgn0033089	-0.388547543
Cp36-PA	FBgn0000359	-0.395828627
ncd-PB	FBgn0002924	-0.420881414
btz-PD	FBgn0045862	-0.443250097
borr-PB	FBgn0032105	-0.448171404
GstE11-PB	FBgn0034354	-0.466492879
Ote-PA	FBgn0266420	-0.500565087
PI31-PF	FBgn0033669	-0.507064633
CG6693-PB	FBgn0037878	-0.508647232
Ssdp-PD	FBgn0011481	-0.512177828
Pp1-87B-PA	FBgn0004103	-0.51600291
His3:CG33866-PA	FBgn0053866	-0.517326426
Gnf1-PA	FBgn0004913	-0.519703744
wde-PB	FBgn0027499	-0.539608886
CG5098-PC	FBgn0034300	-0.551496968
Chrac-14-PB	FBgn0043002	-0.562701134
Fen1-PA	FBgn0025832	-0.585773194
Mes4-PB	FBgn0034726	-0.595915823
CG5290-PA	FBgn0036772	-0.608681843
l(2)k14710-PB	FBgn0021847	-0.624981758
Bx42-PB	FBgn0004856	-0.631706421
Alg-2-PC	FBgn0086378	-0.634930794
Hrb87F-PE	FBgn0004237	-0.653970655
mtSSB-PA	FBgn0010438	-0.661632977
gkt-PA	FBgn0260817	-0.661773825

Name	FBgn	Log2 (Median (15min/4 hrs))	Name	FBgn	Log2 (Median (15min/4 hrs))
sle-PB	FBgn0037810	-0.671133812	CkIIalpha-PG	FBgn0264492	-0.95452664
CG14036-PA	FBgn0031677	-0.674192304	gro-PI	FBgn0001139	-0.954815898
ndl-PA	FBgn0002926	-0.677417342	His2B:CG33910-PA	FBgn0053910	-0.956853337
Fer1HCH-PI	FBgn0015222	-0.689608171	CG3800-PB	FBgn0034802	-0.964873704
CTPsyn-PC	FBgn0266452	-0.717874025	hyd-PB	FBgn0002431	-0.976763557
Hus1-like-PB	FBgn0026417	-0.722203142	PCNA-PB	FBgn0005655	-0.983991752
CG6617-PA	FBgn0030944	-0.729017173	eIF5B-PF	FBgn0026259	-0.987274476
RecQ4-PA	FBgn0040290	-0.730293239	asp-PA	FBgn0000140	-0.988972954
TBCB-PA	FBgn0034451	-0.739024926	Tap42-PA	FBgn0051852	-0.991185615
CG32066-PB	FBgn0052066	-0.743297558	DNApol-alpha50-PA	FBgn0011762	-0.997181487
CG2982-PC	FBgn0266570	-0.745499959	CG4951-PB	FBgn0039563	-1.006378234
CG6950-PD	FBgn0037955	-0.74562936	Caf1-PA	FBgn0263979	-1.008395633
porin-PE	FBgn0004363	-0.753658496	BigH1-PA	FBgn0038252	-1.010790497
Cam-PE	FBgn0000253	-0.773907868	Grip84-PE	FBgn0026430	-1.013670157
CHIP-PA	FBgn0027052	-0.783425184	mor-PA	FBgn0002783	-1.020296276
His4r-PD	FBgn0013981	-0.790849402	BicC-PB	FBgn0000182	-1.036398129
CG11858-PA	FBgn0039305	-0.800307597	Gs1l-PA	FBgn0019982	-1.055041656
CG8142-PA	FBgn0030871	-0.805573188	GlyS-PA	FBgn0266064	-1.055291531
Fmr1-PG	FBgn0028734	-0.824825099	Bap55-PA	FBgn0025716	-1.056911368
CG7966-PA	FBgn0038115	-0.825908081	wupA-PA	FBgn0004028	-1.059592033
mask-PE	FBgn0043884	-0.826794688	AdenoK-PC	FBgn0036337	-1.060659329
Rox8-PH	FBgn0005649	-0.826975545	Fib-PA	FBgn0003062	-1.070722317
Abp1-PA	FBgn0036372	-0.827693016	CG5205-PA	FBgn0038344	-1.083529437
RpS27A-PA	FBgn0003942	-0.839812057	CG30499-PB	FBgn0050499	-1.08879268
Nup93-1-PA	FBgn0027537	-0.842363626	dec-1-PB	FBgn0000427	-1.089705348
CG12129-PA	FBgn0033475	-0.844837829	CG11164-PB	FBgn0030507	-1.089814384
l(3)72Ab-PA	FBgn0263599	-0.847430044	CG13690-PA	FBgn0031252	-1.107673154
CG9853-PC	FBgn0086605	-0.851460734	nonA-PD	FBgn0004227	-1.115309591
eIF2B-delta-PD	FBgn0034858	-0.861291524	CanB2-PB	FBgn0015614	-1.11782225
Vinc-PC	FBgn0004397	-0.862089421	Rpn5-PA	FBgn0028690	-1.125886283
muskelin-PA	FBgn0033757	-0.86618722	CG2046-PA	FBgn0037378	-1.126309927
CLIP-190-PB	FBgn0020503	-0.870999632	Dpy-30L1-PA	FBgn0032293	-1.128313897
Aats-asp-PC	FBgn0002069	-0.875815403	mub-PH	FBgn0262737	-1.134654449
cathD-PA	FBgn0029093	-0.877039249	CG14476-PD	FBgn0027588	-1.137116649
Reps-PB	FBgn0032341	-0.885907838	Ntf-2-PE	FBgn0031145	-1.166357186
His3.3B-PE	FBgn0004828	-0.893710011	dre4-PB	FBgn0002183	-1.167708681
Cdc37-PA	FBgn0011573	-0.912007977	CG1240-PA	FBgn0035370	-1.181613359
Srp9-PA	FBgn0035827	-0.912265637	CG8892-PE	FBgn0031664	-1.194733793
psidin-PA	FBgn0243511	-0.920538316	rump-PA	FBgn0260010	-1.2042216
msps-PC	FBgn0027948	-0.92649673	Su(var)3-7-PA	FBgn0003598	-1.206935285
CG3756-PA	FBgn0031657	-0.930349321	CG9796-PA	FBgn0038149	-1.210768474
yl-PB	FBgn0004649	-0.936552694	sds22-PA	FBgn0028992	-1.21590194
RfC38-PB	FBgn0028700	-0.946932117	Rad23-PC	FBgn0026777	-1.22571158
Sgt1-PA	FBgn0265101	-0.947130878	CG7911-PB	FBgn0039735	-1.225906391
RpS25-PB	FBgn0086472	-0.947396893	Snr1-PA	FBgn0011715	-1.227991629
RpL22-PA	FBgn0015288	-0.949576602			

Name	FBgn	Log2 (Median (15min/4 hrs))
CG18067-PB	FBgn0034512	-1.251978402
mre11-PA	FBgn0020270	-1.252817217
Ssrp-PA	FBgn0010278	-1.256156211
fon-PC	FBgn0032773	-1.265893868
bif-PD	FBgn0014133	-1.273744306
CG13364-PA	FBgn0026879	-1.280507246
for-PI	FBgn0000721	-1.287058327
CG4593-PB	FBgn0029929	-1.28816995
Pxt-PB	FBgn0261987	-1.291314094
pAbp-PB	FBgn0265297	-1.293007076
eIF-3p66-PB	FBgn0040227	-1.295434795
Srp54k-PA	FBgn0010747	-1.298361796
gw-PJ	FBgn0051992	-1.298521145
Rack1-PD	FBgn0020618	-1.307505036
Aats-gln-PA	FBgn0027090	-1.308875077
Aldh-PB	FBgn0012036	-1.30983112
AGO2-PC	FBgn0087035	-1.317450799
CG1703-PB	FBgn0030321	-1.324579366
Tal-PA	FBgn0023477	-1.32769411
mago-PA	FBgn0002736	-1.334351226
Rala-PC	FBgn0015286	-1.3361865
PHGPx-PD	FBgn0035438	-1.340124651
DppIII-PC	FBgn0037580	-1.341655766
Mlf-PC	FBgn0034051	-1.353206072
CG4365-PC	FBgn0037024	-1.354318488
Rpb8-PA	FBgn0037121	-1.35938202
CG4968-PA	FBgn0032214	-1.366649402
Nup43-PA	FBgn0038609	-1.369036861
Cp1-PC	FBgn0013770	-1.370183716
mbf1-PE	FBgn0262732	-1.370654215
CG1646-PB	FBgn0039600	-1.372256015
Clc-PD	FBgn0024814	-1.374819484
SMC2-PA	FBgn0027783	-1.38382268
RfC4-PA	FBgn0260985	-1.385363081
CG10417-PB	FBgn0033021	-1.390639343
shrb-PA	FBgn0086656	-1.392460063
CG33156-PF	FBgn0053156	-1.397274742
Sep2-PA	FBgn0014029	-1.398658038
CG12279-PA	FBgn0038080	-1.399928723
CG7182-PB	FBgn0035878	-1.402611984
lig-PK	FBgn0020279	-1.408020028
lola-PR	FBgn0005630	-1.410627522
pzg-PB	FBgn0259785	-1.412706895
RpS10b-PE	FBgn0261593	-1.414208836
His2Av-PB	FBgn0001197	-1.414267012
CG40045-PD	FBgn0058045	-1.417090618
CG14309-PA	FBgn0038611	-1.420087801
Edc3-PB	FBgn0036735	-1.425681737
tral-PC	FBgn0041775	-1.431542603
CG6195-PA	FBgn0038723	-1.434909079
cl-PC	FBgn0000318	-1.441403632
baf-PB	FBgn0031977	-1.446699632
Tango7-PB	FBgn0033902	-1.448144349
Rae1-PA	FBgn0034646	-1.450540649
Chd64-PB	FBgn0035499	-1.451453503
Dis3-PB	FBgn0039183	-1.456555504
CG15047-PA	FBgn0030938	-1.45703726
bel-PA	FBgn0263231	-1.46313129
CG7054-PA	FBgn0038972	-1.468697195
x16-PB	FBgn0028554	-1.470626112
CG2924-PE	FBgn0023528	-1.47203752
CG2767-PA	FBgn0037537	-1.479677887
Cypl-PA	FBgn0035141	-1.479837323
Tm1-PA	FBgn0003721	-1.479974115
DNApol-alpha73-PC	FBgn0005696	-1.480252334
Smc5-PH	FBgn0052438	-1.480716677
CG9485-PF	FBgn0034618	-1.481554994
Msh6-PA	FBgn0036486	-1.482947537
Capr-PB	FBgn0042134	-1.492070204
Dek-PE	FBgn0026533	-1.497006113
Lis-1-PG	FBgn0015754	-1.498104047
Klp3A-PB	FBgn0011606	-1.501666263
janA-PA	FBgn0001280	-1.508127813
RpS18-PA	FBgn0010411	-1.523031974
Gp93-PA	FBgn0039562	-1.523906434
sw-PK	FBgn0003654	-1.526340499
B52-PO	FBgn0004587	-1.529978852
Jupiter-PC	FBgn0051363	-1.530361076
CG7945-PA	FBgn0036505	-1.537028165
Su(var)205-PB	FBgn0003607	-1.537698354
aub-PA	FBgn0000146	-1.538988134
CG7787-PA	FBgn0032020	-1.539368347
Ubqn-PB	FBgn0031057	-1.53993957
SC35-PD	FBgn0265298	-1.540812169
SF2-PB	FBgn0040284	-1.542221854
Crc-PB	FBgn0005585	-1.543622146
Srp72-PA	FBgn0038810	-1.546092867
beta'COP-PA	FBgn0025724	-1.54610647
Art3-PB	FBgn0038306	-1.548725802
Eb1-PG	FBgn0027066	-1.54898966
Mi-2-PD	FBgn0262519	-1.549208003

Name	FBgn	Log2 (Median (15min/4 hrs))	Name	FBgn	Log2 (Median (15min/4 hrs))
Hsp23-PB	FBgn0001224	-1.554810588	tacc-PI	FBgn0026620	-1.656016853
CSN8-PB	FBgn0261437	-1.55532414	HBS1-PB	FBgn0042712	-1.659582181
iPLA2-VIA-PA	FBgn0036053	-1.556040622	CG3448-PB	FBgn0035996	-1.660629723
CG12702-PC	FBgn0031070	-1.557108258	Bruce-PC	FBgn0266717	-1.662090473
Yp3-PB	FBgn0004047	-1.559673484	LSm3-PB	FBgn0051184	-1.663157002
Grip71-PA	FBgn0032705	-1.560114292	cup-PC	FBgn0000392	-1.668055504
Mp20-PC	FBgn0002789	-1.56217168	CG3609-PC	FBgn0031418	-1.668848624
CG7789-PA	FBgn0039698	-1.562489471	Aats-asn-PB	FBgn0086443	-1.670699029
CG11395-PB	FBgn0034200	-1.563629002	vlc-PI	FBgn0259978	-1.670974464
RpS17-PB	FBgn0005533	-1.563667508	flr-PA	FBgn0260049	-1.676174028
Vha14-1-PA	FBgn0262512	-1.56595403	regucalcin-PD	FBgn0030362	-1.676665768
Hex-A-PA	FBgn0001186	-1.568238579	CG6745-PA	FBgn0035901	-1.679952796
Nup58-PA	FBgn0038722	-1.575151725	Prosbeta2-PA	FBgn0023174	-1.680327822
CG11107-PB	FBgn0033160	-1.577594909	Act5C-PE	FBgn0000042	-1.68324711
dod-PA	FBgn0015379	-1.585243273	26-29-p-PA	FBgn0250848	-1.683807135
Cap-G-PF	FBgn0259876	-1.588888549	Ice-PA	FBgn0019972	-1.686067649
RpLP2-PA	FBgn0003274	-1.590233687	Gga-PB	FBgn0030141	-1.688458819
Vha44-PB	FBgn0262511	-1.591119501	ash2-PC	FBgn0000139	-1.691773738
SpdS-PC	FBgn0037723	-1.59210798	CG9184-PB	FBgn0035208	-1.701556419
Nacalpha-PD	FBgn0086904	-1.592898867	Dp1-PH	FBgn0027835	-1.701963637
CG15717-PE	FBgn0030451	-1.600333107	eIF-2beta-PA	FBgn0004926	-1.705868136
Rad9-PB	FBgn0025807	-1.600590726	VhaSFD-PB	FBgn0027779	-1.709387072
CG11267-PA	FBgn0036334	-1.600617274	lic-PA	FBgn0261524	-1.710397299
eIF-2gamma-PD	FBgn0263740	-1.603005971	CG18190-PB	FBgn0034403	-1.71044088
Galk-PD	FBgn0263199	-1.604878126	tsu-PA	FBgn0033378	-1.712026519
spag-PA	FBgn0015544	-1.60498023	CG9281-PD	FBgn0030672	-1.712229289
vig2-PB	FBgn0046214	-1.617313963	tefu-PB	FBgn0045035	-1.712262912
CHORD-PA	FBgn0029503	-1.617702339	Droj2-PE	FBgn0038145	-1.715607832
Rbp2-PE	FBgn0262734	-1.619408873	CG14715-PA	FBgn0037930	-1.717113399
Prx2540-1-PA	FBgn0033520	-1.622334326	CG8235-PA	FBgn0033351	-1.718031124
l(1)G0255-PA	FBgn0028336	-1.62243638	IM10-PC	FBgn0033835	-1.719642994
CG8149-PA	FBgn0037700	-1.623235657	CG30122-PD	FBgn0050122	-1.723757624
Su(var)2-10-PA	FBgn0003612	-1.630425851	Dlic-PD	FBgn0030276	-1.723944925
AdSS-PA	FBgn0027493	-1.632996685	CG13142-PC	FBgn0032251	-1.724770951
Hsc70-3-PE	FBgn0001218	-1.633543819	Ars2-PE	FBgn0033062	-1.726522473
Map205-PB	FBgn0002645	-1.636287064	Rab1-PA	FBgn0016700	-1.729487551
Rrp46-PA	FBgn0037815	-1.637375785	CG17259-PB	FBgn0031497	-1.731525851
rept-PC	FBgn0040075	-1.639780581	RnrS-PA	FBgn0011704	-1.735418586
vib-PC	FBgn0262468	-1.644271263	Aats-glupro-PA	FBgn0005674	-1.737790944
fit-PA	FBgn0038914	-1.644308191	sta-PF	FBgn0003517	-1.740915118
nero-PA	FBgn0261479	-1.645304515	eIF6-PA	FBgn0034915	-1.745628759
RpLP1-PB	FBgn0002593	-1.648166568	CG1943-PD	FBgn0037468	-1.747897472
hoip-PB	FBgn0015393	-1.648833778	p38b-PA	FBgn0024846	-1.748166255
Sptr-PA	FBgn0014032	-1.649164726	Pp2B-14D-PC	FBgn0011826	-1.748336438
Lsd-2-PA	FBgn0030608	-1.650171982	MBD-R2-PB	FBgn0038016	-1.749870901
lap-PF	FBgn0086372	-1.6505969	pic-PA	FBgn0260962	-1.750389002

Name	FBgn	Log2 (Median (15min/4 hrs))	Name	FBgn	Log2 (Median (15min/4 hrs))
Pect-PE	FBgn0032482	-1.752733434	CG5792-PA	FBgn0032455	-1.834572079
CG10038-PA	FBgn0038013	-1.760534079	egg-PA	FBgn0086908	-1.835315159
Set-PA	FBgn0014879	-1.761629664	Paf-AHalpha-PB	FBgn0025809	-1.835474678
Rho1-PG	FBgn0014020	-1.764121123	sgg-PH	FBgn0003371	-1.838353593
Got2-PA	FBgn0001125	-1.76768033	CG10635-PA	FBgn0035603	-1.838411145
p47-PA	FBgn0033179	-1.768548227	Aps-PC	FBgn0036111	-1.839105867
eIF-2alpha-PB	FBgn0261609	-1.770260261	msd5-PA	FBgn0035210	-1.841888523
Nup154-PD	FBgn0021761	-1.771934312	CSN3-PA	FBgn0027055	-1.842183062
nesd-PA	FBgn0032848	-1.773738713	EndoGI-PC	FBgn0028515	-1.844237372
AP-2alpha-PA	FBgn0264855	-1.775754538	Got1-PB	FBgn0001124	-1.845079751
Mbs-PO	FBgn0005536	-1.777263853	Trx-2-PA	FBgn0040070	-1.846641085
r-PE	FBgn0003189	-1.777802958	CG7656-PF	FBgn0036516	-1.84666412
CG1910-PA	FBgn0022349	-1.778434453	CG5174-PP	FBgn0034345	-1.849252121
Rfabg-PD	FBgn0087002	-1.779197219	CG6523-PA	FBgn0032509	-1.851491694
pch2-PB	FBgn0051453	-1.781591311	CG8525-PD	FBgn0033735	-1.852667003
ade5-PA	FBgn0020513	-1.782970546	CG15141-PA	FBgn0032635	-1.854560446
UbcD2-PD	FBgn0015320	-1.786488201	RanBPM-PF	FBgn0262114	-1.857241901
Arpc3A-PE	FBgn0038369	-1.787888412	Hrb27C-PH	FBgn0004838	-1.858592989
GstO2-PA	FBgn0035906	-1.7908747	Fim-PA	FBgn0024238	-1.858973838
Nup358-PA	FBgn0039302	-1.790994802	Sec31-PB	FBgn0033339	-1.861488269
CG12304-PA	FBgn0036515	-1.793535819	CG10802-PA	FBgn0029664	-1.862018478
CG3689-PC	FBgn0035987	-1.793641017	CG15735-PA	FBgn0030364	-1.86245902
dgt4-PC	FBgn0026085	-1.79520054	CG9436-PA	FBgn0033101	-1.863980287
Adk2-PA	FBgn0022708	-1.795238176	Hsc70-4-PG	FBgn0266599	-1.864952931
Prosbeta7-PB	FBgn0250746	-1.798084793	CG17202-PA	FBgn0038043	-1.864982126
Nplp2-PB	FBgn0040813	-1.79970947	CG8031-PA	FBgn0038110	-1.865855701
pont-PA	FBgn0040078	-1.800565206	CG1707-PA	FBgn0033162	-1.866789019
fax-PC	FBgn0014163	-1.804221422	wdb-PE	FBgn0027492	-1.866852012
eIF-4B-PB	FBgn0020660	-1.806704997	CG4752-PA	FBgn0034733	-1.867404656
Pgi-PC	FBgn0003074	-1.809784	Klc-PC	FBgn0010235	-1.86771927
CG31472-PB	FBgn0051472	-1.812407391	swm-PB	FBgn0002044	-1.877964191
mgr-PA	FBgn0264694	-1.813270364	nocte-PD	FBgn0261710	-1.882285561
bl-PF	FBgn0015907	-1.815332238	La-PA	FBgn0011638	-1.883391211
lolal-PH	FBgn0022238	-1.817403286	DnaJ-1-PB	FBgn0263106	-1.883934877
RpS15-PB	FBgn0034138	-1.81774915	Aats-ile-PD	FBgn0027086	-1.886138682
Hsp27-PB	FBgn0001226	-1.818942798	Prosalpha7-PA	FBgn0023175	-1.887424337
tyf-PM	FBgn0026083	-1.819676348	CoRest-PI	FBgn0261573	-1.887760575
cdc2c-PC	FBgn0004107	-1.819915366	eff-PC	FBgn0011217	-1.889095878
CG8003-PB	FBgn0036096	-1.820079653	PDCD-5-PA	FBgn0036580	-1.891121906
Trip1-PA	FBgn0015834	-1.823446273	Prp19-PA	FBgn0261119	-1.895469415
bnb-PD	FBgn0001090	-1.825361458	CG16712-PB	FBgn0031561	-1.897316602
Pfk-PA	FBgn0003071	-1.827021916	CG17768-PB	FBgn0032240	-1.897428234
Nat1-PB	FBgn0031020	-1.830727814	CG14434-PC	FBgn0029915	-1.898310511
CG3760-PC	FBgn0022343	-1.831646229	CG10638-PD	FBgn0036290	-1.900155024
wmd-PB	FBgn0034876	-1.832106034	Moe-PK	FBgn0011661	-1.900733221
Akap200-PG	FBgn0027932	-1.833453219	eIF3-S8-PB	FBgn0034258	-1.900941024

Name	FBgn	Log2 (Median (15min/4 hrs))	Name	FBgn	Log2 (Median (15min/4 hrs))
LM408-PB	FBgn0027611	-1.901459611	Prosbeta1-PA	FBgn0010590	-1.968212056
Smn-PB	FBgn0036641	-1.902866986	DNA-ligI-PA	FBgn0262619	-1.97063427
Nup153-PC	FBgn0061200	-1.903271188	Bub3-PB	FBgn0025457	-1.97175493
CG1749-PA	FBgn0030305	-1.909111289	Hsp60-PB	FBgn0015245	-1.973150966
Npl4-PD	FBgn0039348	-1.909579524	Amph-PA	FBgn0027356	-1.975103653
CG33722-PE	FBgn0064126	-1.910161308	Ranbp9-PD	FBgn0037894	-1.975393377
Rrp40-PB	FBgn0260648	-1.911511567	CG7519-PB	FBgn0037087	-1.975935332
blw-PA	FBgn0011211	-1.911710347	cin-PA	FBgn0000316	-1.976489056
Oga-PA	FBgn0038870	-1.911861081	CG8636-PA	FBgn0029629	-1.976833682
RfC3-PA	FBgn0032244	-1.913027875	CG7834-PB	FBgn0039697	-1.977096215
trsn-PA	FBgn0033528	-1.913528382	GstO2-PB	FBgn0035906	-1.978603127
Mdh2-PA	FBgn0262559	-1.915161704	Mtpalpha-PA	FBgn0028479	-1.97947063
Acon-PF	FBgn0010100	-1.915519552	CG9149-PA	FBgn0035203	-1.981231555
cpb-PB	FBgn0011570	-1.9175409	betaCOP-PA	FBgn0008635	-1.982063026
Dsor1-PB	FBgn0010269	-1.918722649	smid-PA	FBgn0016983	-1.987648196
ebi-PA	FBgn0263933	-1.918835662	Snx6-PB	FBgn0032005	-1.989465928
cact-PE	FBgn0000250	-1.922697929	CG9674-PD	FBgn0036663	-1.989787764
CG32068-PB	FBgn0052068	-1.925008538	ERp60-PA	FBgn0033663	-1.990241982
Dlc90F-PA	FBgn0024432	-1.925162295	CG5721-PA	FBgn0034315	-1.992107071
Etl1-PA	FBgn0032157	-1.926068974	kra-PE	FBgn0250753	-1.997927656
Not1-PE	FBgn0085436	-1.927865902	lqfR-PD	FBgn0261279	-1.998360075
CG9705-PC	FBgn0036661	-1.92967492	CG17337-PA	FBgn0259979	-1.998897909
CG1416-PC	FBgn0032961	-1.931451403	alph-PC	FBgn0086361	-1.999315866
Pen-PA	FBgn0011823	-1.933123073	CG3511-PB	FBgn0035027	-2.000156106
CG11148-PH	FBgn0039936	-1.933545015	Prosalpha4-PA	FBgn0004066	-2.001536051
Rpn12-PA	FBgn0028693	-1.933892907	Arpc2-PB	FBgn0032859	-2.001898237
Nup107-PA	FBgn0027868	-1.937159797	vas-PC	FBgn0262526	-2.00280831
CG1890-PA	FBgn0039869	-1.938343448	Prosalpha6-PB	FBgn0250843	-2.003438221
RpS8-PG	FBgn0039713	-1.940343402	GstE12-PD	FBgn0027590	-2.004150298
CG10863-PA	FBgn0027552	-1.940351744	ArfGAP1-PB	FBgn0020655	-2.004689769
CG5412-PA	FBgn0038806	-1.940933183	Vha55-PC	FBgn0005671	-2.00495136
CG8243-PA	FBgn0033349	-1.941860422	CG2263-PA	FBgn0030007	-2.00643028
CG5126-PA	FBgn0031320	-1.943948724	Ccs-PC	FBgn0010531	-2.006747443
CG30185-PA	FBgn0050185	-1.945973988	Tsf1-PC	FBgn0022355	-2.007349004
CG31075-PB	FBgn0051075	-1.954218822	CG4199-PI	FBgn0025628	-2.007361915
pod1-PG	FBgn0029903	-1.956682609	ATPsyn-beta-PD	FBgn0010217	-2.008651995
Aats-his-PA	FBgn0027087	-1.956735159	Hrb98DE-PF	FBgn0001215	-2.011379153
CG34455-PC	FBgn0085484	-1.957240161	Aats-arg-PA	FBgn0027093	-2.012250852
pix-PB	FBgn0086706	-1.958477361	TfIIS-PB	FBgn0010422	-2.012373418
Gl-PA	FBgn0001108	-1.959103106	Dak1-PA	FBgn0028833	-2.013038241
Bacc-PD	FBgn0031453	-1.960179188	Ama-PC	FBgn0000071	-2.015761774
me31B-PA	FBgn0004419	-1.961821499	stai-PC	FBgn0266521	-2.015946538
CG2200-PB	FBgn0030447	-1.963499768	UbcD4-PC	FBgn0015321	-2.017073305
CG7546-PE	FBgn0035793	-1.965732163	Orc1-PA	FBgn0022772	-2.021059971
SmE-PA	FBgn0261790	-1.965815979	Pp4-19C-PH	FBgn0023177	-2.022353284
Arp3-PB	FBgn0262716	-1.967048262	CG4390-PA	FBgn0038771	-2.02463118

Name	FBgn	Log2 (Median (15min/4 hrs))
CG8223-PA	FBgn0037624	-2.024757922
Prx5-PB	FBgn0038570	-2.030598412
CG14207-PD	FBgn0031037	-2.031377028
Rab11-PB	FBgn0015790	-2.032281392
Mal-B2-PD	FBgn0032382	-2.032514034
CG32473-PC	FBgn0052473	-2.035089442
His2A:CG33865-PA	FBgn0053865	-2.03594432
CG9330-PA	FBgn0036888	-2.037515612
CG33123-PB	FBgn0053123	-2.038310115
l(2)06496-PB	FBgn0010622	-2.044719192
Sep1-PA	FBgn0011710	-2.045363409
Prosalpha5-PB	FBgn0016697	-2.048174321
CG15100-PA	FBgn0034401	-2.048596425
Srp68-PA	FBgn0035947	-2.049024575
14-3-3zeta-PL	FBgn0004907	-2.049803025
CG11980-PC	FBgn0037652	-2.05273429
CG6028-PA	FBgn0038924	-2.054334016
gammaTub37C-PB	FBgn0010097	-2.054812273
Psi-PC	FBgn0014870	-2.055429505
Drp1-PB	FBgn0026479	-2.057986668
CG10254-PC	FBgn0027512	-2.058443336
poly-PB	FBgn0086371	-2.058820634
mahj-PB	FBgn0034641	-2.061206498
CG5355-PA	FBgn0032242	-2.061964833
Prosbeta4-PB	FBgn0032596	-2.065137118
Nedd8-PB	FBgn0032725	-2.065190036
Irp-1B-PA	FBgn0024957	-2.06540864
CG2246-PG	FBgn0039790	-2.067286751
grsm-PF	FBgn0040493	-2.067305337
eIF4G-PC	FBgn0023213	-2.067748722
Rpn7-PA	FBgn0028688	-2.071739349
CG4603-PC	FBgn0035593	-2.072006583
Aats-gly-PC	FBgn0027088	-2.072335176
casp-PC	FBgn0034068	-2.07263138
dUTPase-PA	FBgn0250837	-2.074766413
Mapmodulin-PD	FBgn0034282	-2.077066739
alphaSnap-PA	FBgn0250791	-2.077619597
nbs-PE	FBgn0261530	-2.07841375
Atx2-PB	FBgn0041188	-2.07857647
Zpr1-PA	FBgn0030096	-2.079344722
CG11089-PB	FBgn0039241	-2.080635896
CG7048-PB	FBgn0038976	-2.081108742
rin-PG	FBgn0015778	-2.083215728
Uch-PB	FBgn0010288	-2.083372988
Yp1-PB	FBgn0004045	-2.083992772
Pglym78-PC	FBgn0014869	-2.084434049
CG42813-PA	FBgn0261995	-2.084675745
Art4-PB	FBgn0037770	-2.08531263
Aats-thr-PD	FBgn0027081	-2.086263622
HIP-R-PD	FBgn0029676	-2.0872298
BubR1-PA	FBgn0263855	-2.089102995
Uch-L5-PB	FBgn0011327	-2.089225799
endos-PF	FBgn0061515	-2.092965041
CG3731-PB	FBgn0038271	-2.093971529
mts-PC	FBgn0004177	-2.094119841
CG10777-PC	FBgn0029979	-2.094509695
fabp-PB	FBgn0037913	-2.094549857
Aos1-PA	FBgn0029512	-2.096346098
Df31-PF	FBgn0022893	-2.099843015
Prat-PB	FBgn0004901	-2.101037988
Nap1-PC	FBgn0015268	-2.101844122
Cbs-PC	FBgn0031148	-2.102070386
CG31673-PB	FBgn0051673	-2.102137737
DhpD-PA	FBgn0261436	-2.105190714
Mtor-PB	FBgn0013756	-2.108507682
Klp10A-PF	FBgn0030268	-2.11238855
Mcm3-PB	FBgn0024332	-2.11728198
CG10289-PC	FBgn0035688	-2.118427816
Fdh-PA	FBgn0011768	-2.119885301
CG1440-PD	FBgn0030038	-2.121743818
CG8498-PB	FBgn0031992	-2.125832564
Txl-PA	FBgn0035631	-2.126654496
Pdi-PE	FBgn0014002	-2.129433378
Cys-PA	FBgn0004629	-2.130741209
CG6180-PA	FBgn0032453	-2.131571245
dgt6-PA	FBgn0039638	-2.132232342
Yp2-PB	FBgn0005391	-2.136591407
Nlp-PB	FBgn0016685	-2.137377742
Eip55E-PB	FBgn0000566	-2.141193916
Cp190-PB	FBgn0000283	-2.141426669
CG1640-PB	FBgn0030478	-2.141839077
CG12173-PA	FBgn0037305	-2.14262668
CG13090-PC	FBgn0032054	-2.142792429
Dmn-PA	FBgn0021825	-2.145628995
Rpt6-PA	FBgn0020369	-2.146758656
CG6767-PI	FBgn0036030	-2.14722888
l(3)01239-PB	FBgn0010741	-2.147480553
NAT1-PD	FBgn0010488	-2.147846868
CG3523-PA	FBgn0027571	-2.148327165
chic-PF	FBgn0000308	-2.150987432
Sod-PA	FBgn0003462	-2.152887952

Name	FBgn	Log2 (Median (15min/4 hrs))
CG5568-PA	FBgn0035641	-2.15596856
Arpc5-PB	FBgn0031437	-2.156042677
ric8a-PB	FBgn0028292	-2.157841892
Ahcy13-PC	FBgn0014455	-2.159886394
Plap-PC	FBgn0024314	-2.16124116
CG1550-PA	FBgn0033225	-2.161779778
ade2-PC	FBgn0000052	-2.163584204
Arp1-PA	FBgn0011745	-2.163966264
CG11984-PI	FBgn0037655	-2.165066525
cnn-PL	FBgn0013765	-2.166230113
Psa-PE	FBgn0261243	-2.16674363
Inos-PA	FBgn0025885	-2.167103948
AdSL-PA	FBgn0038467	-2.167159112
CG11334-PC	FBgn0039849	-2.16749956
Khc-PA	FBgn0001308	-2.16788354
Cul2-PB	FBgn0032956	-2.169057536
eIF3-S10-PD	FBgn0037249	-2.169361309
Prosalpha2-PA	FBgn0086134	-2.170064007
CstF-64-PA	FBgn0027841	-2.170416753
Gpdh-PF	FBgn0001128	-2.171540386
Cul4-PB	FBgn0033260	-2.171643026
Top3alpha-PA	FBgn0040268	-2.172647425
Rrp4-PB	FBgn0034879	-2.175378864
T-cp1-PA	FBgn0003676	-2.177964458
csw-PB	FBgn0000382	-2.179555888
lwr-PD	FBgn0010602	-2.181771995
CG4646-PB	FBgn0033810	-2.182799902
CG10576-PD	FBgn0035630	-2.183876924
mod-PC	FBgn0002780	-2.188523743
eEF1delta-PB	FBgn0032198	-2.1895166
PpD3-PC	FBgn0005777	-2.191224849
Sh3beta-PE	FBgn0035772	-2.196589718
Mcm6-PA	FBgn0025815	-2.196638798
ApepP-PB	FBgn0026150	-2.198204863
GM130-PA	FBgn0034697	-2.200979719
EloB-PA	FBgn0023212	-2.202851298
CG30382-PB	FBgn0050382	-2.202879076
TER94-PA	FBgn0261014	-2.206018462
Art1-PA	FBgn0037834	-2.20702491
UK114-PB	FBgn0086691	-2.208516405
jar-PL	FBgn0011225	-2.208599154
Zwilch-PA	FBgn0061476	-2.209675397
Mdh1-PB	FBgn0262782	-2.209851467
Chc-PG	FBgn0000319	-2.210005012
GstE1-PA	FBgn0034335	-2.214606818
Usp7-PC	FBgn0030366	-2.215171986
Dhc64C-PA	FBgn0261797	-2.21579135
DNApol-alpha180-PA	FBgn0259113	-2.220926366
scu-PA	FBgn0021765	-2.221568381
Aats-val-PA	FBgn0027079	-2.223626754
CG18586-PC	FBgn0035642	-2.223912245
Prosbeta6-PA	FBgn0002284	-2.223989492
CG9135-PD	FBgn0031769	-2.224503917
Dph5-PA	FBgn0024558	-2.224635804
Ef1alpha48D-PE	FBgn0000556	-2.225015697
Arpc1-PA	FBgn0001961	-2.225045338
cib-PE	FBgn0026084	-2.225608008
poe-PB	FBgn0011230	-2.226319323
r-l-PA	FBgn0003257	-2.227258518
Gint3-PE	FBgn0034372	-2.232704747
eRF1-PH	FBgn0036974	-2.23423079
Dip-B-PD	FBgn0000454	-2.238746182
CG4069-PA	FBgn0036301	-2.2391142
CG2862-PC	FBgn0031459	-2.239814372
Chrac-16-PB	FBgn0043001	-2.23988918
Prosbeta3-PA	FBgn0026380	-2.244376647
CG1354-PE	FBgn0030151	-2.244870202
SH3PX1-PA	FBgn0040475	-2.24620423
CG32495-PH	FBgn0052495	-2.2464023
14-3-3epsilon-PC	FBgn0020238	-2.247850899
Hsc70Cb-PI	FBgn0026418	-2.248380714
CG18815-PE	FBgn0042138	-2.249107721
Sgt-PB	FBgn0032640	-2.252292481
bur-PC	FBgn0000239	-2.259107991
CG3011-PA	FBgn0029823	-2.263787348
Hel25E-PB	FBgn0014189	-2.263925178
Ts-PB	FBgn0024920	-2.264952088
Idh-PK	FBgn0001248	-2.266058835
Sec24CD-PC	FBgn0262126	-2.268213373
CG2034-PB	FBgn0015359	-2.268922319
bic-PB	FBgn0000181	-2.270377858
Cyp1-PA	FBgn0004432	-2.270879961
Gdi-PC	FBgn0004868	-2.272496115
Gclc-PD	FBgn0040319	-2.272778027
Ef1beta-PC	FBgn0028737	-2.273226625
primo-1-PB	FBgn0040077	-2.274334441
CG2025-PA	FBgn0030344	-2.275159175
CG11444-PB	FBgn0029715	-2.275401692
FK506-bp2-PA	FBgn0013954	-2.275848031
AnxB10-PA	FBgn0000084	-2.279173159
CG9328-PA	FBgn0032886	-2.279787107

Name	FBgn	Log2 (Median (15min/4 hrs))
Sec13-PB	FBgn0024509	-2.281255052
CG17737-PA	FBgn0035423	-2.282121984
tws-PI	FBgn0004889	-2.28420762
Arp2-PC	FBgn0011742	-2.285339143
CG2051-PA	FBgn0037376	-2.287185718
Rpn6-PC	FBgn0028689	-2.288357352
Pgm-PA	FBgn0003076	-2.291924061
rad50-PD	FBgn0034728	-2.29257763
Vps37B-PC	FBgn0037299	-2.293315631
faf-PC	FBgn0005632	-2.294139632
msk-PA	FBgn0026252	-2.295498647
Cas-PA	FBgn0022213	-2.295759116
Ef1gamma-PD	FBgn0029176	-2.298959452
CG2990-PC	FBgn0030170	-2.301439044
Fs(2)Ket-PE	FBgn0262743	-2.301781613
eIF-4E-PI	FBgn0015218	-2.303845477
spel1-PF	FBgn0015546	-2.303901501
Nup93-2-PA	FBgn0038274	-2.304145881
Hop-PA	FBgn0024352	-2.305690611
ras-PE	FBgn0003204	-2.30710048
AMPdeam-PJ	FBgn0052626	-2.307789383
Prosalpha3-PA	FBgn0261394	-2.308367188
DNApol-delta-PA	FBgn0263600	-2.311027645
capt-PB	FBgn0261458	-2.312875612
smt3-PA	FBgn0264922	-2.313103718
ALiX-PA	FBgn0086346	-2.313128466
Nup50-PA	FBgn0033264	-2.314210644
cpa-PA	FBgn0034577	-2.316239609
Gip-PA	FBgn0011770	-2.319412094
PPP4R2r-PC	FBgn0030208	-2.320479873
REG-PB	FBgn0029133	-2.321038728
RhoGDI-PB	FBgn0036921	-2.321252256
eIF5-PG	FBgn0030719	-2.32147937
CG8036-PC	FBgn0037607	-2.32248182
CG4300-PC	FBgn0036272	-2.324170138
CG6287-PA	FBgn0032350	-2.325549009
CG3704-PA	FBgn0040346	-2.330043238
glob1-PF	FBgn0027657	-2.330913822
Trxr-1-PA	FBgn0020653	-2.332583826
Prosbeta5-PA	FBgn0029134	-2.334568185
CG6664-PE	FBgn0036685	-2.337619176
CG9515-PB	FBgn0032077	-2.337744966
RpII140-PB	FBgn0262955	-2.338679911
Adam-PB	FBgn0027619	-2.338859012
Pp2A-29B-PC	FBgn0260439	-2.338990278
GstD1-PB	FBgn0001149	-2.340074596
CG17333-PA	FBgn0030239	-2.340599111
UGP-PE	FBgn0035978	-2.341564465
Aats-lys-PA	FBgn0027084	-2.341831092
Rpn2-PC	FBgn0028692	-2.3429187
rngo-PB	FBgn0030753	-2.34463354
CG5642-PA	FBgn0036258	-2.351390395
Vha68-2-PF	FBgn0263598	-2.352584208
Rpn10-PB	FBgn0015283	-2.356979567
CG11899-PA	FBgn0014427	-2.357037769
Stam-PA	FBgn0027363	-2.35765035
Vha26-PC	FBgn0015324	-2.358115987
Tudor-SN-PB	FBgn0035121	-2.358251205
CG7261-PA	FBgn0027509	-2.360675962
emb-PA	FBgn0020497	-2.360837096
CG7322-PC	FBgn0030968	-2.365329934
polo-PB	FBgn0003124	-2.367951294
Eno-PD	FBgn0000579	-2.368710698
Cctgamma-PD	FBgn0015019	-2.370889448
Nup98-96-PD	FBgn0039120	-2.373123008
Nmt-PA	FBgn0020392	-2.37561928
AGBE-PA	FBgn0053138	-2.375810848
viaf-PA	FBgn0036237	-2.383077036
Mcm2-PA	FBgn0014861	-2.384561838
RanGAP-PB	FBgn0003346	-2.38541419
Rpt5-PA	FBgn0028684	-2.387799587
CG12321-PA	FBgn0038577	-2.388640907
Mcm5-PA	FBgn0017577	-2.390246858
CG41099-PE	FBgn0039955	-2.39221875
Tctp-PA	FBgn0037874	-2.393400442
CG31549-PB	FBgn0051549	-2.393882261
eIF-4a-PF	FBgn0001942	-2.400399148
CG12018-PA	FBgn0027903	-2.401721949
FANCI-PA	FBgn0033354	-2.406036919
CG2976-PB	FBgn0031633	-2.408416638
PP2A-B'-PQ	FBgn0042693	-2.409666489
Amun-PL	FBgn0030328	-2.410000506
osa-PE	FBgn0261885	-2.413777547
CG3226-PA	FBgn0029882	-2.416938052
FKBP59-PB	FBgn0029174	-2.421282786
Det-PA	FBgn0264291	-2.421401618
CG30105-PA	FBgn0050105	-2.426660305
mst-PB	FBgn0020272	-2.426797816
Tpi-PA	FBgn0086355	-2.426828768
AP-1gamma-PI	FBgn0030089	-2.428565654
Ald-PM	FBgn0000064	-2.432578993

Name	FBgn	Log2 (Median (15min/4 hrs))	Name	FBgn	Log2 (Median (15min/4 hrs))
Atg8a-PA	FBgn0052672	-2.433722431	CSN4-PB	FBgn0027054	-2.51729693
Rpn9-PA	FBgn0028691	-2.434904419	RnrL-PA	FBgn0011703	-2.517701494
Karybeta3-PB	FBgn0087013	-2.435434247	Updo-PA	FBgn0033428	-2.519295955
Pgk-PE	FBgn0250906	-2.43735388	CG4408-PB	FBgn0039073	-2.521259616
Uba2-PA	FBgn0029113	-2.43747606	CG1236-PA	FBgn0037370	-2.521530023
GstE13-PB	FBgn0033381	-2.437706819	CG6726-PC	FBgn0039049	-2.525815013
Lam-PD	FBgn0002525	-2.438049125	lola-PD	FBgn0005630	-2.526412409
GAPsec-PA	FBgn0035916	-2.438408422	Snx1-PA	FBgn0031534	-2.527748037
PyK-PA	FBgn0003178	-2.438451714	Nurf-38-PA	FBgn0016687	-2.528032546
UbcD10-PA	FBgn0026316	-2.439895323	Su(fu)-PA	FBgn0005355	-2.528662756
CG8858-PA	FBgn0033698	-2.440117731	Tcp-1zeta-PA	FBgn0027329	-2.530968767
GstO1-PA	FBgn0035907	-2.440147906	CG5525-PA	FBgn0032444	-2.533886757
clu-PA	FBgn0034087	-2.440710252	und-PC	FBgn0025117	-2.53475315
CG7770-PB	FBgn0036918	-2.44549251	eIF-1A-PC	FBgn0026250	-2.535713915
Atg7-PA	FBgn0034366	-2.445655812	tsr-PA	FBgn0011726	-2.536086557
CG18004-PB	FBgn0033566	-2.446016084	Bet3-PA	FBgn0260859	-2.53783961
Rpn3-PB	FBgn0261396	-2.451985226	sn-PG	FBgn0003447	-2.53937595
Aats-tyr-PA	FBgn0027080	-2.452464619	Sip1-PA	FBgn0010620	-2.541439364
yip2-PA	FBgn0040064	-2.45268524	CG9471-PB	FBgn0037749	-2.542300458
Ran-PD	FBgn0020255	-2.453319592	awd-PD	FBgn0000150	-2.545186176
CG5171-PD	FBgn0031907	-2.453806307	Pex19-PC	FBgn0032407	-2.548420638
CG5706-PA	FBgn0039175	-2.455428066	CG8258-PA	FBgn0033342	-2.551268161
CG9914-PB	FBgn0030737	-2.458481254	GstS1-PC	FBgn0010226	-2.553895521
CG1218-PA	FBgn0037377	-2.466763879	mbo-PA	FBgn0026207	-2.557113193
lost-PA	FBgn0263594	-2.469965189	CtBP-PG	FBgn0020496	-2.557744071
Rpt1-PA	FBgn0028687	-2.474665008	CG17904-PA	FBgn0032597	-2.561790145
twf-PA	FBgn0038206	-2.475981967	Nup205-PA	FBgn0031078	-2.563385911
Mcm7-PA	FBgn0020633	-2.480826916	CG2852-PD	FBgn0034753	-2.568471491
nudC-PB	FBgn0021768	-2.486000562	CIAPIN1-PA	FBgn0001977	-2.570087685
Drep-2-PC	FBgn0028408	-2.486017262	alphaCOP-PA	FBgn0025725	-2.572111922
Adh-PI	FBgn0000055	-2.49085813	Mtap-PC	FBgn0034215	-2.573158763
ATPCL-PF	FBgn0020236	-2.49132957	CG8184-PG	FBgn0030674	-2.576280245
Vha36-1-PA	FBgn0022097	-2.492076863	Gs1-PD	FBgn0001142	-2.577818885
nst-PA	FBgn0036298	-2.493777854	Prx6005-PA	FBgn0031479	-2.578219904
epsilonCOP-PA	FBgn0027496	-2.494100499	CG10418-PA	FBgn0036277	-2.585059747
ade3-PC	FBgn0000053	-2.494738191	Cand1-PB	FBgn0027568	-2.591719724
CG6543-PB	FBgn0033879	-2.496382852	GlyP-PB	FBgn0004507	-2.592031436
dpa-PB	FBgn0015929	-2.496506973	mtd-PU	FBgn0013576	-2.595093924
CG8209-PA	FBgn0035830	-2.50277601	CG5384-PB	FBgn0032216	-2.596772068
rhea-PH	FBgn0260442	-2.50406165	cdc2-PA	FBgn0004106	-2.598518216
kay-PF	FBgn0001297	-2.505854956	Gapdh1-PB	FBgn0001091	-2.599351429
Rpn11-PA	FBgn0028694	-2.50693947	cana-PA	FBgn0040233	-2.602655108
CG6084-PD	FBgn0086254	-2.513262865	CG10565-PB	FBgn0037051	-2.604473228
Rpt4-PB	FBgn0028685	-2.513620375	Uev1A-PC	FBgn0035601	-2.605482475
CG1532-PB	FBgn0031143	-2.513996672	Elf-PD	FBgn0020443	-2.60702549
Cdk7-PA	FBgn0263237	-2.514690326	Argk-PA	FBgn0000116	-2.614112794

Name	FBgn	Log2 (Median (15min/4 hrs))	Name	FBgn	Log2 (Median (15min/4 hrs))
CG2004-PG	FBgn0030060	-2.615240429	CG9934-PB	FBgn0032467	-2.831365185
eIF-5A-PA	FBgn0034967	-2.621198027	coro-PG	FBgn0265935	-2.847392671
deltaCOP-PA	FBgn0028969	-2.621845347	alphaTub84B-PA	FBgn0003884	-2.859709578
SmD3-PA	FBgn0023167	-2.622391189	Arpc4-PA	FBgn0031781	-2.861530414
Tcp-1eta-PA	FBgn0037632	-2.624202925	ben-PE	FBgn0000173	-2.862479093
CG12082-PB	FBgn0035402	-2.625975247	heph-PZ	FBgn0011224	-2.873620096
CG12171-PA	FBgn0037354	-2.626691563	Hsp83-PB	FBgn0001233	-2.876011729
CG10184-PA	FBgn0039094	-2.627394566	betaTub56D-PB	FBgn0003887	-2.889056468
CG2091-PA	FBgn0037372	-2.629422291	GstE6-PA	FBgn0063494	-2.898435307
Rpt2-PB	FBgn0015282	-2.635962143	mad2-PA	FBgn0035640	-2.910017594
Dhpr-PC	FBgn0035964	-2.639714566	CSN5-PB	FBgn0027053	-2.912563745
Ptpa-PA	FBgn0016698	-2.639949588	Aats-cys-PA	FBgn0027091	-2.924976611
Uba1-PA	FBgn0023143	-2.642562971	CG7332-PB	FBgn0030973	-2.930949722
Pgd-PB	FBgn0004654	-2.644669245	CG10306-PA	FBgn0034654	-2.937040403
Tm2-PG	FBgn0004117	-2.644990239	CG6907-PB	FBgn0031711	-2.943649179
CG10602-PE	FBgn0032721	-2.652269853	Rpn8-PB	FBgn0002787	-2.979655301
alphaTub67C-PA	FBgn0087040	-2.652500119	CG10222-PB	FBgn0036356	-2.98806944
RanBP3-PA	FBgn0039110	-2.665868909	Nsun2-PA	FBgn0026079	-2.998289599
CkIIbeta-PE	FBgn0000259	-2.667006858	LSm7-PC	FBgn0261068	-3.021183705
unc-45-PA	FBgn0010812	-2.673219155	Mlc2-PA	FBgn0002773	-3.049291947
Hsp26-PB	FBgn0001225	-2.676193366	Hrs-PC	FBgn0031450	-3.074971271
Jafrac1-PE	FBgn0040309	-2.679214148	Ssb-c31a-PA	FBgn0015299	-3.078432952
Rpi-PC	FBgn0050410	-2.681713815	eIF2B-alpha-PA	FBgn0039726	-3.082675311
Mhc-PU	FBgn0264695	-2.689858356	Cul3-PF	FBgn0261268	-3.119984639
l(2)09851-PB	FBgn0022288	-2.691745138	AP-1-2beta-PA	FBgn0010380	-3.129373132
CG7033-PA	FBgn0030086	-2.693154036	Swip-1-PB	FBgn0032731	-3.133540328
CG16817-PB	FBgn0037728	-2.705950607	CG1578-PC	FBgn0030336	-3.141494136
EF2-PD	FBgn0000559	-2.706226256	CG30118-PA	FBgn0050118	-3.14428251
Aats-ala-PB	FBgn0027094	-2.713745869	eEF1delta-PA	FBgn0032198	-3.144827592
CG30496-PA	FBgn0050496	-2.716964762	dj-1beta-PA	FBgn0039802	-3.205513214
msi-PH	FBgn0011666	-2.717211389	EfTuM-PB	FBgn0024556	-3.209396013
Glycogenin-PE	FBgn0265191	-2.72470984	CG9391-PC	FBgn0037063	-3.211341007
Aats-trp-PB	FBgn0010803	-2.726307951	CG8386-PA	FBgn0034061	-3.229748137
Trn-PD	FBgn0024921	-2.728227557	CG3223-PA	FBgn0037538	-3.267657834
CG10527-PA	FBgn0034583	-2.728276146	yps-PA	FBgn0022959	-3.270107202
Gel-PK	FBgn0010225	-2.728567658	Tm1-PO	FBgn0003721	-3.296504093
TppII-PD	FBgn0020370	-2.748278934	SelD-PA	FBgn0261270	-3.299787883
Gapdh2-PC	FBgn0001092	-2.750141615	sqh-PE	FBgn0003514	-3.301285487
Vps29-PA	FBgn0031310	-2.758389264	CG17746-PB	FBgn0035425	-3.333692771
Prp8-PA	FBgn0033688	-2.781232662	Pmm45A-PA	FBgn0033377	-3.339611585
Rpn1-PA	FBgn0028695	-2.784877149	Sec23-PF	FBgn0262125	-3.347926008
Rpt3-PB	FBgn0028686	-2.792114975	CG32164-PB	FBgn0042177	-3.349232802
vih-PA	FBgn0264848	-2.794768023	CG3909-PA	FBgn0027524	-3.377532703
Vha13-PB	FBgn0026753	-2.795639161	fs(1)N-PA	FBgn0004650	-3.399688243
shi-PP	FBgn0003392	-2.798888375	Mlc-c-PA	FBgn0004687	-3.419888758
Cct5-PA	FBgn0010621	-2.802842952	IntS11-PA	FBgn0039691	-3.424200614

Name	FBgn	Log2 (Median (15min/4 hrs))
pnut-PA	FBgn0013726	-3.436908965
CSN7-PA	FBgn0028836	-3.44014736
Act88F-PA	FBgn0000047	-3.461014581
Act57B-PA	FBgn0000044	-3.465487403
Bre1-PB	FBgn0086694	-3.535807586
Nup62-PB	FBgn0034118	-3.605483232
CG31098-PA	FBgn0051098	-3.629180155
His1:CG33864-PA	FBgn0053864	-3.689160297
Synj-PC	FBgn0034691	-3.707847733
Aprt-PD	FBgn0000109	-3.950808679
nclb-PA	FBgn0263510	-4.043329649
up-PJ	FBgn0004169	-4.053086862
zip-PD	FBgn0265434	-4.248591604
sqd-PB	FBgn0263396	-4.262887269
SmD1-PA	FBgn0261933	-4.28331156
gammaCOP-PA	FBgn0028968	-4.349861052
Arf79F-PJ	FBgn0010348	-4.441871864
S6k-PB	FBgn0015806	-4.47039059
CG3430-PA	FBgn0031875	-4.513702294
CG7737-PB	FBgn0033584	-4.593835336
Rcc1-PC	FBgn0002638	-4.939359731
Act42A-PA	FBgn0000043	-4.960599353
CG9286-PA	FBgn0038183	-5.304293441
CG2918-PB	FBgn0023529	-5.841714837
CG5757-PB	FBgn0034299	-7.957152758

ACKNOWLEDGMENTS

I would like to begin by thanking Axel Imhof for the opportunity to do my PhD thesis in his lab. I appreciate the time and advice very much that you invested in me and it was inspiring for me to experience your continuous enthusiasm about science. Many thanks for your support throughout the entire time of the PhD with regards to scientific but also non-scientific questions.

Furthermore, I like to thank Peter Becker and Michiel Vermeulen for their support during my TAC meetings and in regular other occasions. I value Michiel's advice and personal support during my scientific career as instrumental opportunity to think outside the box and to find new approaches for my projects. Peter's guidance gave me a lot of input and made me aware of crucial questions in science. In addition, Peter's contribution to the chromatin community in Munich is impressive and I am very thankful for having the opportunity to join this network here at the LMU.

I like to thank all past and present members of the Imhof group for constructive feedback, lively discussions and any support for experiments.

Ein ganz herzliches Dankeschön richte ich an Miriam Pusch, Irene Vetter und Edith Mentele. Deine wissenschaftliche Starthilfe, liebe Miriam, wie auch Deine strategischen Ratschläge zu Beginn meiner Doktorarbeit haben mir vieles erleichtert und mir ungemein geholfen! Außerdem werde ich die gemeinsamen Unternehmungen mit Irene und Edith innerhalb und außerhalb des Labors, als auch eure Integrationsmaßnahmen in die bayrische Gesellschaft niemals vergessen. Vielen Dank!
Außerdem danke ich allen früheren Kollegen und Freunden aus dem Adolf Butenandt Institut und dem BMC für eure Unterstützung! Sowohl wissenschaftlich, als auch privat, freue ich mich, mit euch in Kontakt zu sein und euch getroffen zu haben.

Many thanks to Andreas Schmidt, Ignasi Forne, Marc Wirth, Shibojyoti Lahiri and all members of the ZfP team. It was a pleasure to do Mass Spec with you and I am thankful for all advice that I have received from you. You helped me a lot in PTM analysis, SWATH-MS and all other "breakthrough" techniques. Additionally, it was great to not only practice SWATH window adjustments but also some table soccer skills with you. I will miss our daily competitions.
A special thank goes to Anja Groth, Constance Alabert and Kyosuke Nakamura. I would not have been able to perform any NCC experiments without your support and helpful supervision.

During my stay in Copenhagen, I was amazed by your friendly introduction and your patience with me. Moreover, I enjoyed the collaboration very much between our two labs and I will cross my fingers for all upcoming experiments.

Ich danke Lisa Harpprecht für die Zusammenarbeit auf dem Gebiet der Chromatinassemblierung und für den kollegialen Austausch von Protokollen. Außerdem hat es mich gefreut, mit Dir Studentenrepresentant gewesen zu sein.

I also like to thank Elizabeth Schroeder Reiter and all members of the IRTG Graduate Program for financial but also ideational support during my PhD thesis. I gained a lot of knowledge during Conferences and Summer Schools that have been supported by the Graduate network but I also grew personally as member inside the Graduate School. It was a very valuable experience and many thanks Elizabeth for all your support and enthusiasm within the IRTG. In addition, I like to say a very big “thank you” for proofreading this thesis, Elizabeth.

Many thanks to all colleagues within the Adolf Butenandt Institute and BMC for sharing reagents, protocols and experience. It was fun to work with you.
Ein besonderer Dank gilt auch Edith Müller und Carolin Brieger für alle administrativen Aufgaben!

Ein unendlich großer Dank gilt meiner Mutter, ohne deren Unterstützung ich nicht bis zu diesem Punkt gekommen wäre. Diese Unterstützung und die vielen wertvollen Ratschläge während meiner Schul- und Studienzeit haben mir für meinen wissenschaftlichen und auch beruflichen Werdegang viel gelehrt und ich bin mehr als dankbar dafür!

Diese Arbeit wäre nicht ohne die Hilfe und Unterstützung von meiner Frau zustande gekommen. Liebe Christine, ich danke Dir, dass Du die „Launen eines Wissenschaftlers“ mehr als einmal ertragen hast und mir immerzu den Rücken stärkst. Ich freue mich sehr auf die weitere gemeinsame Zeit mit Dir!